



**NAM**

# **EUCentre Shaketable Test of Terraced House Modelling Predictions and Analysis Cross Validation**

---

**Staff from ARUP, EUCentre (Pavia) and TU Delft**

Datum November 2015

Editors Jan van Elk & Dirk Doornhof



## General Introduction

The response of buildings and the structural strength of the buildings in the Groningen area is an important issue for the assessment of risk resulting from induced earthquakes. As the building stock in the Groningen region is quite different from that in other seismically active areas, detailed studies into the structural strength response to earthquakes of the buildings typical for the Groningen area are required.

Especially modelling of the unreinforced masonry (URM) buildings typical for the Groningen area is challenging. Therefore a test of a terraced house was planned with modelling prior to the test, comparison of the modelling with the test results and modelling of the test results based on updated models. This test is part of a much larger study program into building response to earthquakes. A typical Groningen terraced house was built on a shake table in the laboratory of EUCENTRE in Pavia, Italy, and subjected to representative accelerograms.

This report describes the test of a terraced house (build to Groningen specifications) at the shake table of EUCentre in Pavia and the modelling done before and after the test results were evaluated. In this respect the current report is a further step in understanding the behavior URM buildings and an extension of the URM Modelling and Analysis Cross-Validation study. The same teams of modelers that took part in the Cross-Validation study also collaborated in the shake-table test; ARUP, EUCENTRE Pavia and Technical University Delft.

The test was designed and carried out by EUCentre. The modelling study supporting this test has been coordinated by ARUP, who also compiled the report from the individual contributions from the three participants.

The test and modelling results have been fed into the fragility functions development work stream, which is coordinated by the following experts:

External Expert	Affiliation	Main Expertise Area
Rui Pinho	EUCentre	Fragility of buildings
Helen Crowley	EUCentre	Fragility of buildings
Peter Stafford	EUCentre / Imperial College London	Ground Motion Prediction
Barbara Polidoro	EUCentre	Fragility of buildings

Assurance for this study is primarily based on cross-validation between the parties involved. This test and the studies into the fragility of buildings have further been reviewed by a panel of independent experts in October during a workshop in London:

<b>External Expert</b>	<b>Affiliation</b>	<b>Role</b>	<b>Main Expertise Area</b>
Jack Baker	Stanford University, US	Independent Reviewer	Building Fragility and Risk
Paolo Franchin	University of Rome "La Sapienza"	Independent Reviewer	Building Fragility and Risk
Michael Griffith	University of Adelaide, Australia	Independent Reviewer	Modeling and Testing of Masonry structures
Curt Haselton	California State University, US	Independent Reviewer	Structural Modeling and Fragility
Jason Ingham	University of Auckland	Independent Reviewer	Modeling and Testing of Masonry structures
Nico Luco	United States Geological Survey	Independent Reviewer	Building Fragility and Risk
Dimitrios Vamvatsikos	NTUA, Greece	Independent Reviewer	Building Fragility and Risk



**NAM**

<b>Title</b>	<b>EUcentre Shaketable Test of Terraced House Modelling Predictions and Analysis Cross Validation</b>		<b>Date</b>	November 2015
			<b>Initiator</b>	NAM
<b>Author(s)</b>	Staff from EUcentre, ARUP and TU Delft	<b>Editors</b>	Jan van Elk Dirk Doornhof	
<b>Organisation</b>	ARUP, EUCENTRE, TUDelft	<b>Organisation</b>	NAM	
<b>Place in the Study and Data Acquisition Plan</b>	<u>Study Theme:</u> Building Structural Strength <u>Comment:</u> This report describes the test of a terraced house (build to Groningen specifications) at the shake table of EUcentre in Pavia and the modelling done before and after the test results were evaluated.			
<b>Directly linked research</b>	(1) Ground Motion Prediction (incl. duration and spectral acceleration)m, (2) Structural upgrading of buildings, (3) Definition of Risk Metrics.			
<b>Used data</b>	Test results of a terraced house (build to Groningen specifications) at the shake table of EUcentre in Pavia			
<b>Associated organisation</b>	EUcentre, University of Pavia, Mosayk, University of Delft and ARUP.			
<b>Assurance</b>	Assurance team has met in London in October 2015. Recommendations of the assurance team have been included in the report: "Development of v2 Partial Collapse Fragility and Consequence Functions for the Groningen Field".			

Client: Nederlandse Aardolie  
Maatschappij

**Arup Project Title: Groningen  
Earthquakes - Structural  
Upgrading**

**EUC-BUILD: Modelling Predictions  
and Analysis Cross Validation**

229746\_031.0\_REP1004

Issue | 21 December 2015

This report was prepared by Arup in December 2015 on the basis of a scope of services agreed with our client. It is not intended for and should not be relied upon by any third party and no responsibility or liability is undertaken to any third party.

Job number 229746

**Arup b.v.**  
Naritaweg 118  
1043 CA Amsterdam  
PO box 57145  
1040 BA Amsterdam  
The Netherlands

This document is part of scientific work and is based on information available at the time of writing. Work is still in progress and the contents may be revised during this process, or to take account of further information or changing needs. This report is in the public domain only for the purpose of allowing thorough scientific discussion and further scientific review. The findings are only estimated outcomes based upon the available information and certain assumptions. We cannot accept any responsibility for actual outcomes, as events and circumstances frequently do not occur as expected

**ARUP**

# Contents

---

	Page
<b>Executive Summary</b>	<b>1</b>
<b>1 Introduction</b>	<b>2</b>
<b>2 Analysis Predictions of EUC-BUILD</b>	<b>3</b>
2.1 Comparison of Blind Predictions	5
2.2 Comparison of Blind Predictions using Measured Ground Motions	62
2.3 Comparison of Post-Test Refined Predictions	113

## References

## Appendices

### Appendix A

Modelling Approach and Assumptions

## Executive Summary

---

Currently, very limited data is available on the seismic response of construction typologies specific to Dutch practice. Therefore, in addition to benchmarking, cross-validation against newly planned experimental data is needed to study material characteristics and the response of components and full buildings in order to validate and update the guidance.

This report compares the performance of three different modelling approaches used by Arup, EUCENTRE and TU-Delft against their ability to predict the performance of the shake table test of a terraced house that embodies typical modern Dutch residential building construction. The shake table test was administered at EUCENTRE.

All teams performed a blind prediction of the experiment before the experiment took place as well as a post-test refined prediction after the experimental test results were released to the teams. All numerical models achieved improved results with each post-test refined prediction model.

An outcome of the performed predictions is a summary of software pros and cons for all three utilized modelling approaches as well as a list of lessons learnt from each party. While improvements in the numerical modelling results achieved by all parties are significant, there is still much to learn regarding the behaviour of typical Dutch buildings. Therefore, it is recommended that the test campaign is continued in order to better understand the behaviour of full scale structural connections and other building components that exemplify typical Dutch building construction. It is also recommended that more validation regarding the variability of masonry material properties, such as calcium-silicate material, be performed so that the most accurate and robust modelling and analysis method of this material can be determined.



# 1 Introduction

---

There are a number of modelling and analysis approaches presently used for assessment of the seismic performance of unreinforced masonry (URM) structures. The approaches employ different idealisations for modelling the behaviour of masonry and other features of URM buildings construction, potentially leading to differences in the resulting assessment of the expected seismic performance.

A benchmarking and cross-validation exercise [1] was performed by Arup, the European Centre for Training and Research in Earthquake Engineering (EUCENTRE) and the Technical University of Delft (TU-Delft) in 2014. The three Consultants used different analysis software: LS-DYNA, TREMURI and DIANA (see Appendix A). A number of experimental benchmarks were tested in two laboratories at EUCENTRE and TU-Delft. The focus of this document is on the shake table test performed at EUCENTRE on the full-scale “index building” with typical geometry representative of the Groningen terraced house building stock. The three consultants prepared computational solutions for this shake table test to calibrate and validate their models.

The previous work [1] highlighted the need to perform further large scale component tests and full scale building tests. It was determined that to demonstrate the robustness of each approach, each Consultant should generate a “blind-prediction” of the expected laboratory result, based on the planned test protocol. The specimen would then be tested and the blind prediction compared to the test. A “post-test refined prediction” would then be analysed, in order to establish the sensitivity of each model to salient parameters.

This report presents the results of the blind and post-test refined predictions for the EUCENTRE full scale shake table test, which was performed in September 2015.



Figure 1: Collaboration partners of Arup



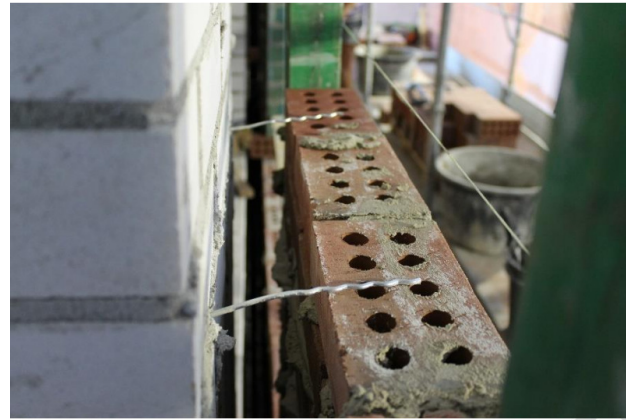


Figure 13. Laying of the ties

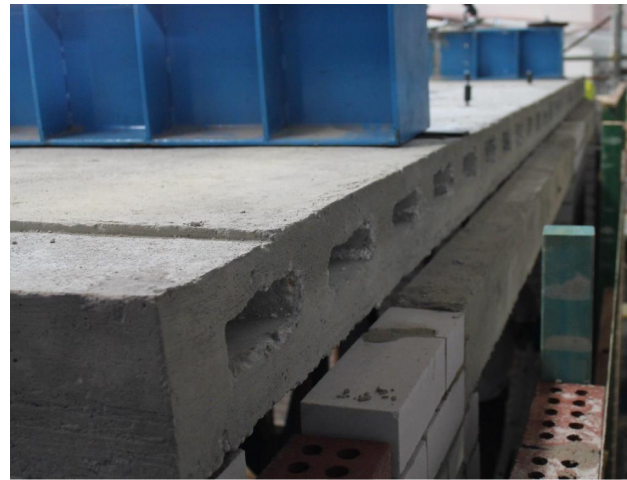


Figure 17. View of the r.c. slab of the first floor - East side



Figure 24. Roof and c.s. gable - South side



Figure 30. Detail of the connection between the girder and the clay gable - 2

Figure 4: Photographs of test house from EUCENTRE Report

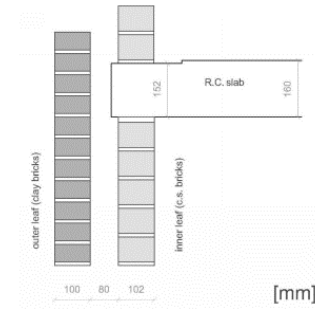


Figure 276. Detail of the connection between the r.c. slab of the first and second floor and the inner leaf (c.s. walls) - South side.

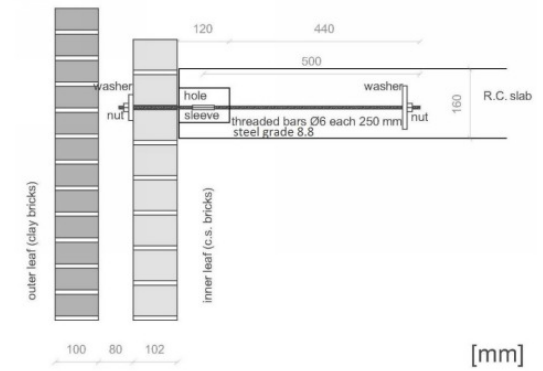


Figure 277. Detail of the connection between the r.c. slab of the first floor and the inner leaf (c.s. walls) - East and West side.

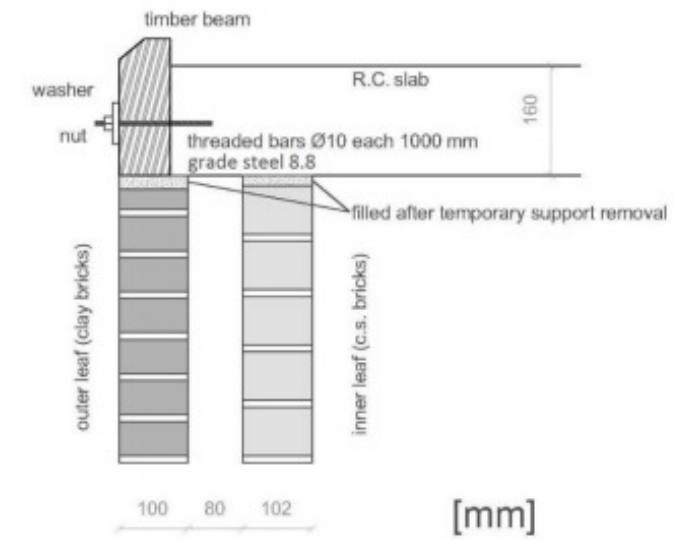


Figure 280. Detail of the connection between the r.c. slab of the second floor and the inner leaf (c.s. walls) - East and West side.

Figure 5: Connection details from EUCENTRE Report

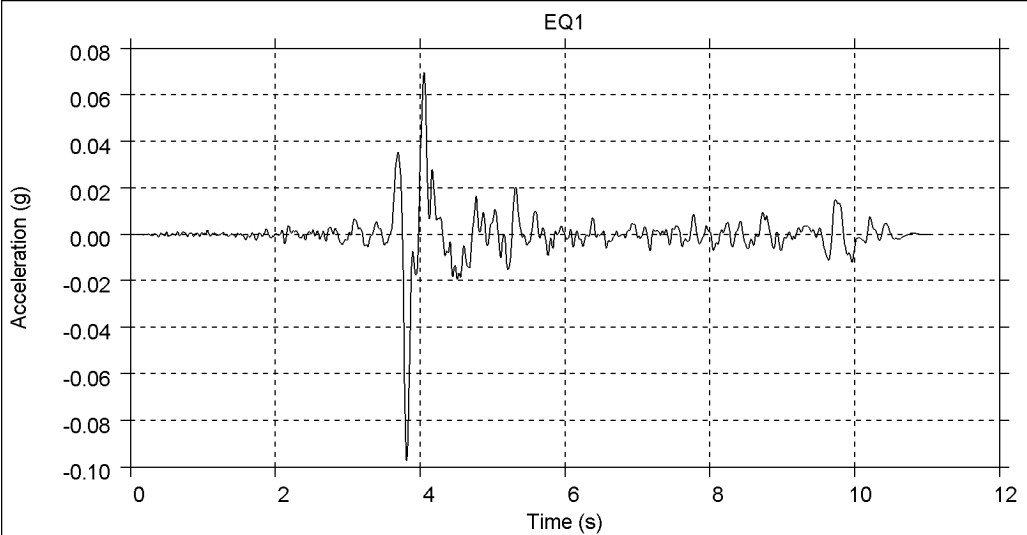
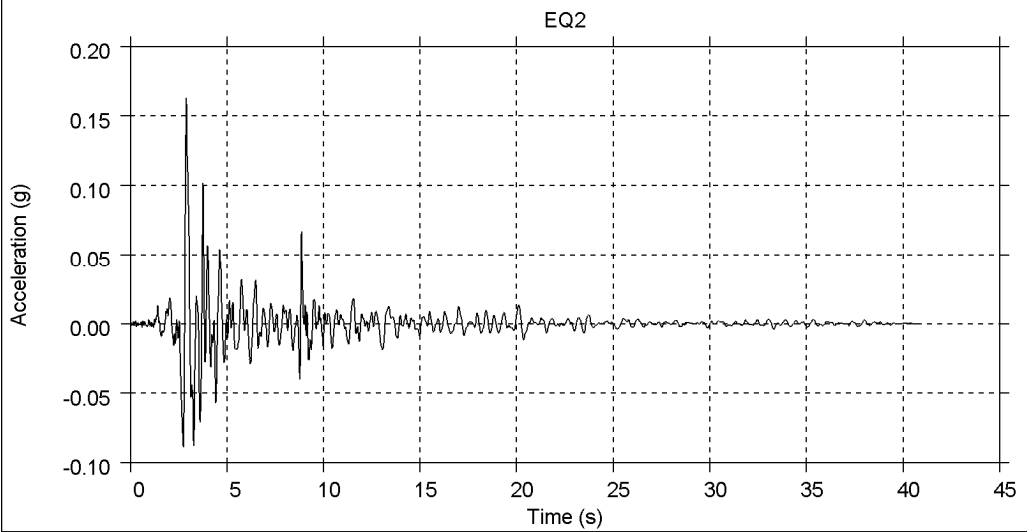
## 2.1 Comparison of Blind Predictions

This section compares the results of the blind prediction models from each consultant to the lab results.

### 2.1.1 Model Assumptions

The assumed loading protocol for the blind prediction numerical models is as illustrated in Table 1.

Table 1: Assumed loading protocol

Earthquake	Graph	Protocol
EQ1		EQ1 @ 50%
		EQ1 @ 100%
		EQ1 @ 150%
EQ2		EQ2 @ 100%
		EQ2 @ 150%
		EQ2 @ 200%

Assumptions on material properties made by each consultant are summarized in Table 2 through Table 4. Modelling techniques and assumptions are summarized in Table 5 and Table 6. More information on such assumptions are described in sections 2.1.2 through 2.1.3.

Table 2: Calcium silicate (inner leaf) material properties (based on summary table dated 13/07/2015 unless noted otherwise)

Symbol	Description	Value	Arup	EUCENTRE	TU-Delft
$\rho$	Mass density [kg/m <sup>3</sup> ]	---	1785	1800	1785
E	Masonry Young's modulus in the direction perpendicular to bed joints [GPa]	E <sub>1</sub> = 3.256	4.182	4.182	3.256
		E <sub>2</sub> = 4.182			
		E <sub>3</sub> = 3.236			
$\nu$	Poisson's ratio of masonry	0.14 <sup>1</sup>	0.14	---	0.14
$f_c$	Masonry compressive strength in the direction perpendicular to bed joints [MPa]	6.3	6.3	6.3	6.3
$f_t$	Tensile strength (flexural bond strength) of mortar joints [MPa]	0.238	0.238	---	---
$f_s$	Shear strength (cohesion) of mortar joints [MPa]	0.21	0.21	0.21	0.14 <sup>3</sup>
$G_t$	Energy release rate for tensile failure of mortar [N/m]	---	15 <sup>2</sup>	---	15 <sup>2</sup>
$G_s$	Energy release rate for shear failure of mortar [N/m]	---	21	---	---
$\mu$	Coefficient of friction for sliding of joints	0.42	0.42	0.42	---

<sup>1</sup> Value from TU-Delft material tests as listed in the 13/07/2015 summary document

<sup>2</sup> Value not provided in summary document and referenced from NAM BfD rev 3

<sup>3</sup> See section 2.1.3 for further explanation of assumption

Table 3: Clay material (outer leaf) properties (based on summary table dated 13/07/2015)

Symbol	Description	Value	Arup	EUCENTRE	TU-Delft
$\rho$	Mass density [kg/m <sup>3</sup> ]	---	1867	1700	1831
E	Masonry Young's modulus in the direction perpendicular to bed joints [GPa]	$E_1 = 5.760$	6.033	6.033	5.760
		$E_2 = 6.033$			
		$E_3 = 5.967$			
$\nu$	Poisson's ratio of masonry	$0.20^2$	0.20	---	0.20
$f_c$	Masonry compressive strength in the direction perpendicular to bed joints [MPa]	11.32	11.32	11.32	11.32
$f_t$	Tensile strength (flexural bond strength) of mortar joints [MPa]	0.158	0.158	---	--- <sup>3</sup>
$f_s$	Shear strength (cohesion) of mortar joints [MPa]	$0.15^1$	0.15	0.15	$0.15^3$
$G_t$	Energy release rate for tensile failure of mortar [N/m]	---	$35^2$	---	15
$G_s$	Energy release rate for shear failure of mortar [N/m]	---	15	---	---
$\mu$	Coefficient of friction for sliding of joints	$0.87^1$	0.87	0.87	---

<sup>1</sup> Value from TU-Delft material tests as listed in the 13/07/2015 summary document<sup>2</sup> Value not provided in summary document and referenced from NAM BfD rev 3<sup>3</sup> See section 2.1.3 for further explanation of assumption

Table 4: Other material properties

Symbol	Description	Value	Arup	EUCENTRE	TU-Delft
<b>Concrete</b>					
$\rho$	Mass density [kg/m <sup>3</sup> ]	---	2400	2500	2400
$f'_c$	Concrete compressive strength [MPa]	29.8 <sup>2</sup>	29.8	28	---
$f'_t$	Concrete tensile strength [MPa]	---	2.7	---	---
<b>Reinforcement in slab</b>					
$\rho$	Mass density [kg/m <sup>3</sup> ]	---	7860	---	---
E	Young's modulus [GPa]	---	200	---	---
$\sigma_y$	Yield strength [MPa]	---	585	---	---
<b>Timber</b>					
$\rho$	Mass density [kg/m <sup>3</sup> ]	---	500	420	600
E	Elastic modulus [GPa]	11.6 – 14.7 <sup>2</sup>	13.2	11	9.0
<b>Wall Ties</b>					
$\sigma_t$	Tensile strength of ties [kN]	4.35 <sup>1</sup>	1.0	2.90	1.20

<sup>1</sup> Value from EUCENTRE material tests as listed in the 13/07/2015 summary document<sup>2</sup> Value provided by EUCENTRE

Table 5: Additional modelling assumptions

Component	Arup	EUCENTRE	TU-Delft
Roof diaphragm	Roof girders and planks are modelled with 1D linear elastic beam elements. Nails are modelled as nonlinear hysteretic beam elements. Nails rigidly connect the plank and girder elements. Diaphragm flexibility and nonlinearity is captured by the behaviour of the nails.	Modelled by means of two inclined (43.5°) 4-node orthotropic membrane finite elements with equivalent thickness, shear modulus (tangential stiffness of the diaphragm) and moduli of elasticity (normal stiffness of the membrane).	The roof plywood is modelled with eight-node quadrilateral isoparametric curved shell elements with linear material properties. The plywood is fully clamped to the girders, whilst it is not connected with the North/South walls.
Wall ties	Wall ties are modelled as 1D discrete beam elements with defined nonlinear axial strength and stiffness only in tension and compression.	<p>The cavity ties connecting the in-plane (east and west side) walls are modelled by means of equivalent membrane elements with equivalent thickness and shear modulus, introduced at the levels of the floor slabs.</p> <p>The connecting ties between the CaSi leaf and the veneer of the northern side are modelled as elastic beams by means of 2D finite elements, each one of them defined between 2 nodes. These beams are distributed at certain spacing along the wall height, with properties equivalent to the properties of the total number of ties located at that specific level. Due to the need to introduce the required number of nodes in order to realize the aforementioned modelling approach, the two masonry leafs are discretized.</p>	Modelled with two-node truss elements, with nonlinear behaviour both in tension and compression.
Connection between first floor slab and East/West walls	The first floor slab and East/West inner leaves are connected via discrete beam elements that represent the threaded bar anchors for out-of-plane displacements only. Beams have defined elastic axial stiffness only. These elements become activated after the inherent gravity load is applied to replicate the actual construction sequence.	In the model implemented for the blind prediction, the kinematic coupling is effective only between the slab and the corner piers.	Connected for the out-of-plane displacements only through the use of tyings.
Connection between first floor slab and North/South walls	First floor slab elements are fully merged with the North/South inner leaf wall elements	Ideal connection, with perfect displacement coupling. The in-plane moment transfer is achieved by introducing a fictitious beam, connecting the two out-of-plane CaSi leafs, with equivalent to the RC slab flexural stiffness.	Fully clamped.
Connection between second floor slab and East/West inner leaves	Second floor slab elements and East/West wall elements are connected for the vertical displacements. Sliding is potentially resisted by friction only (representing the mortar between the slab and the walls) but due to the modelling of the construction sequence, there is no weight on this connection. Vertical loads occur only as a result of dynamic behaviour during the shaking motion, therefore frictional resistance to sliding is small and intermittent.	Fictitious beams with axial and flexural stiffness equivalent to those of an effective width of the RC slab are introduced at the top of the 2 <sup>nd</sup> storey piers in order to model the presence of the slab.	Connected for the vertical displacements only through the use of tyings.
Connection between timber beam at gutter level and East/West outer leaves		No connection	
Connection between second floor slab and North/South walls	Second floor slab elements are fully merged with the North/South inner leaf wall elements	Ideal connection, with perfect displacement coupling. The in-plane moment transfer is achieved by introducing a fictitious beam, connecting the two out-of-plane CaSi leafs, with equivalent to the RC slab flexural stiffness.	Fully clamped.



Table 6: Additional modelling assumptions (continued)

Component	Arup	EUCENTRE	TU-Delft
Connection between roof girders and North/South walls	Roof girders are fully merged with the North/South inner leaf wall elements.	Ideal connection, with perfect displacement coupling and in-plane moment transfer.	Fully clamped.

## 2.1.2 Arup

In addition to the information presented in section 2.1.1, the slabs are modelled as nonlinear 2D shell elements that are subdivided into layers defined explicitly for concrete and for reinforcement. Elastic properties of the concrete and reinforcement are those specified in Table 4. Nonlinearity of the composite slab beyond the elastic range is accounted for in the model.

The concrete lintels above window and door openings are modelled as 1D linear elastic beam elements with concrete properties specified in Table 4.

The masonry inner and outer leaves are modelled with a homogenized masonry material model with 2D, fully integrated shell elements and five through-thickness integration points that evaluate the behaviour of masonry where the damage is assumed to be lumped at the joints. Crack plane directions are pre-defined to model mortar bonds.

Some numerical instability occurred during the GM2 200% ground motion, resulting in unrealistically high levels of damage. The stability problem has been fixed in the LS-DYNA software, and the updated version has been used for subsequent analyses including that described in Sections 2.2 and 2.3 of this report. Hence, the damage shown in this blind prediction is more extensive than in the analysis described in Sections 2.2 and 2.3.

See Figure 6 for a schematic of the LS-DYNA blind prediction model with annotations.

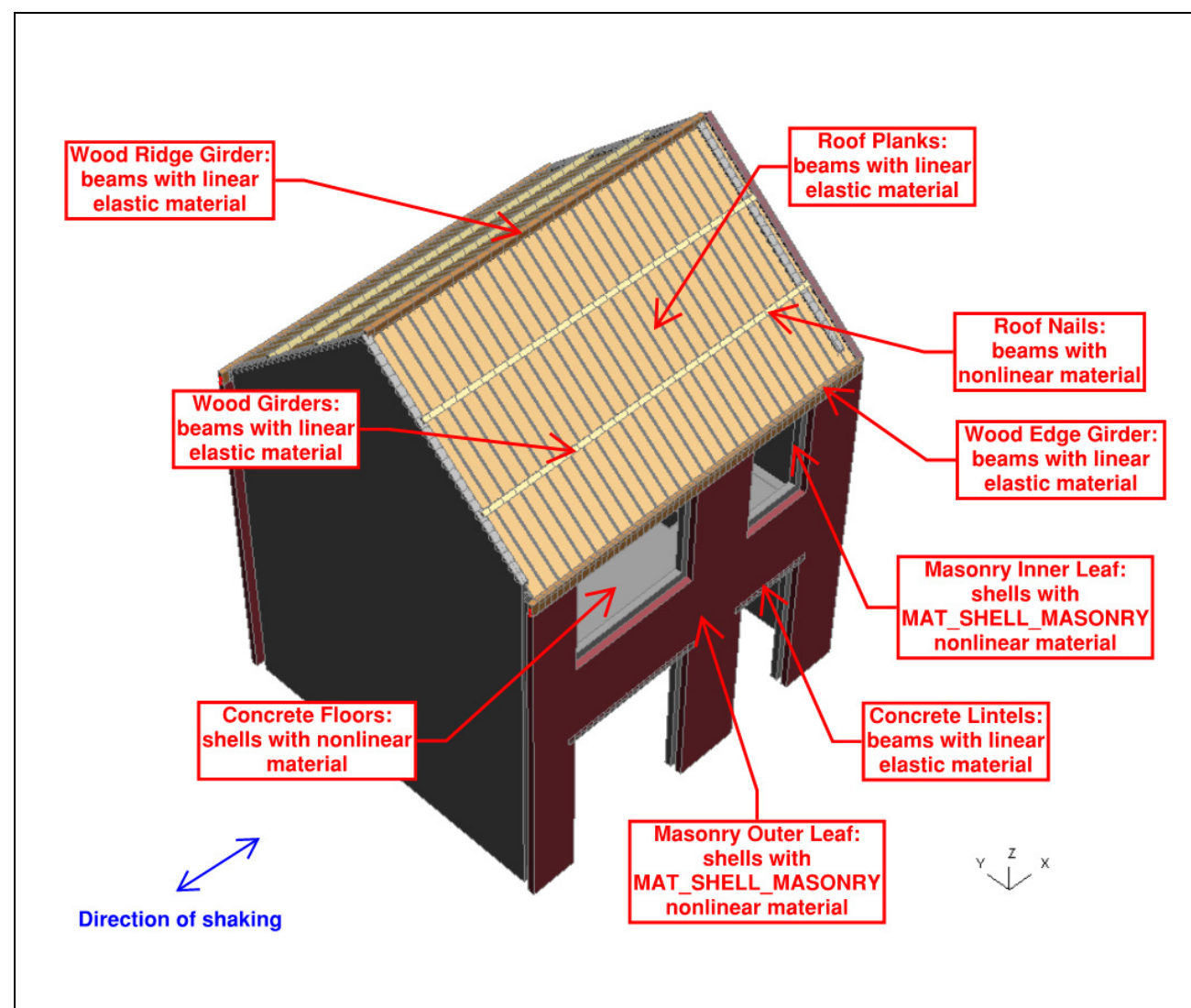


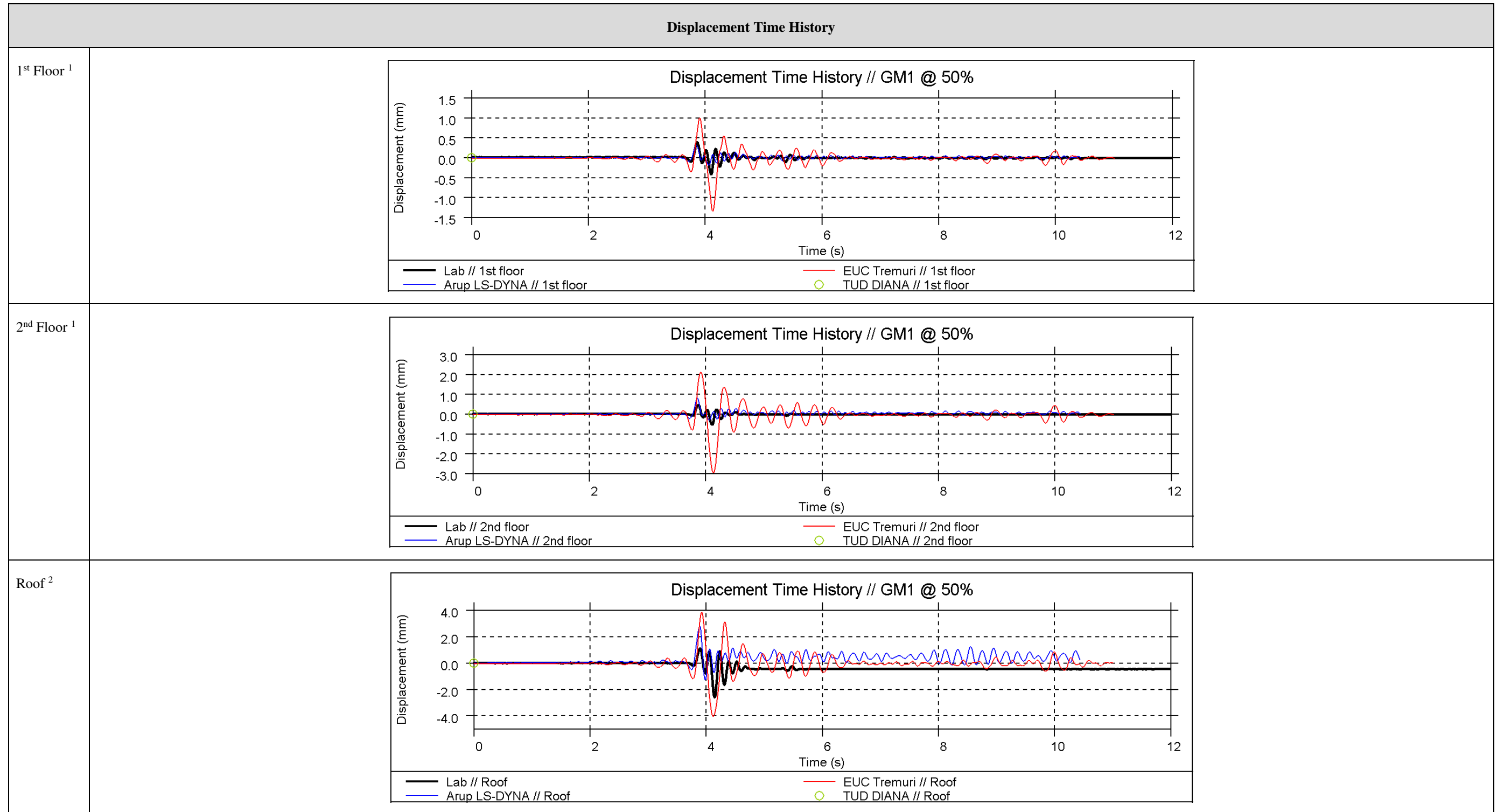
Figure 6: LS-DYNA shell model with annotations

### 2.1.3 TU-Delft

The DIANA finite element model of EUC-BUILD has been subjected to 3 separate analyses, namely EQ1-100%, EQ2-100% and EQ2-150%, with no accumulated damage, i.e. a separate analysis has been executed for each accelerogram and PGA level. Since in the fixed smeared crack approach the behavior is defined in terms of total stress vs total strains in fixed crack directions, a uniaxial tensile strength is needed for calcium silicate and clay brick masonry respectively. For each material, this value has been set equal to the average between the tensile strength associated to rocking (assumed equal to  $f_s$ ) and the one associated to the development of diagonal cracks in the middle of the panel (assumed equal to  $1.5 \cdot f_s$ ).

## 2.1.4 Summary of Results

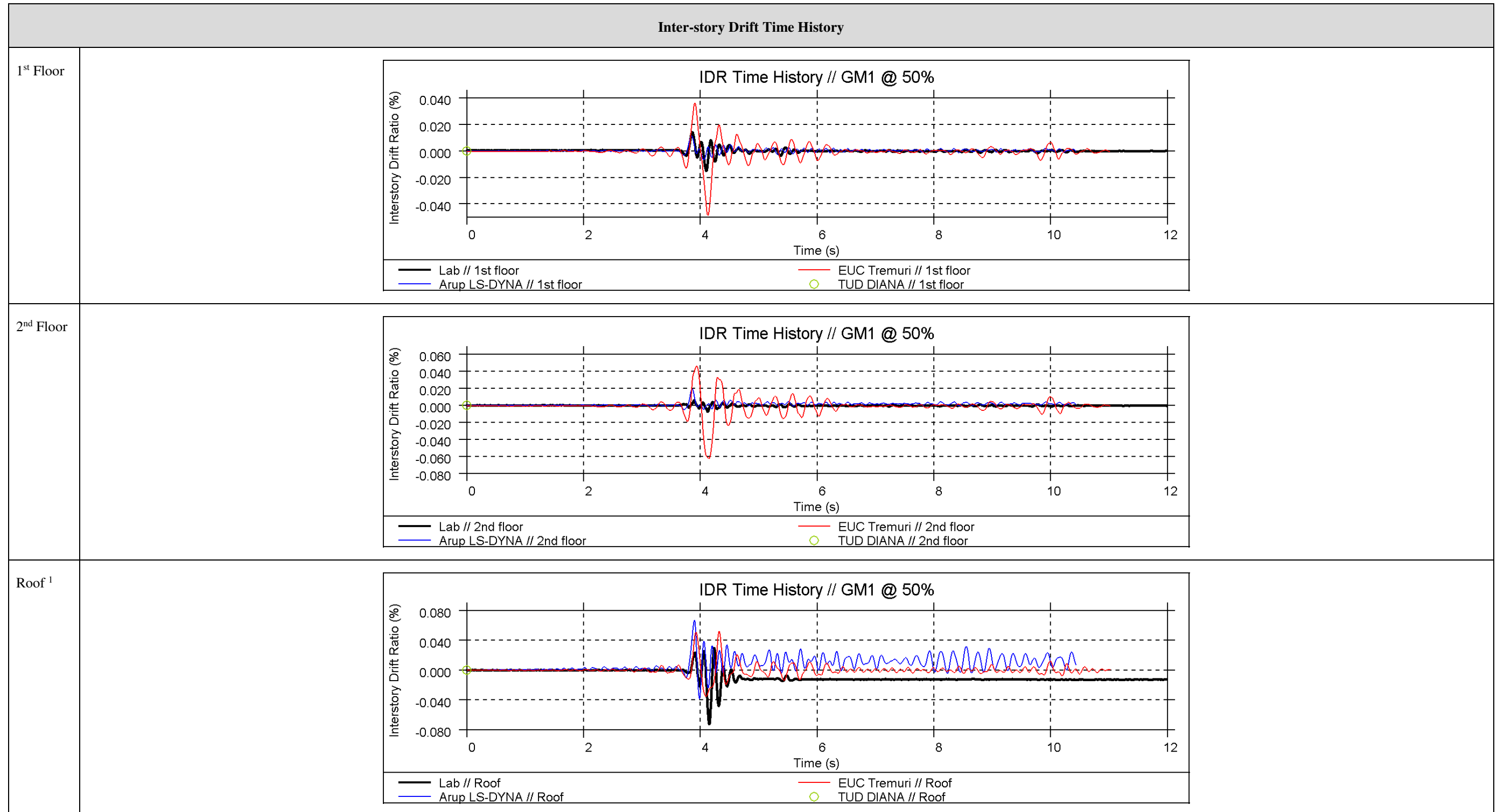
EQ1 at 50%



<sup>1</sup> Displacement of the 1<sup>st</sup> floor and 2<sup>nd</sup> floor is calculated as the average displacement measured at the four corners of the slab

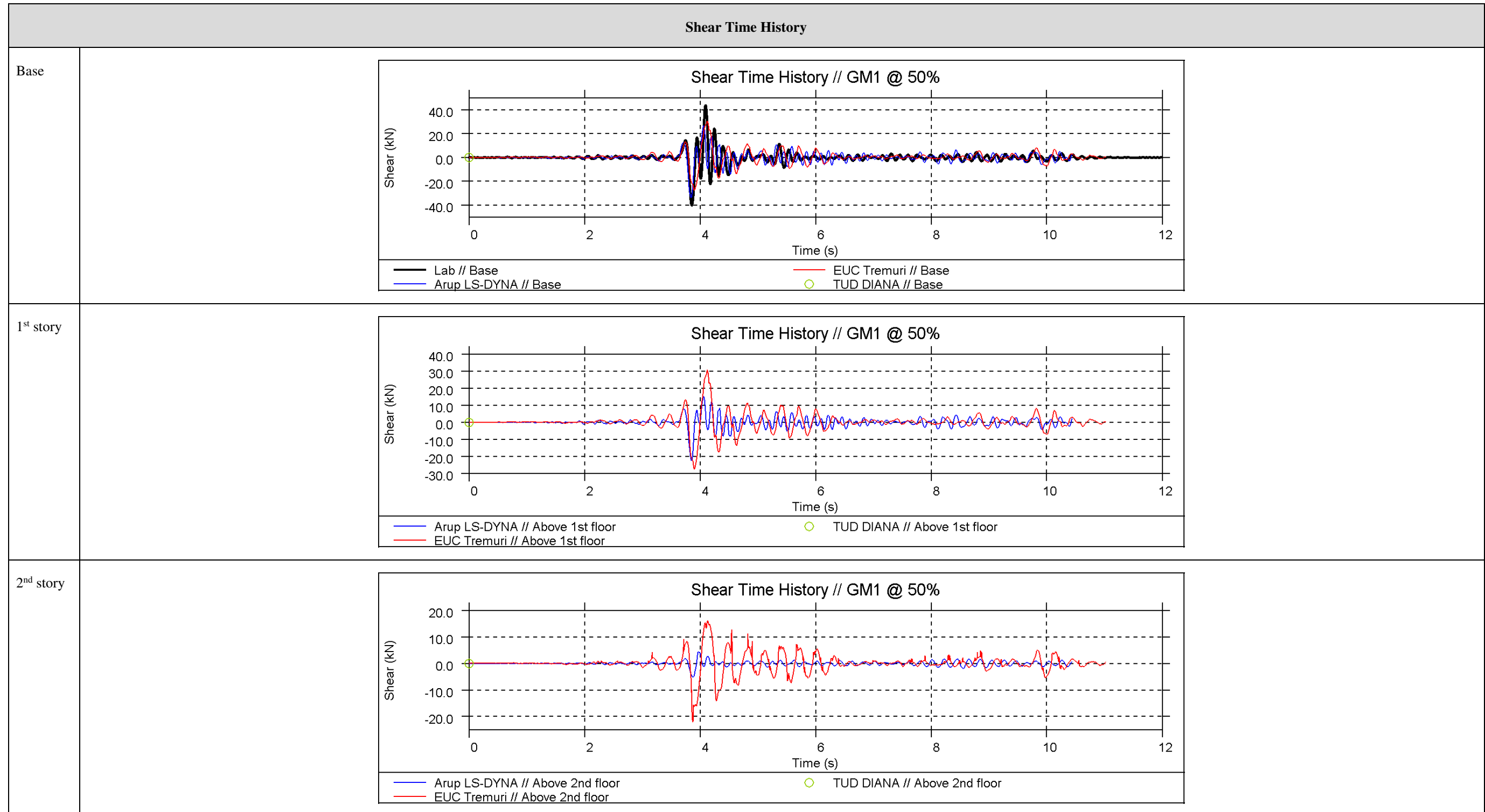
<sup>2</sup> Displacement of the roof is measured as the average displacement at the two ends of the ridge beam

EQ1 at 50%



<sup>1</sup> Roof drift is calculated using a diagonal length from the gable peak to the 2<sup>nd</sup> floor along the roof slope (3.5m)

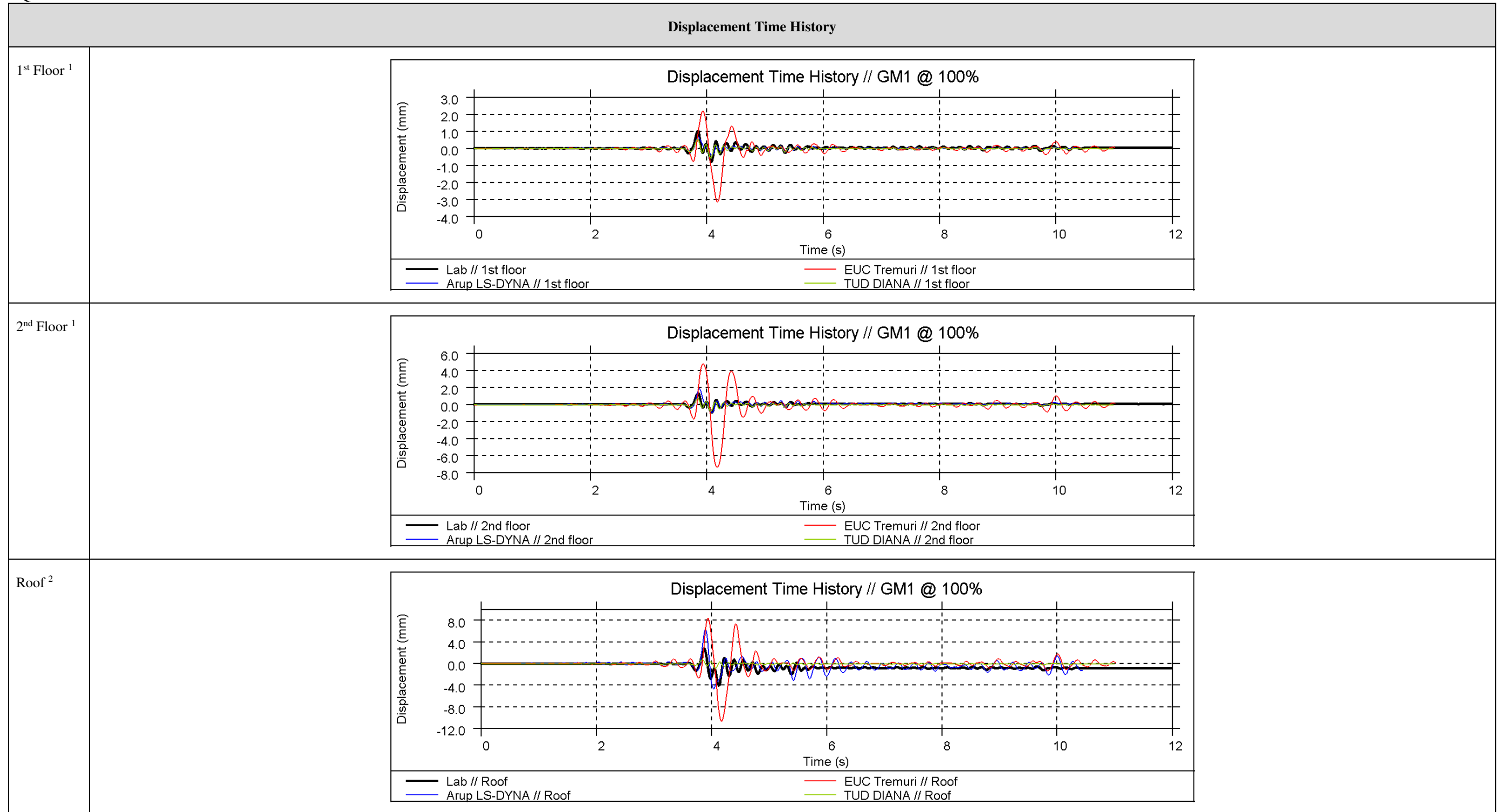
EQ1 at 50%



EQ1 at 50%

Global Hysteresis <sup>1</sup>	
<p>Global Hysteresis // GM1 @ 50%</p> <p>Shear (kN)</p> <p>Displacement (mm)</p> <p>— Lab      — Arup LS-DYNA</p>	<p>- Results not provided -</p>
<p>Arup</p>	<p>TU-Delft</p>
<p>Global Hysteresis // GM1 @ 50%</p> <p>Shear (kN)</p> <p>Displacement (mm)</p> <p>— Lab      — EUC Tremuri</p>	
<p>EUCENTRE</p>	<p><sup>1</sup> Base shear vs. 2<sup>nd</sup> floor displacement</p>

EQ1 at 100%

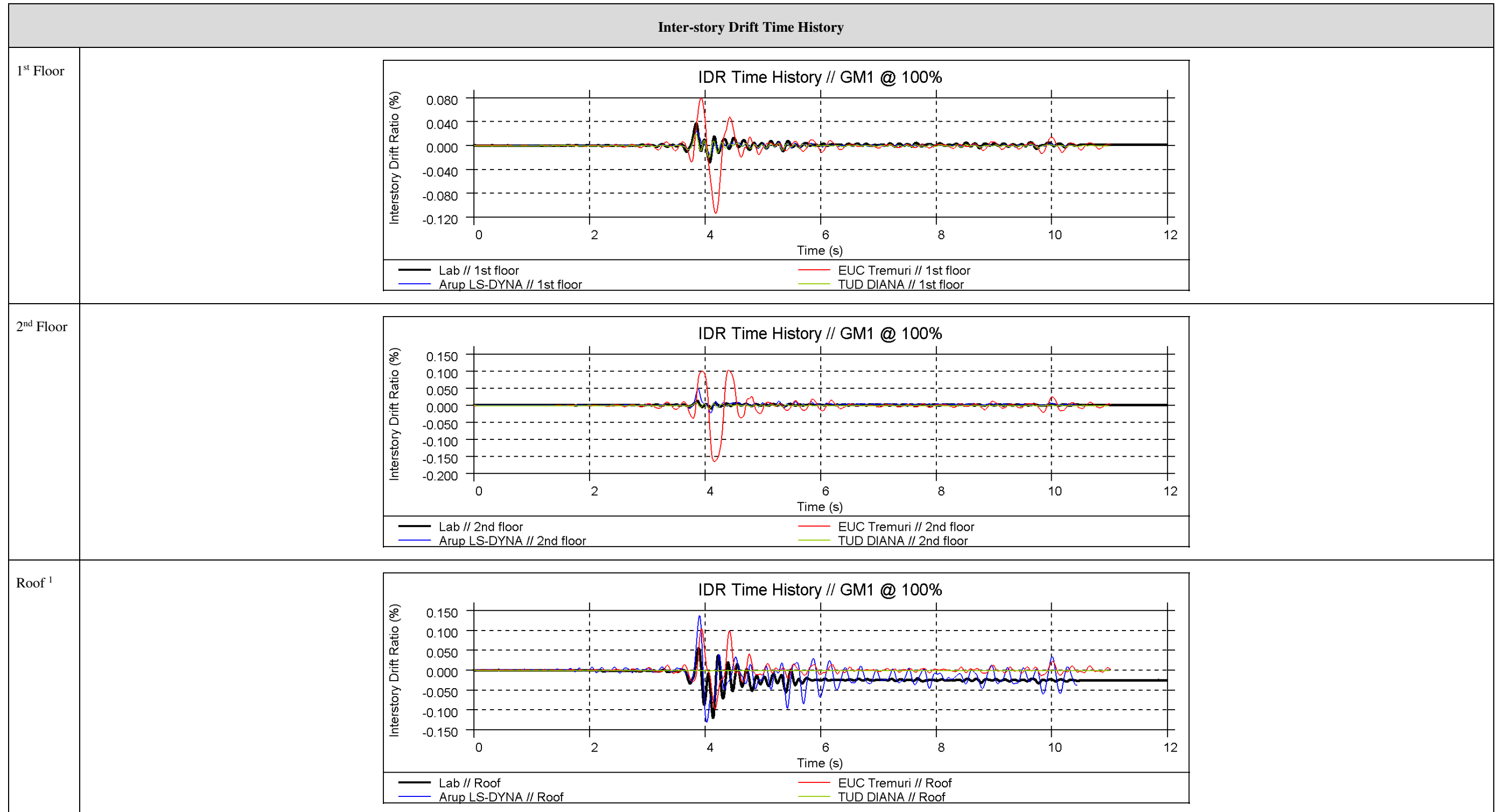


<sup>1</sup> Displacement of the 1<sup>st</sup> floor and 2<sup>nd</sup> floor is calculated as the average displacement measured at the four corners of the slab

<sup>2</sup> Displacement of the roof is measured as the average displacement at the two ends of the ridge beam

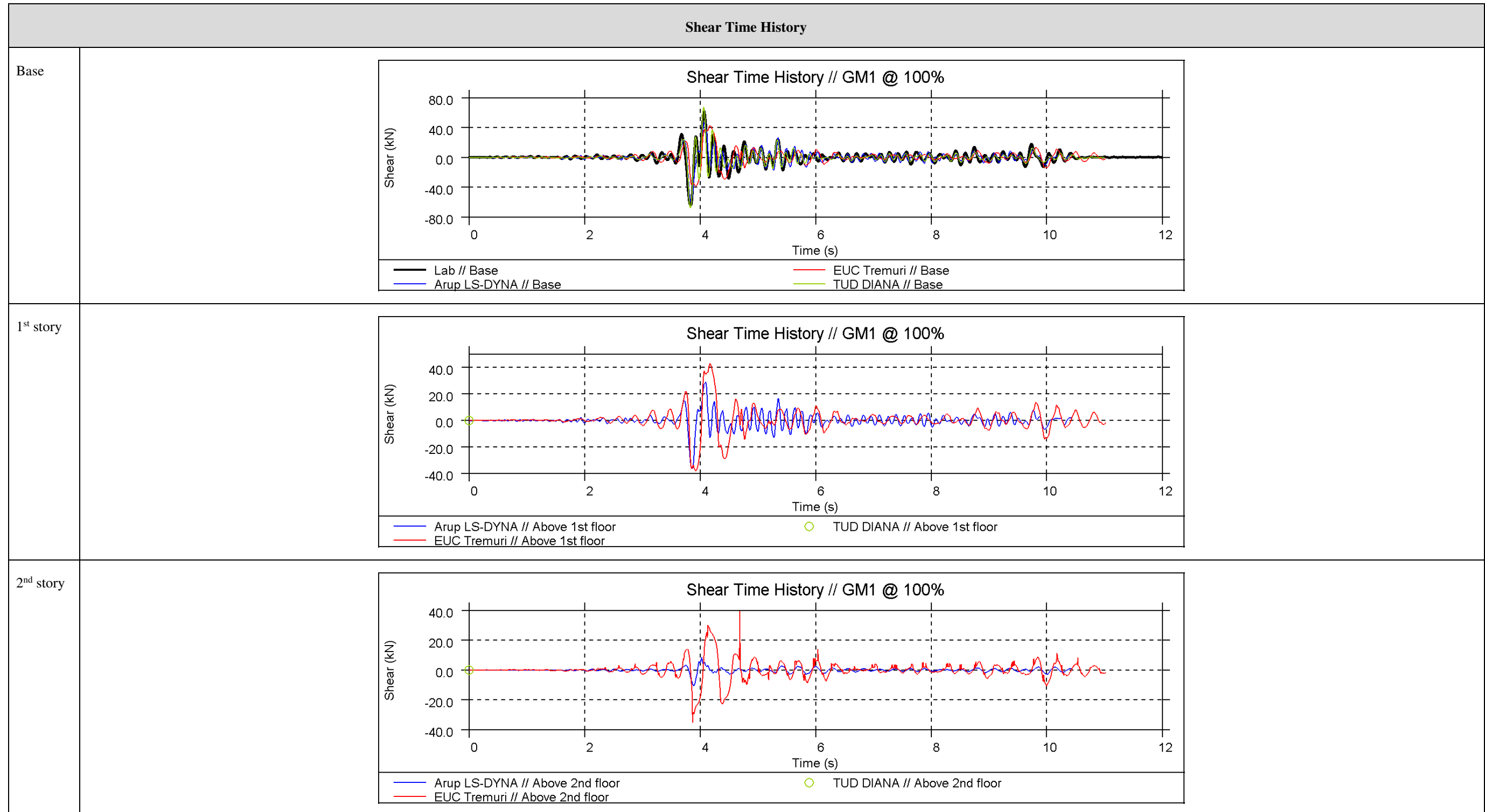


EQ1 at 100%



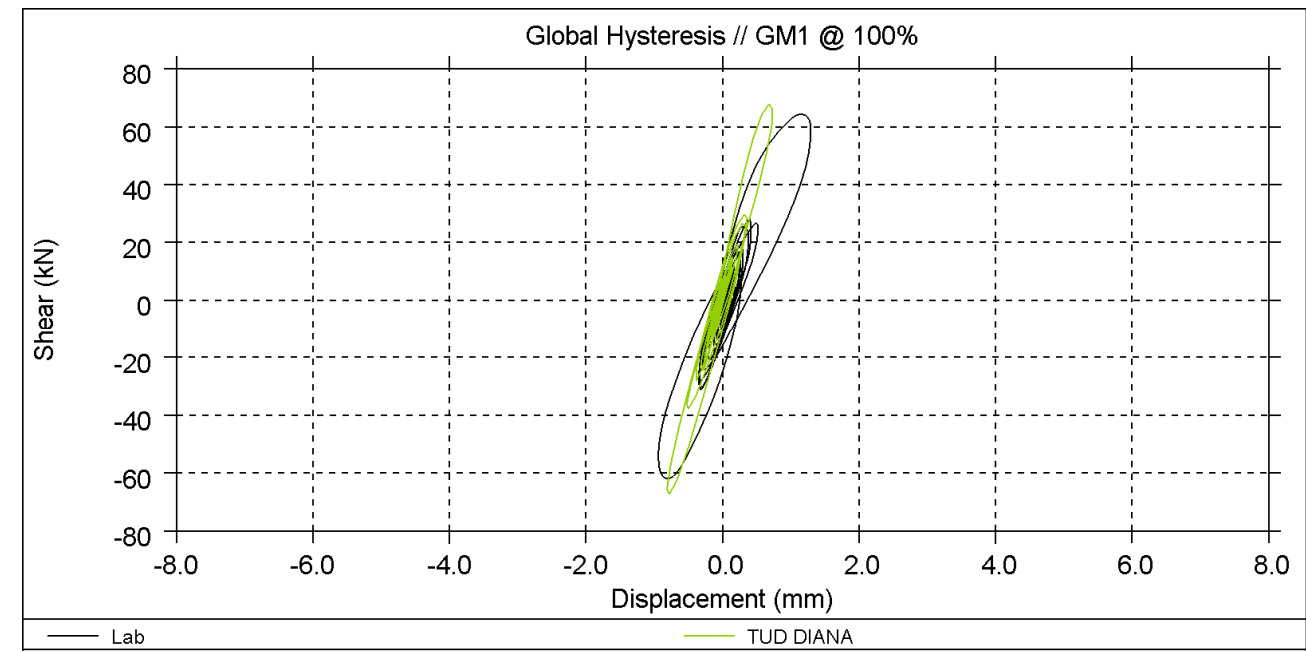
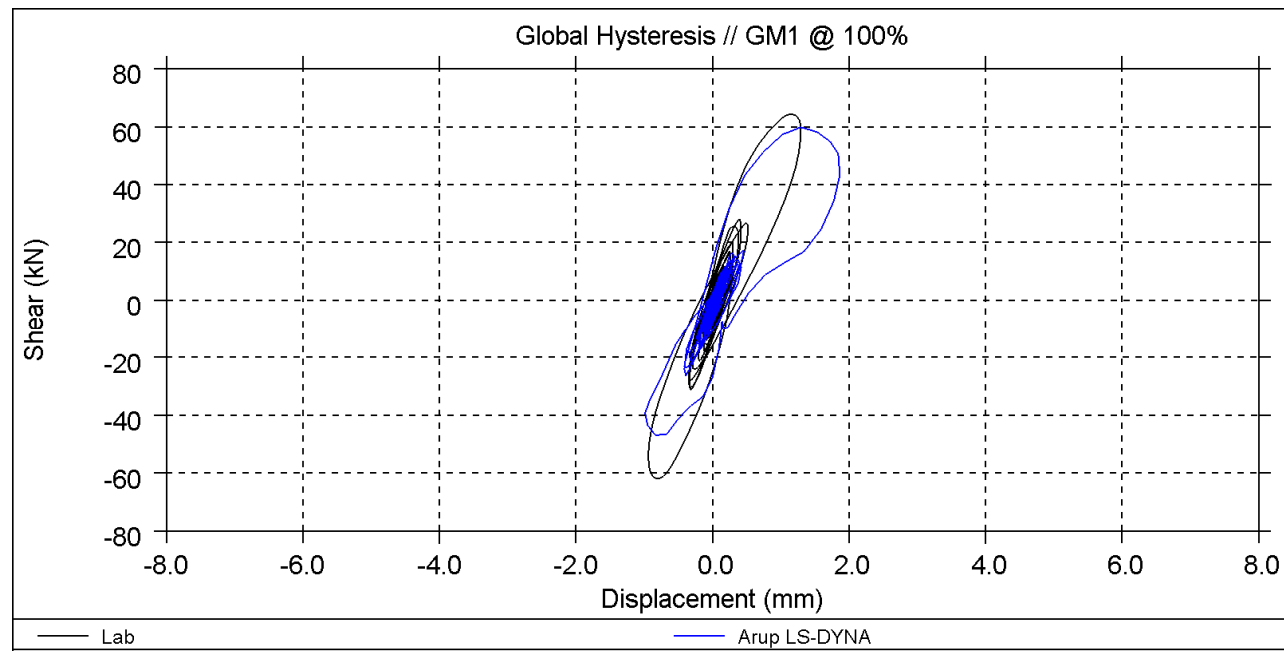
<sup>1</sup> Roof drift is calculated using a diagonal length from the gable peak to the 2<sup>nd</sup> floor along the roof slope (3.5m)

EQ1 at 100%



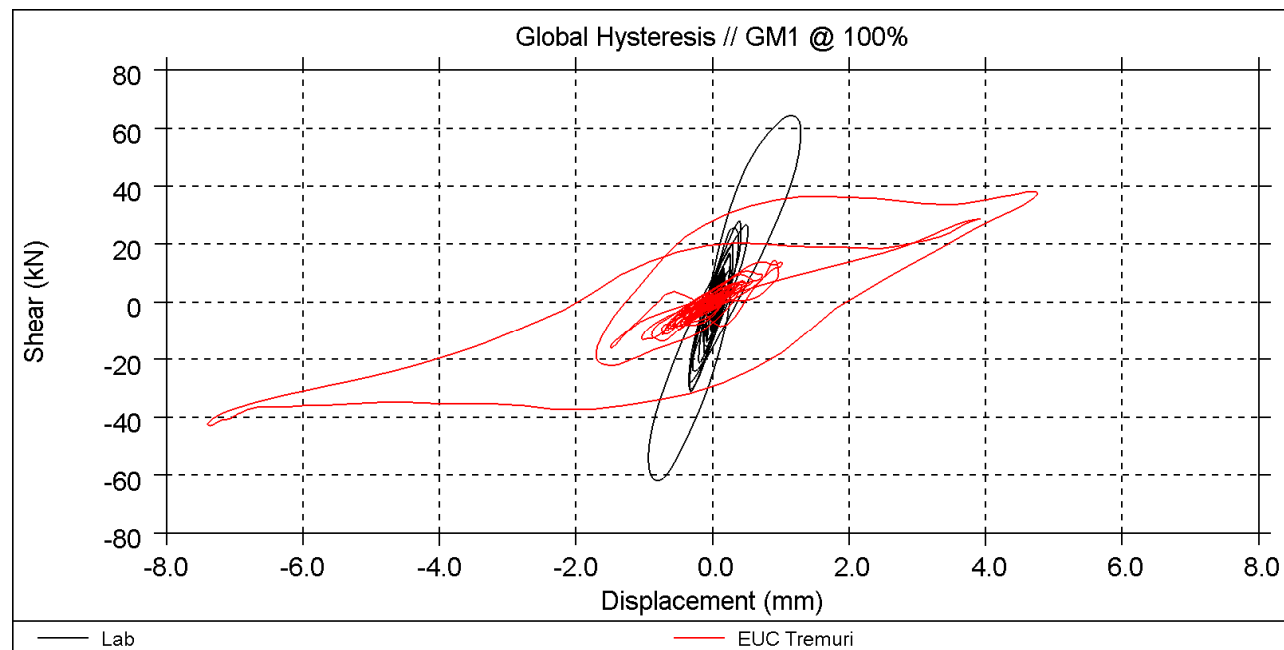
EQ1 at 100%

Global Hysteresis <sup>1</sup>



Arup

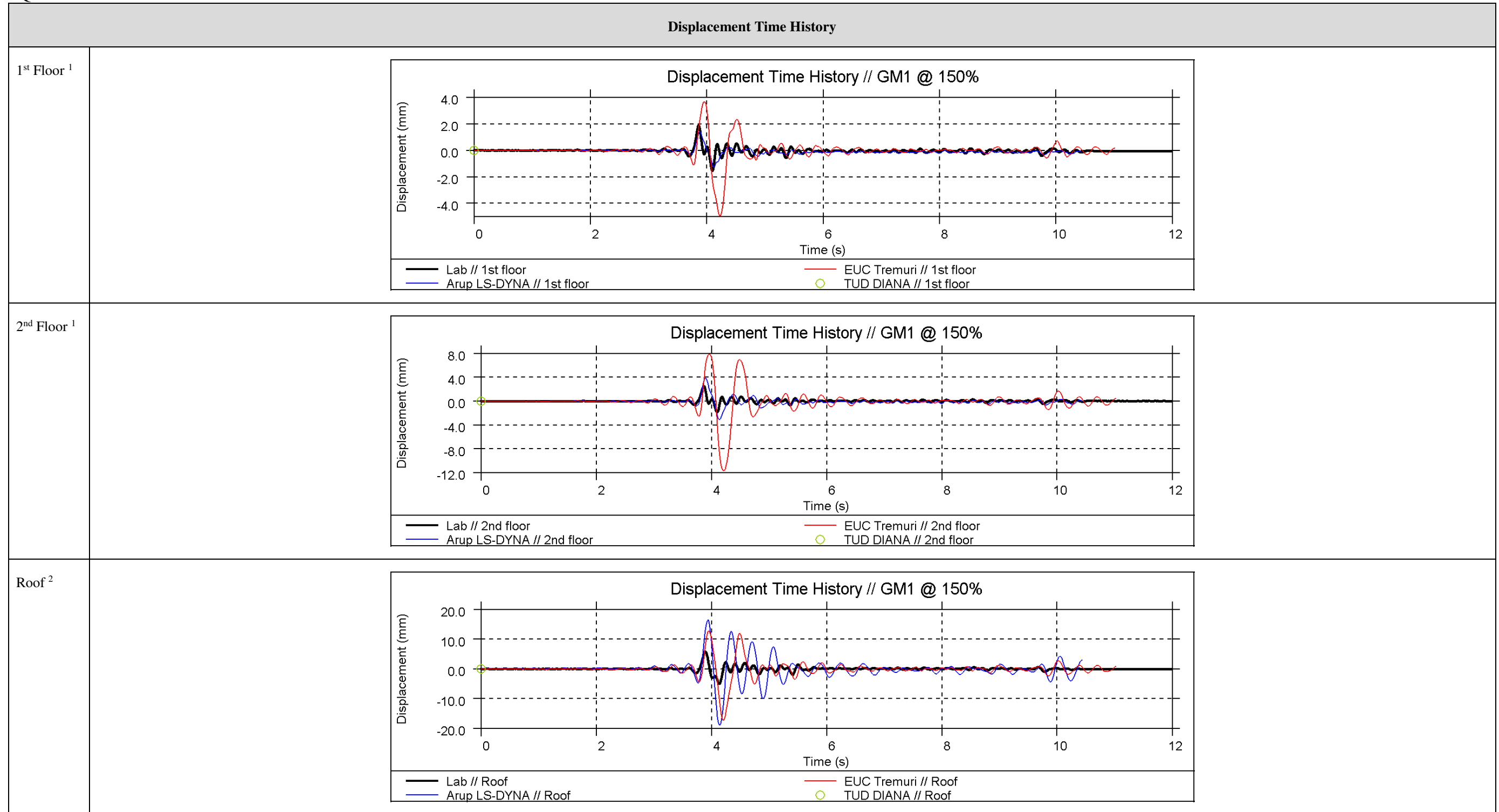
TU-Delft



EUCENTRE

<sup>1</sup> Base shear vs. 2<sup>nd</sup> floor displacement

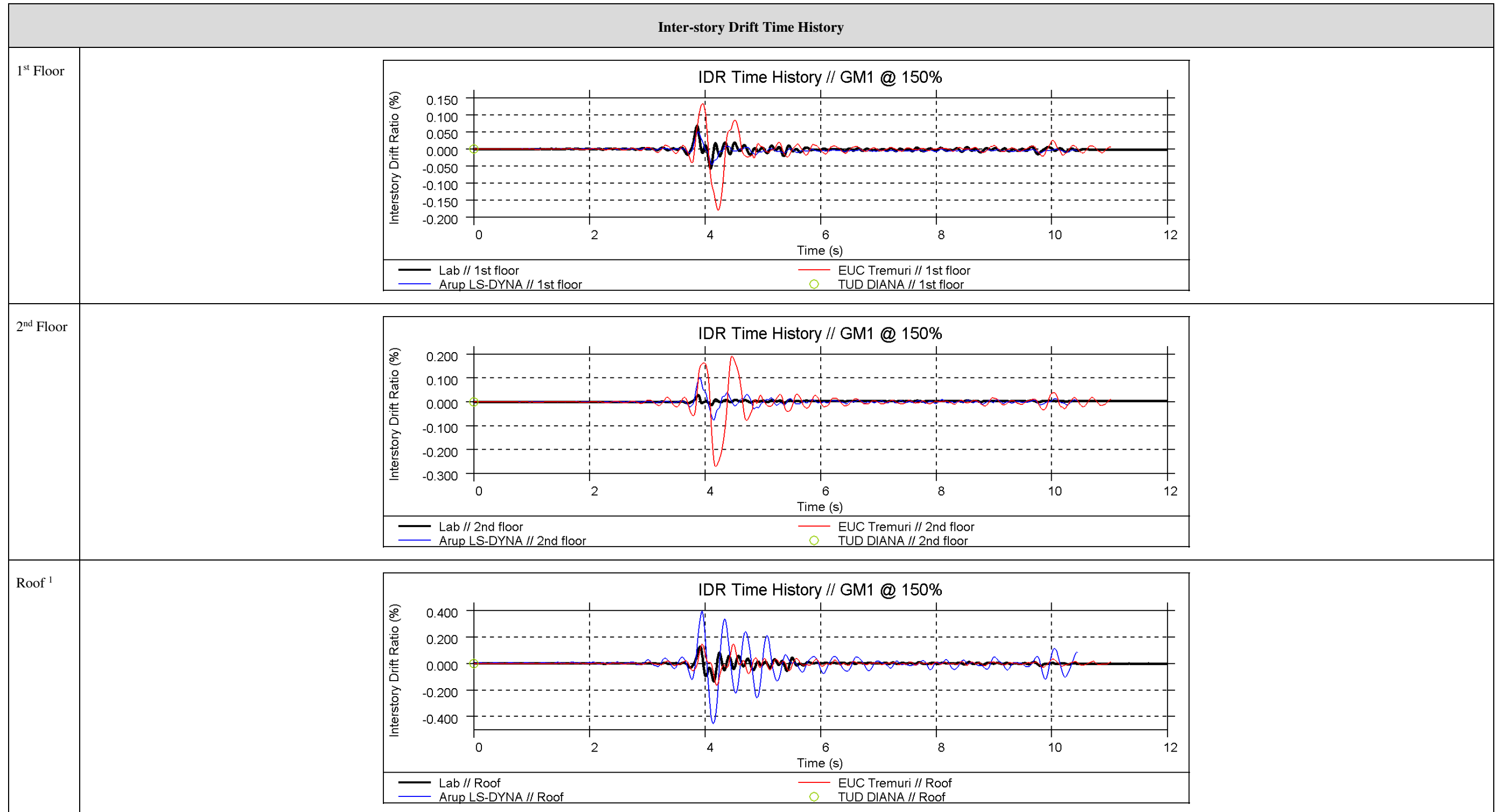
EQ1 at 150%



<sup>1</sup> Displacement of the 1<sup>st</sup> floor and 2<sup>nd</sup> floor is calculated as the average displacement measured at the four corners of the slab

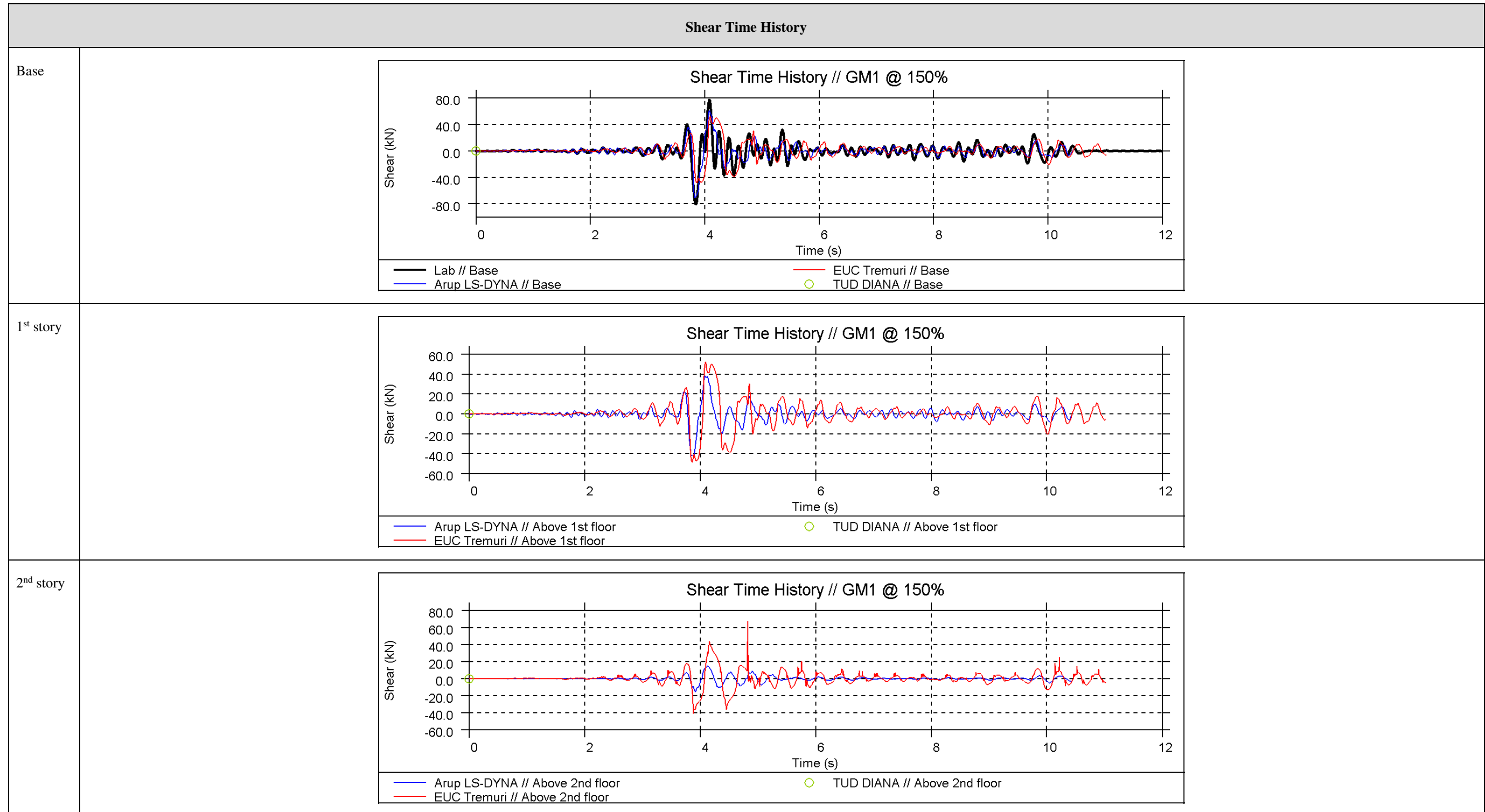
<sup>2</sup> Displacement of the roof is measured as the average displacement at the two ends of the ridge beam

EQ1 at 150%



<sup>1</sup> Roof drift is calculated using a diagonal length from the gable peak to the 2<sup>nd</sup> floor along the roof slope (3.5m)

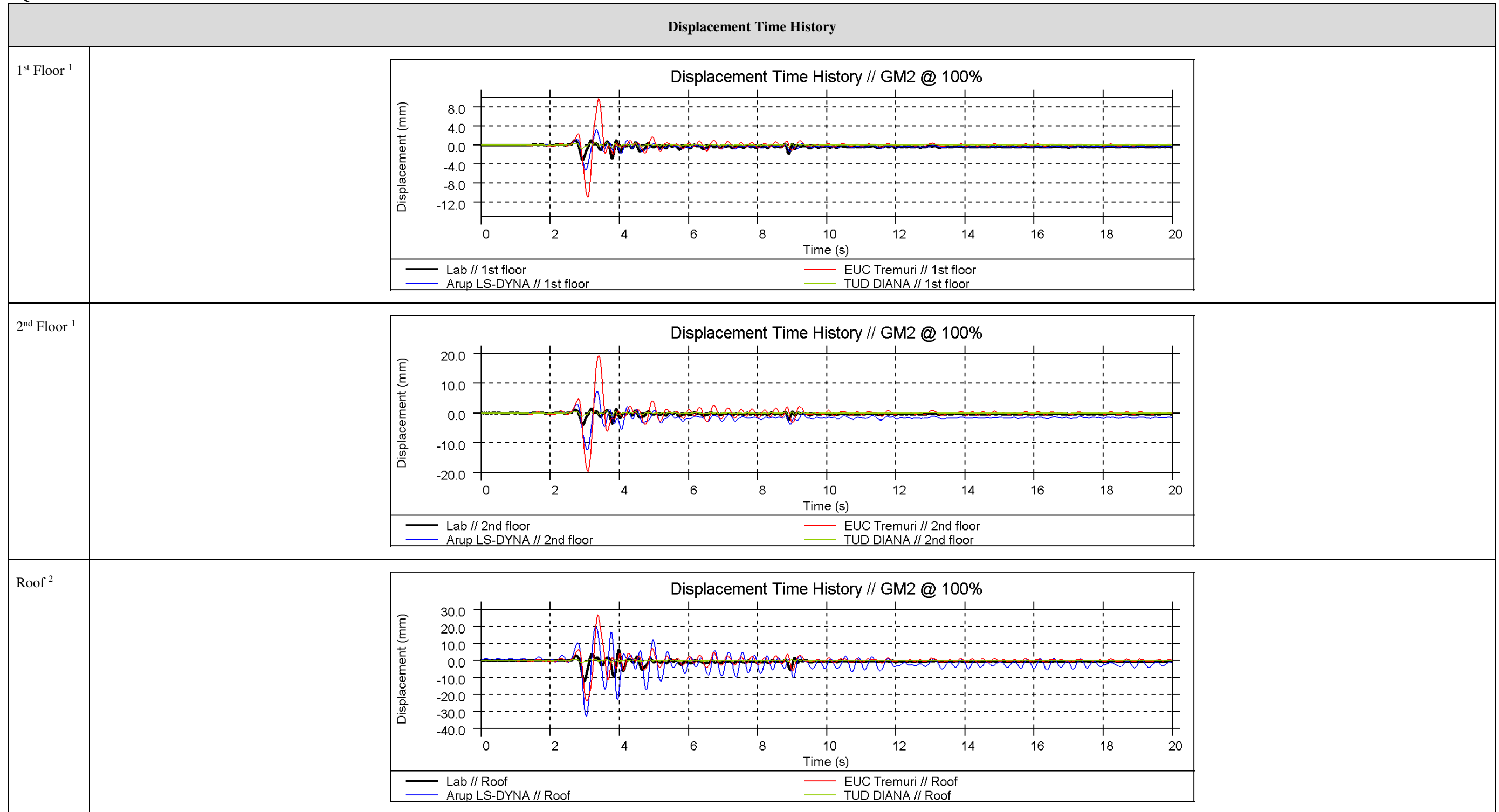
EQ1 at 150%



EQ1 at 150%

Global Hysteresis <sup>1</sup>	
<p>Global Hysteresis // GM1 @ 150%</p> <p>Shear (kN)</p> <p>Displacement (mm)</p> <p>— Lab      — Arup LS-DYNA</p>	<p>- Results not provided -</p>
<p>Arup</p>	<p>TU-Delft</p>
<p>Global Hysteresis // GM1 @ 150%</p> <p>Shear (kN)</p> <p>Displacement (mm)</p> <p>— Lab      — EUC Tremuri</p>	
<p>EUCENTRE</p>	<p><sup>1</sup> Base shear vs. 2<sup>nd</sup> floor displacement</p>

EQ2 at 100%

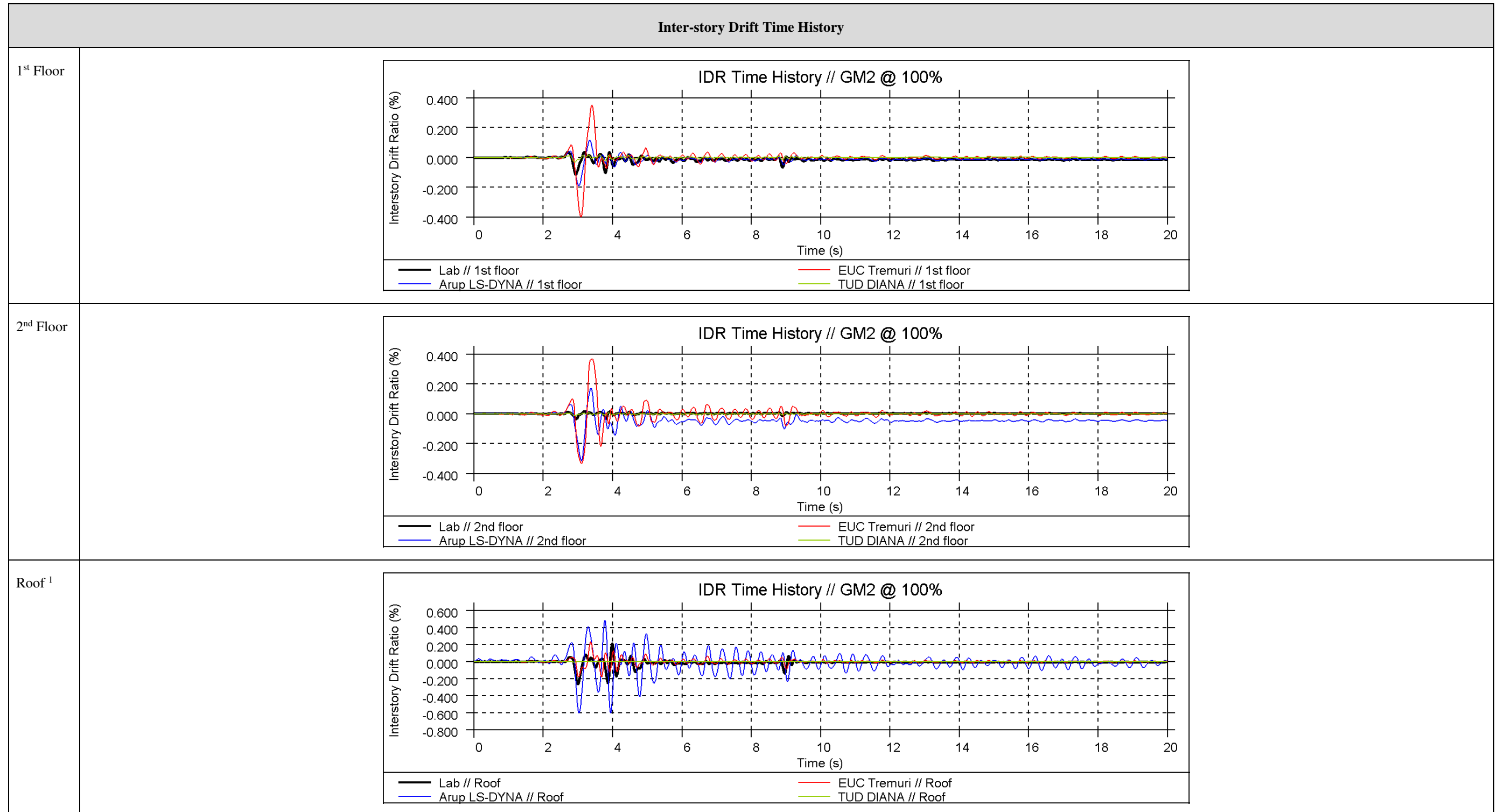


<sup>1</sup> Displacement of the 1<sup>st</sup> floor and 2<sup>nd</sup> floor is calculated as the average displacement measured at the four corners of the slab

<sup>2</sup> Displacement of the roof is measured as the average displacement at the two ends of the ridge beam

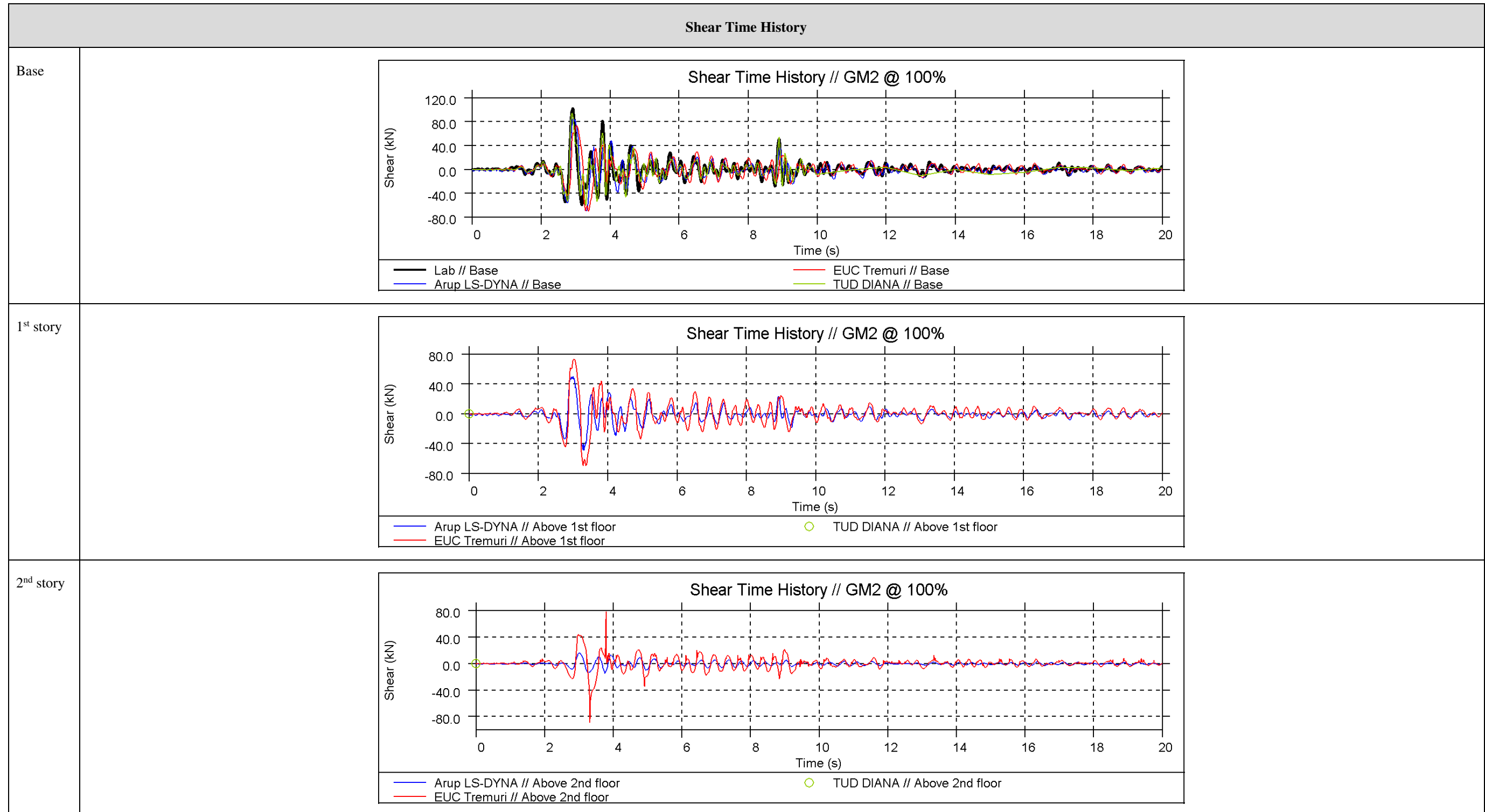


EQ2 at 100%



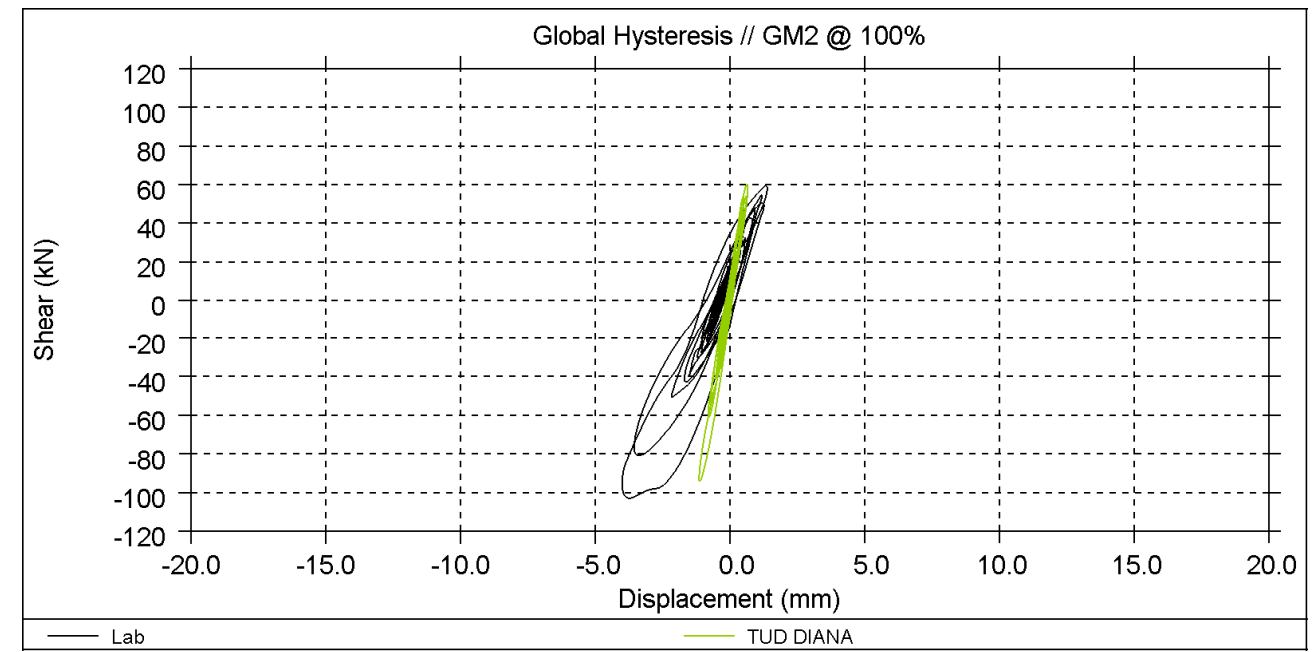
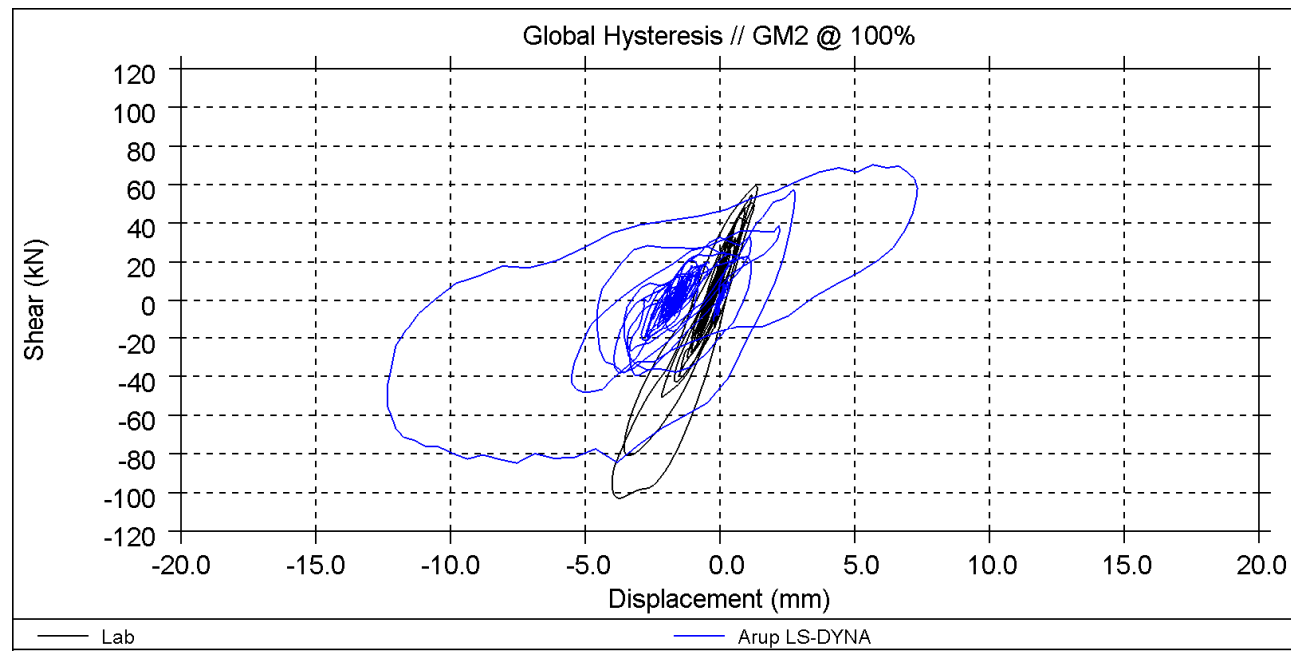
<sup>1</sup> Roof drift is calculated using a diagonal length from the gable peak to the 2<sup>nd</sup> floor along the roof slope (3.5m)

EQ2 at 100%



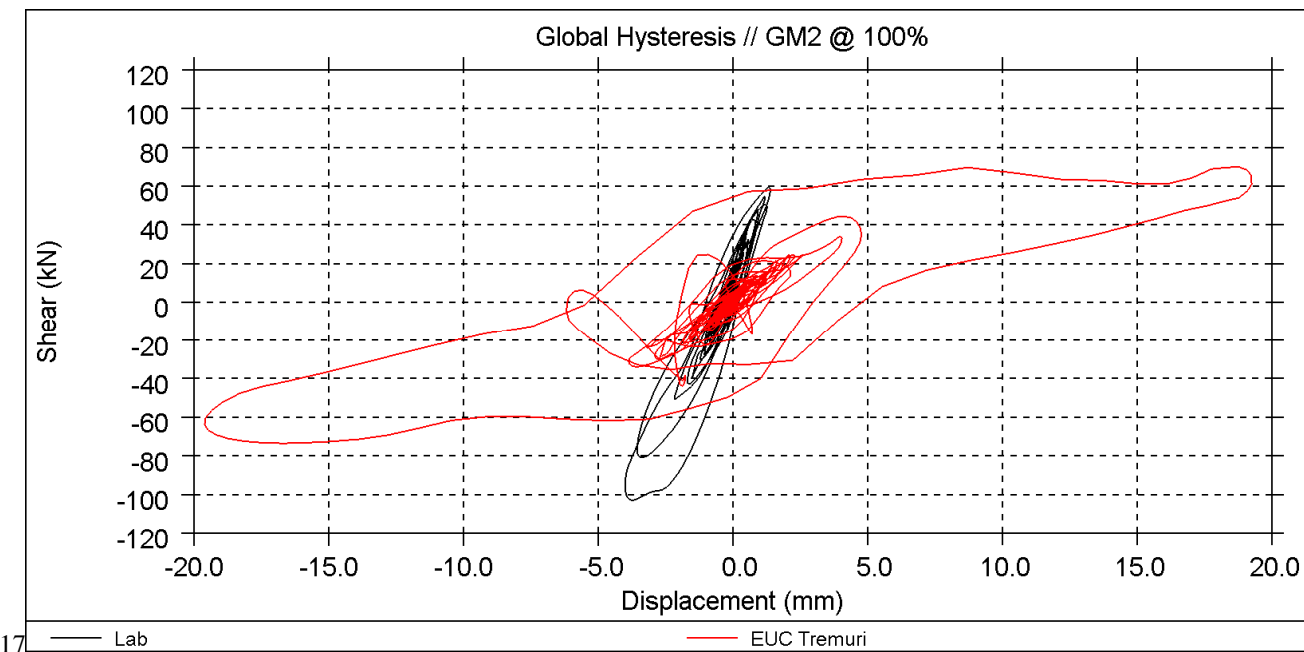
EQ2 at 100%

Global Hysteresis <sup>1</sup>



Arup

TU-Delft



17

EUCENTRE

<sup>1</sup> Base shear vs. 2<sup>nd</sup> floor displacement

EQ2 at 100%

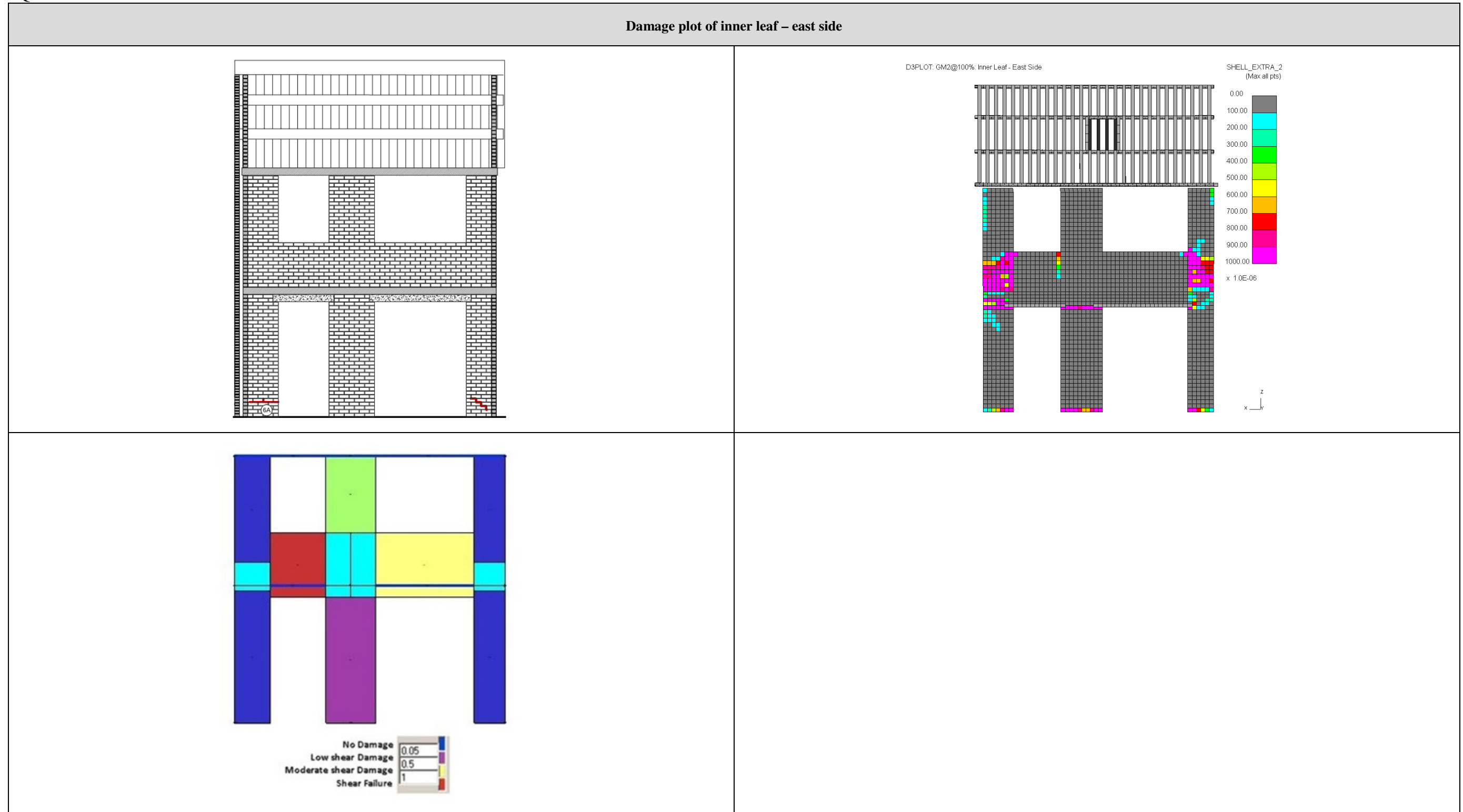


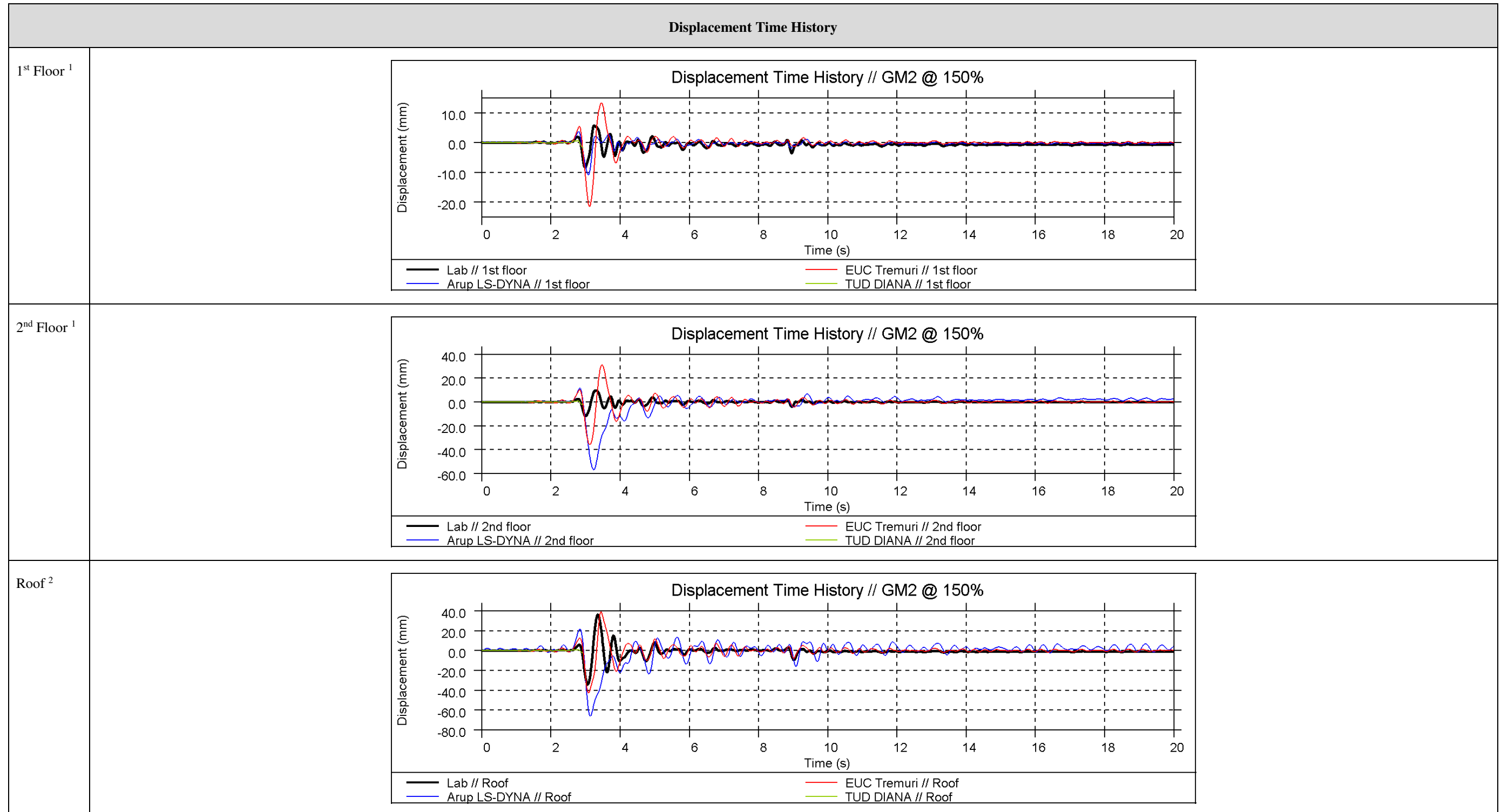
Figure 7: Damage plot of inner leaf - east side of test result (top left), Arup LS-DYNA (top right), and EUCENTRE (bottom left)

EQ2 at 100%



Figure 8: Damage plot of inner leaf - west side of test result (top left), Arup LS-DYNA (top right), and EUCENTRE (bottom left)

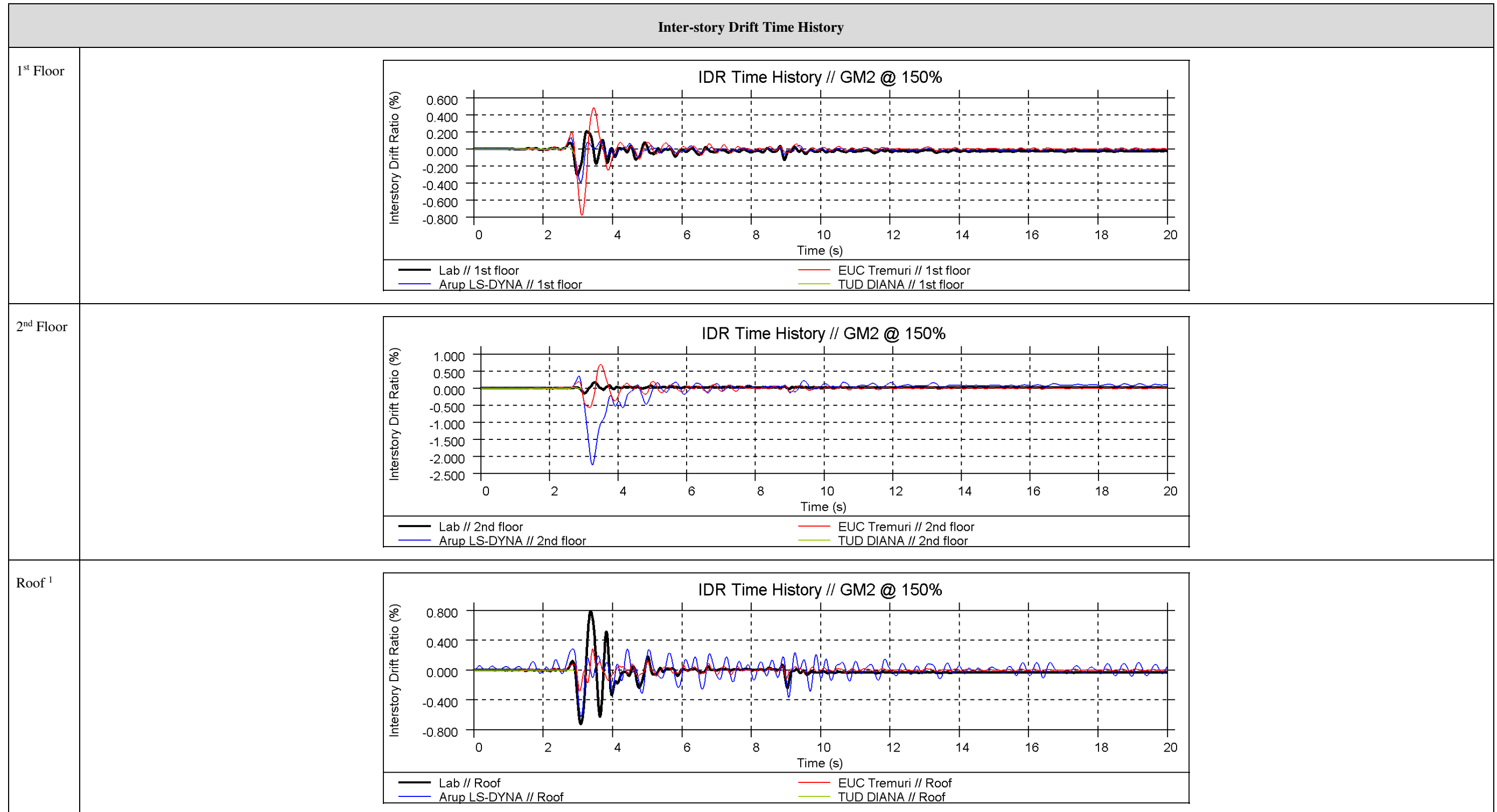
EQ2 at 150%



<sup>1</sup> Displacement of the 1<sup>st</sup> floor and 2<sup>nd</sup> floor is calculated as the average displacement measured at the four corners of the slab

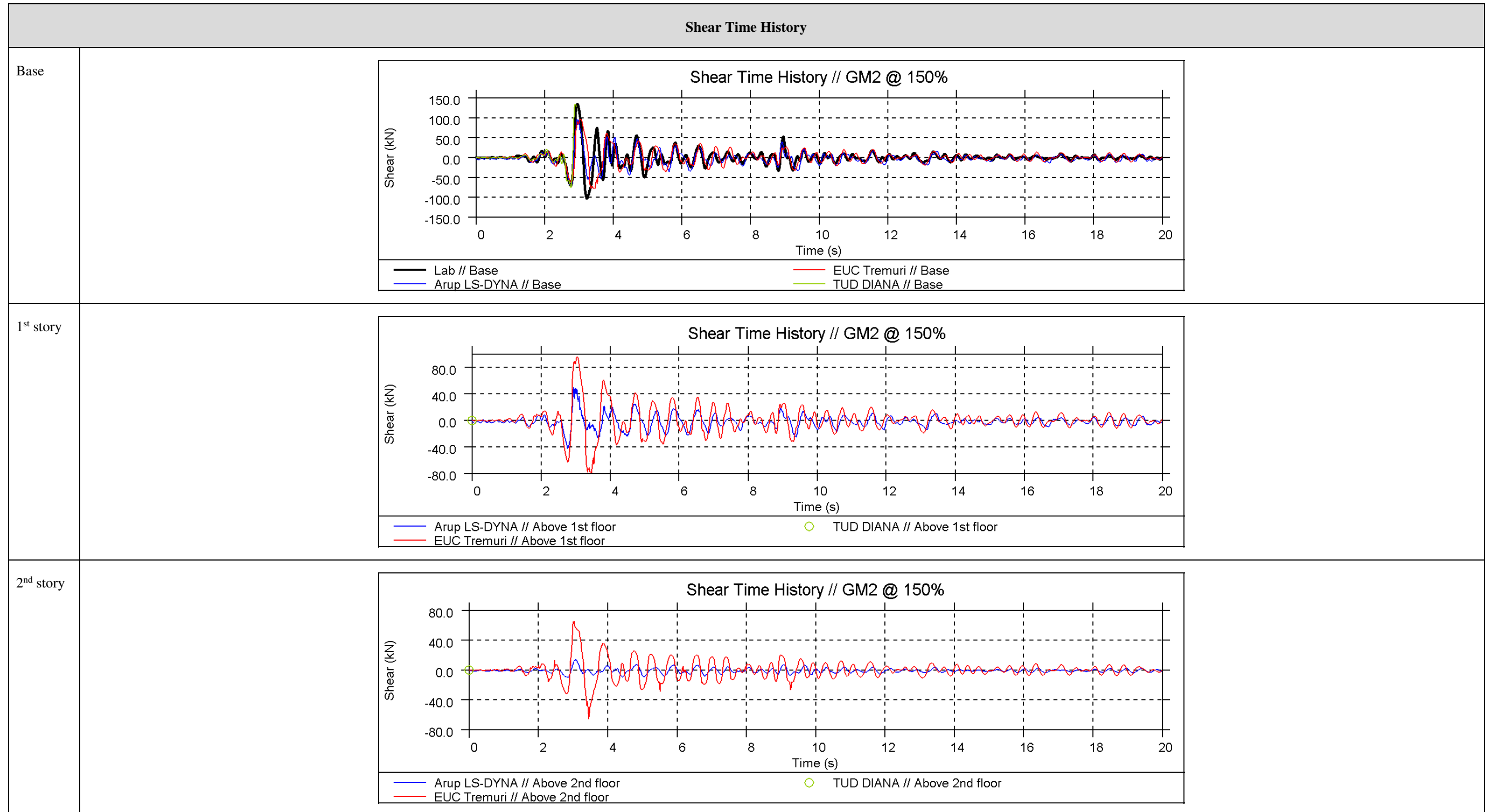
<sup>2</sup> Displacement of the roof is measured as the average displacement at the two ends of the ridge beam

EQ2 at 150%



<sup>1</sup> Roof drift is calculated using a diagonal length from the gable peak to the 2<sup>nd</sup> floor along the roof slope (3.5m)

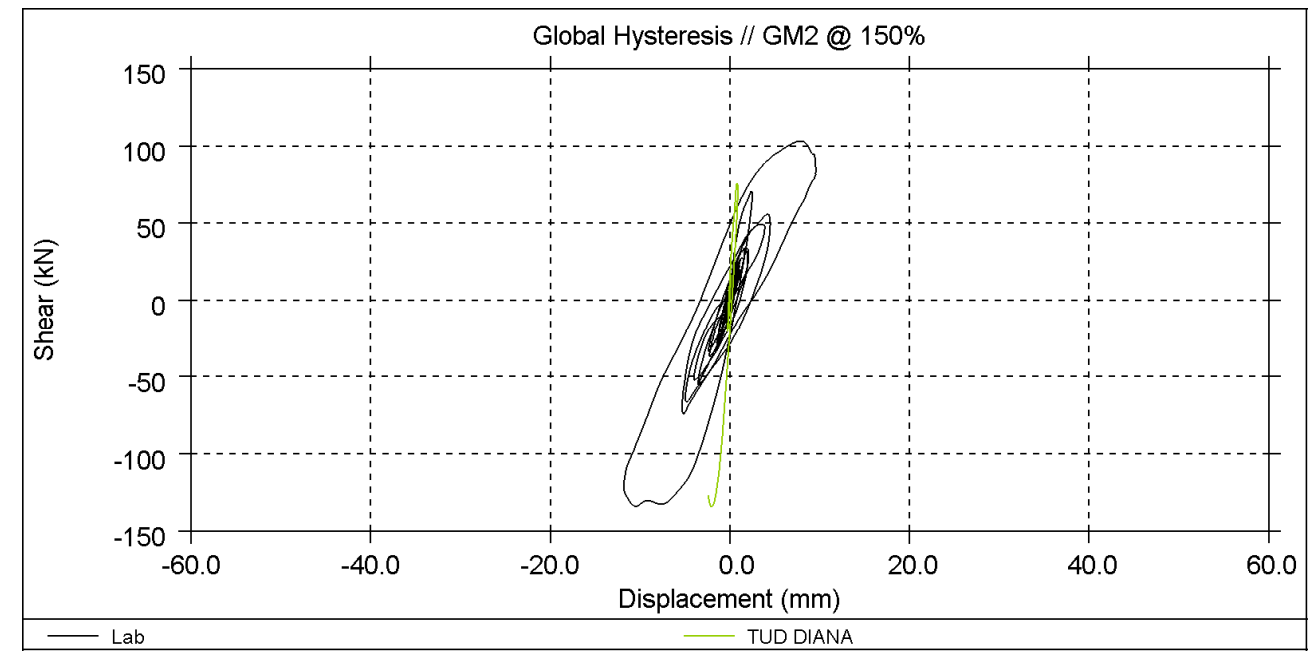
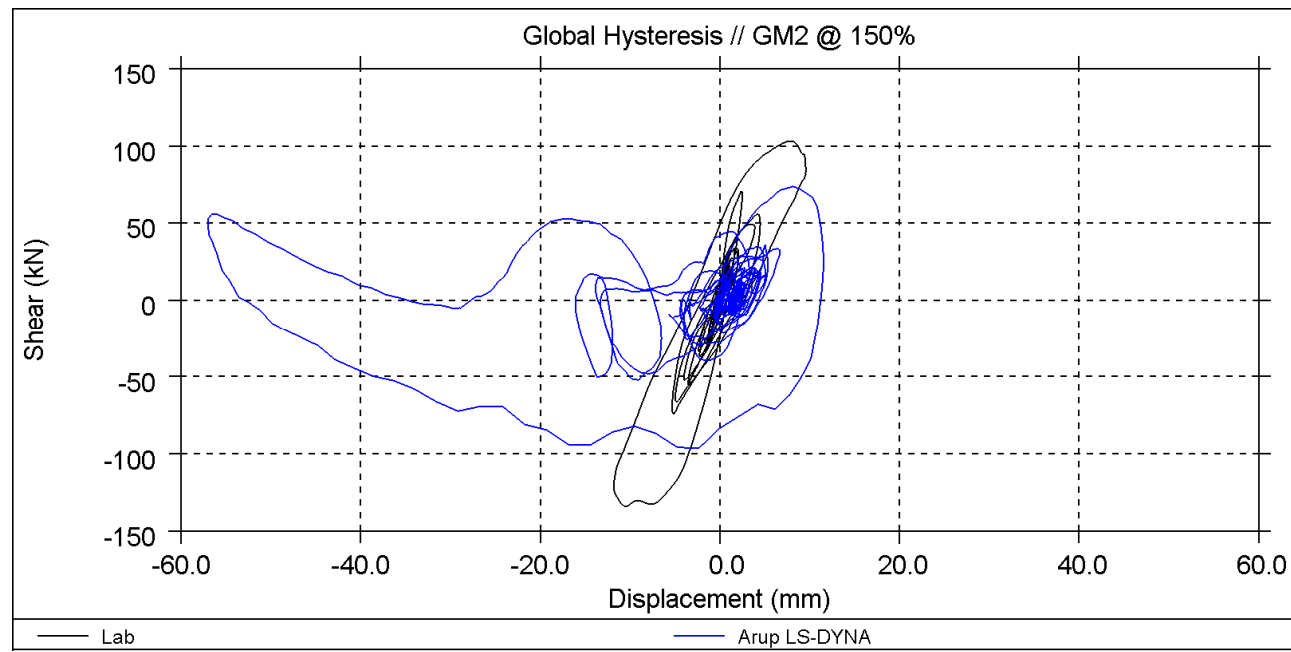
EQ2 at 150%





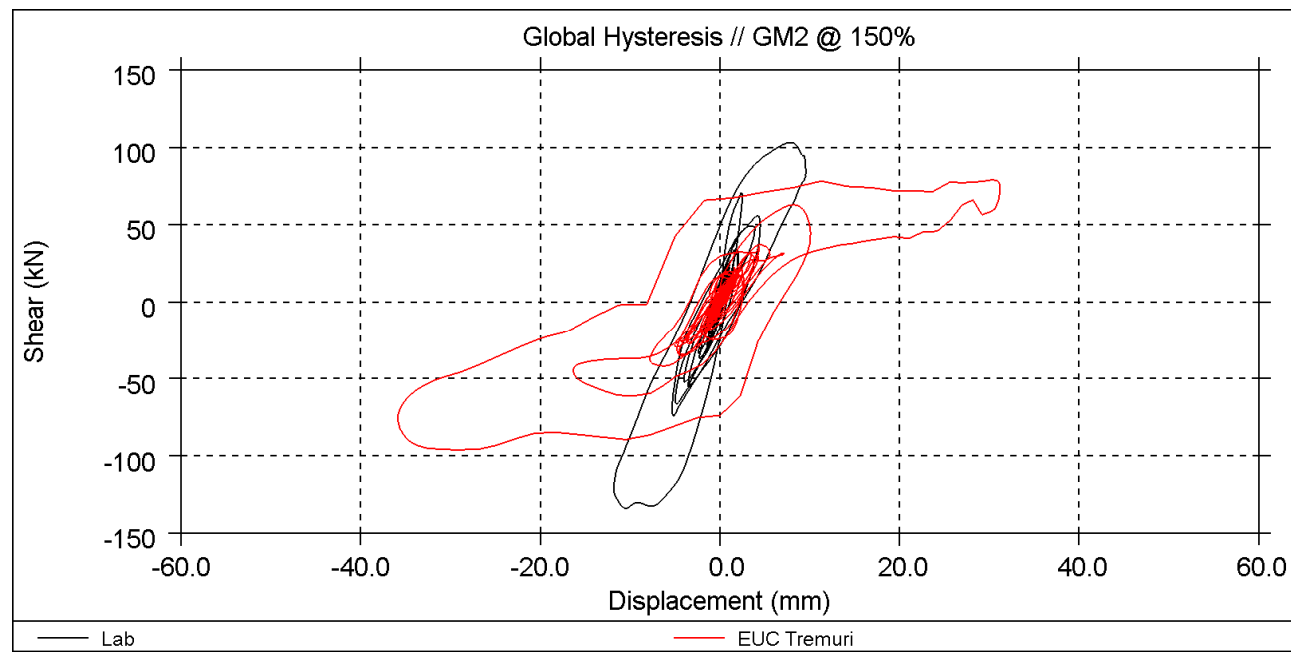
EQ2 at 150%

Global Hysteresis <sup>1</sup>



Arup

TU-Delft



EUCENTRE

<sup>1</sup> Base shear vs. 2<sup>nd</sup> floor displacement

EQ2 at 150%

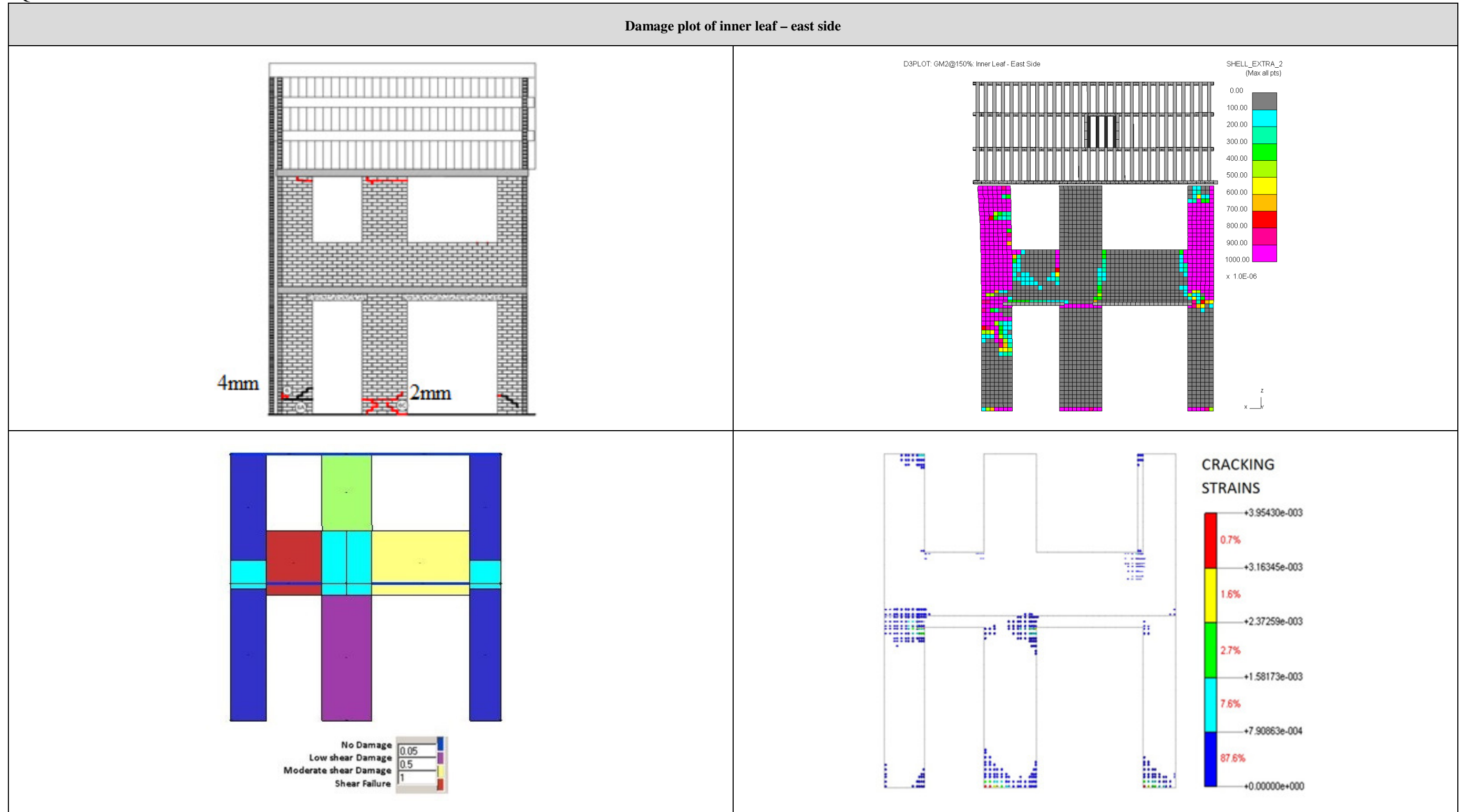


Figure 9: Damage plot of inner leaf - east side of test result (top left), Arup LS-DYNA (top right), EUCENTRE (bottom left), and TU-Delft (bottom right)

EQ2 at 150%

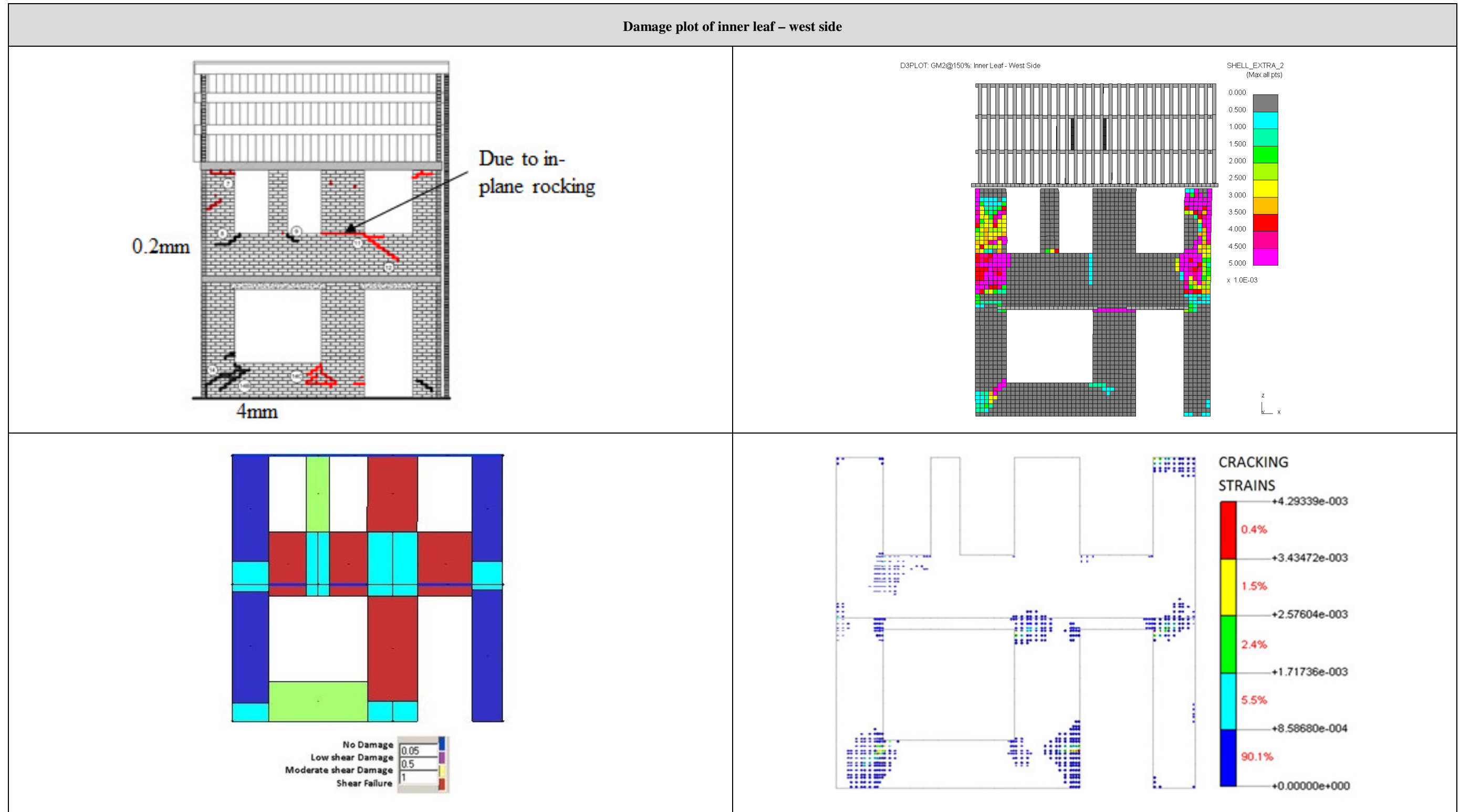
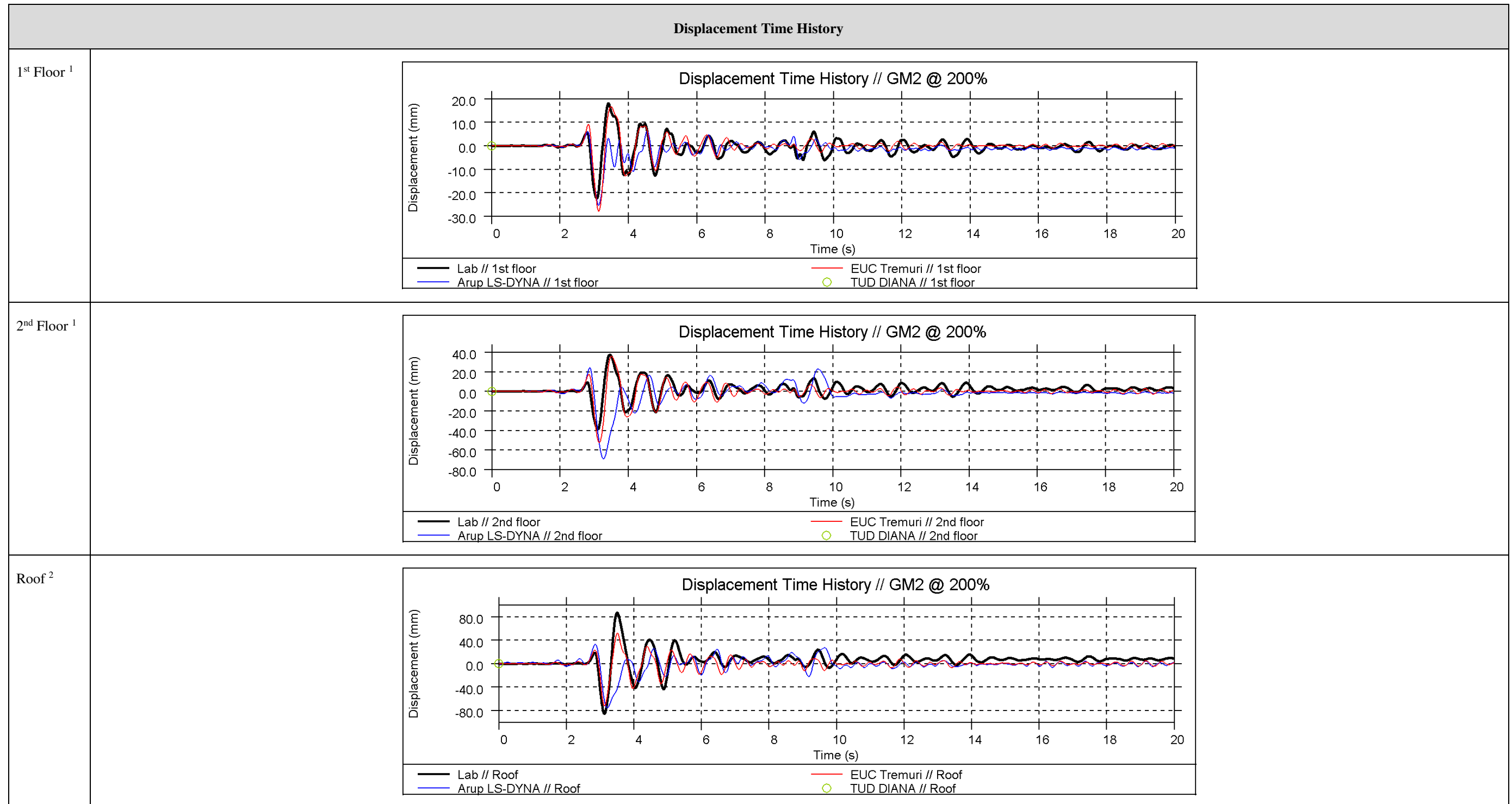


Figure 10: Damage plot of inner leaf - west side of test result (top left), Arup LS-DYNA (top right), EUCENTRE (bottom left), and TU-Delft (bottom right)

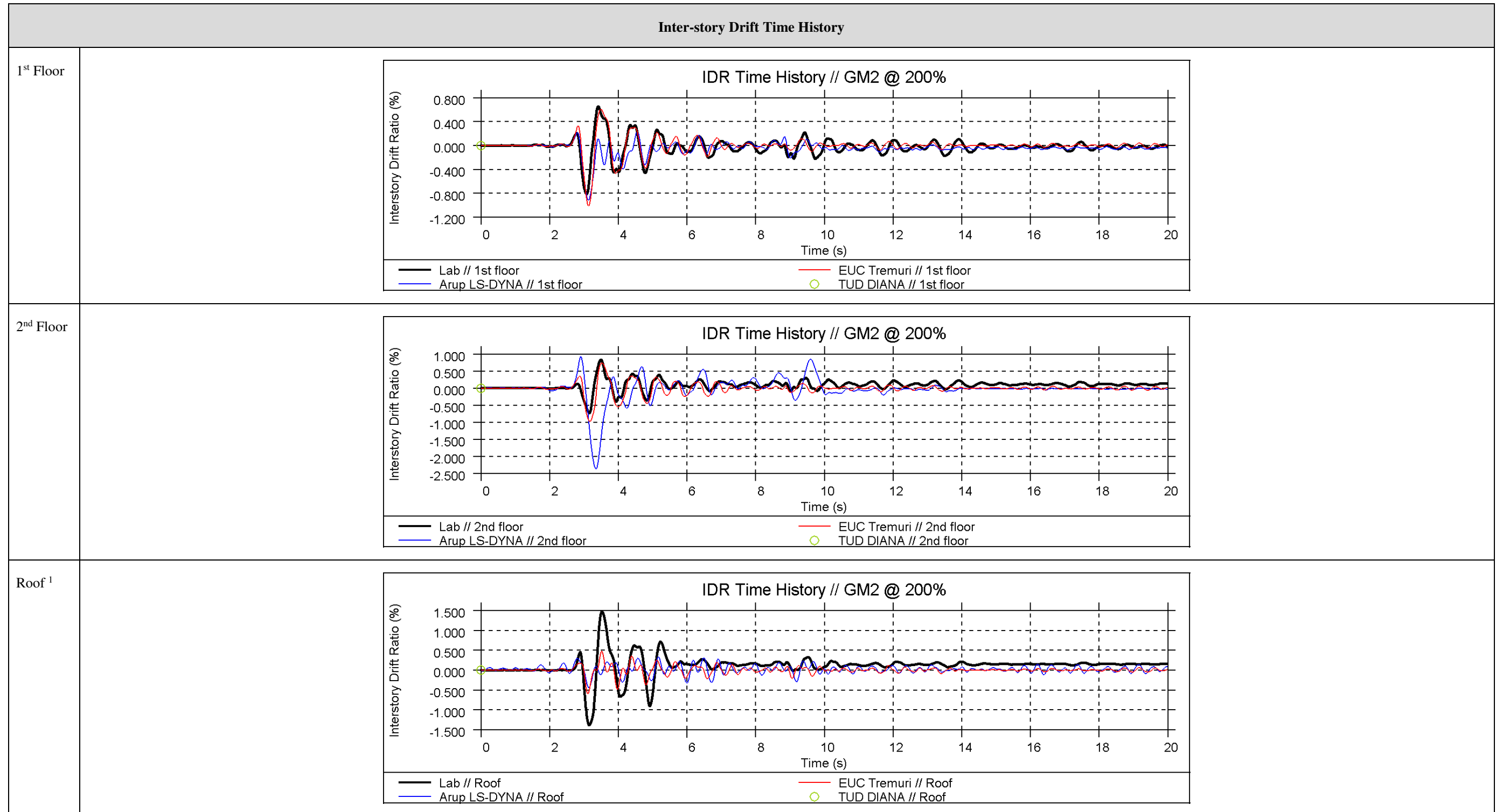
EQ2 at 200%



<sup>1</sup> Displacement of the 1<sup>st</sup> floor and 2<sup>nd</sup> floor is calculated as the average displacement measured at the four corners of the slab

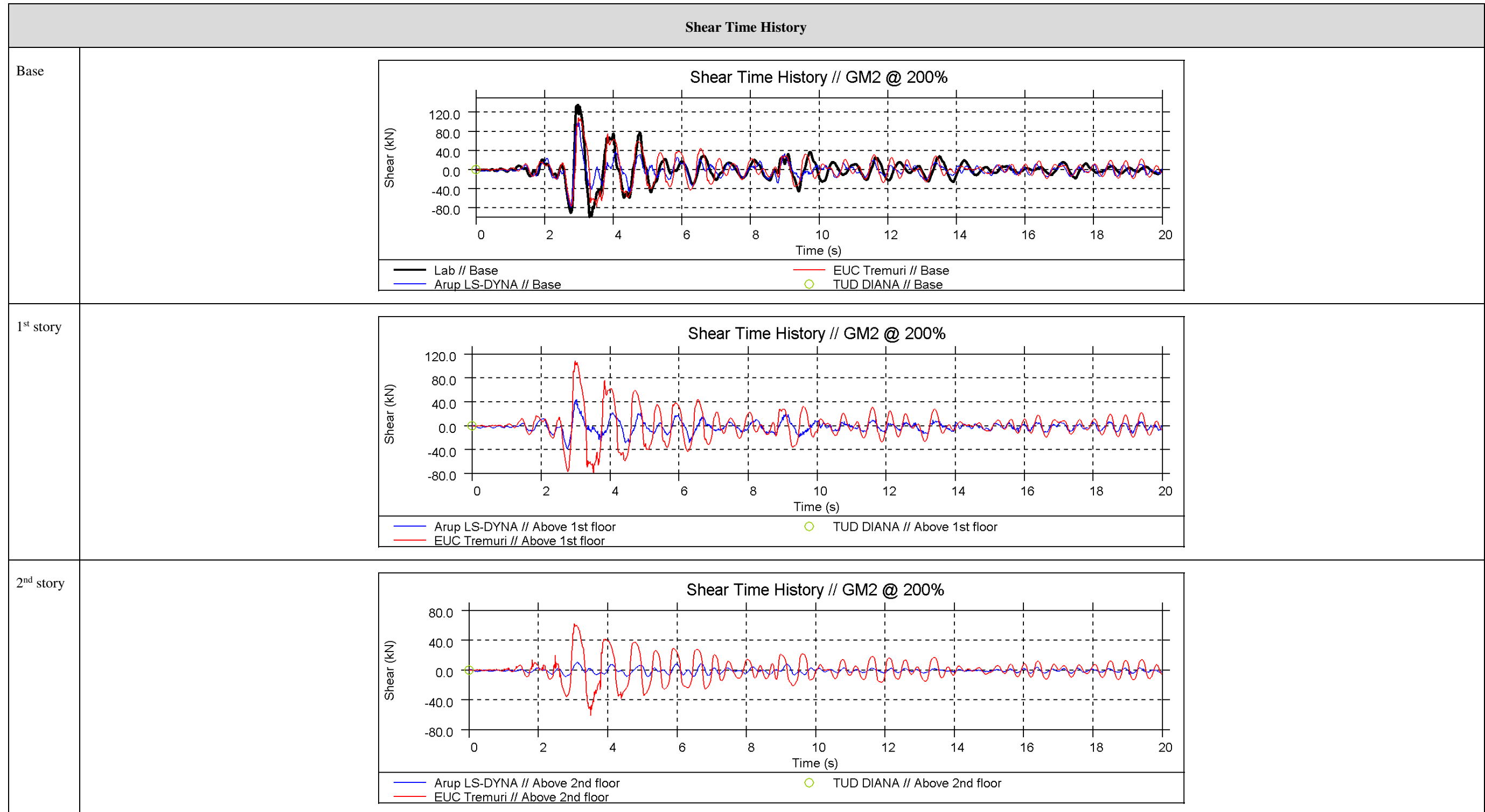
<sup>2</sup> Displacement of the roof is measured as the average displacement at the two ends of the ridge beam

EQ2 at 200%



<sup>1</sup> Roof drift is calculated using a diagonal length from the gable peak to the 2<sup>nd</sup> floor along the roof slope (3.5m)

EQ2 at 200%



EQ2 at 200%

Global Hysteresis <sup>1</sup>	
<p>Global Hysteresis // GM2 @ 200%</p> <p>Shear (kN)</p> <p>Displacement (mm)</p> <p>— Lab      — Arup LS-DYNA</p>	<p>- Results not provided -</p>
<p>Arup</p>	<p>TU-Delft</p>
<p>Global Hysteresis // GM2 @ 200%</p> <p>Shear (kN)</p> <p>Displacement (mm)</p> <p>— Lab      — EUC Tremuri</p>	<p>EUCENTRE</p>
<p><sup>1</sup> Base shear vs. 2<sup>nd</sup> floor displacement</p>	

EQ2 at 200%

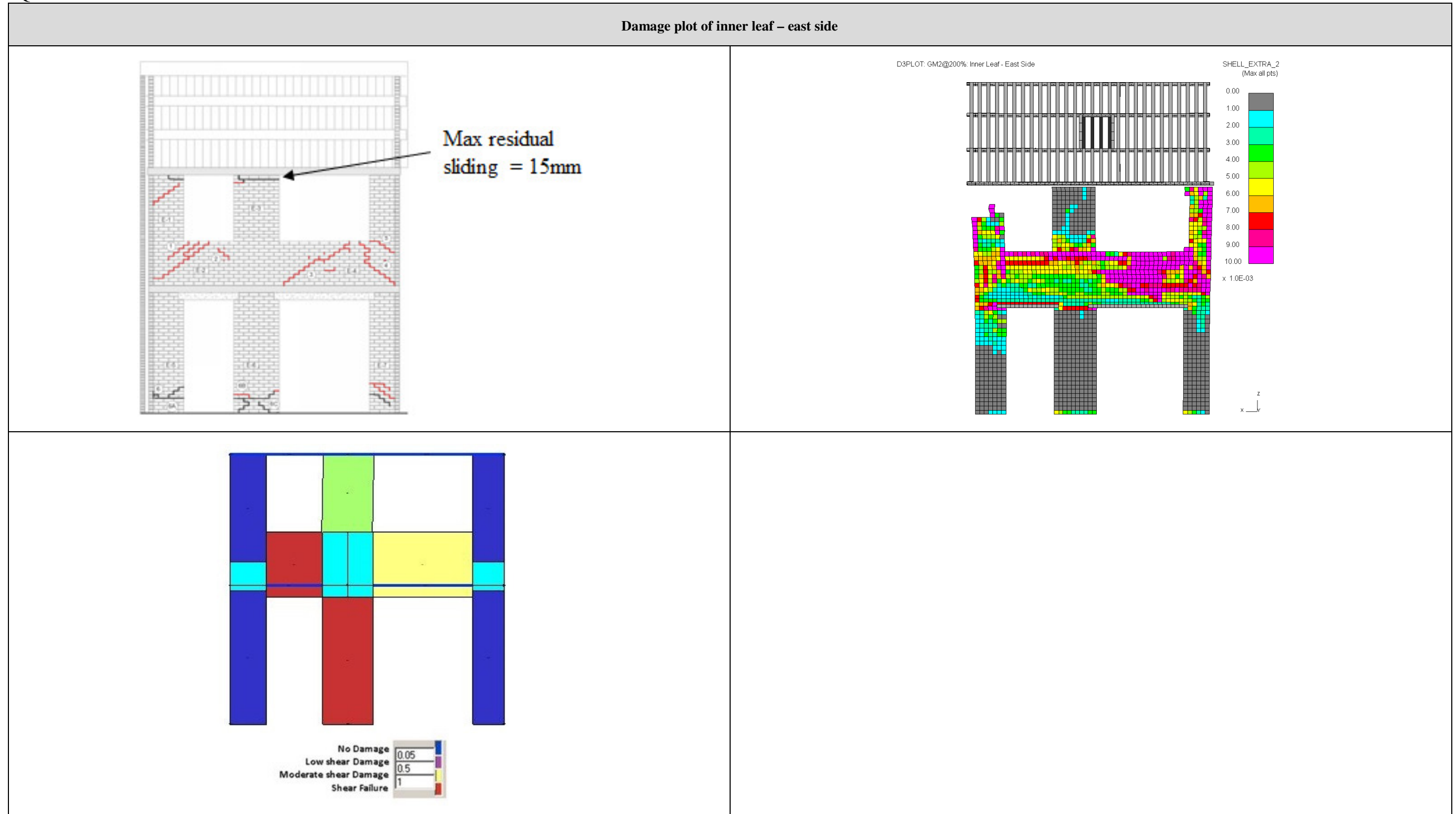


Figure 11: Damage plot of inner leaf - east side of test result (top left), Arup LS-DYNA (top right), and EUCENTRE (bottom left)



EQ2 at 200%

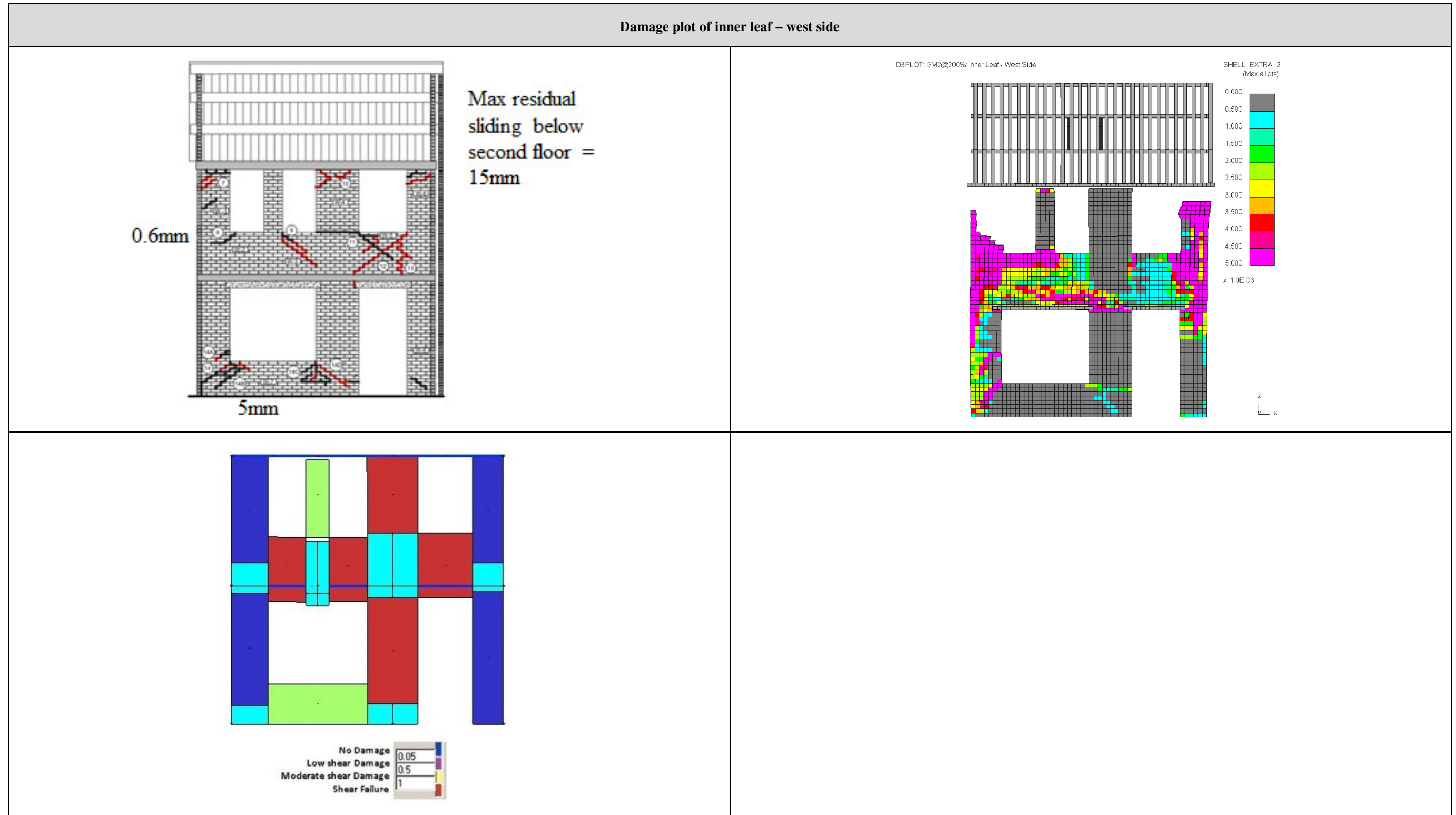


Figure 12: Damage plot of inner leaf - west side of test result (top left), Arup LS-DYNA (top right), and EUCENTRE (bottom left)

EQ2 at 200%

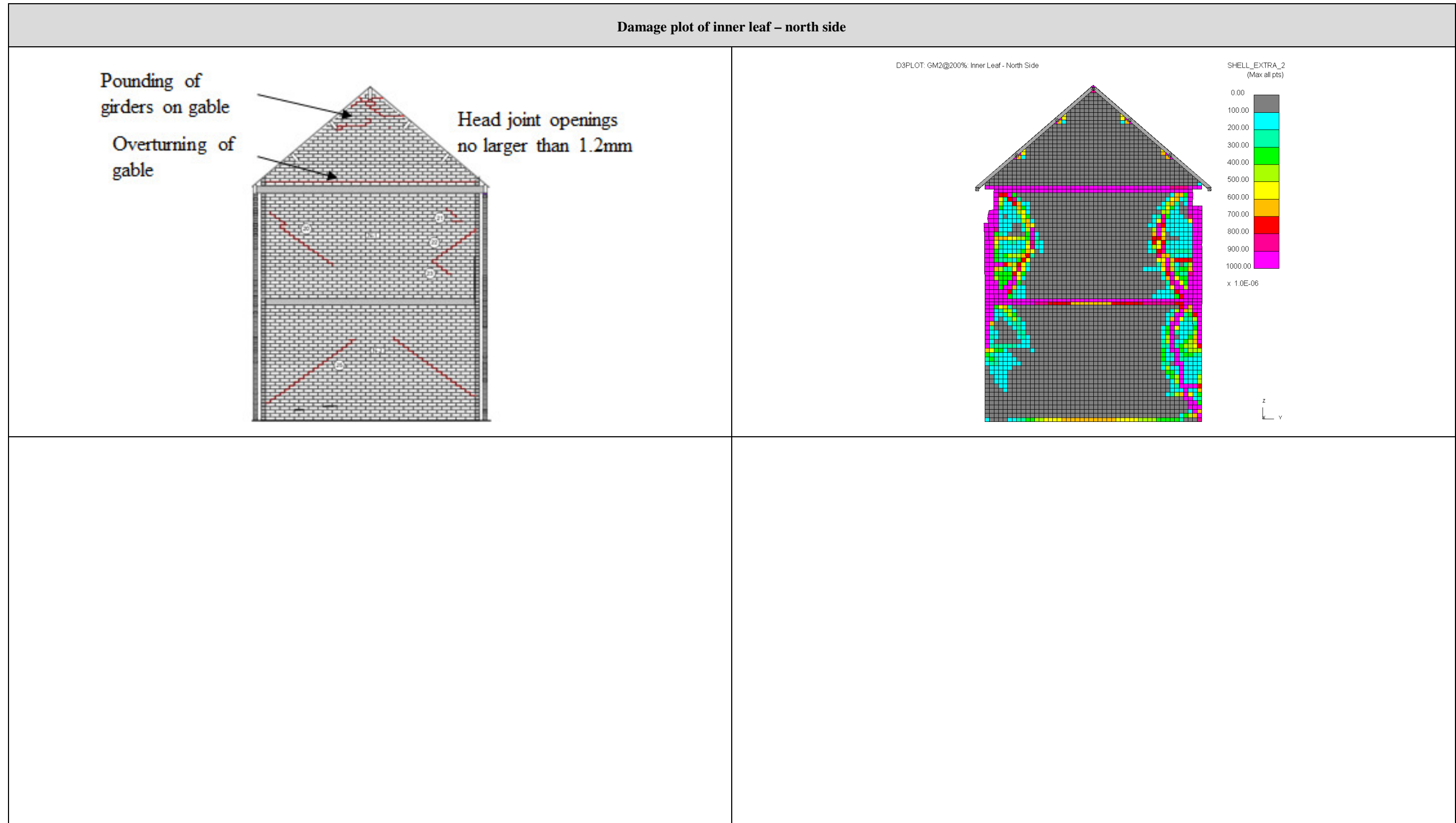


Figure 13: Damage plot of inner leaf - north side of test result (top left) and Arup LS-DYNA (top right)

EQ2 at 200%

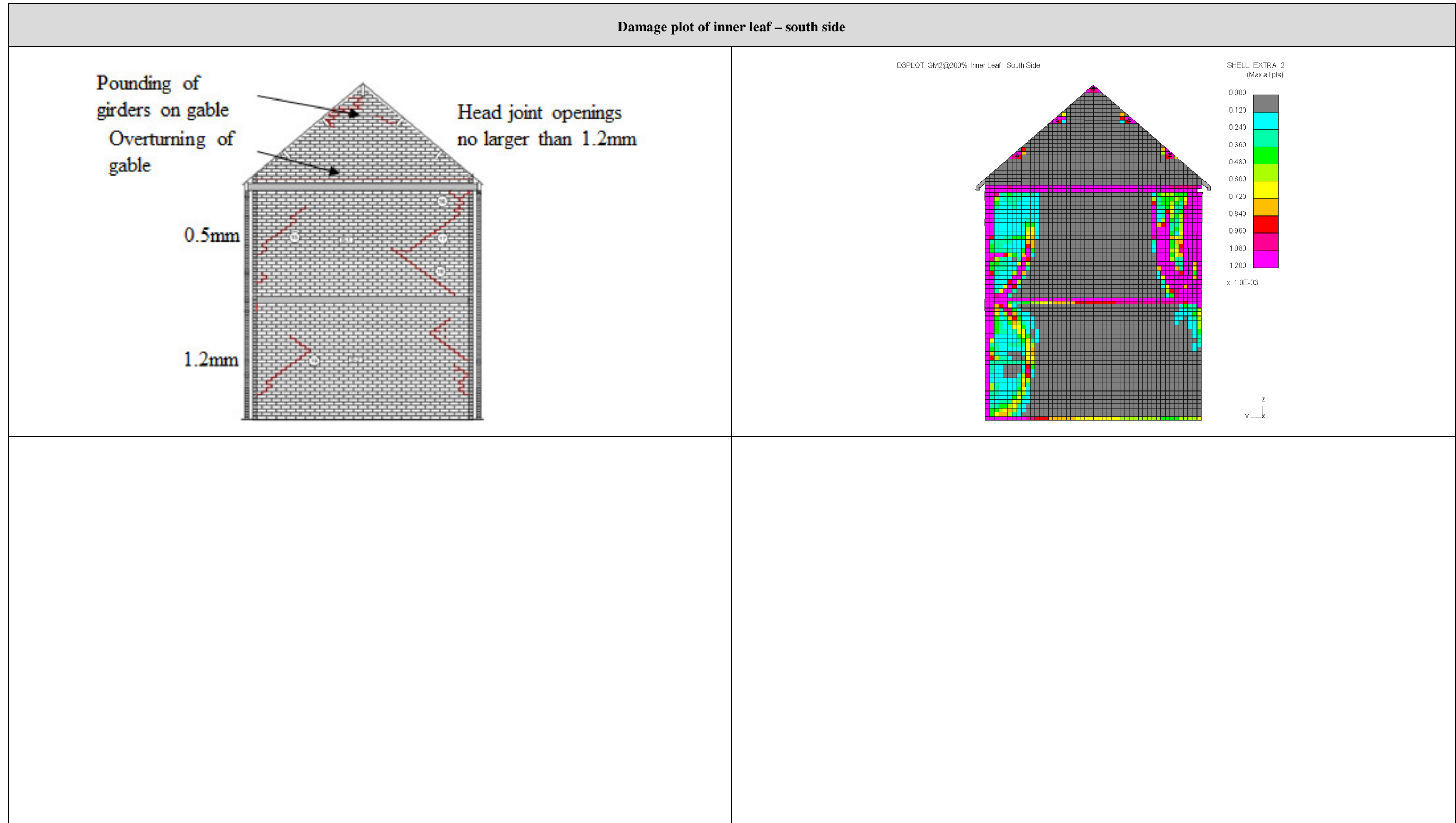


Figure 14: Damage plot of inner leaf - south side of test result (top left) and Arup LS-DYNA (top right)

EQ2 at 200%

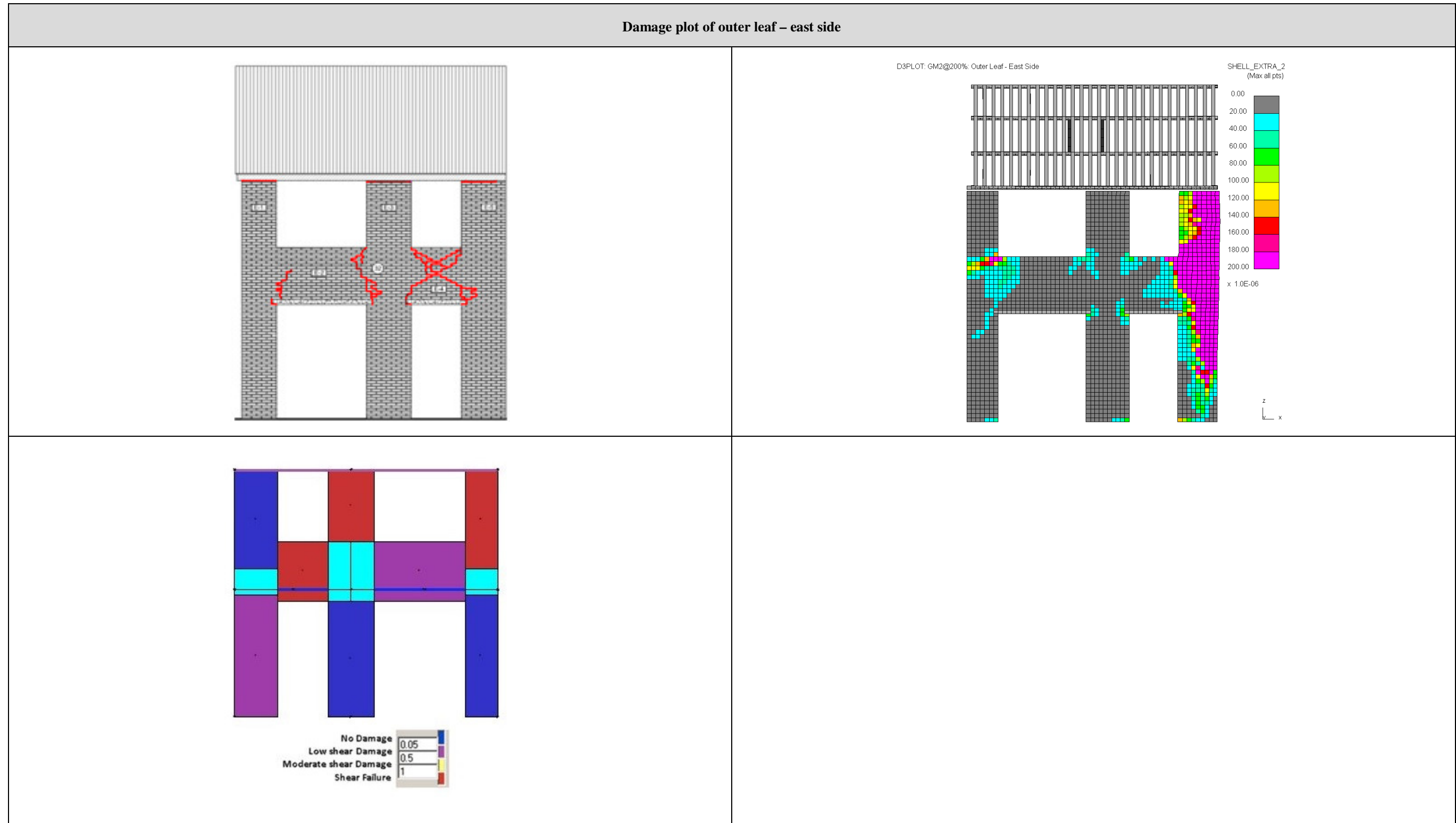


Figure 15: Damage plot of outer leaf - east side of test result (top left), Arup LS-DYNA (top right), and EUCENTRE (bottom left)

EQ2 at 200%



Figure 16: Damage plot of outer leaf - west side of test result (top left), Arup LS-DYNA (top right), and EUCENTRE (bottom left)

EQ2 at 200%

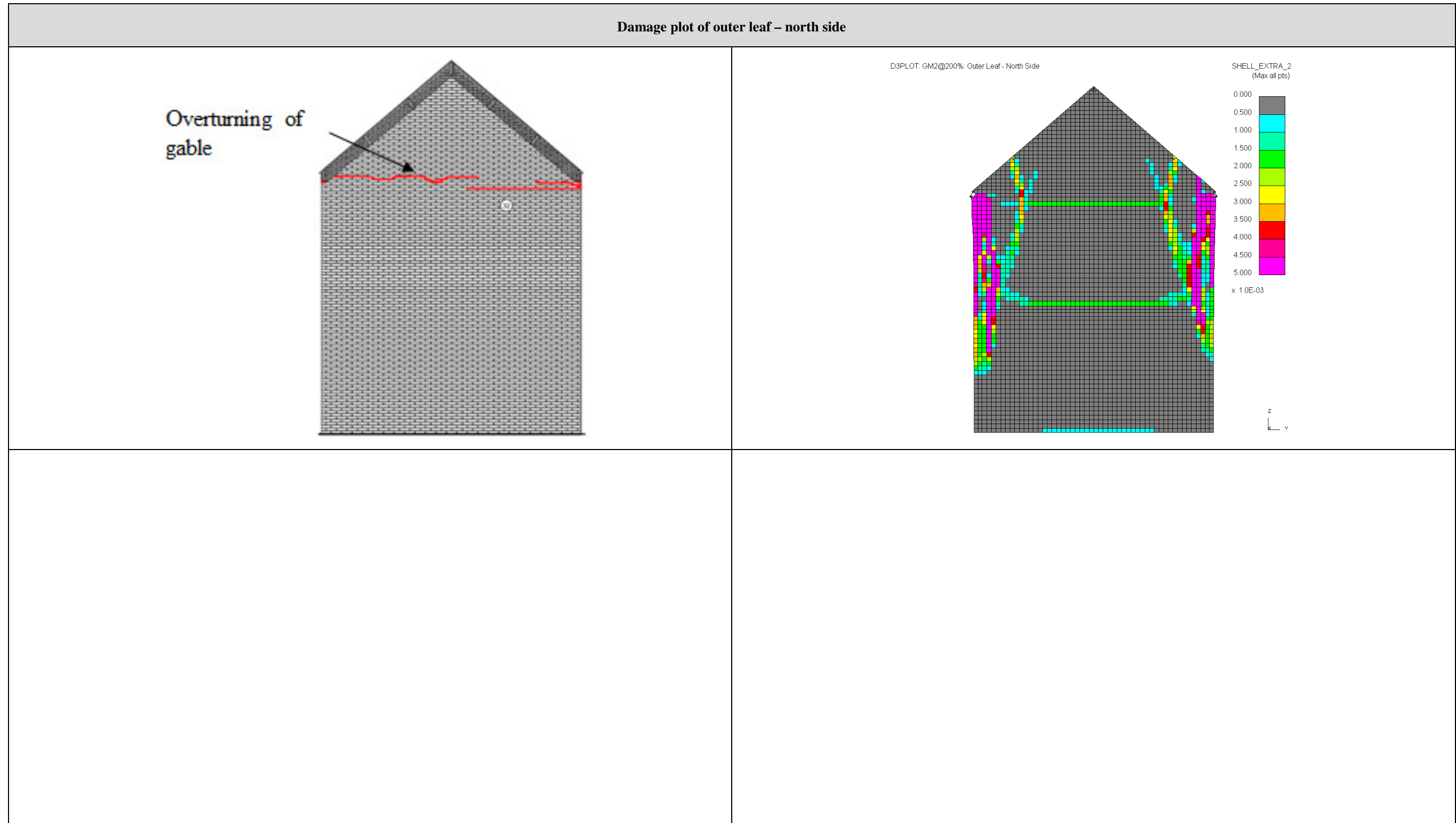


Figure 17: Damage plot of outer leaf - north side of test result (top left), and Arup LS-DYNA (top right)

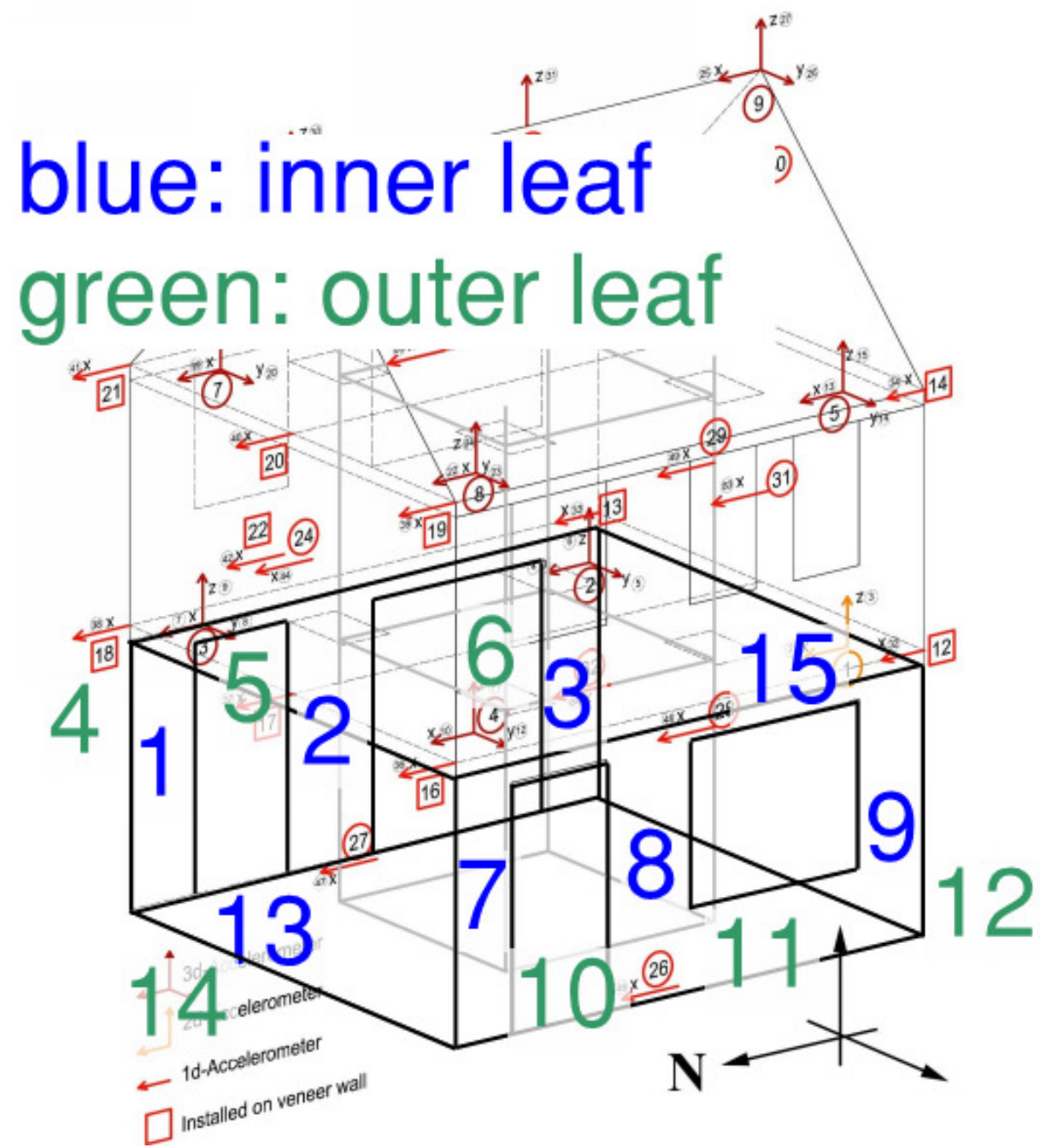


Figure 18: Legend for pier labelling. Refer to tables below

Table 7: Axial force summary (kN) <sup>1</sup>

		Total	East wall, inner			East wall, outer			West wall, inner			West wall, outer			North wall, inner	North wall, outer	South wall
			Pier 1	Pier 2	Pier 3	Pier 4	Pier 5	Pier 6	Pier 7	Pier 8	Pier 9	Pier 10	Pier 11	Pier 12	Pier 13	Pier 14	Pier 15
t = 0	Arup	552	59.1			33.5			62.9			37.4			146	63.4	150.2
	EUCENTRE	541	37.0	12.5	37.0	10.50	12.31	8.44	35.6	14.8	40.3	9.1	14.5	11.2	120	56.9	120
	TU-Delft	528	16.7	16.0	16.0	15.99	19.91	19.61	14.8	14.3	16.3	14.3	17.8	18.7	112	86.8	129
EQ1 @ 50%	Arup	553	57.4			28.2			62.4			32.7			171	74.1	128
	EUCENTRE	537	39.9	13.5	32.6	8.92	12.20	8.27	38.6	16.8	34.4	7.7	14.4	11.2	125	60	114
	TU-Delft																
EQ1 @ 100%	Arup	553	55.4			24.7			61.3			29.4			191	80.8	110
	EUCENTRE	544	41.8	13.2	32.8	6.1	12.1	7.9	39.4	19.8	35.5	4.9	14.7	10.5	130	68.3	107
	TU-Delft																
EQ1 @ 150%	Arup	554	53.5			23.6			58.6			28.2			196	83.1	111
	EUCENTRE	558	44.0	14.5	33.5	5.4	11.9	7.8	42.2	21.3	37.7	3.7	14.6	10.5	136	74.2	101
	TU-Delft																

<sup>1</sup> Unless noted otherwise, reported axial forces occur at time "A." Time "A" is the time at which the total base shear force is the absolute maximum during that run



Table 8: Axial force summary (kN) (continued)<sup>1 2</sup>

		Total	East wall, inner			East wall, outer			West wall, inner			West wall, outer			North wall, inner	North wall, outer	South wall
			Pier 1	Pier 2	Pier 3	Pier 4	Pier 5	Pier 6	Pier 7	Pier 8	Pier 9	Pier 10	Pier 11	Pier 12	Pier 13	Pier 14	Pier 15
EQ2 @ 100%	Arup	562	68.6			46.2			77.3			46.2			56.0	42.1	225
	EUCENTRE	544	44.4	16.9	35.4	4.7	10.8	6.9	39.2	27.7	40.5	2.0	14.0	9.8	132	76.9	82.8
	TU-Delft																
EQ2 @ 150%	Arup	558	66.8			55.0			68.0			55.2			65	37.6	211
	EUCENTRE	540	49.1	22.3	41.6	10.0	8.5	6.2	40.7	36.6	49.7	3.6	12.9	8.2	124	75.8	50.8
	TU-Delft																
EQ2 @ 200%	Arup	554	60.3			46.0			90.8			62.0			57	40.7	197
	EUCENTRE	518	54.5	18.9	48.4	13.7	7.1	5.9	56.6	12.4	63.4	8.4	11.9	7.6	115	65.5	28.9
	TU-Delft																

<sup>1</sup> Unless noted otherwise, reported axial forces occur at time "A." Time "A" is the time at which the total base shear force is the absolute maximum during that run<sup>2</sup> Positive values are compression loads. Negative values are tension loads due to uplift.

Table 9: Base shear force summary (kN): EQ1 @ 50%

			Total	East wall, inner			East wall, outer			West wall, inner			West wall, outer			North wall, inner	North wall, outer	South wall
				Pier 1	Pier 2	Pier 3	Pier 4	Pier 5	Pier 6	Pier 7	Pier 8	Pier 9	Pier 10	Pier 11	Pier 12	Pier 13	Pier 14	Pier 15
EQ1 @ 50%	t = A <sup>1</sup>	Arup	-33.9	-8.9			-5.1			-11.3			-5.3			-1.9	-2.1	0.5
		EUCENTRE	30.7	2.29	3.79	3.82	0.36	0.31	-0.02	1.83	5.62	6.41	0.29	0.61	-0.25	2.16	1.15	2.25
		TU-Delft																
	Max Envelope	Arup		-8.9			-5.1			-11.3			-5.3			-1.9	-2.1	2.3
		EUCENTRE		4.16	4.49	3.83	0.60	0.66	0.33	3.19	5.98	6.41	0.39	0.95	0.76	2.44	1.23	2.37
		TU-Delft																

<sup>1</sup> Time “A” is the time at which the total base shear force is the absolute maximum during that run

Table 10: Base shear force summary (kN): EQ1 @ 100%

			Total	East wall, inner			East wall, outer			West wall, inner			West wall, outer			North wall, inner	North wall, outer	South wall
				Pier 1	Pier 2	Pier 3	Pier 4	Pier 5	Pier 6	Pier 7	Pier 8	Pier 9	Pier 10	Pier 11	Pier 12	Pier 13	Pier 14	Pier 15
EQ1 @ 100%	t = A	Arup	-59.7	-16.2			-8.3			-19.9			-8.8			-3.0	-3.2	-0.3
		EUCENTRE	42.9	4.01	3.90	5.05	0.84	0.92	0.16	3.13	6.84	7.94	0.58	1.37	0.13	3.16	1.69	3.20
		TU-Delft	49.1	3.4	5.5	3.4	6.6	6.9	2.3	2.5	2.0	1.4	4.8	2.7	-0.3	2.8	3.9	1.2
	Max Envelope	Arup		-16.2			-8.3			-20.0			-8.8			-3.0	-3.3	3.0
		EUCENTRE		5.16	5.53	5.08	1.00	1.12	0.58	4.01	7.90	8.09	0.63	1.44	1.10	3.16	1.93	3.20
		TU-Delft		4.7	5.6	3.4	6.6	6.9	3.1	3.4	2.1	1.40	4.8	2.8	1.0	2.8	3.9	2.14

Table 11: Base shear force summary: EQ1 @ 150%

			Total	East wall, inner			East wall, outer			West wall, inner			West wall, outer			North wall, inner	North wall, outer	South wall
				Pier 1	Pier 2	Pier 3	Pier 4	Pier 5	Pier 6	Pier 7	Pier 8	Pier 9	Pier 10	Pier 11	Pier 12	Pier 13	Pier 14	Pier 15
EQ1 @ 150%	t = A	Arup	-70.9	-18.2			-9.9			-22.7			-10.6			-4.1	-4.3	-1.1
		EUCENTRE	52.1	5.92	6.82	4.46	0.94	1.02	0.23	4.11	9.84	7.03	0.60	1.24	0.09	4.09	2.22	3.44
		TU-Delft																
	Max Envelope	Arup		-18.2			-10.6			-24.0			-11.7			-4.6	-4.4	4.5
		EUCENTRE		5.94	7.02	5.71	1.25	1.62	0.80	4.37	10.66	8.86	0.74	2.03	1.41	4.14	3.05	3.84
		TU-Delft																

Table 12: Base shear force summary: EQ2 @ 100%

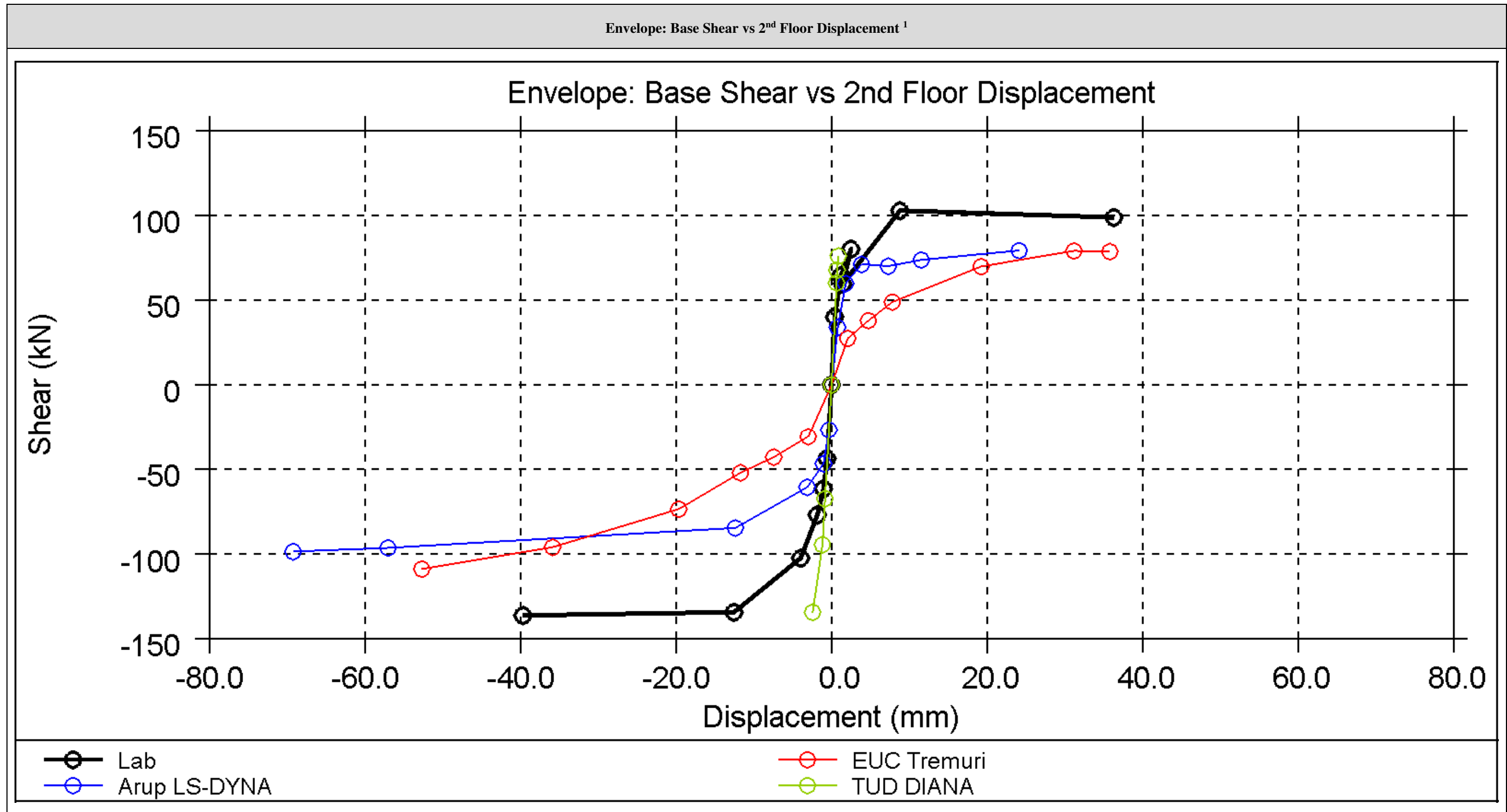
			Total	East wall, inner			East wall, outer			West wall, inner			West wall, outer			North wall, inner	North wall, outer	South wall
				Pier 1	Pier 2	Pier 3	Pier 4	Pier 5	Pier 6	Pier 7	Pier 8	Pier 9	Pier 10	Pier 11	Pier 12	Pier 13	Pier 14	Pier 15
EQ2 @ 100%	t = A	Arup	85.7	19.3			9.6			22.6			12.5			4.5	3.0	14.2
		EUCENTRE	73.4	9.31	6.40	6.42	1.47	2.65	1.01	6.75	12.66	9.94	0.44	3.37	1.32	4.33	3.59	3.77
		TU-Delft	63.4	6.2	7.5	1.7	8.4	8.5	4.8	4.3	1.3	1.7	5.9	1.6	1.3	2.5	3.9	3.8
	Max Envelope	Arup		21.4			12.3			-27.0			14.8			-6.0	-5.8	14.9
		EUCENTRE		9.31	10.34	6.57	1.60	2.67	1.15	6.75	12.66	13.29	1.01	3.67	2.52	4.89	3.69	4.80
		TU-Delft		6.2	7.5	4.1	8.5	8.5	4.8	4.3	2.1	1.8	6.0	2.6	1.3	2.5	3.9	3.8

Table 13: Base shear force summary: EQ2 @ 150%

			Total	East wall, inner			East wall, outer			West wall, inner			West wall, outer			North wall, inner	North wall, outer	South wall
				Pier 1	Pier 2	Pier 3	Pier 4	Pier 5	Pier 6	Pier 7	Pier 8	Pier 9	Pier 10	Pier 11	Pier 12	Pier 13	Pier 14	Pier 15
EQ2 @ 150%	t = A	Arup	98.9	16.2			17.7			17.4			22.8			5.9	3.9	15.1
		EUCENTRE	96.0	12.50	8.46	7.66	3.01	3.17	1.31	8.68	17.97	12.86	1.01	4.83	1.88	4.09	4.91	3.64
		TU-Delft	87.9	9.6	9.7	3.1	12.2	6.8	6.4	6.3	0.5	5.4	8.8	1.0	2.6	4.4	4.2	6.9
	Max Envelope	Arup		21.4			17.7			-26.6			22.8			-15.3	-4.9	20.6
		EUCENTRE		12.76	13.50	8.30	11.18	5.23	2.20	9.18	18.60	15.62	3.85	8.56	5.73	6.57	5.36	5.85
		TU-Delft		9.7	9.9	4.6	12.6	9.0	6.5	6.28	2.9	5.9	9.0	3.6	3.7	4.7	8.5	5.0

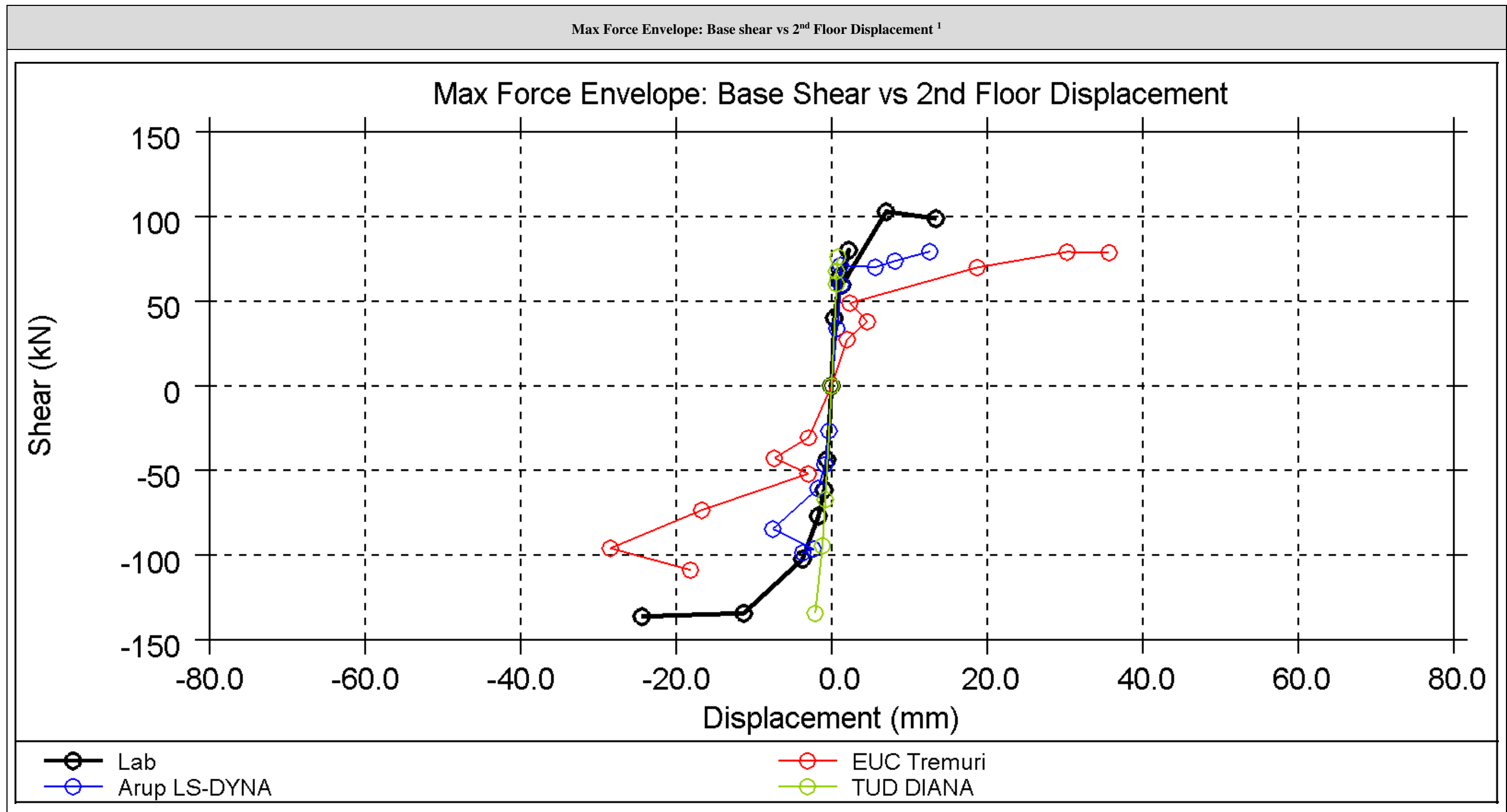
Table 14: Base shear force summary: EQ2 @ 200%

			Total	East wall, inner			East wall, outer			West wall, inner			West wall, outer			North wall, inner	North wall, outer	South wall
				Pier 1	Pier 2	Pier 3	Pier 4	Pier 5	Pier 6	Pier 7	Pier 8	Pier 9	Pier 10	Pier 11	Pier 12	Pier 13	Pier 14	Pier 15
EQ2 @ 200%	t = A	Arup	100.2	17.0			10.5			25.3			18.9			3.1	3.5	21.9
		EUCENTRE	108.9	12.39	11.44	7.70	2.89	3.49	1.35	9.02	21.64	14.37	1.01	5.06	1.98	5.43	5.62	5.48
		TU-Delft																
	Max Envelope	Arup		-19.2			14.3			-25.9			21.6			-13.3	5.8	24.4
		EUCENTRE		13.56	12.39	9.49	15.03	6.47	2.47	10.68	21.64	16.42	4.20	8.95	4.96	7.17	6.47	7.09
		TU-Delft																

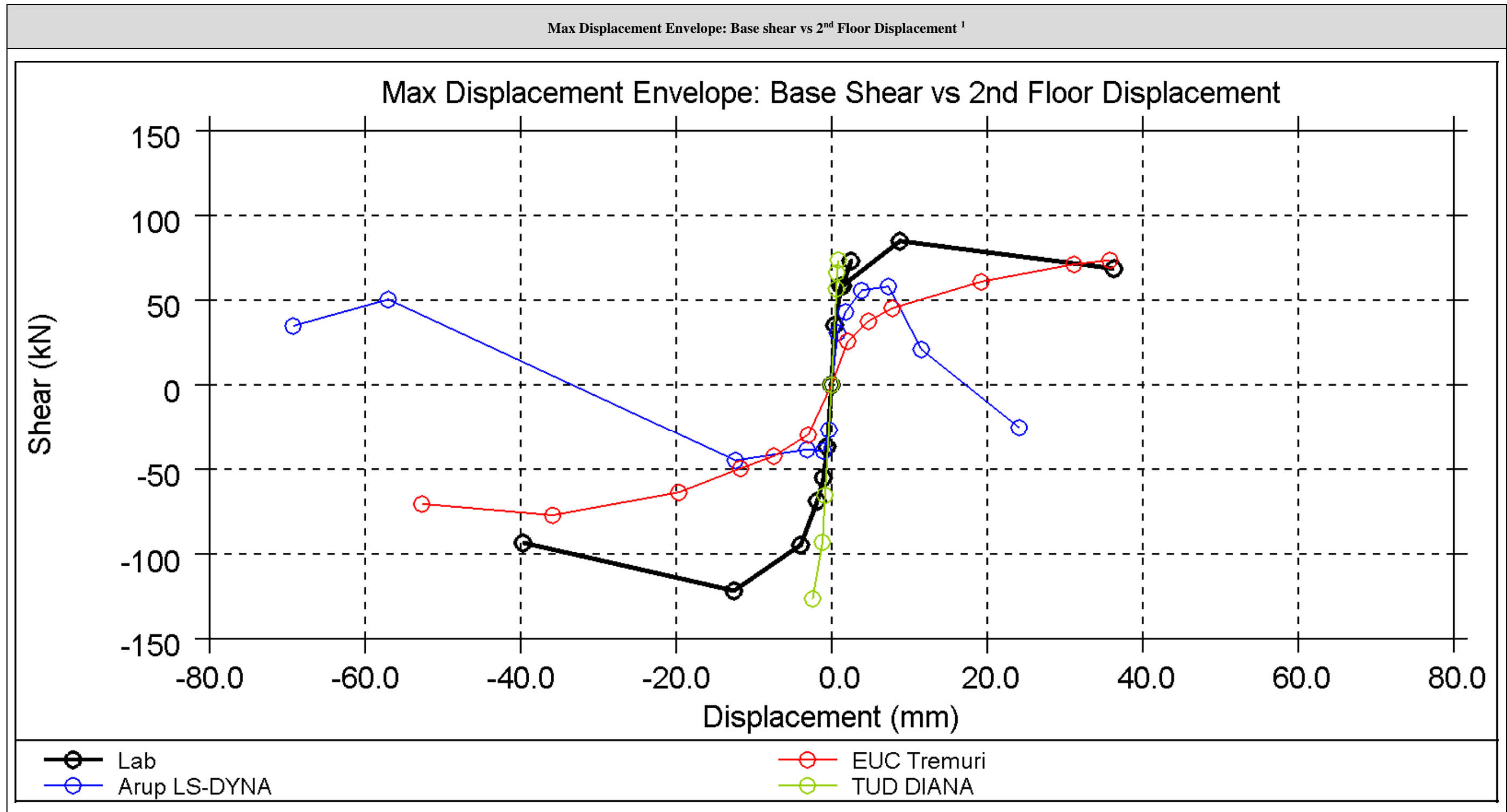


<sup>1</sup> Plot is defined as maximum base shear in +x direction vs. maximum displacement in +x direction, and maximum base shear in -x direction vs. maximum displacement in -x direction for each ground motion.





<sup>1</sup> Plot is defined as maximum base shear in +x direction vs. corresponding displacement at that instant, and maximum base shear in -x direction vs. corresponding displacement at that instant for each ground motion.



<sup>1</sup> Plot is defined as instantaneous base shear vs. maximum displacement in +x direction, and instantaneous base shear vs. maximum displacement in -x direction for each ground motion.

## 2.1.5 Conclusion

In summary, the LS-DYNA model has reasonably accurate stiffness, as shown by good prediction for the weaker ground motions but has only about two thirds of the strength of the real structure, as shown by excessive displacements in the stronger ground motions. The TREMURI model has a stiffness much less than the real structure, leading to excessive displacements in the weaker ground motions that ultimately match the structure's response during the final run of EQ2 scaled at 200%. The DIANA model has reasonably accurate stiffness as shown by good prediction for the weaker ground motions, but has post-elastic stiffness much larger than the real structure, leading to under-predicted displacements and global response for the stronger ground motions.

All models will incorporate refinements in the post-test refined prediction that aim to address the limitations described above. More detail is provided in the individual sections below.

### Arup – LS-DYNA

The LS-DYNA model of the full scale shake table building predicts the response of the structure subjected to ground shaking fairly well during the first portion of the protocol during which different levels of EQ1 are applied. However, the model consistently overestimates the deformations and resulting damage during the application of EQ2. A major source of difference appears to be that sliding of the 2<sup>nd</sup> floor relative to the East and West walls, predicted by the LS-DYNA model, did not occur in the test specimen. The model assumes a non-load-bearing, sliding interface between the top of the wall and the slab. However, the test results are consistent with that connection having significant resistance to sliding and/or uplift, perhaps arising from the cohesive strength of the mortar packing the gap. The first floor slab also appears to be more rigidly connected to the East and West walls than assumed in the model, although this has less influence on results than the second floor slab connectivity. Possibly, the threaded bars (intended to restrain the East-West walls out of plane at the first floor) may have been tensioned during construction, providing frictional resistance to sliding between the sides of the slab and the walls.

The global hysteresis is in general well predicted during the application of EQ1, although the initial stiffness is slightly underestimated. As the analysis progresses through the loading protocol, the second floor slab experienced a large amount of sliding due to the flexible connection to the East-West inner and outer leaves. As a result, the deformation predicted is much higher than in the lab. In addition, there is a lag in the acceleration applied at the base and the subsequent movement of slab, which explains how as the base shear increases in one direction, the slab is still moving in the opposite direction.

The flexibility of the gable walls in the model is overestimated and results in larger drifts of the roof than observed in the lab. This may be due to the structural members of the roof being less well-tied into the gable walls in the model than was the case in reality.

After investigating the results of the LS-DYNA blind prediction model, the following areas of improvement have been identified for post-test refined prediction model:

- Connections: Assumptions are made for the connections as described in Table 5 and Table 6. After observing the lab results, these assumptions will be revisited and modified to better replicate the real conditions. This is expected to improve the results. Example of connections to modify:
  - 1<sup>st</sup> floor slab to East/West inner leaves—account for more than just the axial threaded bar capacity, add resistance to sliding as suggested above. As an upper bound, assume a full rigid connection.
  - 2<sup>nd</sup> floor slab to the East/West inner and outer leaves—current modelling accounts for contact with friction only (no cohesion) and very little compression load. As an upper bound, assume a full rigid connection assuming the mortar packed in the joint has adequate cohesive strength. The actual strength of this joint is not known.
  - Roof girders to North wall—provide a connection between the girders and the North outer leaf
- Material properties: Properties from the latest material test results will be implemented to better represent the real structure.

### EUCENTRE - TREMURI

The comparison of the global hysteresis curves, as well as the displacement time histories, between the TREMURI blind prediction model and the lab tests makes clear that the model is quite more flexible, resulting in a general response far from the real dynamic response of the test building, at least during the first tests. The model presents systematically a more flexible structure when subjected to GM1, and captures in a satisfying degree the global stiffness of the specimen only under stronger ground motions (200% of GM2). Being so flexible, the model predicts displacements higher than those achieved during the shaking table tests. It also provides base shear time histories with amplitudes lower than those attained during the tests, showing a response generally weaker than the observed one. The aforementioned remarks are easily perceived after closely observing the global hysteresis curves and are aptly summarized in the base shear vs 2nd floor displacement envelope. These observations are also confirmed by the comparison of the final damage pattern at the end of the different runs, which show a relatively good consistency only for the stronger ground motions.

After closely observing the IDR time histories comparison plots, it is evident that the 1st and 2nd storey IDRs predicted by the TREMURI model overestimate those obtained in the lab. On the contrary, the roof IDR seems to be in a good agreement with the experimental results and this supplies a strong evidence that the assumptions made for modelling the gable-roof system behaviour were suitable, at least at capturing the elastic behaviour of the system. Only under the 200% of GM2 test the model underestimates the roof IDR, which leads to the belief that the in-plane stiffness of the roof diaphragm changes significantly, a fact that should be considered in refining the model. However, greater effort should be put into attributing more accurately the response of the 1st and 2nd storeys, by accounting accordingly for the collaboration of the longitudinal inner and outer leaves (revising the conservative assumptions made when modelling connections), as well as for the contribution of the out-of-plane walls by means of the flange effect. Specifically, as an example, the connection between the first floor slab and East/West walls will be refined in the model used for the post-diction analysis by adding beams of equivalent slab stiffness in order to guarantee an appropriate connection also with the central piers.

### TU-Delft - DIANA

The DIANA finite element model of EUC-BUILD is subjected to 3 separate analyses, namely EQ1-100%, EQ2-100% and EQ2-150%, with no accumulated damage, i.e. a separate analysis has been executed for each accelerogram and PGA level.

The comparison between experimental and DIANA numerical results in terms of hysteresis plots shows a satisfactory agreement for EQ1-100%. The global stiffness is slightly higher leading to underestimated displacement levels. For EQ2-100% instead the model results stiffer than the real specimen and the numerical hysteresis plot diverges from the experimental one; the maximum shear levels are correctly predicted but the displacements are much lower. Eventually for EQ2-150%, before the divergence the model again shows a stiffer behaviour with respect to the real specimen.

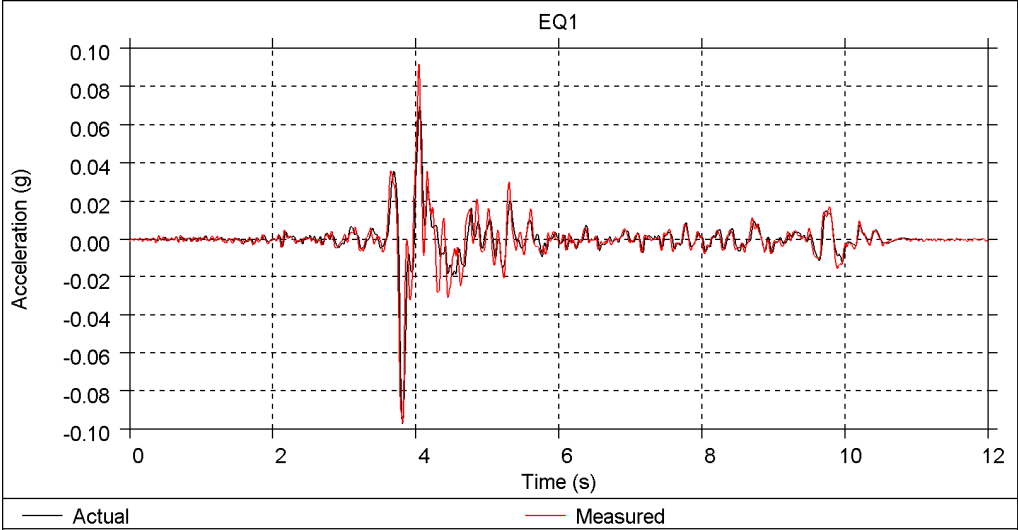
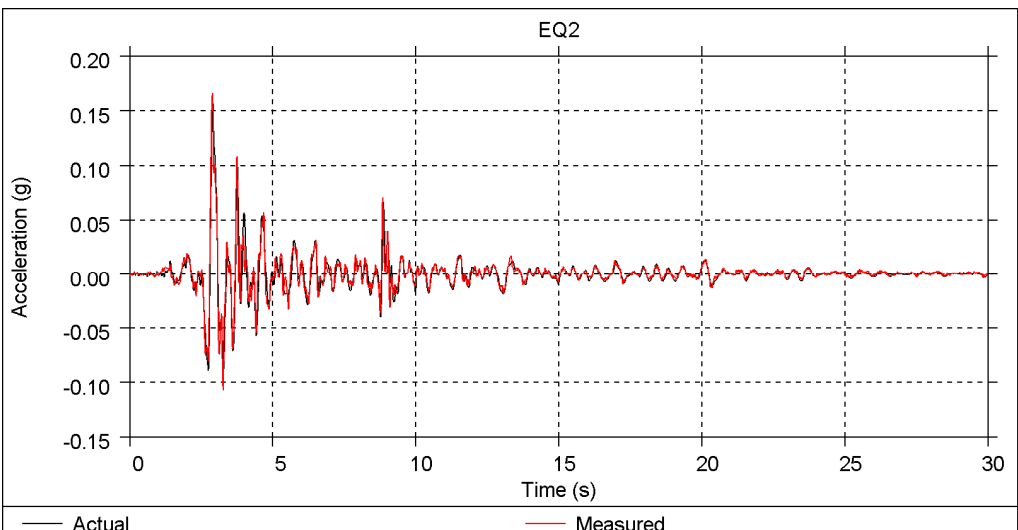
Concerning the IDR time histories, the model does not correctly predict the shape of the drift profile along the height, being the second storey of the real specimen more stiff with respect to the first one and the roof level and consequently showing a lower IDR. In the model instead the IDR increases progressively from 1<sup>st</sup> to 2<sup>nd</sup> floor and it is drastically reduced for the roof level.

Concerning the damage scenario, the model underwent the first 2 earthquakes (EQ1-100% and EQ2-100%) with limited damage on both inner and outer masonry leaves, mainly characterized by slight rocking of the piers and crack initiation at the corners of the openings. The stresses in the ties remain below the strength, both in tension and compression. The application of EQ2-150% caused much more damage in the structure. The inner leaf of East and West walls present high level rocking of piers, and severe diagonal cracks at the opening corners was also observed in the experiment. Additionally, the model shows severe damage on the outer leaf of East and West walls and diagonal cracks related to out-of-plane behaviour of the North and South walls not observed during the experiment for EQ2-150%. The analysis diverges around 2.5 s and shows a local failure with out-of-plane damage of the North wall and high deformation in tension of some of the ties that went far beyond their resistance.

## 2.2 Comparison of Blind Predictions using Measured Ground Motions

This section compares the results of the blind prediction models after they were updated to include the actual measured ground motions, but without any other changes to the models. The ground motions are illustrated in Table 15.

Table 15: Actual loading protocol

Earthquake	Graph	Protocol
EQ1		#4: 50%_EQ1_050 (Data: 02-EQ1-050)
		#7: 100%_EQ1_100 (Data: 04-EQ1-100)
		#9: 150%_EQ1_150 (Data: 05-EQ1-150)
EQ2		#14: 50%_EQ2_080 (Data: 09-EQ2-080)
		#16: 100%_EQ2_160 (Data: 10-EQ2-160)
		#18: 50%_EQ2_080 (Data: 11-EQ2-080-COMP)
		#19: 125%_EQ2_200 (Data: 12-EQ2-240)
		#21: 150%_EQ2_240 (Data: 13-EQ2-250)
#23: 200%_EQ2_320 (Data: 14-EQ2-320)		

### **2.2.1 Changes to Blind Prediction model - Arup**

Other than the update of the loading protocol, no changes were made to the blind prediction model. However, as mentioned in Section 2.1.2, the previous version of the LS-DYNA software, which was used to produce the blind prediction results of Section 2.1, showed some tendency for damage, once initiated, to become exaggerated in an unrealistic manner. This stability problem has been fixed in the updated version of the software, which has been used to produce blind prediction results of Section 2.2 and post-test refined prediction results of Section 2.3. Hence, the damage shown in the blind prediction in this section is more extensive than those in Sections 2.2 and 2.3.

### **2.2.2 Changes to Blind Prediction model - EUCENTRE**

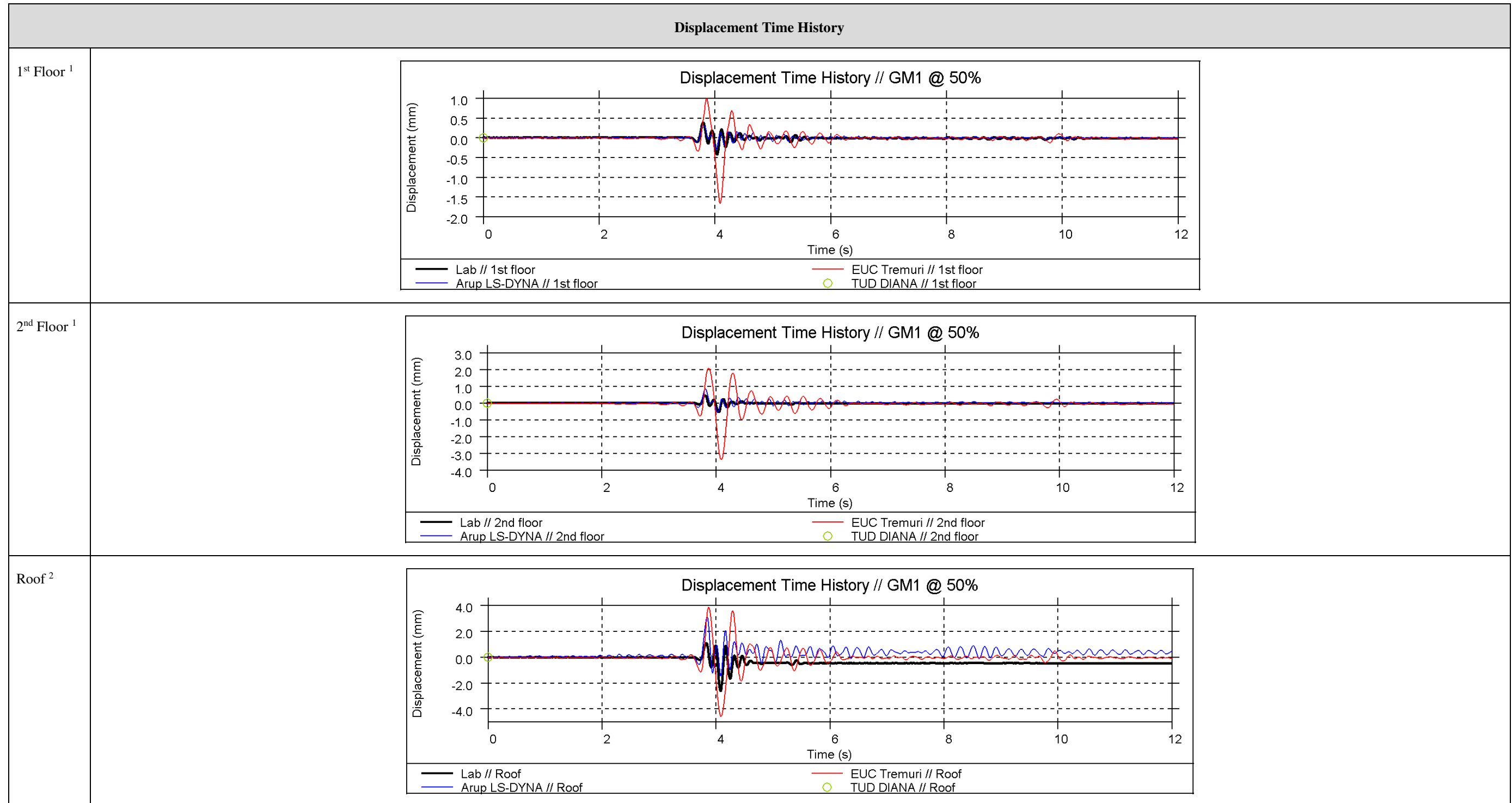
Only the loading protocol was changed.

### **2.2.3 Changes to Blind Prediction model - TU-Delft**

Only the loading protocol was changed.

## 2.2.4 Summary of Results

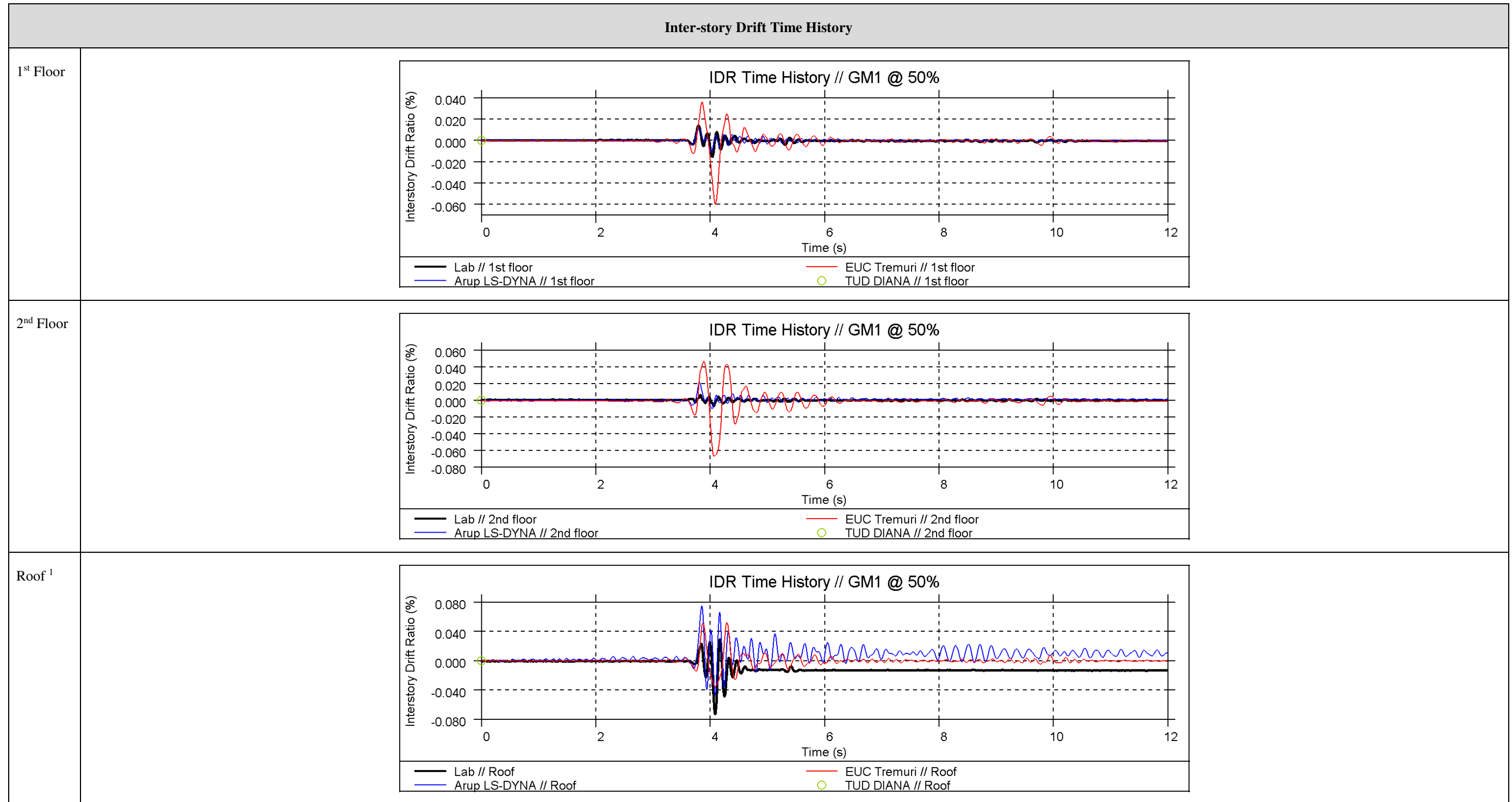
EQ1 at 50%



<sup>1</sup> Displacement of the 1<sup>st</sup> floor and 2<sup>nd</sup> floor is calculated as the average displacement measured at the four corners of the slab

<sup>2</sup> Displacement of the roof is measured as the average displacement at the two ends of the ridge beam

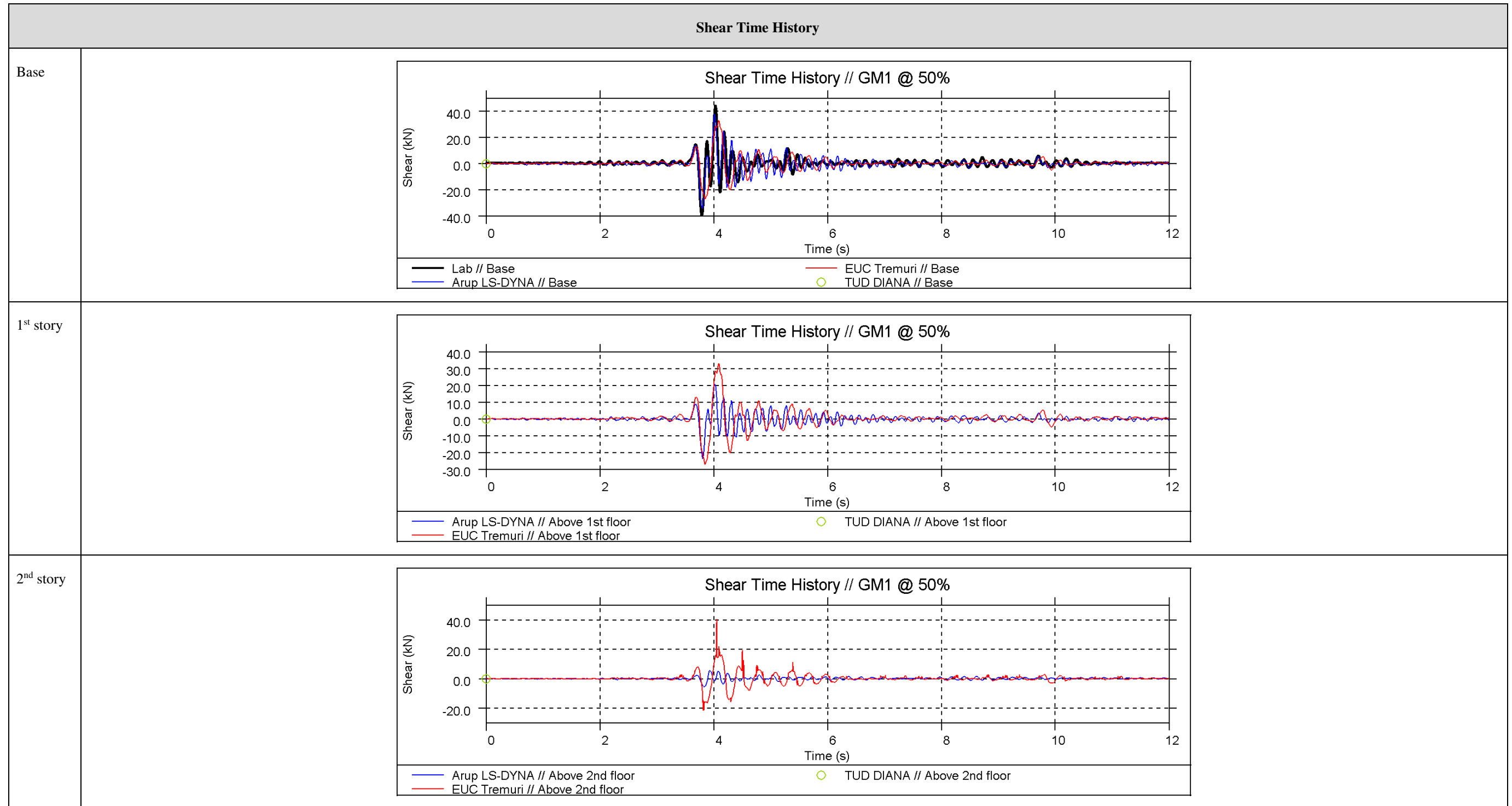
EQ1 at 50%



<sup>1</sup> Roof drift is calculated using a diagonal length from the gable peak to the 2<sup>nd</sup> floor along the roof slope (3.5m)



EQ1 at 50%

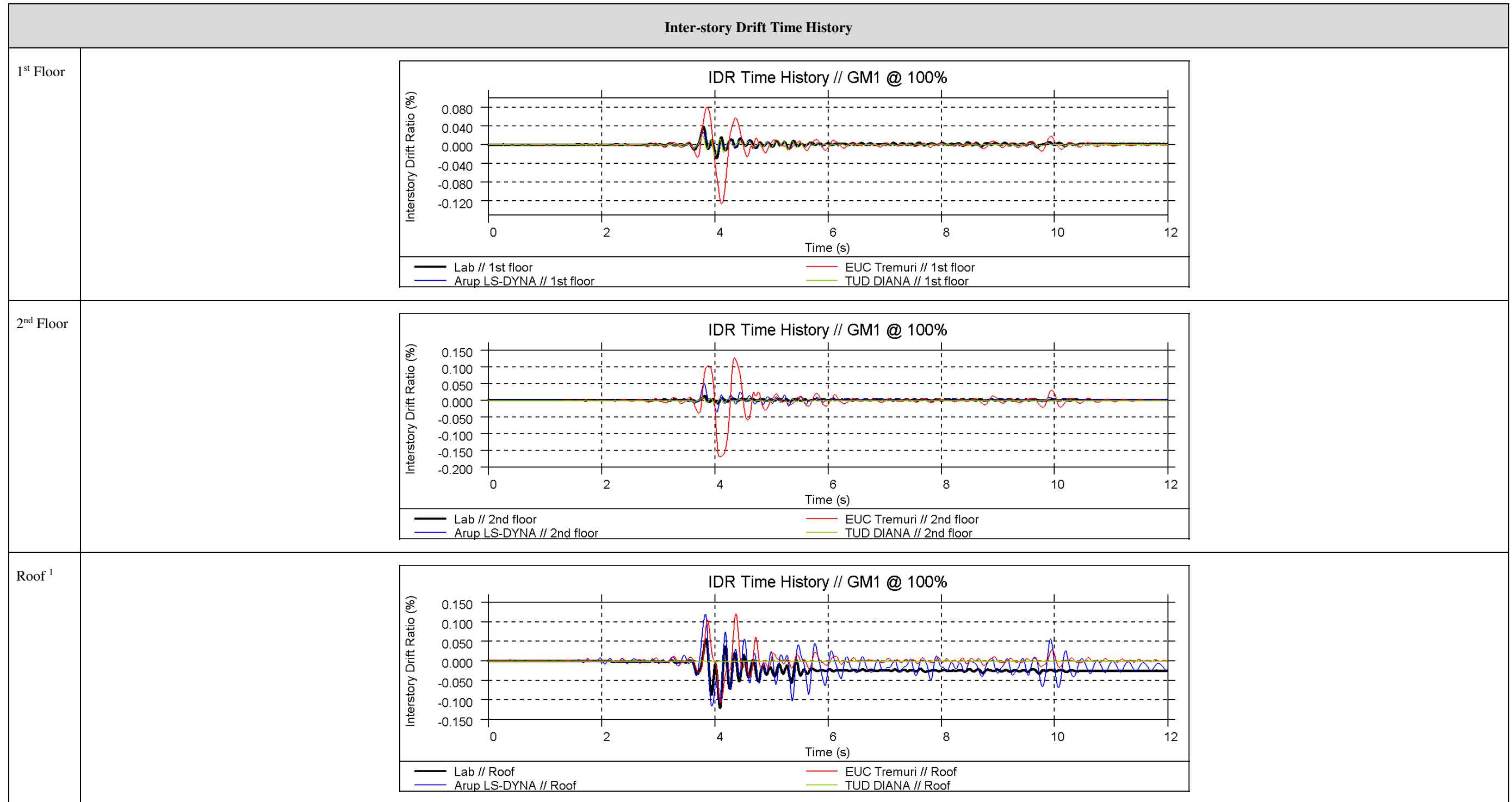


EQ1 at 50%

Global Hysteresis <sup>1</sup>	
<p>Global Hysteresis // GM1 @ 50%</p> <p>Shear (kN)</p> <p>Displacement (mm)</p> <p>— Lab      — Arup LS-DYNA</p>	<p>- Results not provided -</p>
<p>Arup</p>	<p>TU-Delft</p>
<p>Global Hysteresis // GM1 @ 50%</p> <p>Shear (kN)</p> <p>Displacement (mm)</p> <p>— Lab      — EUC Tremuri</p>	
<p>EUCENTRE</p>	<p><sup>1</sup> Base shear vs. 2<sup>nd</sup> floor displacement</p>



EQ1 at 100%

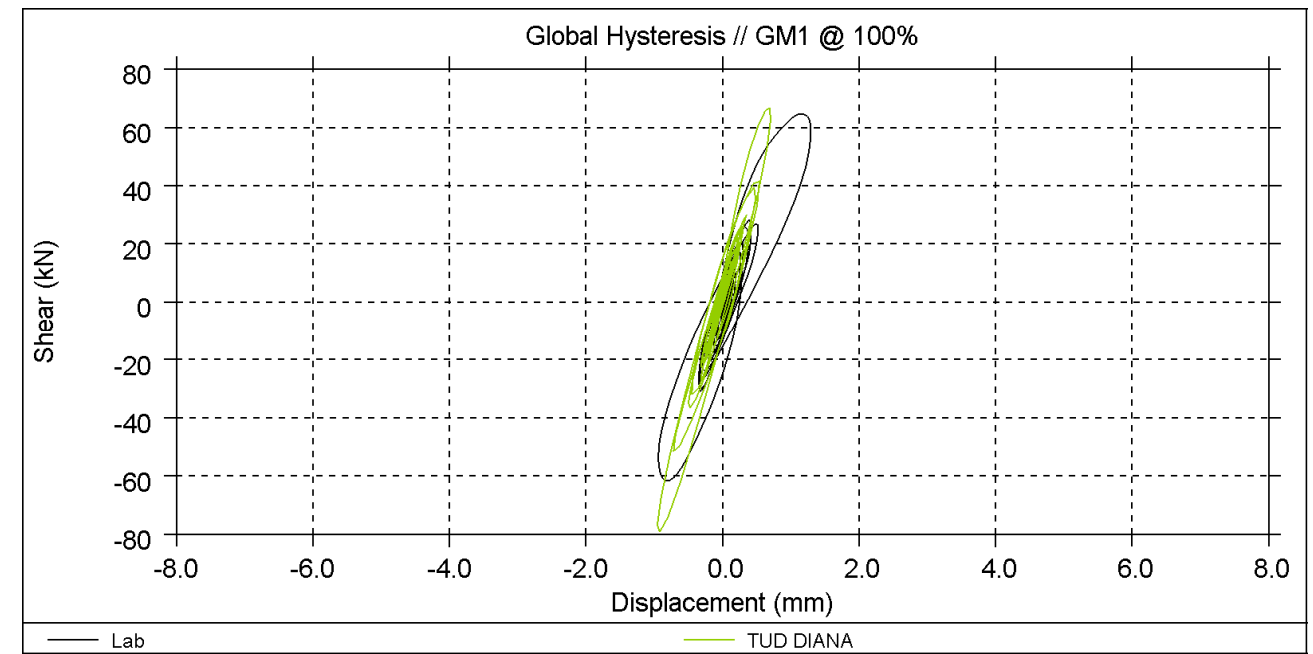
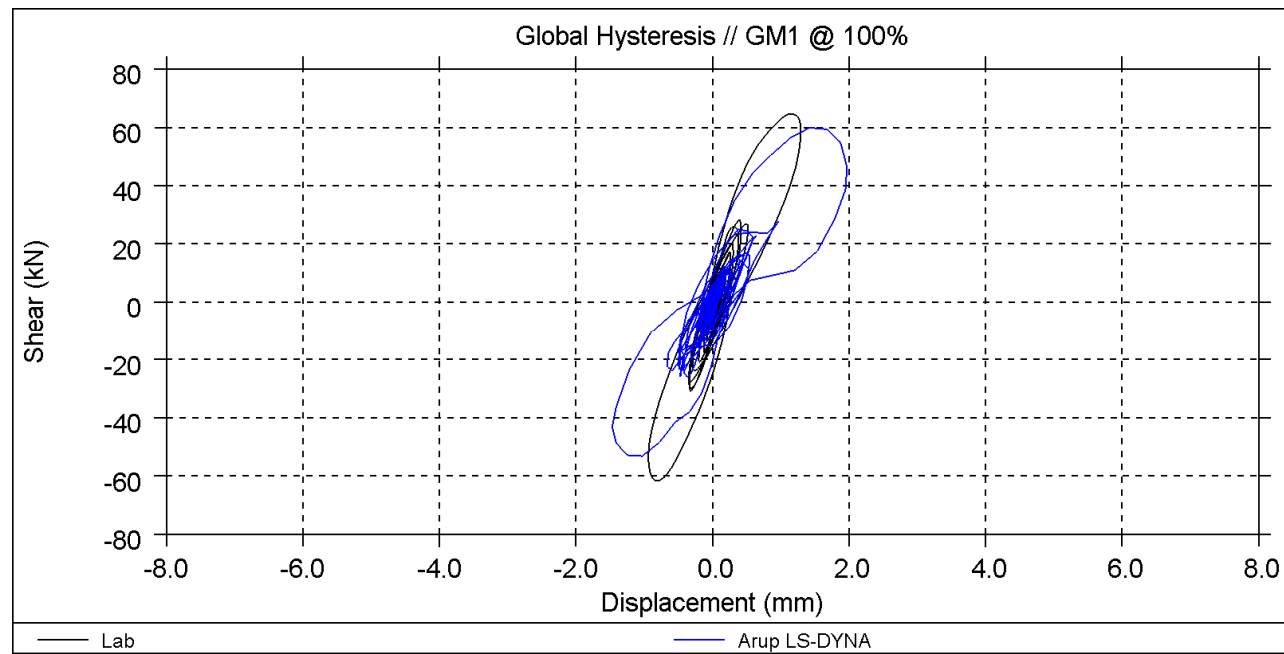


<sup>1</sup> Roof drift is calculated using a diagonal length from the gable peak to the 2<sup>nd</sup> floor along the roof slope (3.5m)



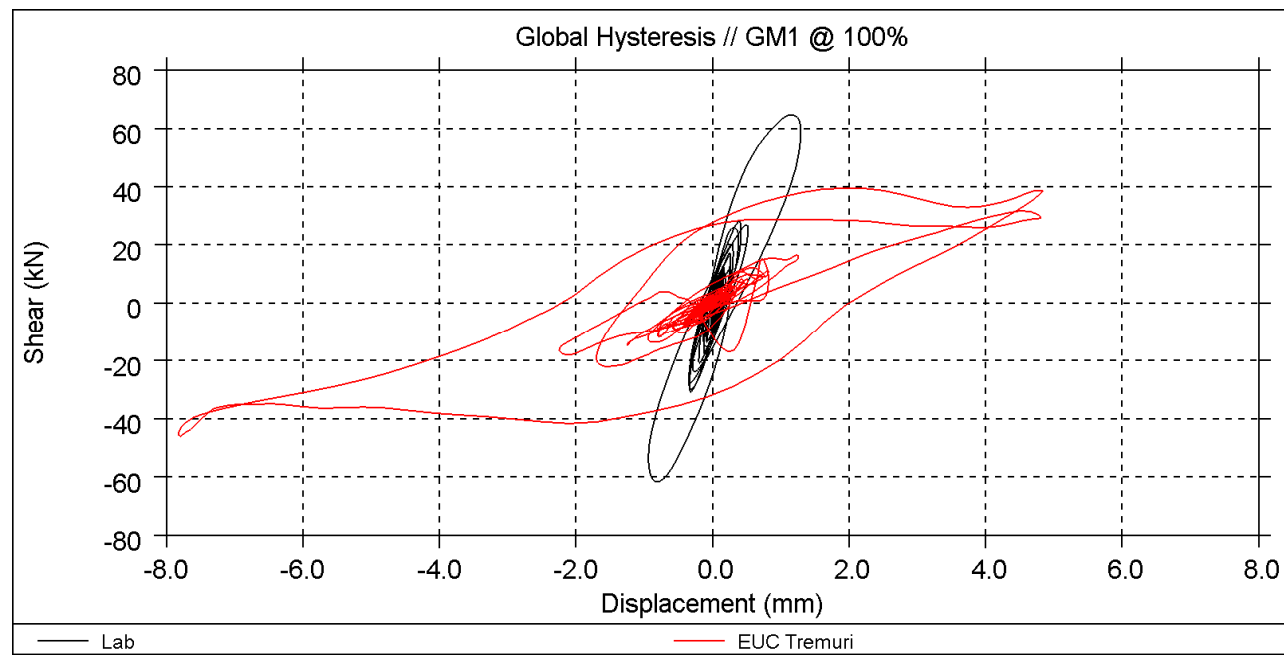
EQ1 at 100%

Global Hysteresis <sup>1</sup>



Arup

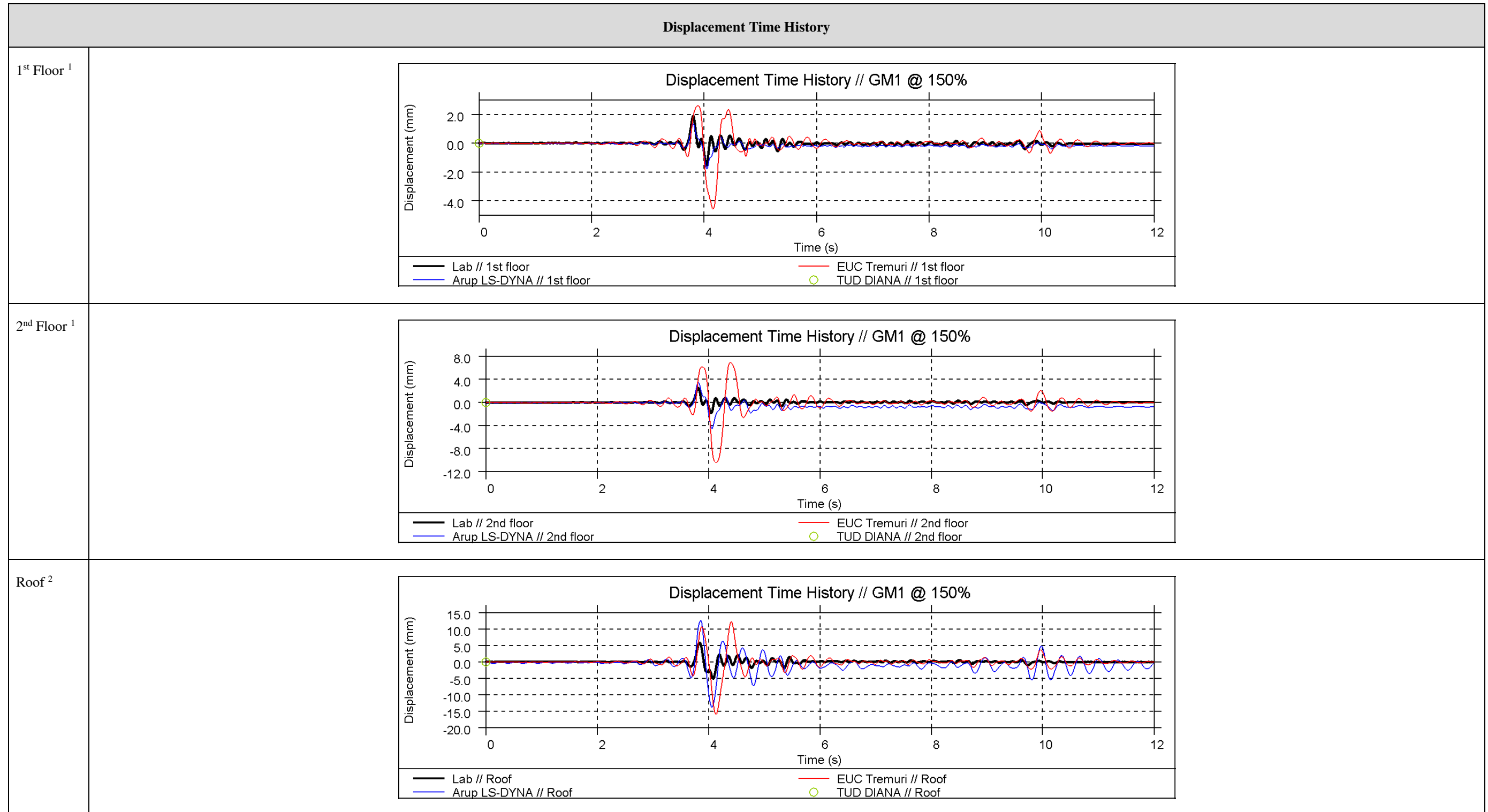
TU-Delft



EUCENTRE

<sup>1</sup> Base shear vs. 2<sup>nd</sup> floor displacement

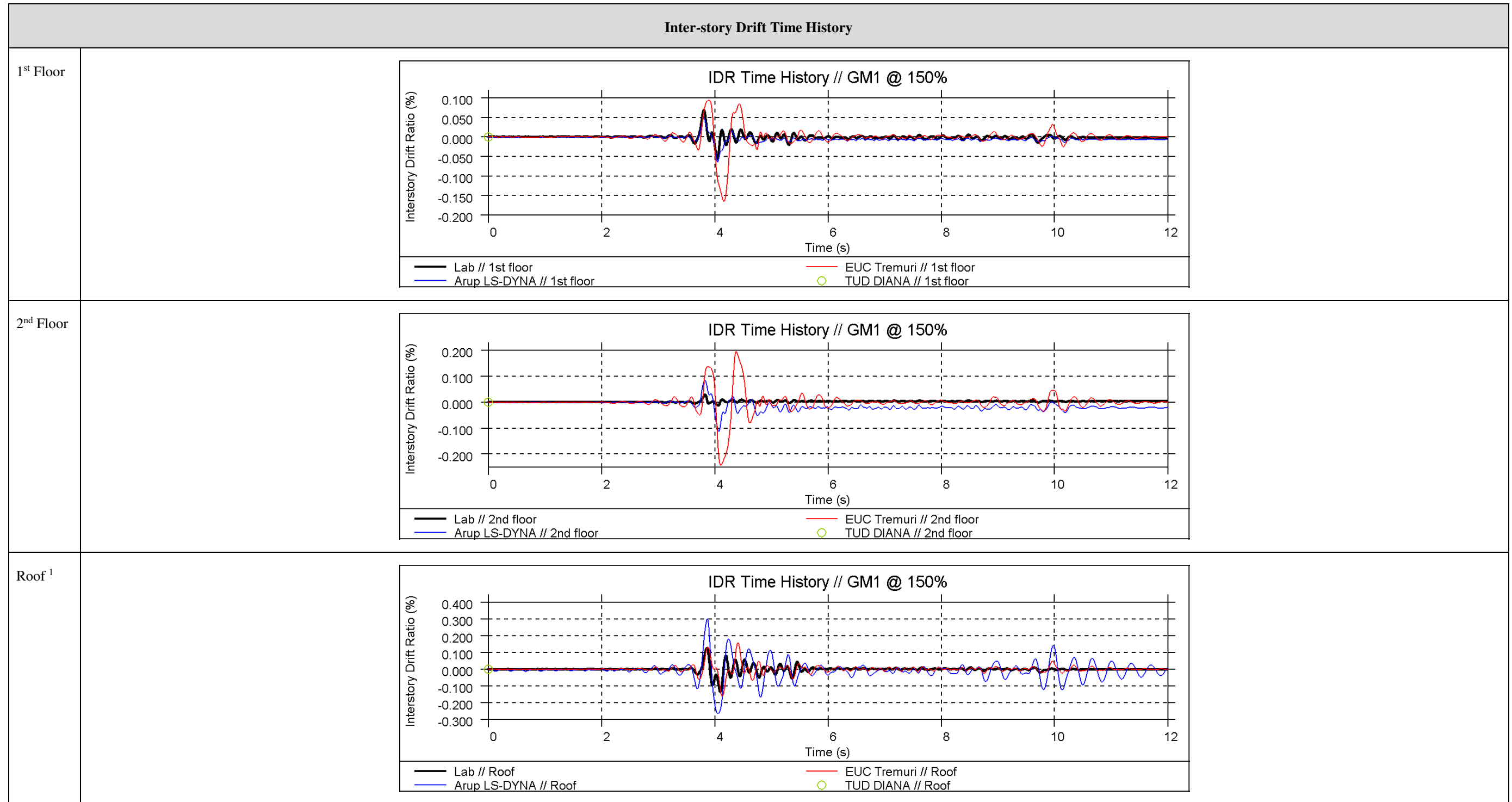
EQ1 at 150%



<sup>1</sup> Displacement of the 1<sup>st</sup> floor and 2<sup>nd</sup> floor is calculated as the average displacement measured at the four corners of the slab

<sup>2</sup> Displacement of the roof is measured as the average displacement at the two ends of the ridge beam

EQ1 at 150%

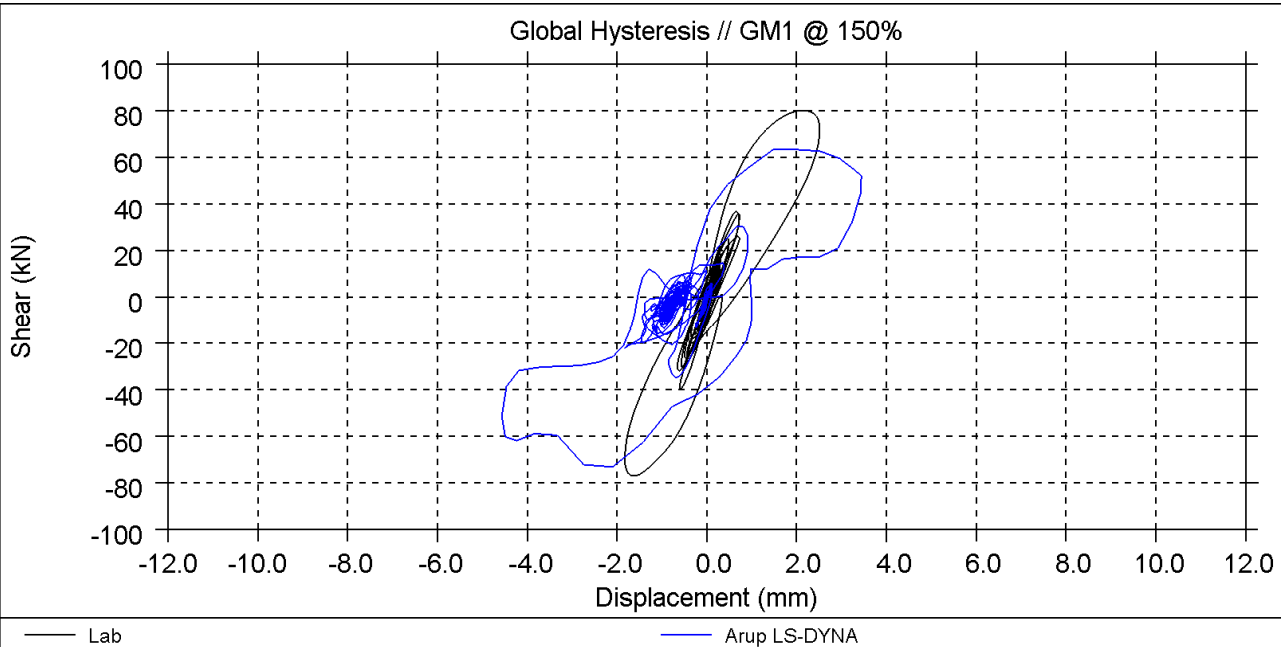
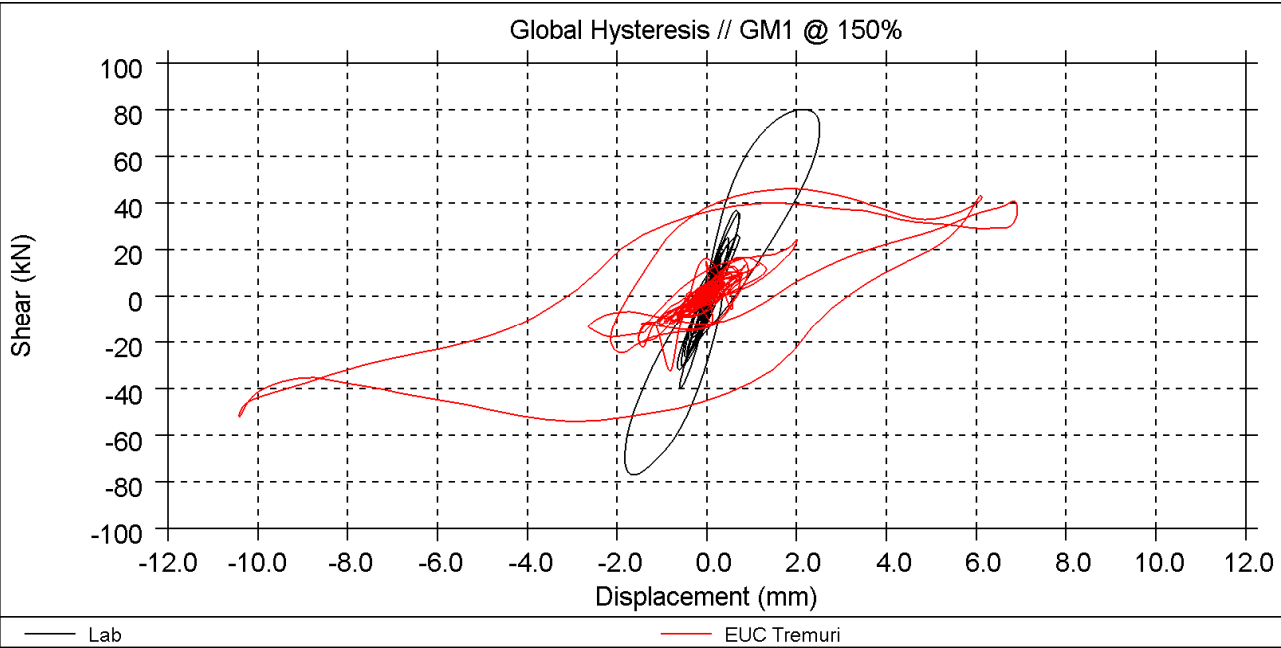


<sup>1</sup> Roof drift is calculated using a diagonal length from the gable peak to the 2<sup>nd</sup> floor along the roof slope (3.5m)

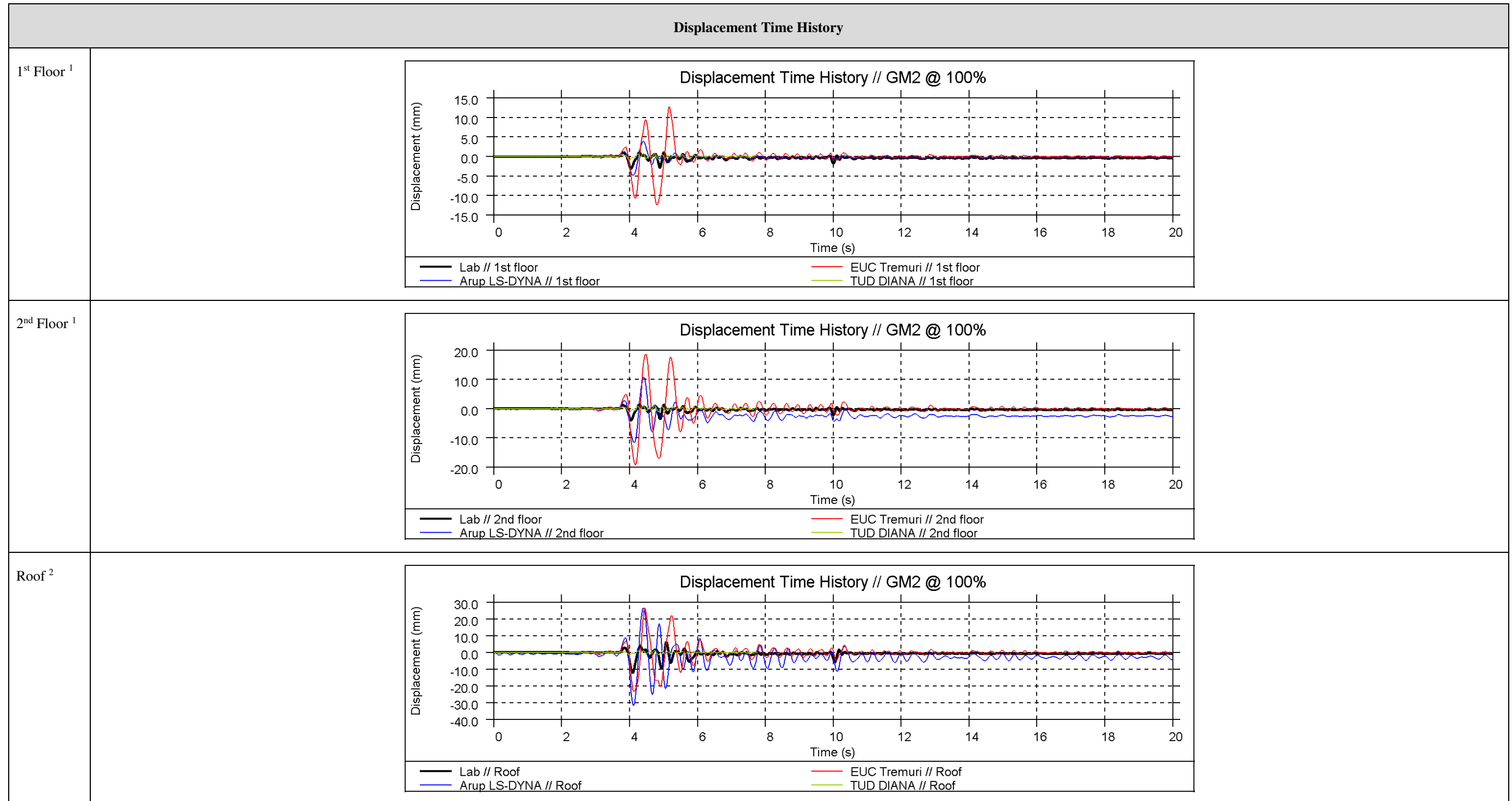




EQ1 at 150%

Global Hysteresis <sup>1</sup>	
	<p>- Results not provided -</p>
<p>Arup</p>	<p>TU-Delft</p>
	
<p>EUCENTRE</p>	<p><sup>1</sup> Base shear vs. 2<sup>nd</sup> floor displacement</p>

EQ2 at 100%



<sup>1</sup> Displacement of the 1<sup>st</sup> floor and 2<sup>nd</sup> floor is calculated as the average displacement measured at the four corners of the slab

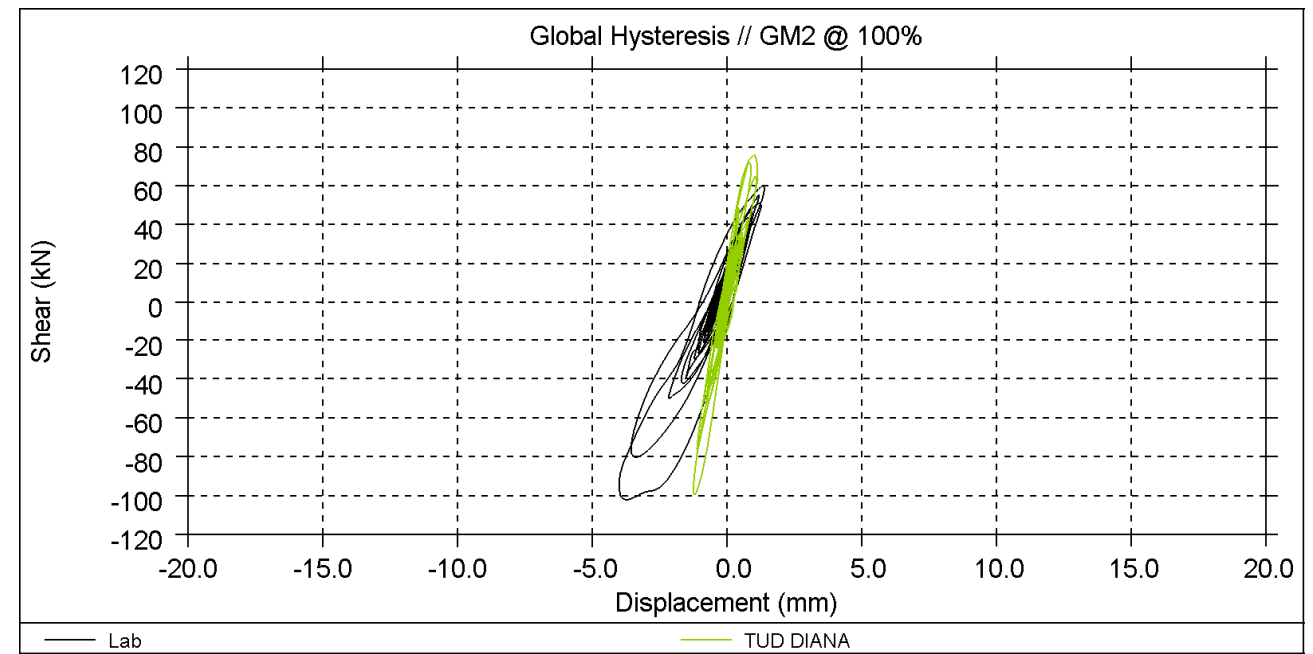
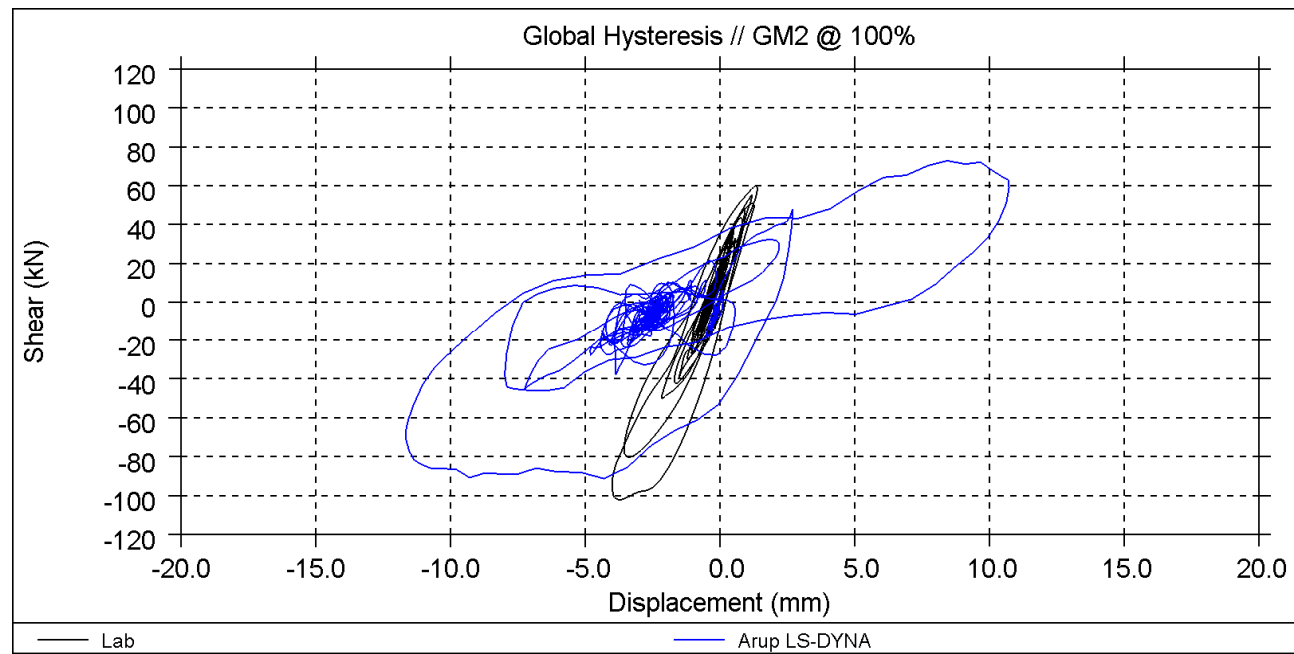
<sup>2</sup> Displacement of the roof is measured as the average displacement at the two ends of the ridge beam





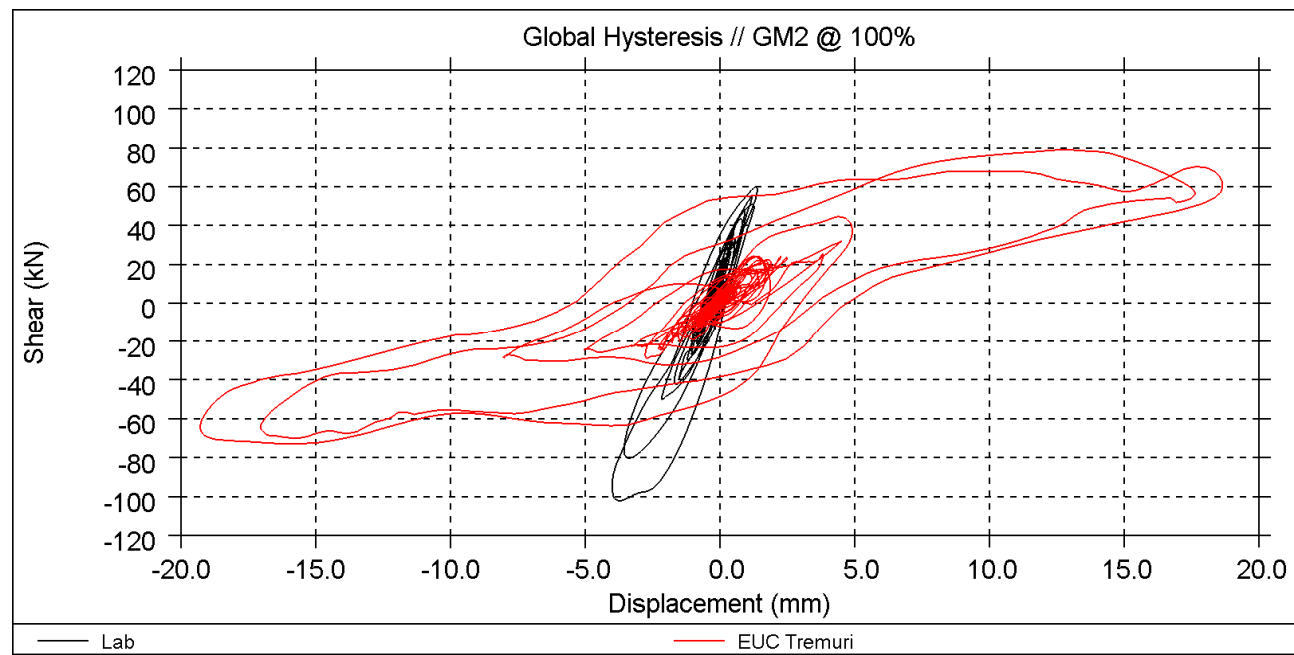
EQ2 at 100%

Global Hysteresis <sup>1</sup>



Arup

TU-Delft



EUCENTRE

<sup>1</sup> Base shear vs. 2<sup>nd</sup> floor displacement

EQ2 at 100%

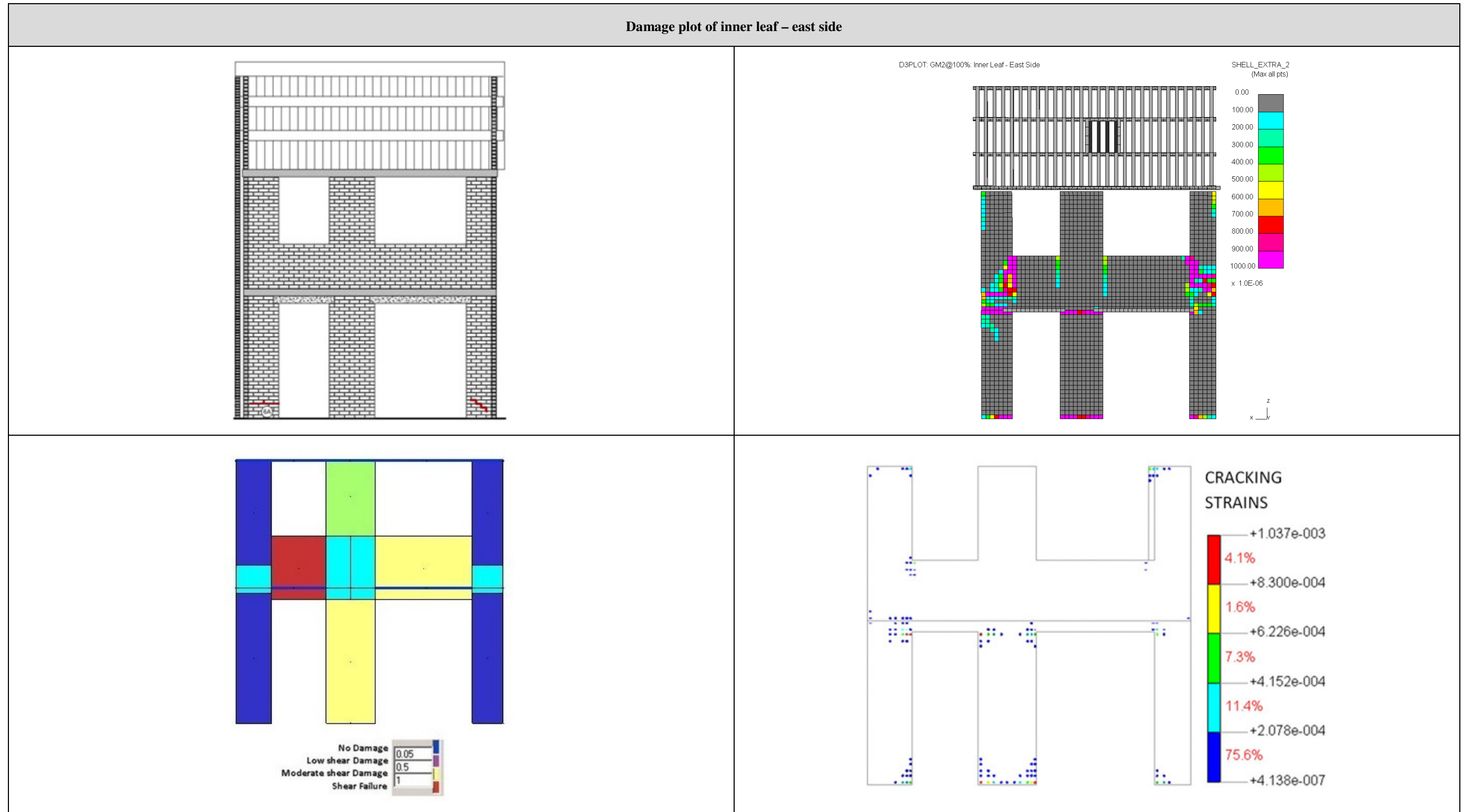


Figure 19: Damage plot of inner leaf - east side of test result (top left), Arup LS-DYNA (top right), EUCENTRE (bottom left), and TU-Delft (bottom right)

EQ2 at 100%

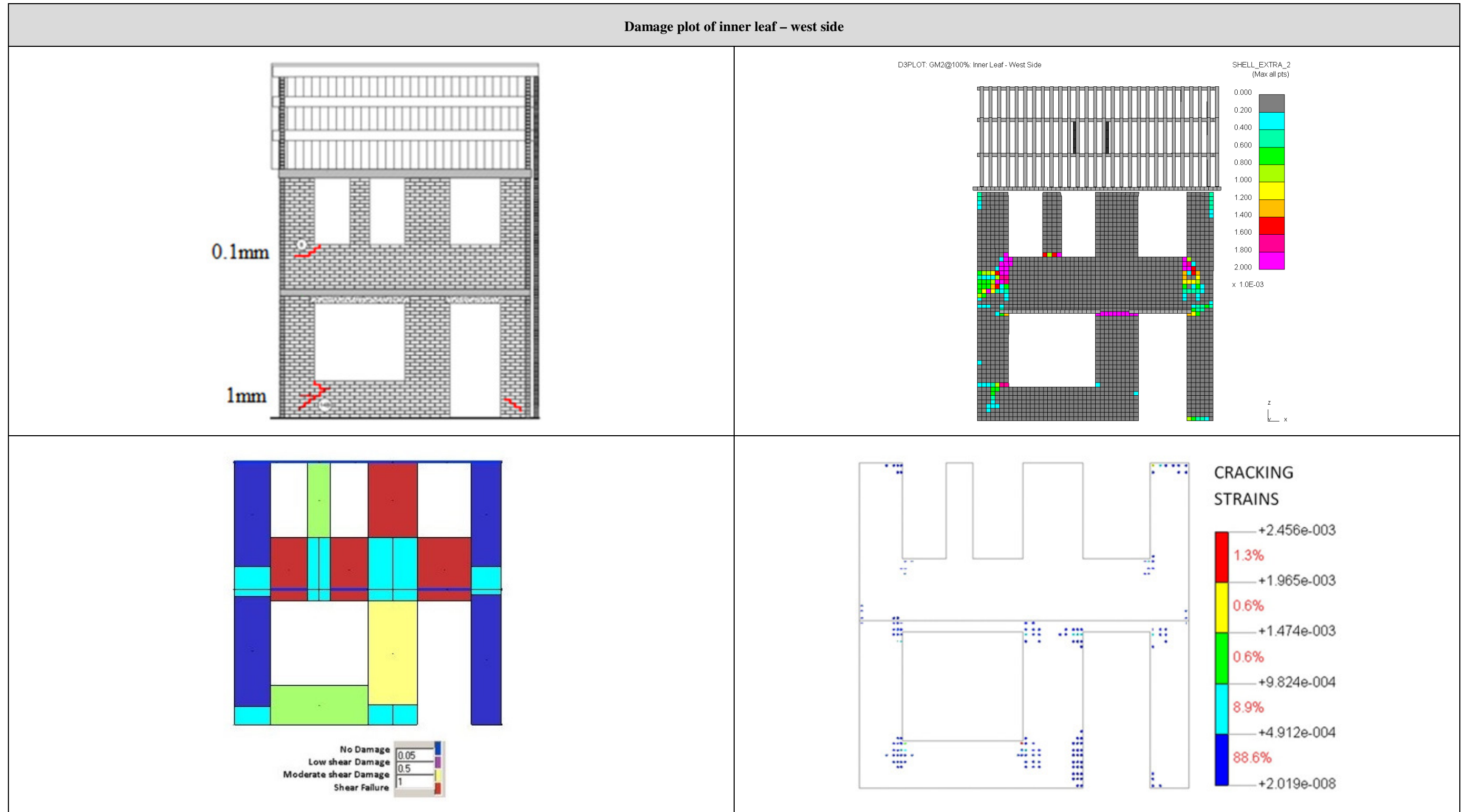
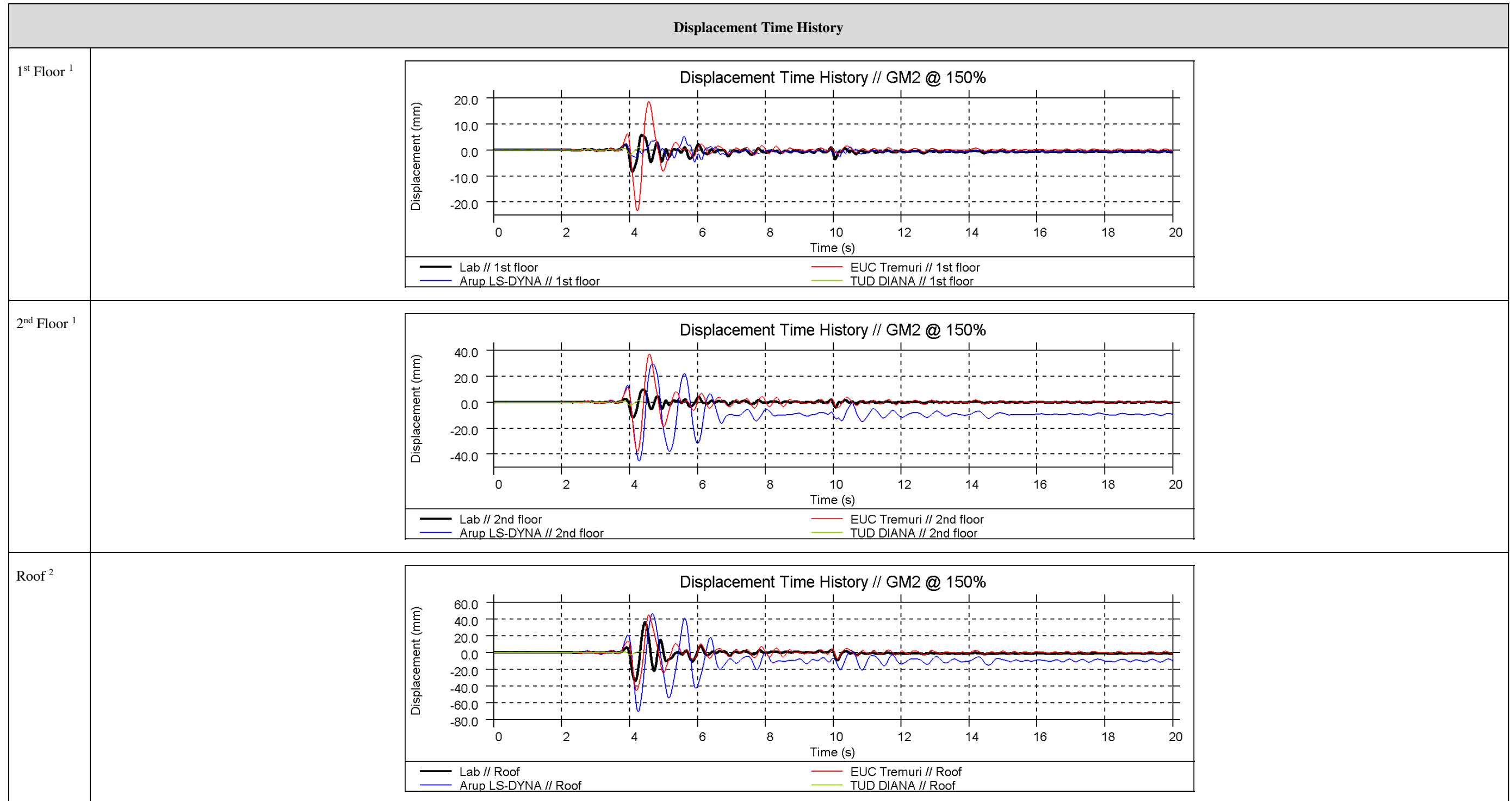


Figure 20: Damage plot of inner leaf - west side of test result (top left), Arup LS-DYNA (top right), EUCENTRE (bottom left), and TU-Delft (bottom right)



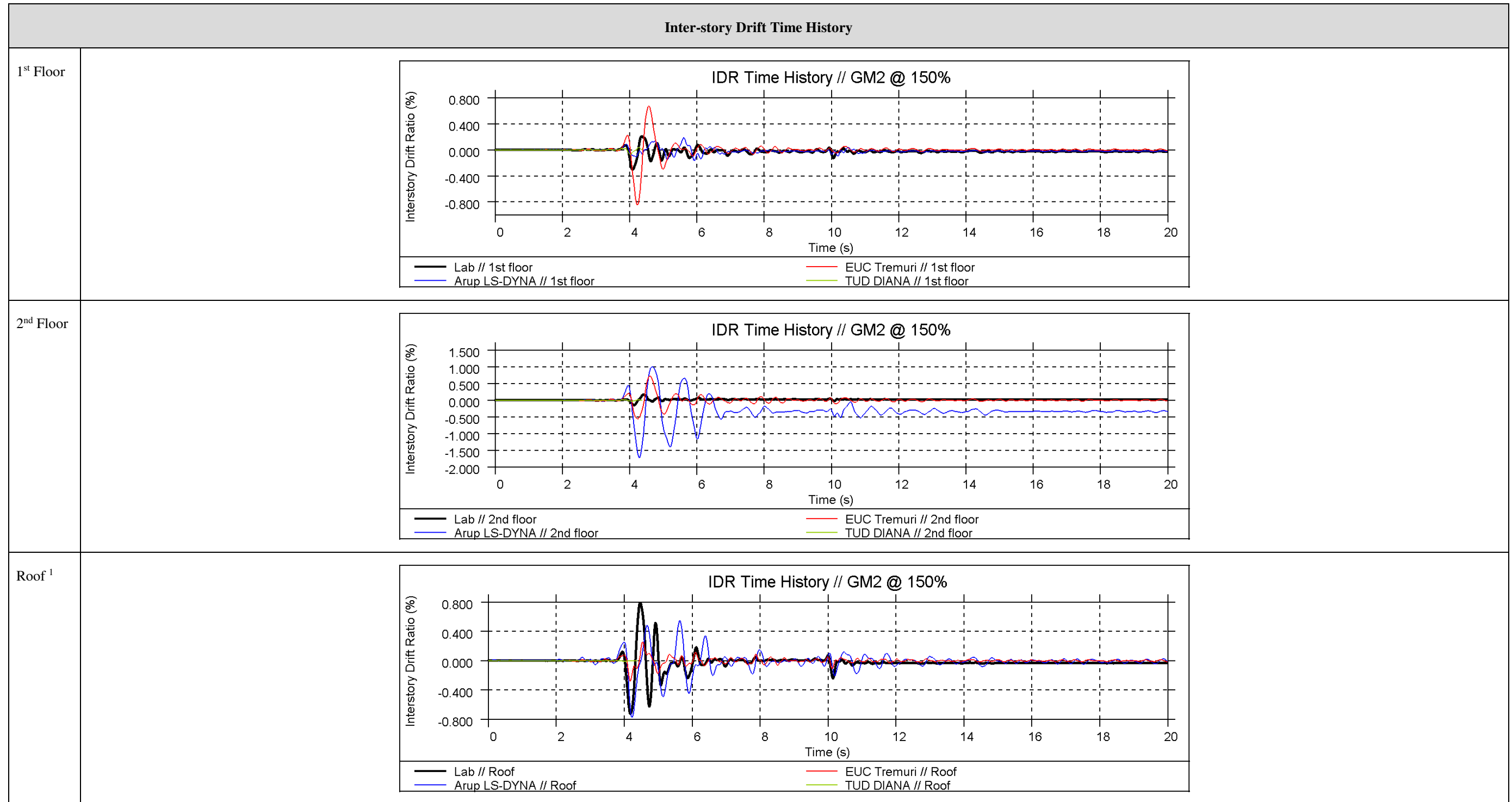
EQ2 at 150%



<sup>1</sup> Displacement of the 1<sup>st</sup> floor and 2<sup>nd</sup> floor is calculated as the average displacement measured at the four corners of the slab

<sup>2</sup> Displacement of the roof is measured as the average displacement at the two ends of the ridge beam

EQ2 at 150%

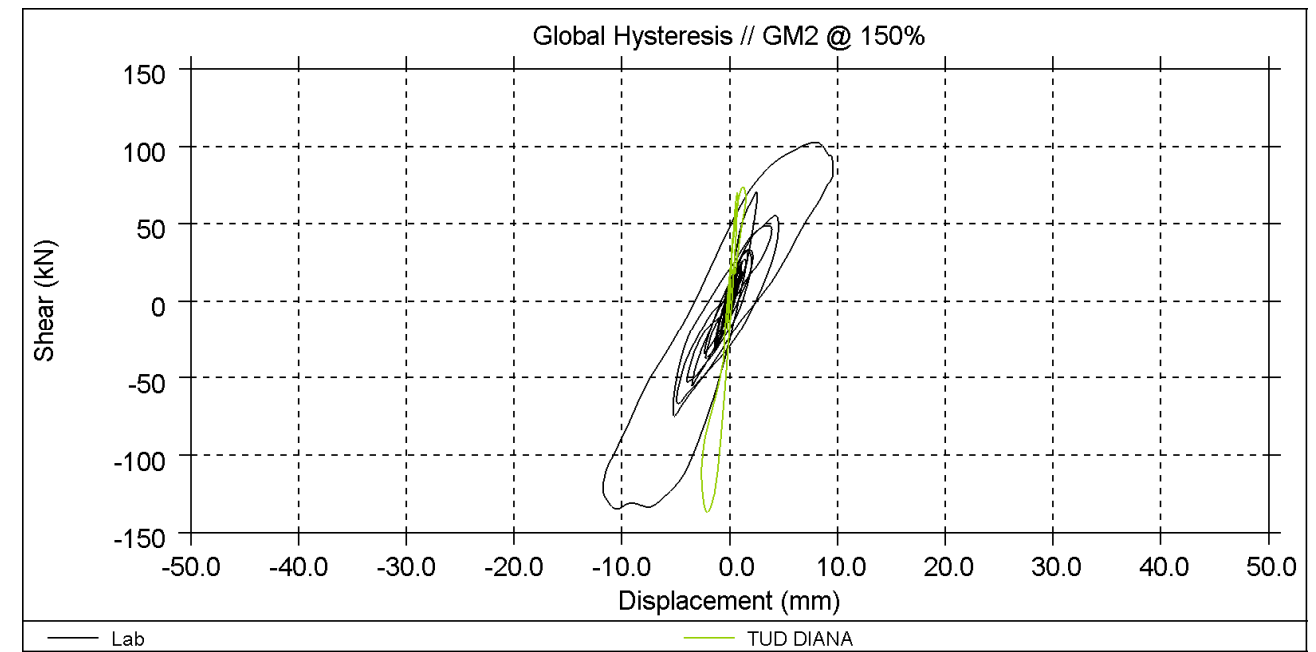
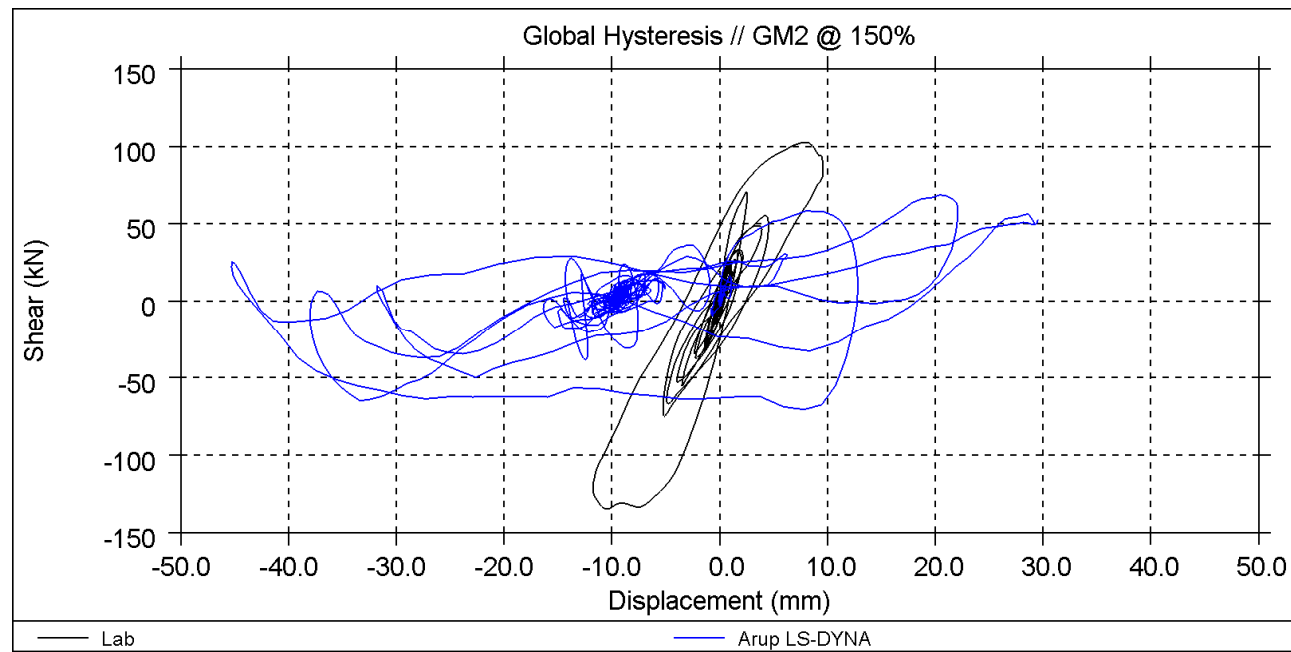


<sup>1</sup> Roof drift is calculated using a diagonal length from the gable peak to the 2<sup>nd</sup> floor along the roof slope (3.5m)



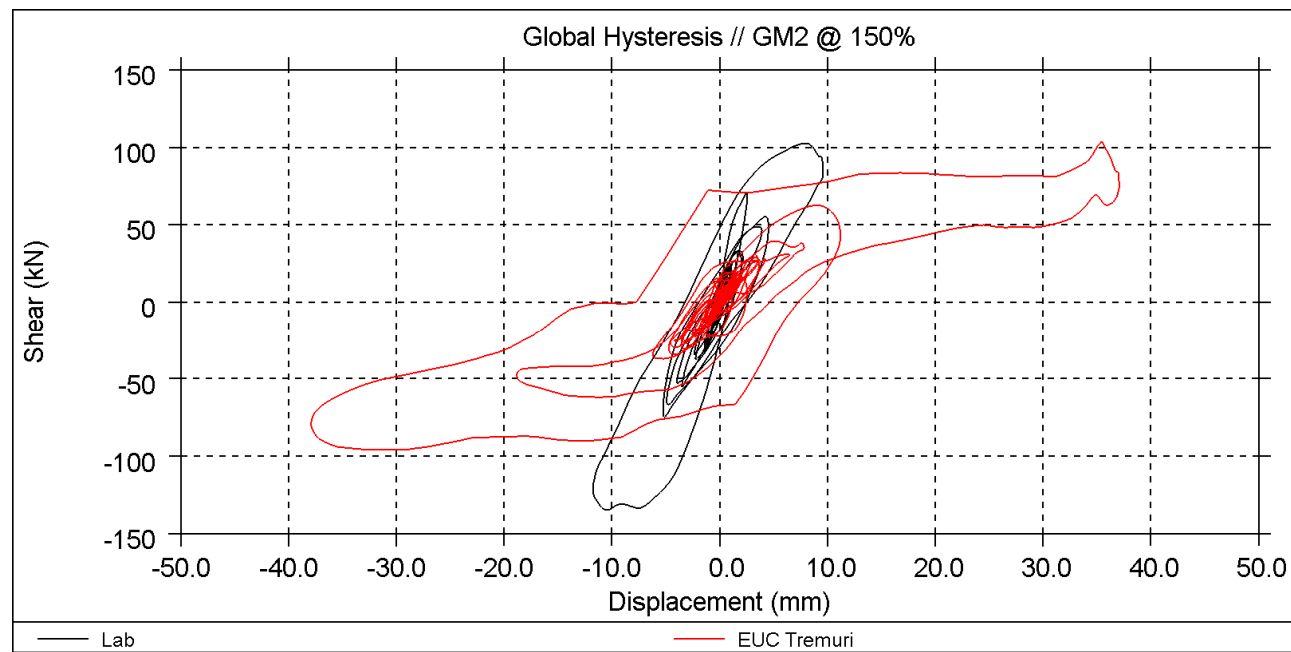
EQ2 at 150%

Global Hysteresis <sup>1</sup>



Arup

TU-Delft



EUCENTRE

<sup>1</sup> Base shear vs. 2<sup>nd</sup> floor displacement

EQ2 at 150%

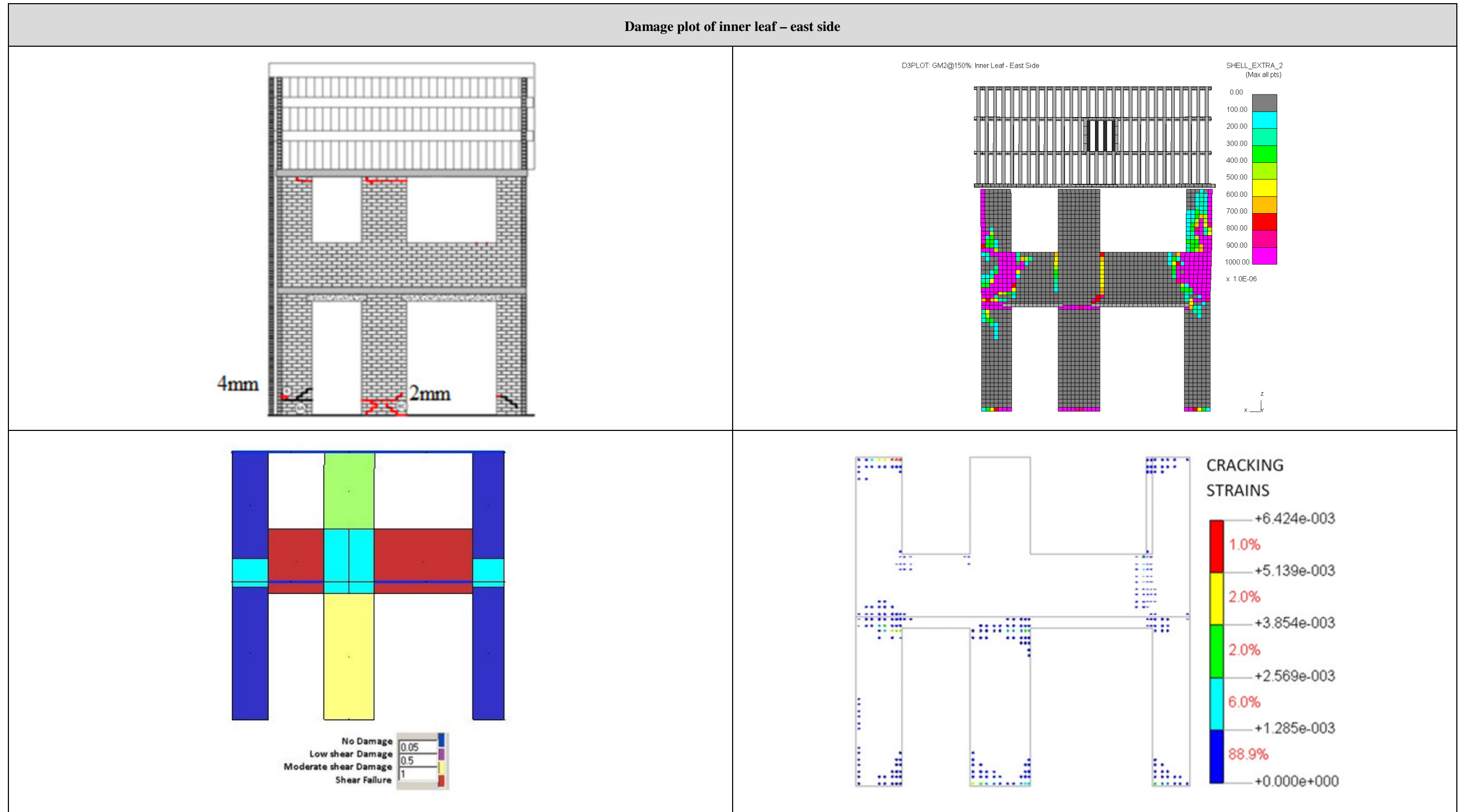


Figure 21: Damage plot of inner leaf - east side of test result (top left), Arup LS-DYNA (top right), EUCENTRE (bottom left), and TU-Delft (bottom right)

EQ2 at 150%

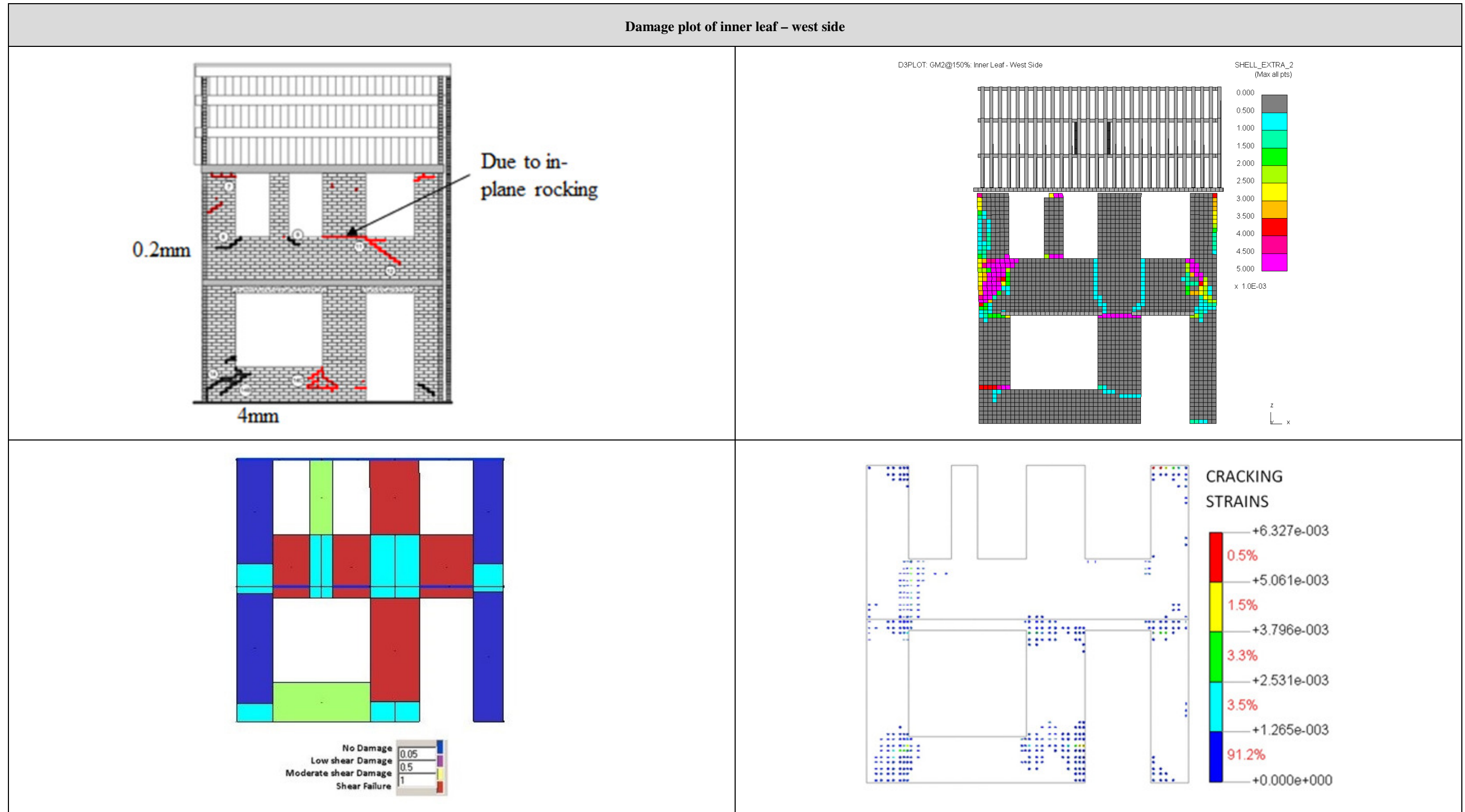
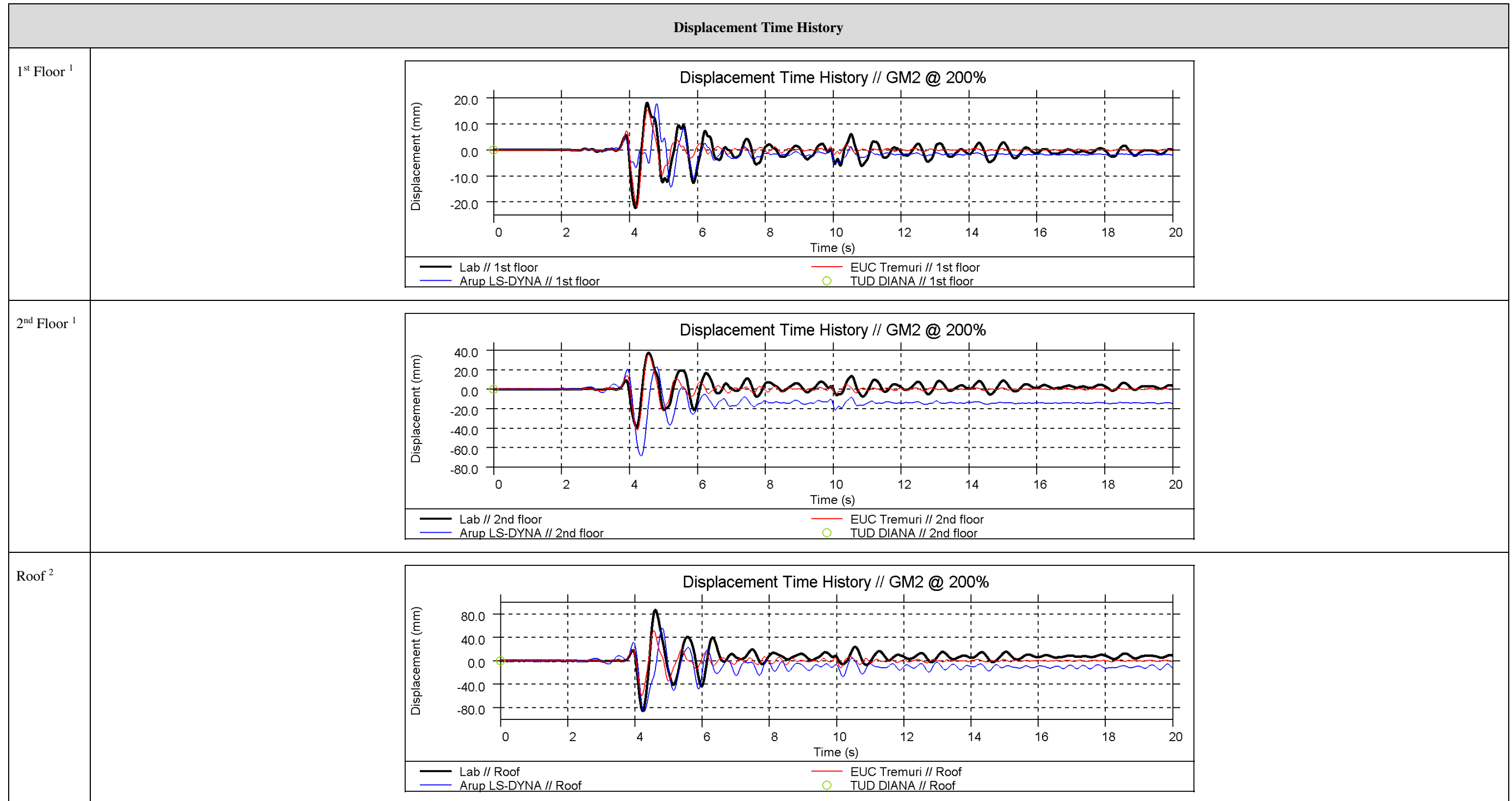


Figure 22: Damage plot of inner leaf - west side of test result (top left), Arup LS-DYNA (top right), EUCENTRE (bottom left), and TU-Delft (bottom right)

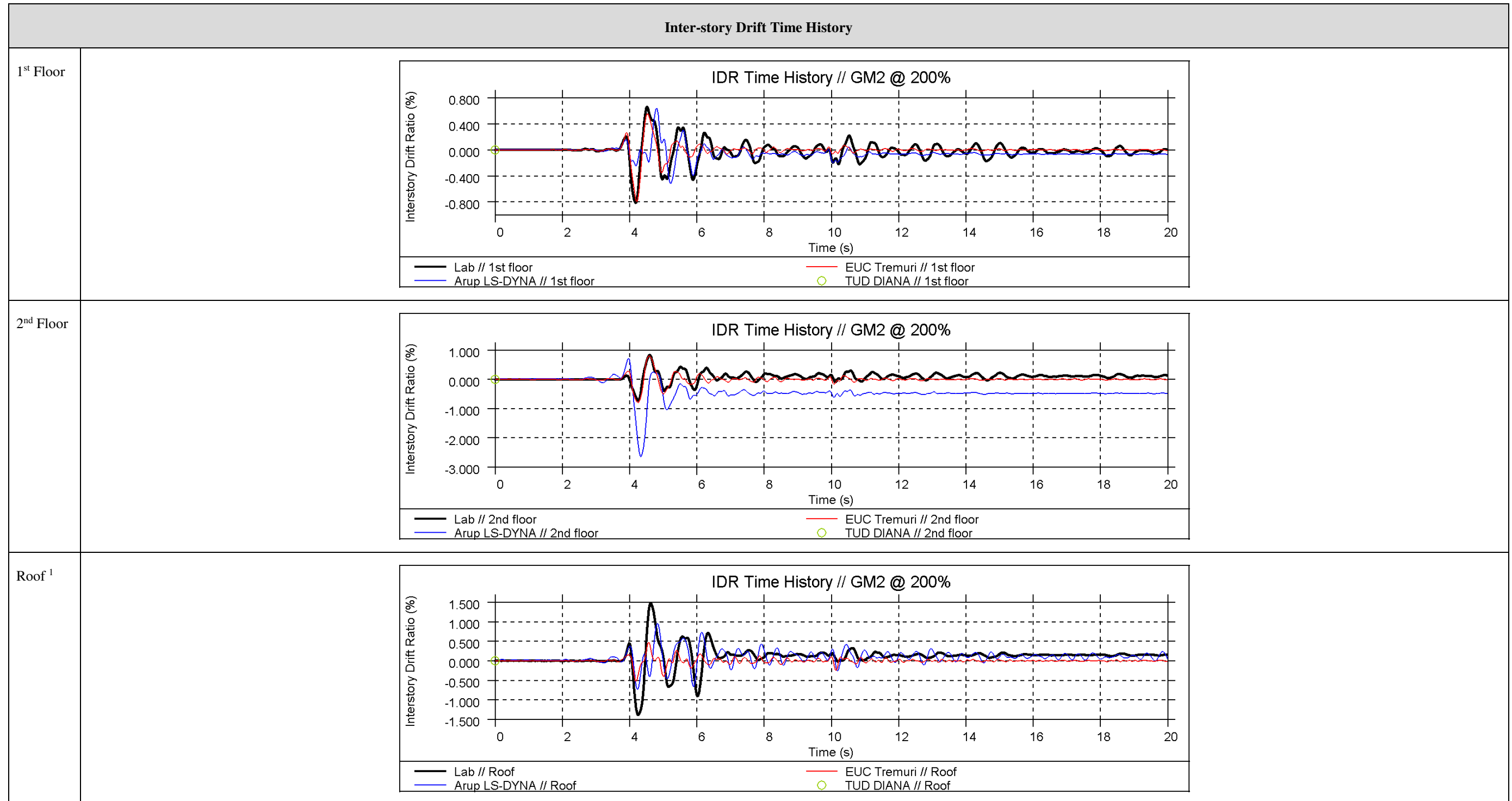
EQ2 at 200%



<sup>1</sup> Displacement of the 1<sup>st</sup> floor and 2<sup>nd</sup> floor is calculated as the average displacement measured at the four corners of the slab

<sup>2</sup> Displacement of the roof is measured as the average displacement at the two ends of the ridge beam

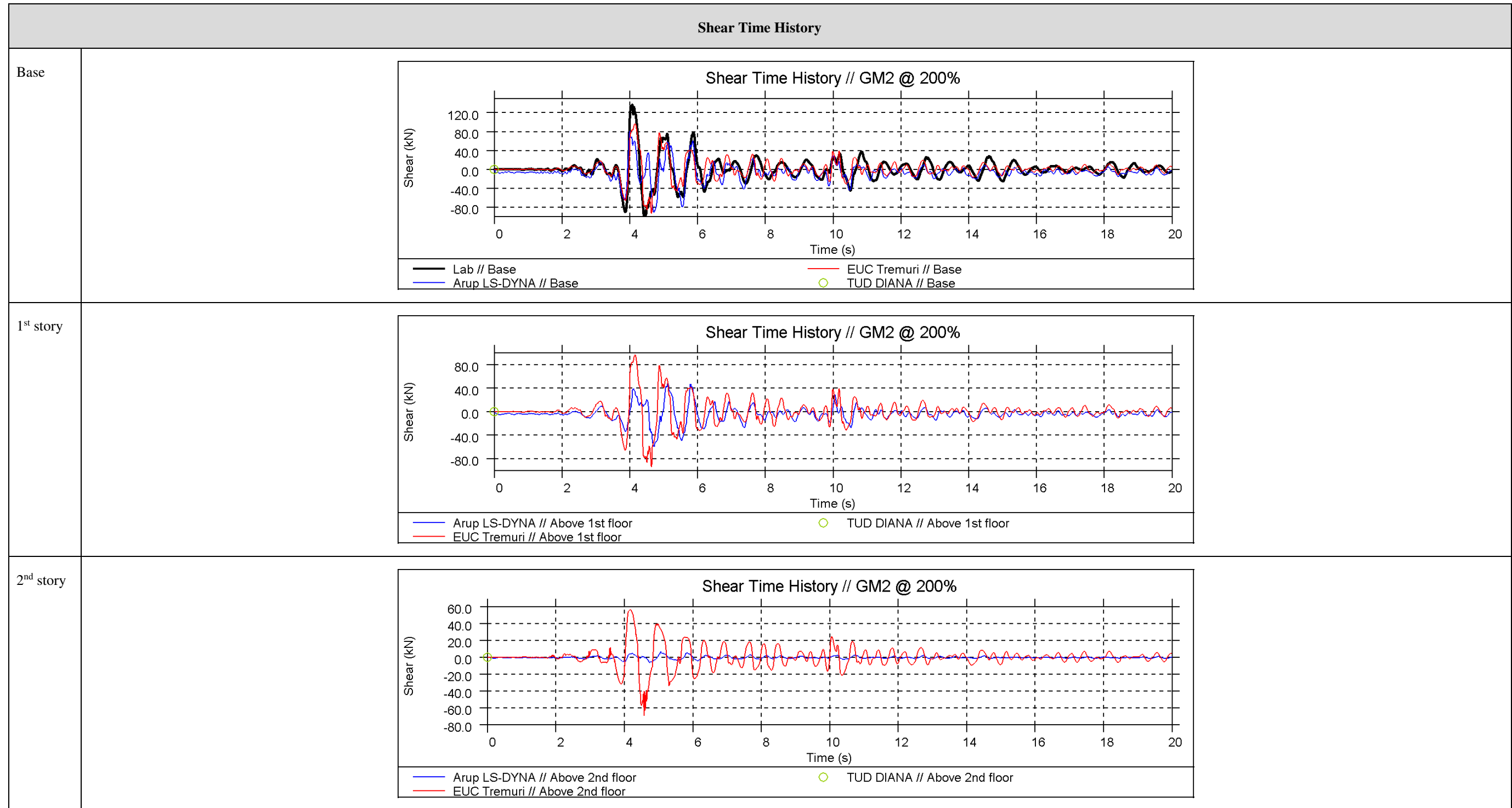
EQ2 at 200%



<sup>1</sup> Roof drift is calculated using a diagonal length from the gable peak to the 2<sup>nd</sup> floor along the roof slope (3.5m)



EQ2 at 200%



EQ2 at 200%

Global Hysteresis <sup>1</sup>	
<p style="text-align: center;">Global Hysteresis // GM2 @ 200%</p> <p>Shear (kN)</p> <p>Displacement (mm)</p> <p>— Lab      — Arup LS-DYNA</p>	<p>- Results not provided -</p>
<p>Arup</p> <p style="text-align: center;">Global Hysteresis // GM2 @ 200%</p> <p>Shear (kN)</p> <p>Displacement (mm)</p> <p>— Lab      — EUC Tremuri</p>	<p>TU-Delft</p>
<p>EUCENTRE</p>	<p><sup>1</sup> Base shear vs. 2<sup>nd</sup> floor displacement</p>

EQ2 at 200%

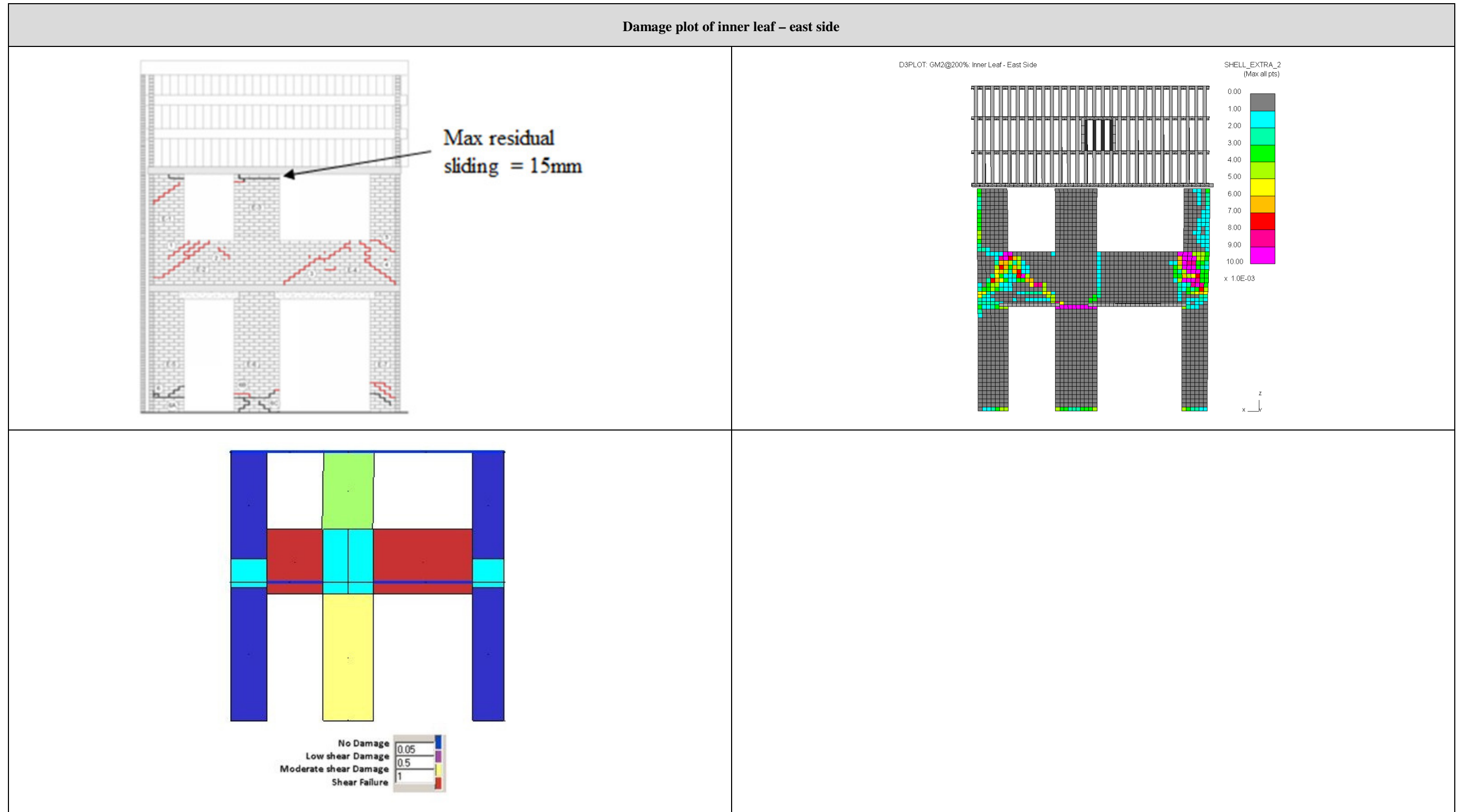


Figure 23: Damage plot of inner leaf - east side of test result (top left), Arup LS-DYNA (top right), and EUCENTRE (bottom left)

EQ2 at 200%

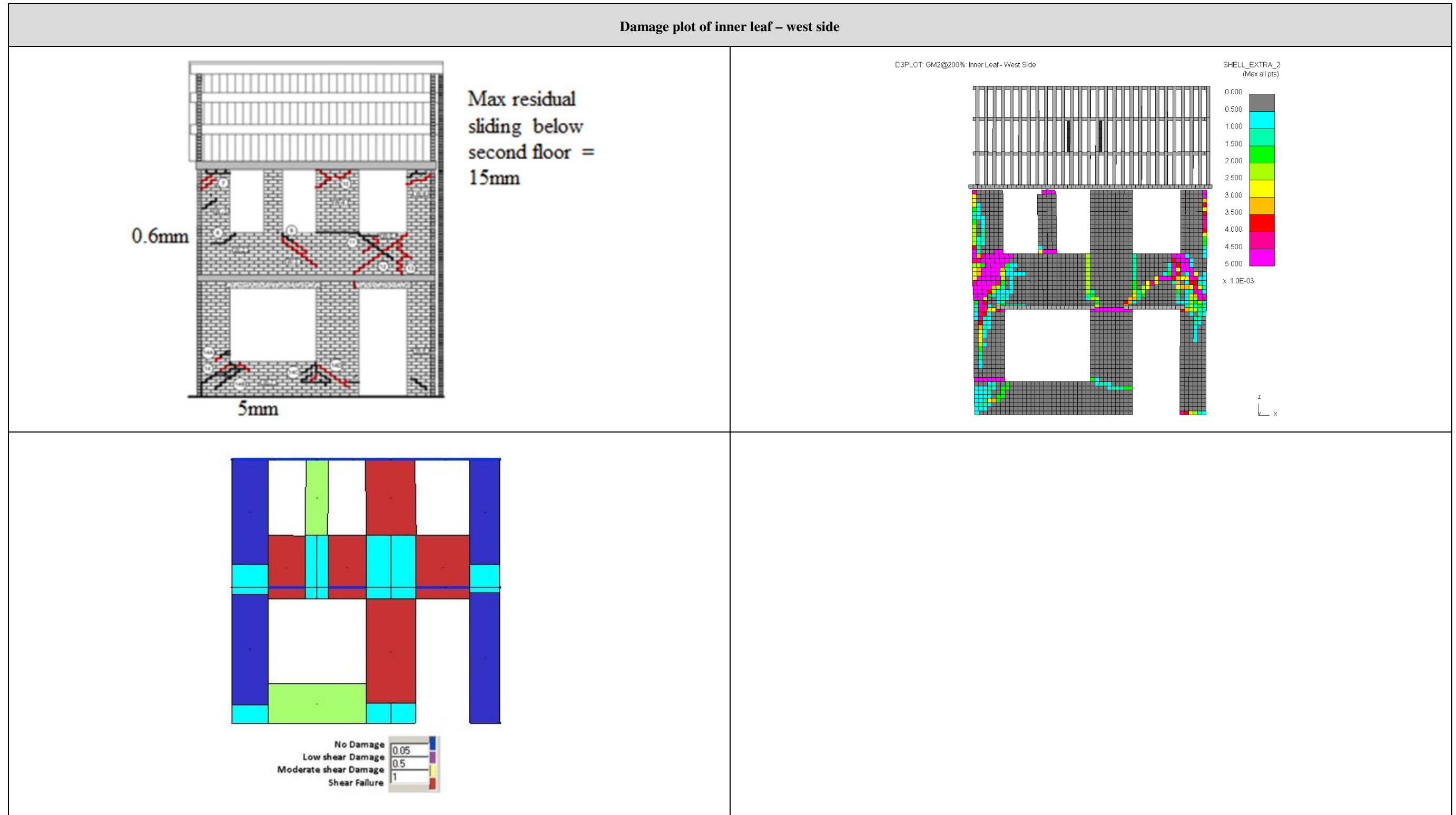


Figure 24: Damage plot of inner leaf - west side of test result (top left), Arup LS-DYNA (top right), and EUCENTRE (bottom left)

EQ2 at 200%

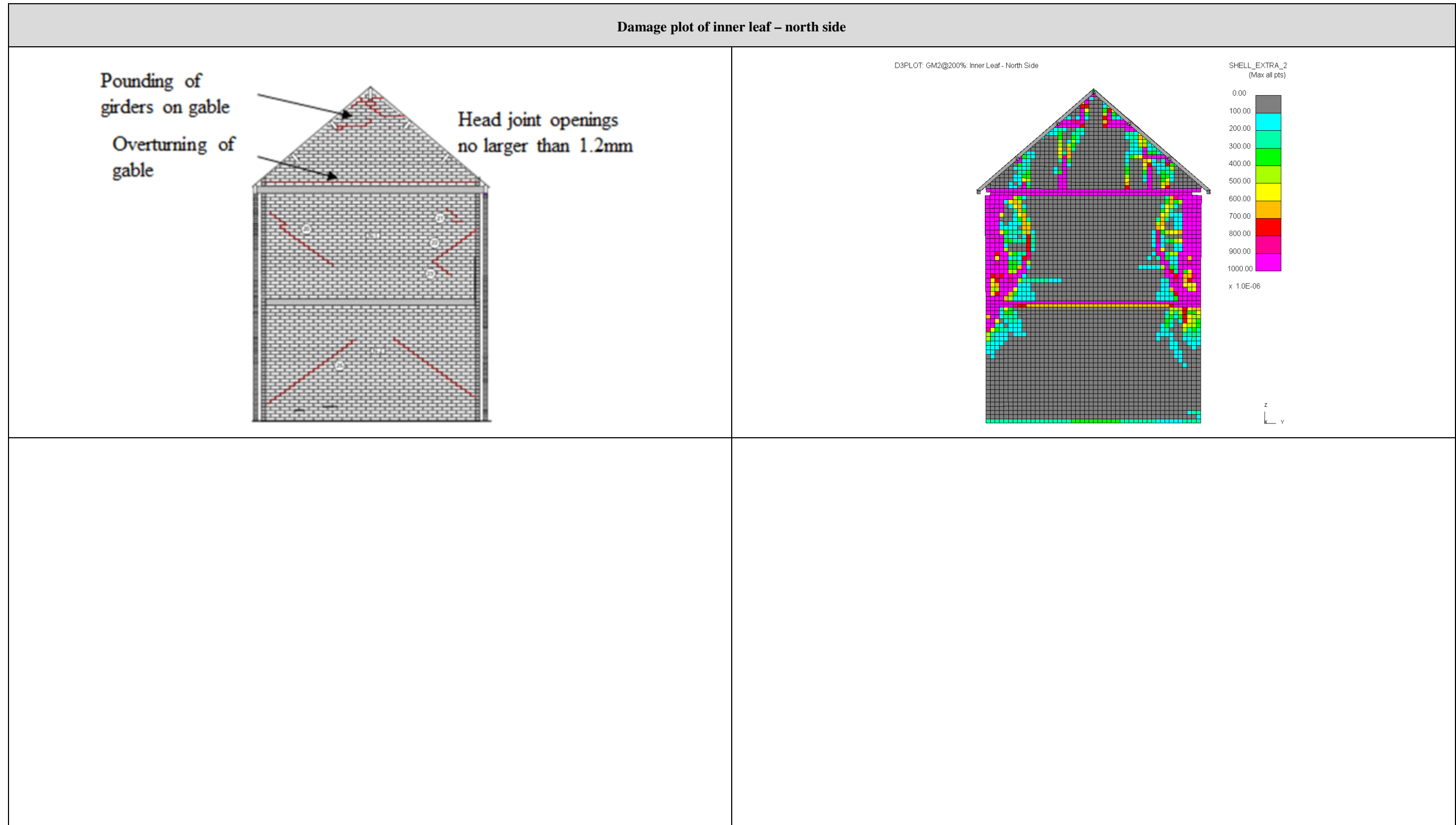


Figure 25: Damage plot of inner leaf - north side of test result (top left) and Arup LS-DYNA (top right)

EQ2 at 200%

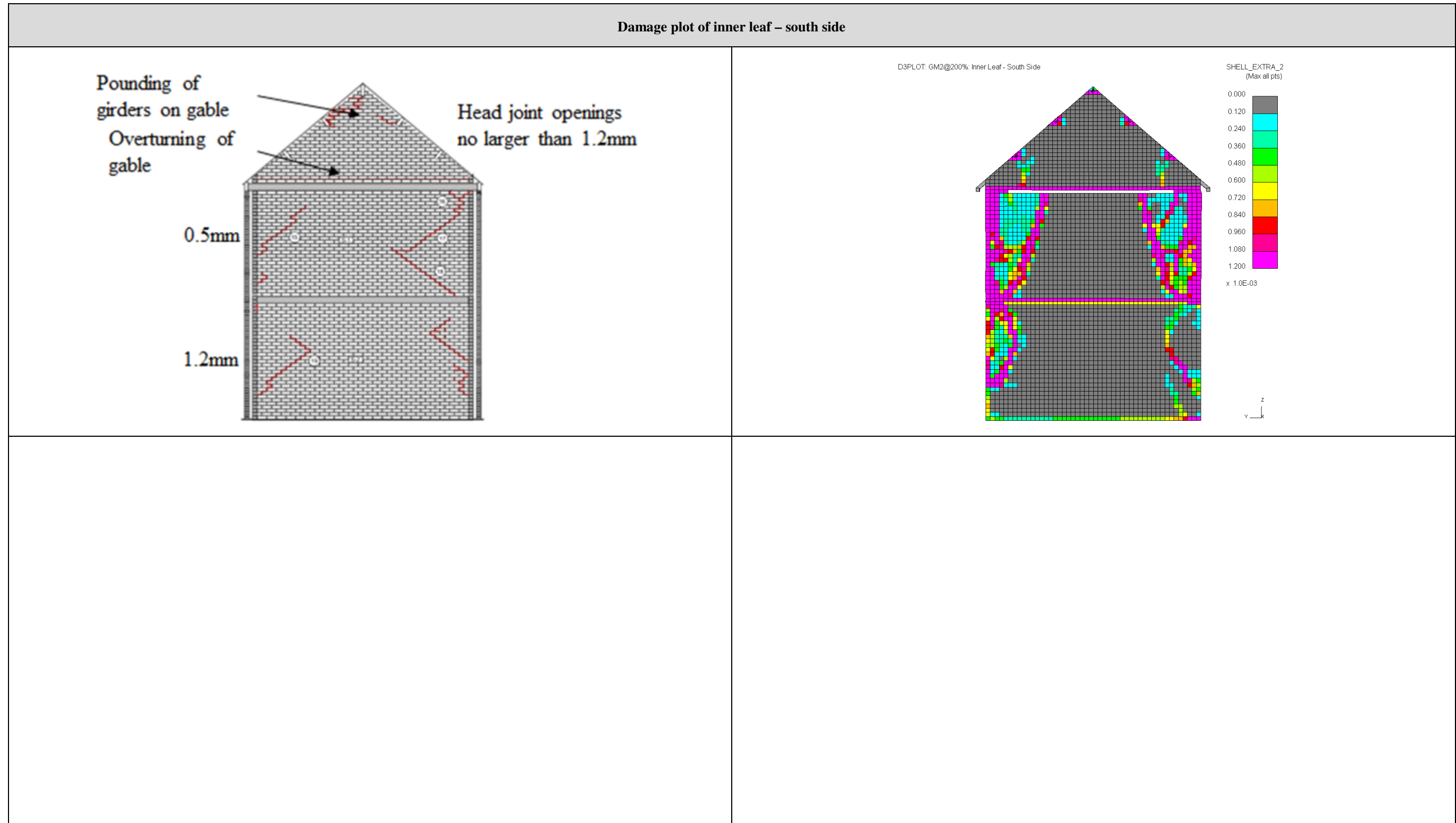


Figure 26: Damage plot of inner leaf - south side of test result (top left) and Arup LS-DYNA (top right)

EQ2 at 200%

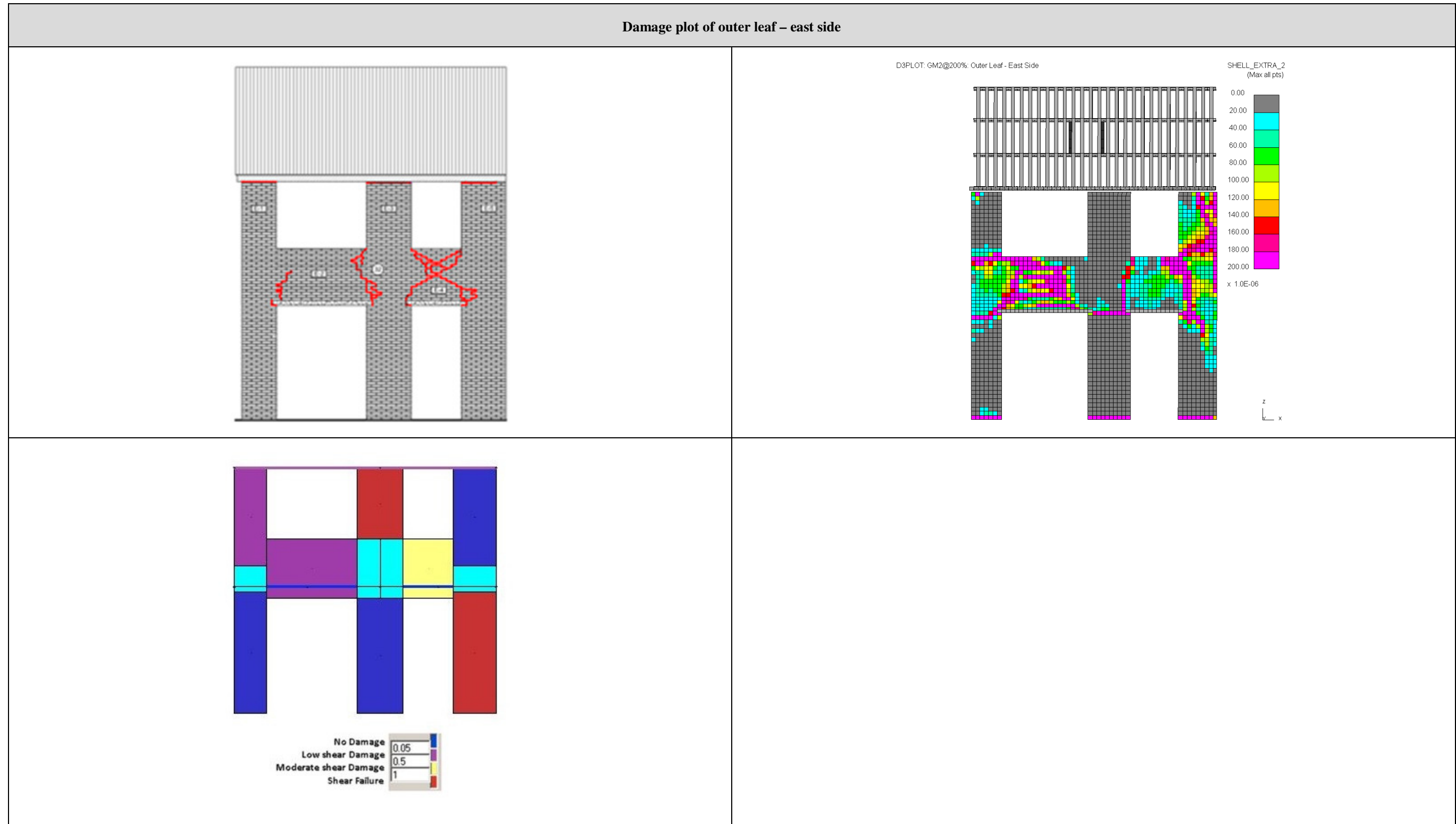


Figure 27: Damage plot of outer leaf - east side of test result (top left), Arup LS-DYNA (top right), and EUCENTRE (bottom left)

EQ2 at 200%

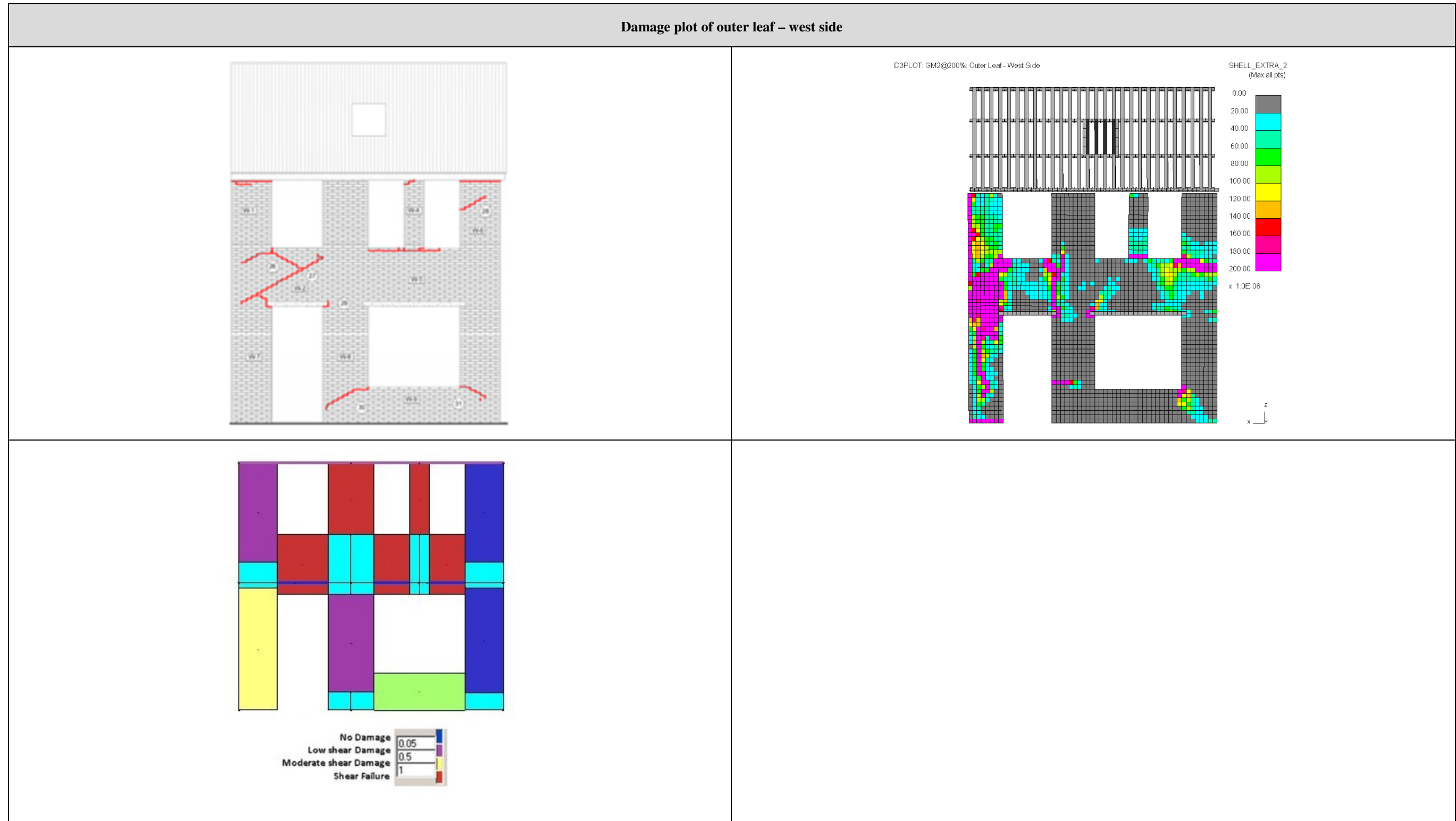


Figure 28: Damage plot of outer leaf - west side of test result (top left), Arup LS-DYNA (top right), and EUCENTRE (bottom left)



EQ2 at 200%

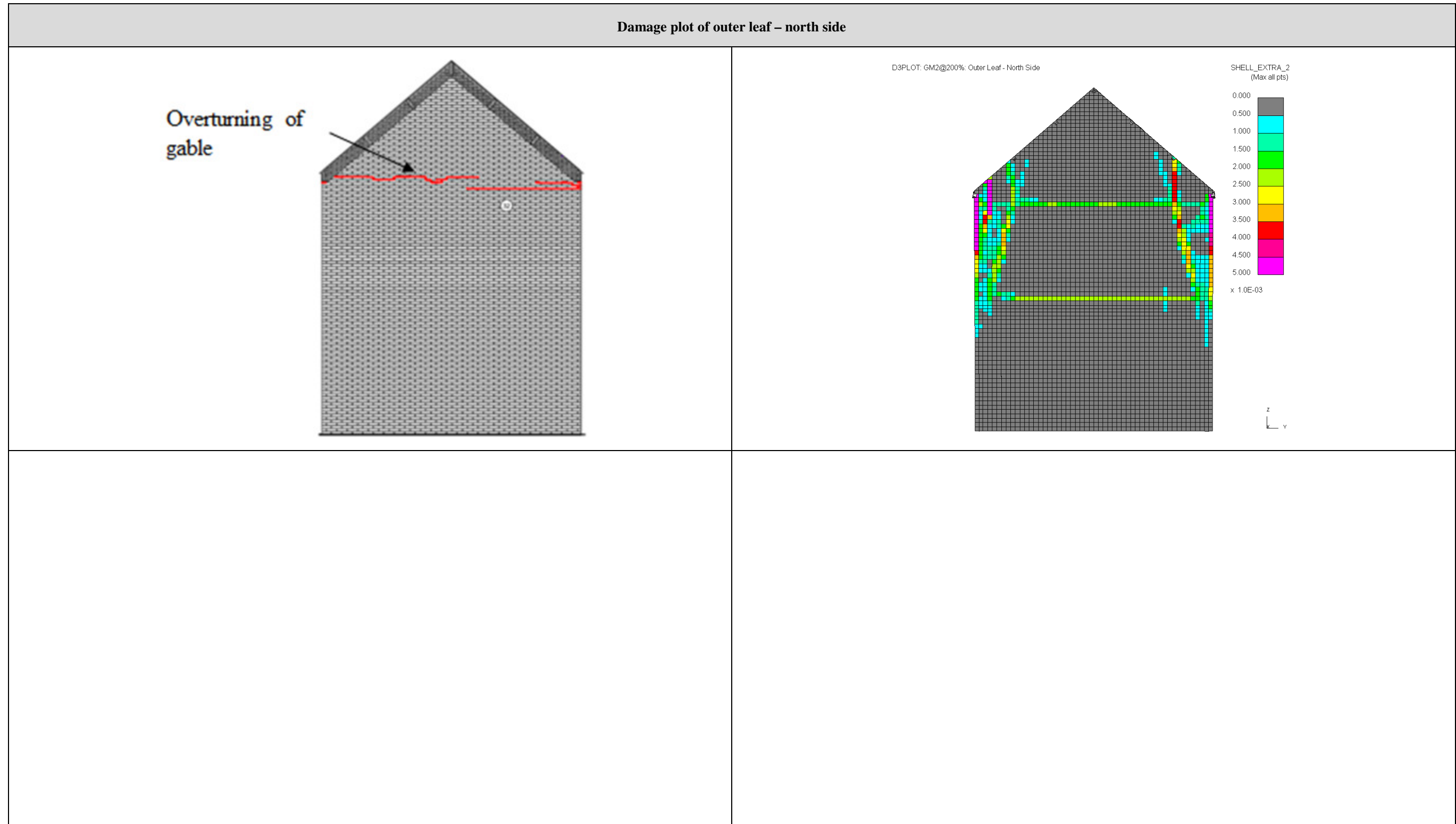


Figure 29: Damage plot of outer leaf - north side of test result (top left) and Arup LS-DYNA (top right)

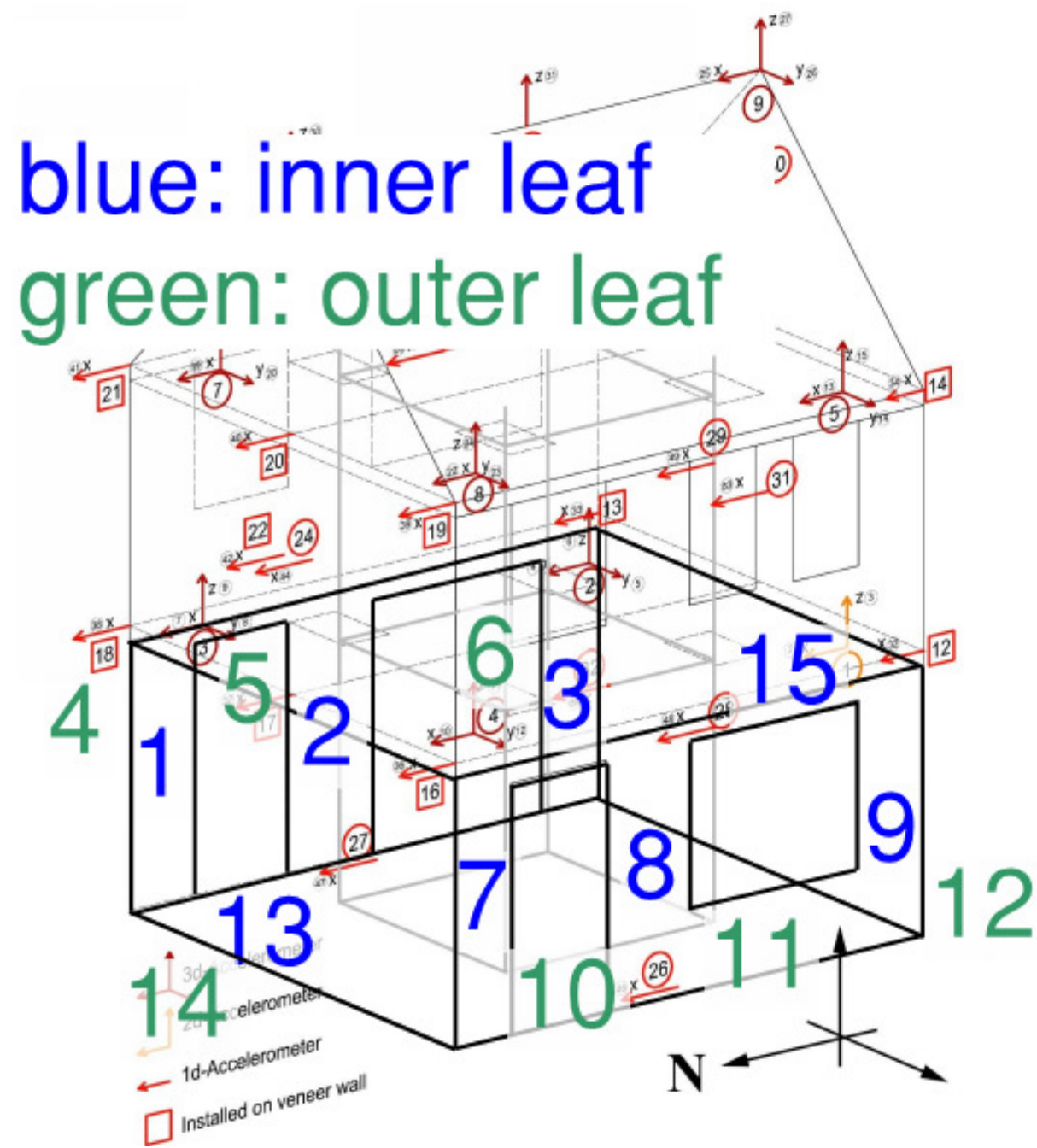


Figure 30: Legend for pier labelling. Refer to tables below

Table 16: Axial force summary (kN) <sup>1</sup>

		Total	East wall, inner			East wall, outer			West wall, inner			West wall, outer			North wall, inner	North wall, outer	South wall
			Pier 1	Pier 2	Pier 3	Pier 4	Pier 5	Pier 6	Pier 7	Pier 8	Pier 9	Pier 10	Pier 11	Pier 12	Pier 13	Pier 14	Pier 15
t = 0	Arup	552	21.2	19.0	18.7	10.9	13.5	9.2	18.6	16.5	15.8	9.7	12.6	8.4	146	63.3	150
	EUCENTRE <sup>2</sup>	541	37.0	12.5	37.0	10.5	12.3	8.4	35.6	14.8	40.3	9.1	14.5	11.2	120	56.9	120
	TU-Delft	527	16.7	16.0	16.0	16.1	19.9	19.6	14.8	14.3	15.4	14.3	17.8	18.7	112	86.8	128.8
EQ1 @ 50%	Arup	553	27.1	20.6	12.6	14.8	15.5	10.3	23.0	11.8	15.9	12.5	11.1	11.9	125	49.9	171
	EUCENTRE	543	41.0	12.8	8.2	8.2	12.2	8.2	38.3	17.9	35.3	7.1	14.4	11.1	126	63.5	114
	TU-Delft																
EQ1 @ 100%	Arup	552	7.1	17.9	30.6	5.4	11.3	7.6	7.9	23.0	16.4	4.9	15.0	3.8	191	81.9	109
	EUCENTRE	549	42.7	13.6	32.6	6.0	12.1	7.8	41.8	20.2	35.5	4.7	14.7	10.4	131	69.2	107
	TU-Delft	523	28.0	19.4	6.8	29.9	26.7	24.0	23.8	8.1	14.1	24.7	13.3	28.9	80.6	30.3	165
EQ1 @ 150%	Arup	558	36.4	25.3	1.0	16.8	17.5	11.2	30.2	7.1	8.2	14.1	10.2	14.0	89.1	40.8	209
	EUCENTRE	557	43.3	14.5	33.2	7.2	11.2	7.5	41.0	20.7	37.8	4.8	14.4	10.0	135	72.7	104
	TU-Delft																

<sup>1</sup> Unless noted otherwise, reported axial forces occur at time "A." Time "A" is the time at which the total base shear force is the absolute maximum during that run

Table 17: Axial force summary (kN) (continued)<sup>1</sup>

		Total	East wall, inner			East wall, outer			West wall, inner			West wall, outer			North wall, inner	North wall, outer	South wall
			Pier 1	Pier 2	Pier 3	Pier 4	Pier 5	Pier 6	Pier 7	Pier 8	Pier 9	Pier 10	Pier 11	Pier 12	Pier 13	Pier 14	Pier 15
EQ2 @ 100%	Arup	549	50.2	30.0	-2.3	18.9	17.6	11.7	49.8	6.3	-3.0	16.7	9.7	15.0	55.2	34.7	213
	EUCENTRE	540	43.5	16.9	35.4	5.5	10.5	6.8	38.5	27.1	40.9	2.3	13.9	9.4	131	75.0	83.1
	TU-Delft	521	32.0	21.4	4.0	33.7	29.3	24.3	26.9	6.7	11.6	27.0	12.4	30.4	71.4	16.7	173
EQ2 @ 150%	Arup	548	27.6	14.5	-0.7	15.6	16.3	12.2	30.6	1.4	0.5	14.9	6.0	16.2	135	42.7	192
	EUCENTRE	553	50.3	24.0	42.6	10.8	8.7	6.2	44.6	34.1	52.1	3.7	13.5	8.2	125	79.2	50.2
	TU-Delft	476	45.13	27.60	0.70	42.57	36.21	25.96	37.51	7.17	4.27	33.90	11.09	32.51	43.7	-19.1	188
EQ2 @ 200%	Arup	542	39.3	12.2	-1.0	15.1	16.1	12.1	31.8	2.7	0.4	14.8	6.5	16.8	118	41.9	191
	EUCENTRE	553	63.6	17.8	59.4	15.7	21.2	15.1	58.9	4.1	79.2	21.4	17.9	14.7	37.5	31.5	94.8
	TU-Delft																

<sup>1</sup> Unless noted otherwise, reported axial forces occur at time "A." Time "A" is the time at which the total base shear force is the absolute maximum during that run

Table 18: Base shear force summary (kN): EQ1 @ 50%

			Total	East wall, inner			East wall, outer			West wall, inner			West wall, outer			North wall, inner	North wall, outer	South wall
				Pier 1	Pier 2	Pier 3	Pier 4	Pier 5	Pier 6	Pier 7	Pier 8	Pier 9	Pier 10	Pier 11	Pier 12	Pier 13	Pier 14	Pier 15
EQ1 @ 50%	t = A <sup>1</sup>	Arup	37.7	3.4	4.6	1.9	2.5	2.1	1.2	2.3	1.2	0.5	1.8	0.2	0.6	0.3	0.4	2.6
		EUCENTRE	33.0	2.97	3.69	4.24	0.50	0.44	0.03	2.35	5.61	6.77	0.33	0.65	-0.23	2.36	1.07	2.22
		TU-Delft																
	Max Envelope	Arup		3.5	-5.3	-2.4	2.5	-2.3	1.2	2.4	-2.3	-0.5	1.8	-1.0	0.6	-1.9	-2.0	2.6
		EUCENTRE		4.14	4.50	4.24	0.75	0.81	0.36	3.17	5.95	6.86	0.48	1.14	0.80	2.67	1.18	2.29
		TU-Delft																

<sup>1</sup> Time “A” is the time at which the total base shear force is the absolute maximum during that run

Table 19: Base shear force summary (kN): EQ1 @ 100%

			Total	East wall, inner			East wall, outer			West wall, inner			West wall, outer			North wall, inner	North wall, outer	South wall
				Pier 1	Pier 2	Pier 3	Pier 4	Pier 5	Pier 6	Pier 7	Pier 8	Pier 9	Pier 10	Pier 11	Pier 12	Pier 13	Pier 14	Pier 15
EQ1 @ 100%	t = A	Arup	-60.3	-3.5	-8.8	-3.9	-3.6	-3.7	-1.2	-2.3	-6.4	-0.3	-2.9	-1.8	0.2	-2.9	-3.2	-0.3
		EUCENTRE	45.9	4.44	4.07	5.19	0.86	1.10	0.22	3.44	7.05	8.14	0.58	1.58	0.23	3.52	1.99	3.52
		TU-Delft	54.8	5.40	6.61	3.01	7.44	8.11	3.17	3.78	1.60	1.11	5.30	1.10	1.06	1.68	2.87	2.55
	Max Envelope	Arup		4.4	-9.0	-3.9	-3.6	-3.8	1.6	3.0	-7.1	-0.6	-2.9	-1.8	0.7	-2.9	-3.2	3.2
		EUCENTRE		5.22	5.59	5.19	1.19	1.38	0.59	4.04	8.45	8.27	0.76	1.71	1.16	3.52	2.33	3.56
		TU-Delft		5.40	6.61	3.35	7.44	8.11	3.17	3.78	2.24	1.43	5.30	2.72	1.06	2.27	3.87	2.55

Table 20: Base shear force summary: EQ1 @ 150%

			Total	East wall, inner			East wall, outer			West wall, inner			West wall, outer			North wall, inner	North wall, outer	South wall
				Pier 1	Pier 2	Pier 3	Pier 4	Pier 5	Pier 6	Pier 7	Pier 8	Pier 9	Pier 10	Pier 11	Pier 12	Pier 13	Pier 14	Pier 15
EQ1 @ 150%	t = A	Arup	70.0	5.4	10.1	2.1	4.0	4.4	2.1	4.2	3.2	0.2	3.2	0.7	0.8	1.9	1.5	3.7
		EUCENTRE	54.2	5.83	6.56	4.40	1.21	1.54	0.43	4.10	10.19	7.28	0.74	1.68	0.35	4.13	2.27	3.44
		TU-Delft																
	Max Envelope	Arup		8.6	10.1	-5.9	-4.2	4.4	2.1	6.3	-8.4	0.8	-3.4	-2.1	0.8	-4.2	-4.1	4.1
		EUCENTRE		5.83	6.82	5.57	1.35	1.92	0.80	4.24	10.78	8.76	0.83	2.37	1.40	4.20	2.93	3.77
		TU-Delft																

Table 21: Base shear force summary: EQ2 @ 100%

			Total	East wall, inner			East wall, outer			West wall, inner			West wall, outer			North wall, inner	North wall, outer	South wall
				Pier 1	Pier 2	Pier 3	Pier 4	Pier 5	Pier 6	Pier 7	Pier 8	Pier 9	Pier 10	Pier 11	Pier 12	Pier 13	Pier 14	Pier 15
EQ2 @ 100%	t = A	Arup	84.1	9.6	10.7	0.1	5.2	5.5	2.6	7.4	0.9	2.6	4.0	1.0	1.0	3.5	3.5	7.2
		EUCENTRE	-79.0	-7.41	-9.70	-9.31	0.00	-1.91	-1.38	-5.06	-16.7	-15.0	0.00	-0.74	-1.99	-2.72	-3.29	-3.83
		TU-Delft	69.2	6.56	7.69	3.72	8.99	9.88	4.32	4.53	1.83	2.11	6.24	1.65	1.39	2.67	3.90	3.76
	Max Envelope	Arup		9.6	10.9	-11.9	5.2	5.5	2.6	11.9	-8.1	3.5	4.0	-2.4	1.0	-5.4	-4.8	14.4
		EUCENTRE		14.0	9.70	9.31	4.19	3.29	1.40	8.93	16.7	15.2	1.06	4.36	2.59	4.93	3.96	4.96
		TU-Delft		6.56	7.83	4.41	9.00	9.88	4.35	4.53	4.07	2.30	6.30	4.08	1.43	2.73	4.52	3.86

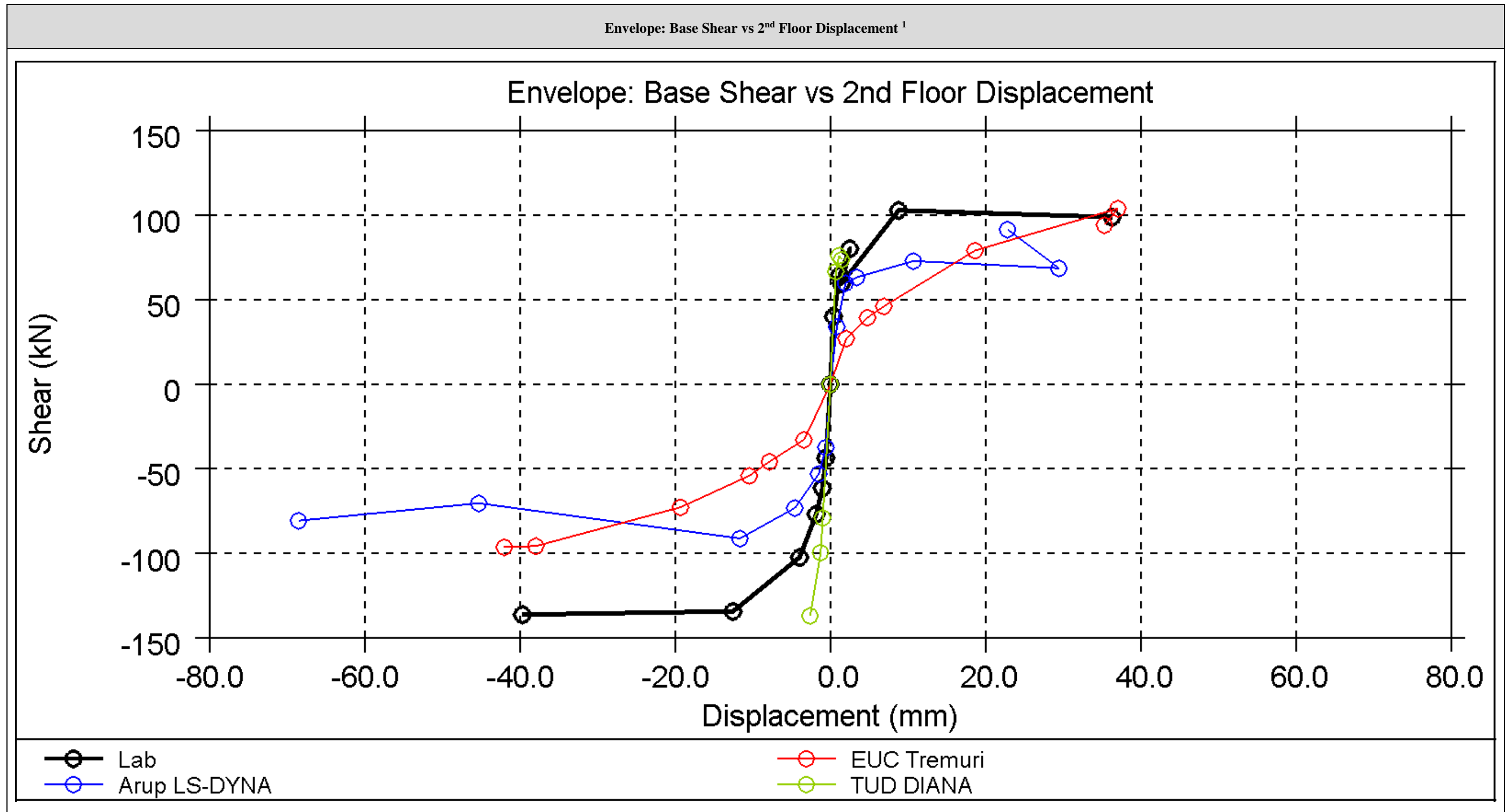


Table 22: Base shear force summary: EQ2 @ 150%

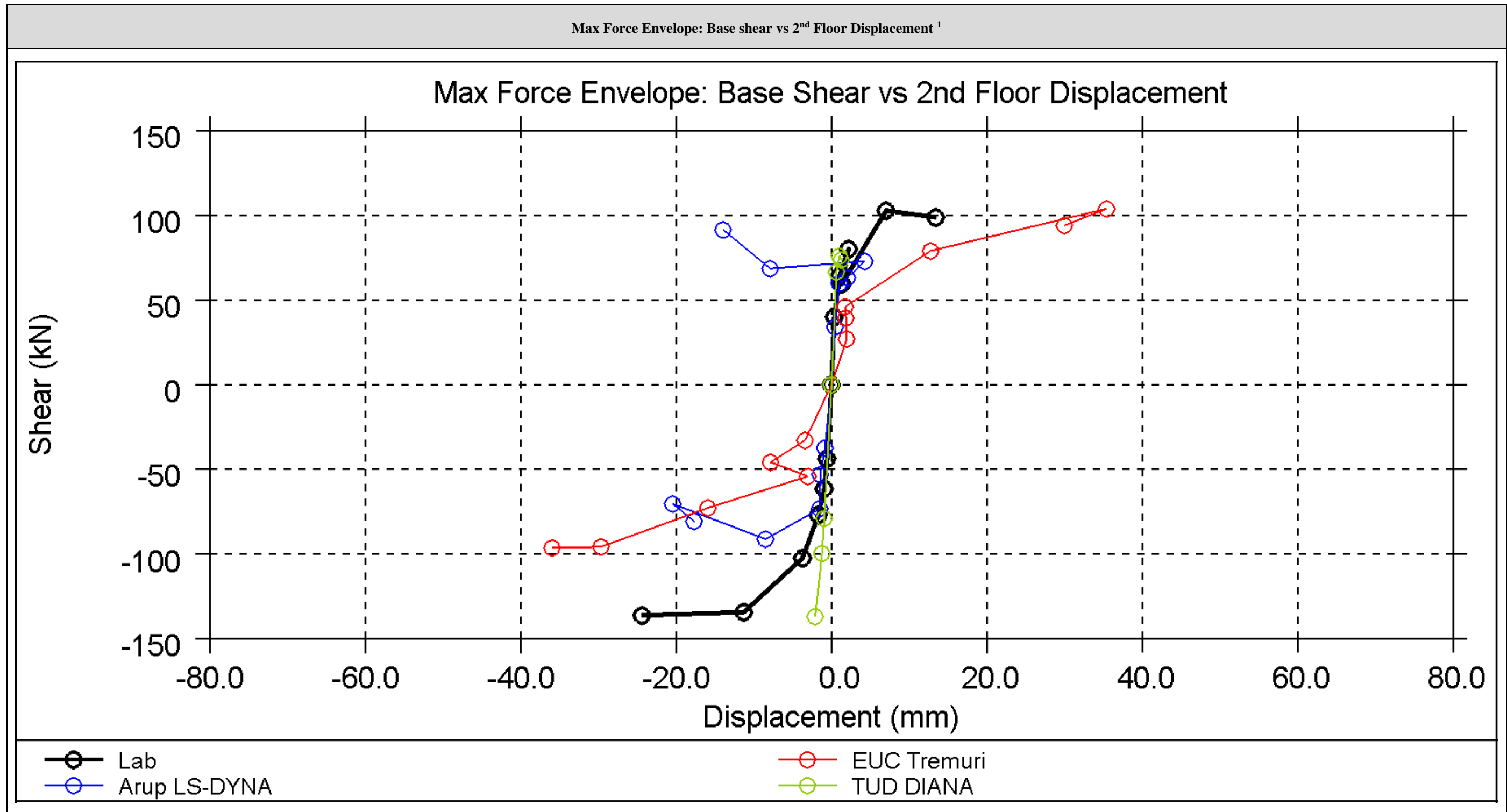
			Total	East wall, inner			East wall, outer			West wall, inner			West wall, outer			North wall, inner	North wall, outer	South wall
				Pier 1	Pier 2	Pier 3	Pier 4	Pier 5	Pier 6	Pier 7	Pier 8	Pier 9	Pier 10	Pier 11	Pier 12	Pier 13	Pier 14	Pier 15
EQ2 @ 150%	t = A	Arup	73.3	3.3	5.3	0.5	3.5	7.1	3.5	5.2	-0.3	-0.5	3.2	1.4	1.2	5.6	2.6	13.4
		EUCENTRE	-105	-9.13	-10.0	-8.41	-7.76	-4.05	-1.82	-6.86	-10.8	-14.1	-9.22	-7.78	-6.05	-2.14	-2.62	-3.93
		TU-Delft	95.9	9.64	10.0	2.61	12.3	12.9	6.28	6.43	1.43	5.51	8.88	1.41	2.55	4.61	4.03	7.28
	Max Envelope	Arup		6.8	9.0	-11.1	3.5	7.4	3.7	7.3	-7.7	2.4	3.3	-2.1	1.2	-6.5	-4.5	14.3
		EUCENTRE		12.9	14.5	9.15	11.5	5.49	2.28	10.1	16.3	17.6	9.22	9.26	6.69	7.03	5.61	5.92
		TU-Delft		9.70	10.0	5.28	12.7	13.4	6.28	6.43	4.95	6.00	9.09	5.02	4.19	4.61	5.52	9.69

Table 23: Base shear force summary: EQ2 @ 200%

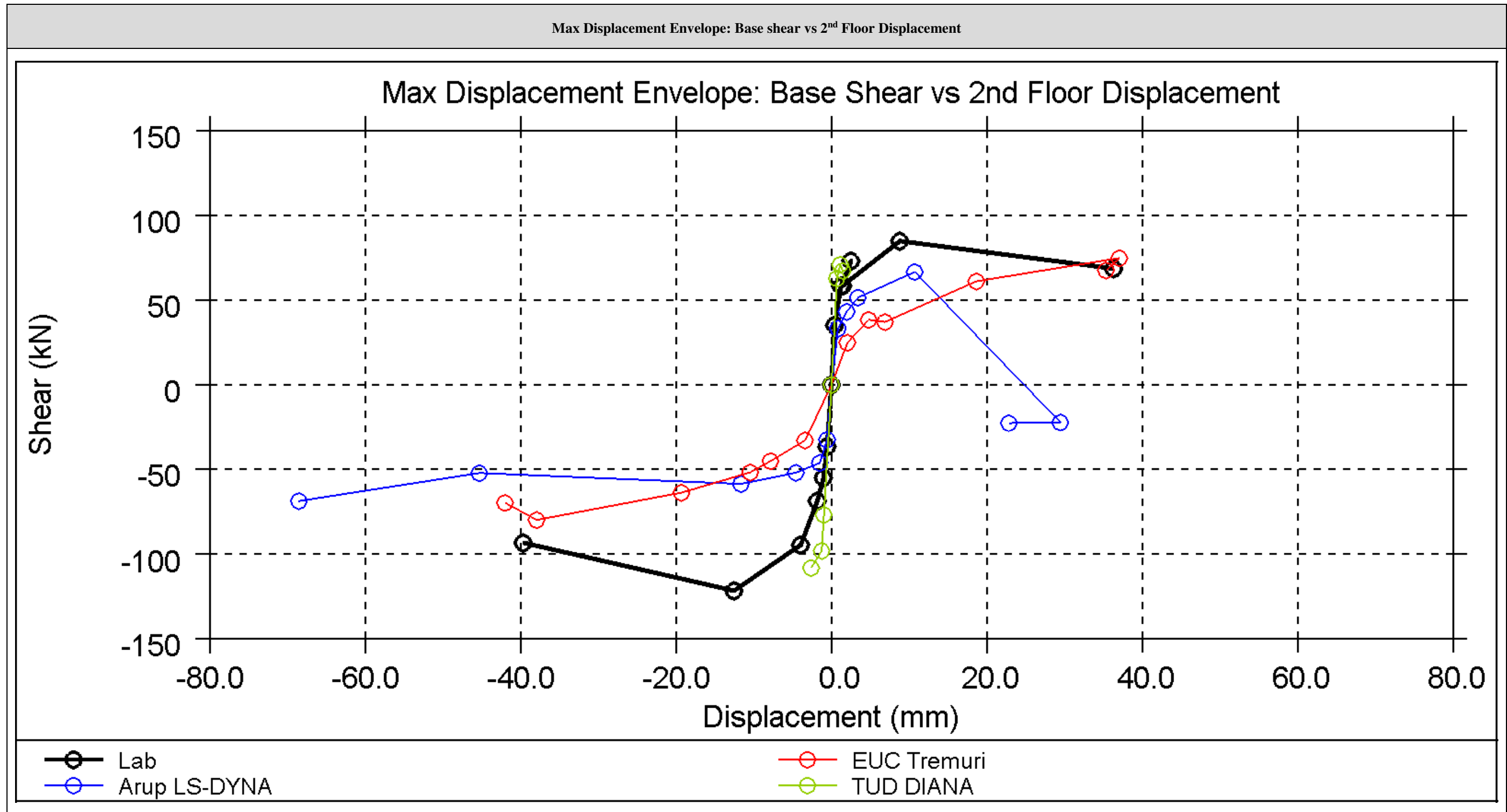
			Total	East wall, inner			East wall, outer			West wall, inner			West wall, outer			North wall, inner	North wall, outer	South wall
				Pier 1	Pier 2	Pier 3	Pier 4	Pier 5	Pier 6	Pier 7	Pier 8	Pier 9	Pier 10	Pier 11	Pier 12	Pier 13	Pier 14	Pier 15
EQ2 @ 200%	t = A	Arup	87.3	4.8	5.0	-0.3	3.7	7.0	3.6	4.5	1.0	1.0	3.6	1.8	1.5	8.9	4.7	16.1
		EUCENTRE	96.4	11.6	8.80	8.50	4.15	3.41	1.39	8.96	15.2	13.6	1.49	5.68	1.98	3.91	4.49	3.15
		TU-Delft																
	Max Envelope	Arup		9.3	14.4	-12.2	4.9	-11.8	5.3	8.8	-10.7	2.0	3.6	-3.2	10.1	-13.3	-13.3	18.0
		EUCENTRE		11.7	11.2	9.07	23.0	6.11	2.46	9.19	15.6	16.0	11.2	11.1	7.84	6.35	5.93	6.19
		TU-Delft																



<sup>1</sup> Plot is defined as maximum base shear in +x direction vs. maximum displacement in +x direction, and maximum base shear in -x direction vs. maximum displacement in -x direction for each ground motion.



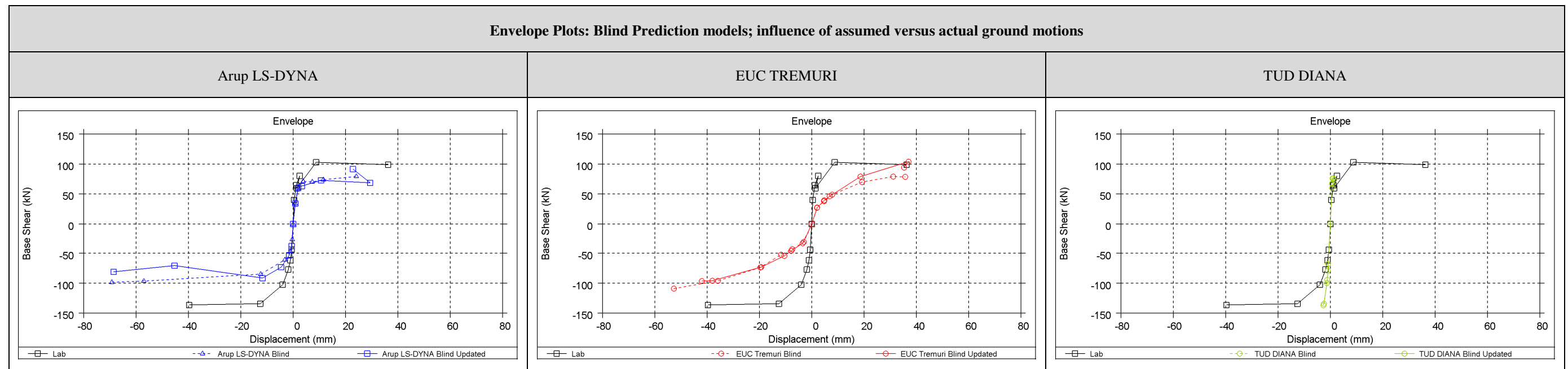
<sup>1</sup> Plot is defined as maximum base shear in +x direction vs. corresponding displacement at that instant, and maximum base shear in -x direction vs. corresponding displacement at that instant for each ground motion.



<sup>1</sup> Plot is defined as instantaneous base shear vs. maximum displacement in +x direction, and instantaneous base shear vs. maximum displacement in -x direction for each ground motion.

## 2.2.5 Conclusion

The ground motions measured during the tests (instead of the motions assumed pre-test) were applied to all three models. In summary, the change of ground motions made little difference to the results. The limitations of the models described in Section 2.1.5 remain valid. All models will incorporate refinements in the post-test refined prediction that aim to address these limitations. More detail is provided in the individual sections below.



### Arup – LS-DYNA

The LS-DYNA model with updated ground motions generally follows the same trends described in Section 2.1.5. One difference is that at larger ground motions, the blind prediction model with updated ground motions predicts larger displacements and inter-story deformations in comparison to the original blind prediction model. This is because the actual protocol contains more runs than the originally assumed protocol.

### EUCENTRE - TREMURI

When comparing the results of the incremental dynamic analyses of the blind prediction model under the waveforms originally specified by the theoretical test protocol versus those obtained after running the same model using as input ground motions the base acceleration histories supplied by the accelerometers installed on the shaking table, no significant differences are observed. The agreement achieved during this comparison implies that a substantial deviation of the numerical from the experimental results cannot be attributed to any possible distortion in the content of the input signals after their passing through the shaking table. The aforementioned verification therefore adds value to the blind prediction process, renders its outcome meaningful, and so, comparable to the results obtained during the experimental campaign.

As far as the TREMURI model is concerned, under the recorded shaking table accelerations it demonstrates a response similar to the one observed when subjected to the original ground motions, differing only during the last run (200% of EQ2), where the maximum displacement and base shear are better predicted. This could be partially justified by the fact that, during this test, the applied base accelerations were not as strong as defined in the protocol (lower value of PGA by 6%).

### TU-Delft - DIANA

The analyses run and reported in this chapter aim to investigate if any significant change occurs in the behaviour of EUC-BUILD specimen by applying the real ground motions recorded during the test with respect to the ones provided in the protocol. For consistency with the previously performed analyses of section 2.1, also in this case the DIANA finite element model of EUC-BUILD is subjected to 3 separate analyses, namely EQ1-100%, EQ2-100% and EQ2-150%, with no accumulated damage, i.e. a separate analysis has been executed for each accelerogram and PGA level. Divergence of the numerical analysis is encountered for both EQ2-100%, at 7.78 s and EQ2-150% at 4.38 s. Slightly higher displacements are observed with the application of the real ground motions, but no substantial changes are recorded in terms of hysteresis plots, interstorey drift time-histories and damage pattern. Therefore, the same comments reported in section 2.1 apply to this section as well.

The differences between experimental and numerical behaviour concerning the stiffer response of the model, the different IDR profile along the height of the building and the damage pattern are consequently not related to the different applied ground motions and will be further investigated in the post-test refined prediction phase.

## 2.3 Comparison of Post-Test Refined Predictions

### 2.3.1 Post-Test Model Assumptions

Assumptions on material properties made by each consultant are summarized in Table 24 through Table 25. Modelling techniques and assumptions are summarized in Table 27. More information on such assumptions are described in sections 2.3.2 through 2.3.4.

EUCENTRE carried out two sets of tests on the masonry materials: one using specimens constructed at the same time as the component test specimens, and one using specimens constructed at the same time as the house. The masonry materials in the house were nominally the same as those used for the component tests. The two sets of tests on the clay masonry showed very similar results, as expected. However, the calcium silicate masonry used in the house showed bond strengths ( $f_t$ ,  $f_s$ ) very much lower than the masonry used in the component tests, and elastic stiffness half the value obtained for the component test specimens. This may have been due to the weather conditions during construction of the house and/or inadequate soaking of the bricks, resulting in water being sucked rapidly out of the mortar and a weak bond between mortar and bricks. Comparison of calcium silicate material properties from the two sets of tests is made in Table 26.

Table 24: Calcium silicate (inner leaf) material properties (based on EUCENTRE Unified Report dated 06-11-215 unless noted otherwise)

Symbol	Description	Value	Arup	EUCENTRE	TU-Delft
$\rho$	Mass density [kg/m <sup>3</sup> ]	1835	1785	1835	1785
E	Masonry Young's modulus in the direction perpendicular to bed joints [GPa]	E <sub>1</sub> = 1.736 E <sub>2</sub> = 2.132 E <sub>3</sub> = 1.66	2.132	2.132	2.132
$\nu$	Poisson's ratio of masonry	0.14 <sup>1</sup>	0.14	---	0.14
$f_c$	Masonry compressive strength in the direction perpendicular to bed joints [MPa]	5.49	5.26 <sup>3</sup>	5.49	5.49
$f_t$	Tensile strength (flexural bond strength) of mortar joints [MPa]	0.056	0.056	---	--- <sup>3</sup>
$f_s$	Shear strength (cohesion) of mortar joints [MPa]	0.035	0.21 <sup>4</sup>	0.035×10 <sup>4</sup>	---
$G_t$	Energy release rate for tensile failure of mortar [N/m]	---	15 <sup>2</sup>	---	15 <sup>2</sup>
$G_s$	Energy release rate for shear failure of mortar [N/m]	---	21	---	---
$\mu$	Coefficient of friction for sliding of joints	0.50	0.42 <sup>4</sup>	0.50	---

<sup>1</sup> Value from TU-Delft material tests as listed in the 13/07/2015 summary document

<sup>2</sup> Value not provided in summary document and referenced from NAM BfD rev 3

<sup>3</sup> See section 2.3.2 (for Arup value) or 2.3.4 (for TU-Delft value) for further explanation of assumption

<sup>4</sup> Model was run before the new value from laboratory test became available



Table 25: Clay material (outer leaf) properties (based on EUCENTRE Unified Report)

Symbol	Description	Value	Arup	EUCENTRE	TU-Delft
$\rho$	Mass density [kg/m <sup>3</sup> ]	1905	1867	1905	1831
E	Masonry Young's modulus in the direction perpendicular to bed joints [GPa]	E <sub>1</sub> = 4.742	3.926	5.339	4.742
		E <sub>2</sub> = 3.926			
		E <sub>3</sub> = 5.339			
$\nu$	Poisson's ratio of masonry	0.20 <sup>2</sup>	0.20	---	0.20
f <sub>c</sub>	Masonry compressive strength in the direction perpendicular to bed joints [MPa]	12.72	12.27 <sup>3</sup>	12.72	12.72
f <sub>t</sub>	Tensile strength (flexural bond strength) of mortar joints [MPa]	0.152	0.152	---	--- <sup>3</sup>
f <sub>s</sub>	Shear strength (cohesion) of mortar joints [MPa]	0.15	0.15	0.15	---
G <sub>t</sub>	Energy release rate for tensile failure of mortar [N/m]		35 <sup>2</sup>	---	35 <sup>2</sup>
G <sub>s</sub>	Energy release rate for shear failure of mortar [N/m]	---	15	---	---
$\mu$	Coefficient of friction for sliding of joints	0.7	0.87	0.70	---

<sup>1</sup> Value from TU-Delft material tests as listed in the 13/07/2015 summary document<sup>2</sup> Value not provided in summary document and referenced from NAM BfD rev 3<sup>3</sup> See section 2.3.2 (for Arup value) or 2.3.4 (for TU-Delft value) for further explanation of assumption

Table 26: Comparison of calcium silicate material properties obtained from two sets of tests--component specimen material tests vs test house material tests (major differences are highlighted in bold)

Symbol	Description	Value from component specimen material tests	Value from test house material test
$\rho$	Mass density [kg/m <sup>3</sup> ]	---	1835
E	Masonry Young's modulus in the direction perpendicular to bed joints [GPa]	E <sub>1</sub> = 3.256	E <sub>1</sub> = 1.736
		E <sub>2</sub> = 4.182	E <sub>2</sub> = 2.132
		E <sub>3</sub> = 3.236	E <sub>3</sub> = 1.66
$\nu$	Poisson's ratio of masonry	0.14 <sup>1</sup>	0.14 <sup>1</sup>
$f_c$	Masonry compressive strength in the direction perpendicular to bed joints [MPa]	6.3	5.49
<b><math>f_t</math></b>	<b>Tensile strength (flexural bond strength) of mortar joints [MPa]</b>	<b>0.238</b>	<b>0.056</b>
<b><math>f_s</math></b>	<b>Shear strength (cohesion) of mortar joints [MPa]</b>	<b>0.210</b>	<b>0.035</b>
G <sub>t</sub>	Energy release rate for tensile failure of mortar [N/m]	---	---
G <sub>s</sub>	Energy release rate for shear failure of mortar [N/m]	---	---
$\mu$	Coefficient of friction for sliding of joints	0.42	0.50

Modelling techniques and assumptions are summarized in Table 27 and Table 28 below. Bold entries differ from the assumptions made in the blind prediction models as presented in Table 5 and Table 6.

Table 27: Additional modelling assumptions

Component	Arup	EUCENTRE	TU-Delft
Roof diaphragm	Roof girders and planks are modelled with linear elastic beam elements. Nails are modelled as nonlinear hysteretic beam elements. Nails rigidly connect the plank and girder elements. Diaphragm flexibility and nonlinearity is captured by the behaviour of the nails.	Modelled by means of two inclined (43.5°) 4-node orthotropic membrane finite elements with equivalent thickness, shear modulus (tangential stiffness of the diaphragm) and moduli of elasticity (normal stiffness of the membrane).	The roof plywood is modelled with eight-node quadrilateral isoparametric curved shell elements with linear material properties. The plywood is fully clamped to the girders, whilst it is not connected with the North/South walls.
Wall ties	Wall ties are modelled as 1D discrete beam elements with defined nonlinear axial strength and stiffness only in tension and compression.	<p>The cavity ties connecting the in-plane (east and west side) walls are modelled by means of equivalent membrane elements with equivalent thickness and shear modulus, introduced at the levels of the floor slabs.</p> <p>The connecting ties between the CaSi leaf and the veneer of the northern side are modelled as elastic beams by means of 2D finite elements, each one of them defined between 2 nodes. These beams are distributed at certain spacing along the wall height, with properties equivalent to the properties of the total number of ties located at that specific level. Due to the need to introduce the required number of nodes in order to realize the aforementioned modelling approach, the two masonry leaves are discretized.</p>	Modelled with two-node, truss elements, with nonlinear behaviour both in tension and compression.
Connection between first floor slab and East/West walls	<b>First floor slab elements are fully merged with the East/West inner leaf wall elements after the application of inherent gravity loading of the slab</b>	<p><b>Beams of equivalent slab axial stiffness connect the top nodes of the 1<sup>st</sup> storey East/West CaSi piers (providing in-plane displacement coupling).</b></p> <p><b>No equivalent beams are introduced to represent connections between the 1<sup>st</sup> floor slab and the East/West clay-brick walls.</b></p>	Connected for the out-of-plane displacements only through the use of tyings.
Connection between first floor slab and North/South walls	First floor slab elements are fully merged with the North/South inner leaf wall elements	Ideal connection, with perfect displacement coupling. The in-plane moment transfer is achieved by introducing a fictitious beam, connecting the two out-of-plane CaSi leaves, with equivalent to the RC slab flexural stiffness.	Fully clamped.

Table 28: Additional modelling assumptions (continued)

Component	Arup	EUCENTRE	TU-Delft
Connection between second floor slab and East/West inner leaves	<b>Second floor slab elements are fully merged with the East/West inner and outer leaf wall elements after the application of inherent gravity loading of the slab</b>	Fictitious beams with axial and flexural stiffness equivalent to those of an effective width of the RC slab have been introduced at the top of the 2 <sup>nd</sup> storey piers in order to model the presence of the slab and its connection to the walls.	Connected for the vertical displacements only through the use of tyings.
Connection between timber beam at gutter level and East/West outer leaves		<p><b>Introduction of short-height macro-elements on the top of the elements representing the 2<sup>nd</sup> storey in-plane veneer piers, in order to model the presence of the 1 cm thin layer of mortar. Interface elements, are inserted just below the timber beams that exist on the top of the longitudinal clay-brick walls.</b></p> <p><b>In order to better match the last stage of the test (EQ2-200%) the interface elements on top of the veneers were removed, allowing for free sliding</b></p>	
Connection between second floor slab and North/South walls	Second floor slab elements are fully merged with the North/South inner leaf wall elements	Ideal connection, with perfect displacement coupling. The in-plane moment transfer is achieved by introducing a fictitious beam, connecting the two out-of-plane CaSi leaves, with equivalent to the RC slab flexural stiffness.	Fully clamped.
Connection between roof girders and North/South walls	<b>Roof girders are fully merged with the North/South inner and outer leaf wall elements.</b>	Ideal connection, with perfect displacement coupling and in-plane moment transfer.	Fully clamped.

### 2.3.2 Arup

Further information about the modelling methods used is given in the bullet points below (these are the same as in the blind prediction model):

- The slabs are modelled as nonlinear 2D shell elements that are subdivided into layers defined explicitly for concrete and for reinforcement.
- The concrete lintels above the window and door openings are modelled as 1D linear elastic beam elements. More information on the modelling of the slabs and lintels is included in section 2.1.
- The masonry inner and outer leaves are modelled with a homogenized masonry material model with 2D, fully integrated shell elements and five through-thickness integration points that evaluate the behaviour of masonry where the damage is assumed to be lumped at the joints. Crack plane directions are pre-defined to model mortar bonds.

The compression stress-strain definition of masonry has changed from a linear elastic, perfectly plastic relationship in the blind prediction model to a nonlinear relationship in the post-test refined prediction model. The nonlinear compressive stress-strain relationship used in the LS-DYNA post-test refined model is drawn as an average of the individual stress-strain curves generated from each wallet specimen compression test as reported in the EUCENTRE Unified Report. As a result, the peak compressive strength does not exactly match the reported average peak compressive strength.

The model has been run with the “production” version of the masonry model released within Arup in October 2015. This is the same version of the LS-DYNA software with which the model reported in section 2.2 was run.

Differences in modelling techniques utilized in the post-test refined model in comparison to the blind prediction model are highlighted in bold in Table 27 and Table 28 above and compared side-by-side in Table 29 below.

Table 29: Comparison of LS-DYNA modelling assumptions between blind prediction model and post-test refined prediction model

Component	Blind prediction model	Post-test refined prediction model
Connection between first floor slab and East/West walls	The first floor slab and East/West inner leaves are connected via discrete beam elements that represent the threaded bar anchors for out-of-plane displacements only. Beams have defined elastic axial stiffness only. These elements become activated after the inherent gravity load is applied to replicate the actual construction sequence.	First floor slab elements are fully merged with the East/West inner leaf wall elements after the application of inherent gravity loading of the slab
Connection between second floor slab and East/West walls (inner and outer leaves)	Second floor slab elements and East/West wall elements are connected for the vertical displacements. Sliding is potentially resisted by friction only (representing the mortar between the slab and the walls) but due to the modelling of the construction sequence, there is no weight on this connection. Vertical loads occur only as a result of dynamic behaviour during the shaking motion, therefore frictional resistance to sliding is small and intermittent.	Second floor slab elements are fully merged with the East/West inner and outer leaf wall elements after the application of inherent gravity loading of the slab
Connection between roof girders and North/South walls	Roof girders are fully merged with the North/South inner leaf wall elements.	Roof girders are fully merged with the North/South inner and outer leaf wall elements.

Further explanation of these changes is discussed below.

## First floor slab to East-West wall connections

After the execution of the laboratory test, it was learnt that the threaded bars were tightened during the construction of the full scale specimen. This imposed post-tensioning between the slab and inner leaf resulted in a friction surface between the slab and the inner leaf that had the ability to transfer shear. In response, the modelling of the connection between the inner leaf elements and the first floor slab was changed. In the blind prediction model, beam elements with axial stiffness only were used to connect only in the out-of-plane direction. In the post-test model, fully merged 2D slab elements are used to make this connection. Figure 31 below illustrates the aforementioned change.

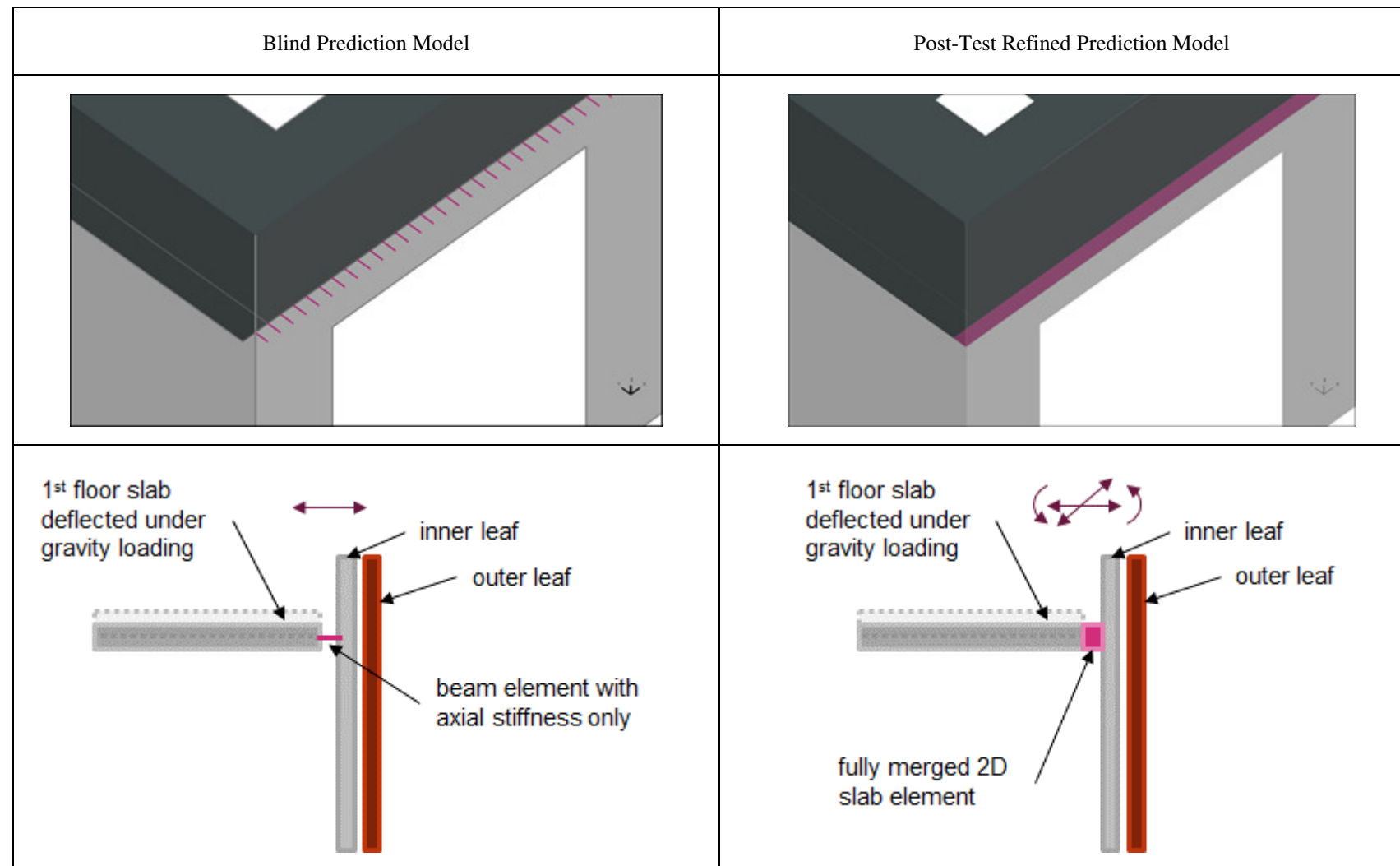


Figure 31: Change in connection between first floor slab and East/West walls in LS-DYNA post-test refined model

## Second floor slab to East-West wall connections

The second floor slab is constructed on the North and South walls, leaving a gap between the underside of the slab and the tops of the East and West walls. Later, the gap is packed with mortar. In the blind prediction model, it was assumed that the connection provided by the mortar was weak and free-sliding, and was modelled with beam elements offering only frictional resistance. However, after the execution of the laboratory test, it was learnt that the East and West walls behaved as if well connected to the slab. In response, fully merged 2D slab elements are used to connect the second floor slab to the tops of the East and West walls. In the model, a staged construction method was used to avoid transferring gravity load from the slab to the East and West walls. Figure 32 below illustrates the aforementioned change.

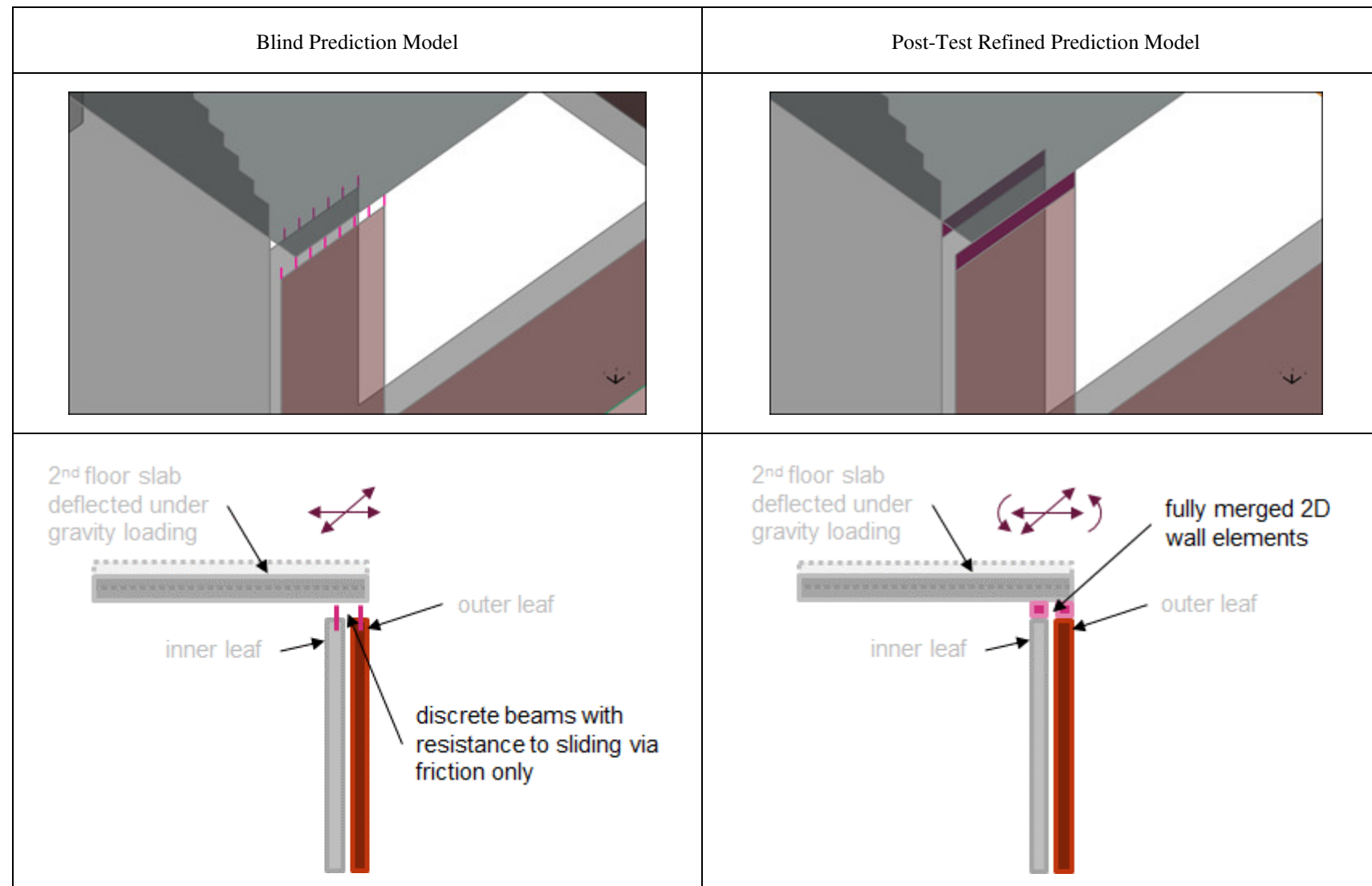


Figure 32: Change in connection between second floor slab and East/West walls in LS-DYNA post-test refined model

### 2.3.3 EUCENTRE

Differences in modelling techniques utilized in the post-test refined model in comparison to the blind prediction model are highlighted in bold in Table 27 above and compared side-by-side in Table 30 below.

Table 30: Comparison of TREMURI modelling assumptions between blind prediction model and post-test refined prediction model

Component	Blind prediction model	Post-test refined prediction model
Connection between first floor slab and East/West walls	In the model implemented for the blind prediction, the kinematic coupling is effective only between the slab and the corner piers.	Beams of equivalent slab axial stiffness connect the top nodes of the 1 <sup>st</sup> storey East/West CaSi piers (providing in-plane displacement coupling).  No equivalent beams are introduced to represent connections between the 1 <sup>st</sup> floor slab and the East/West clay-brick walls.
Connection between timber beam at gutter level and East/West outer leaves	No connection	Introduction of short-height macro-elements on the top of the elements representing the 2 <sup>nd</sup> storey in-plane veneer piers, in order to model the presence of the 1 cm thin layer of mortar. Interface elements, are inserted just below the timber beams that exist on the top of the longitudinal clay-brick walls.  In order to better match the last stage of the test (EQ2-200%) the interface elements on top of the veneers were removed, allowing for free sliding

A significant improvement of modelling assumptions incorporated in the post-test refined TREMURI model regards the introduction of short-height macro-elements on the top of the elements representing the 2<sup>nd</sup> storey in-plane veneer piers, in order to model the presence of the 1 cm thin layer of mortar. These interface elements, are inserted just below the timber beams that exist on the top of the longitudinal clay-brick walls, and their material properties are calibrated accordingly so that a failure occurs only at late stages of the test. This failure allows the sliding of the timber beams (which are attached on the 2<sup>nd</sup> floor slab), and consequently results in the uncoupled horizontal displacements of inner and outer leaves at these locations. This type of detailed connection modelling would not be usual in a macroelement model of a building. The experiment has shown that the connection provided by the timber beam is not sufficient to constrain the inner and outer leaf to be subjected to the same displacement, hence it seems that the modeling refinement introduced in the post-diction is necessary to capture the uncoupled motion of the inner and outer leaf.

Another important consideration that affected the refined model's ability to simulate the specimen's behavior with competence throughout the whole test procedure is the re-evaluation of the effective height of the masonry piers during the evolution of the tests. The pattern of the cracks developed is taken into account in order to properly define the geometry of spandrels and piers, by adjusting (reducing) at the same time the dimensions of the rigid nodes. In general, the crack pattern is not known a priori, so this refinement would not be possible in a blind prediction, where the definition of the effective height must be chosen based on expert judgment or existing proposals, which often would not match the specific single case.



### 2.3.4 TU-Delft

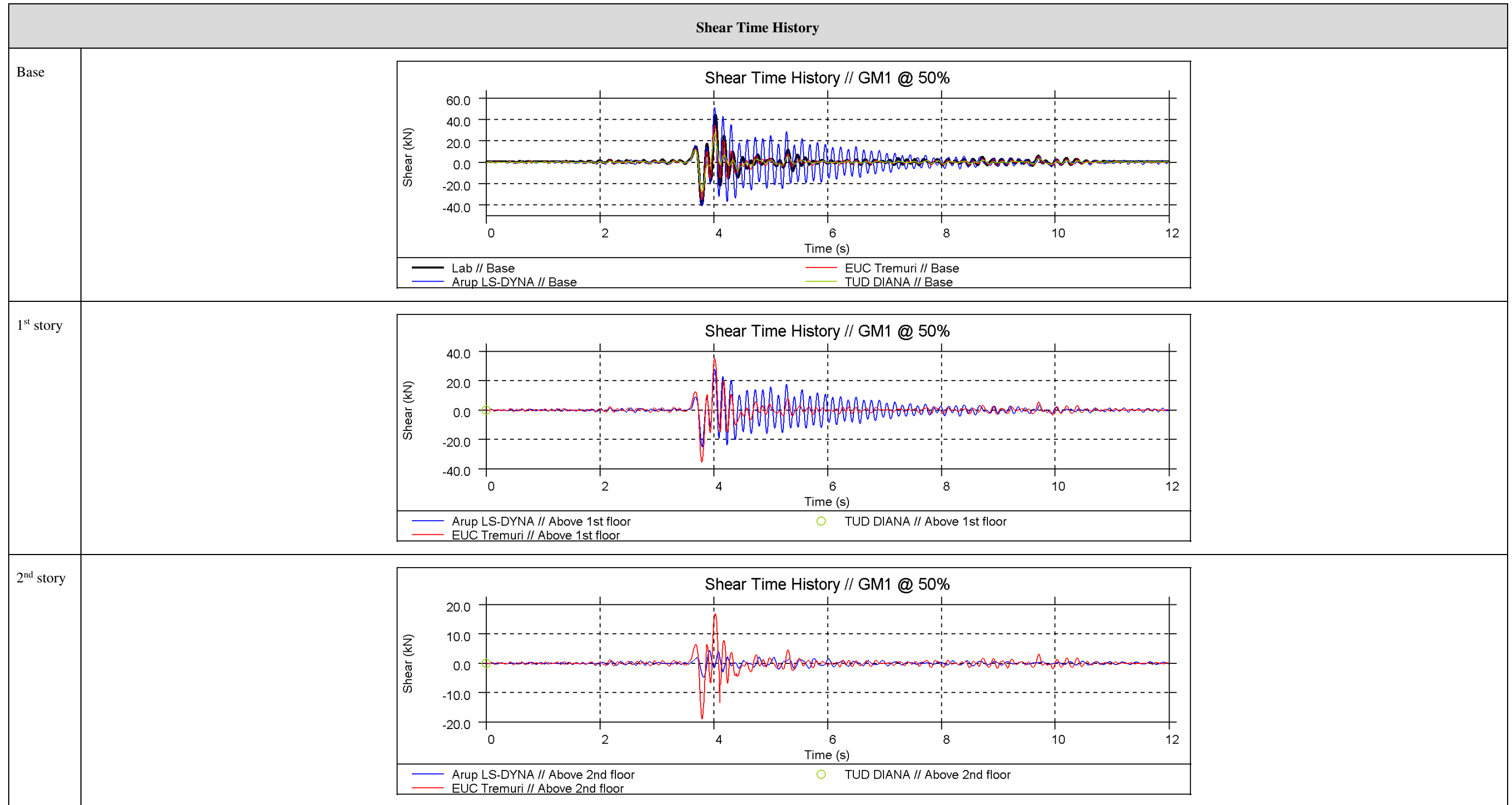
The finite element model for the post-test prediction has been refined by adjusting some over-constrained nodes at the connection between outer leaf and roof and by replacing some missing tyings for the floor-facades connection. Nevertheless, the general hypothesis on the connections have been kept the same as for the blind prediction (see Table 5 and Table 6). Differently from what has been done for the blind predictions, the whole set of ground motions has been applied in sequence so to account for accumulated damage in the structure.

The material properties have been updated according to new material tests. Young moduli, compressive and tensile strengths have been updated for both calcium silicate and clay. The updated tensile strength for the masonry material has been derived from the flexural bond strength divided by 1.5. Additionally, the fracture energy of clay has been increased from 15 N/m to 35 N/m according to NAM Basis for Design document.



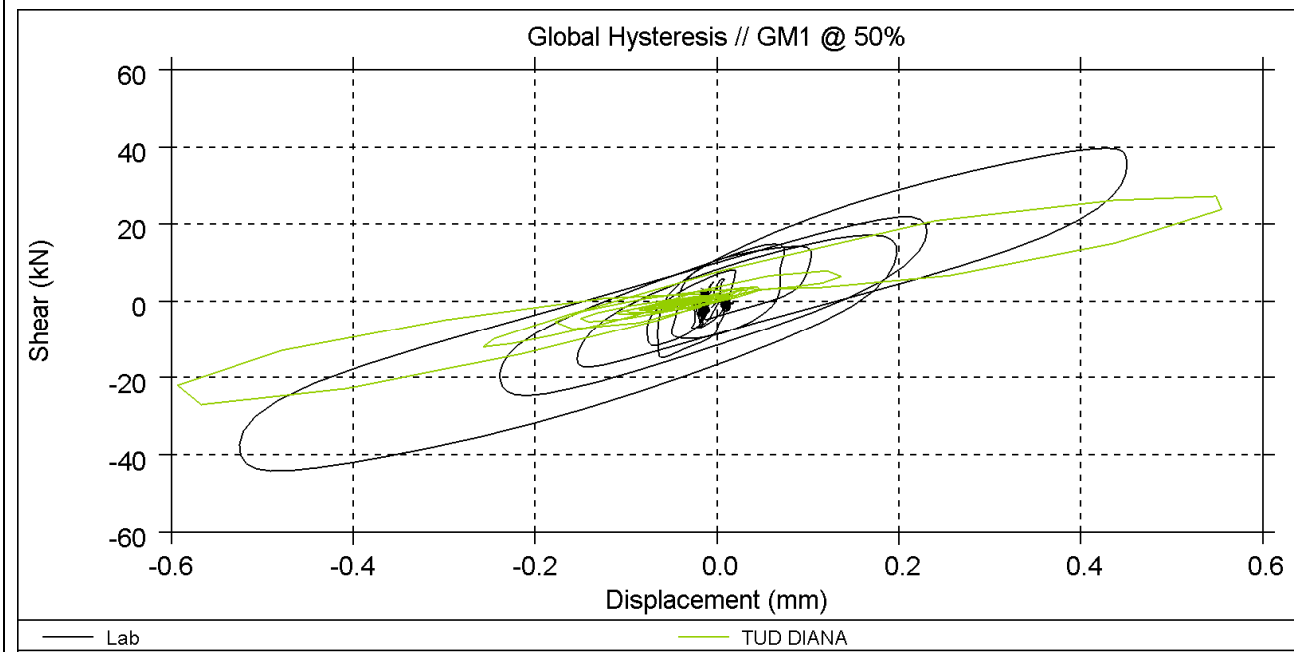
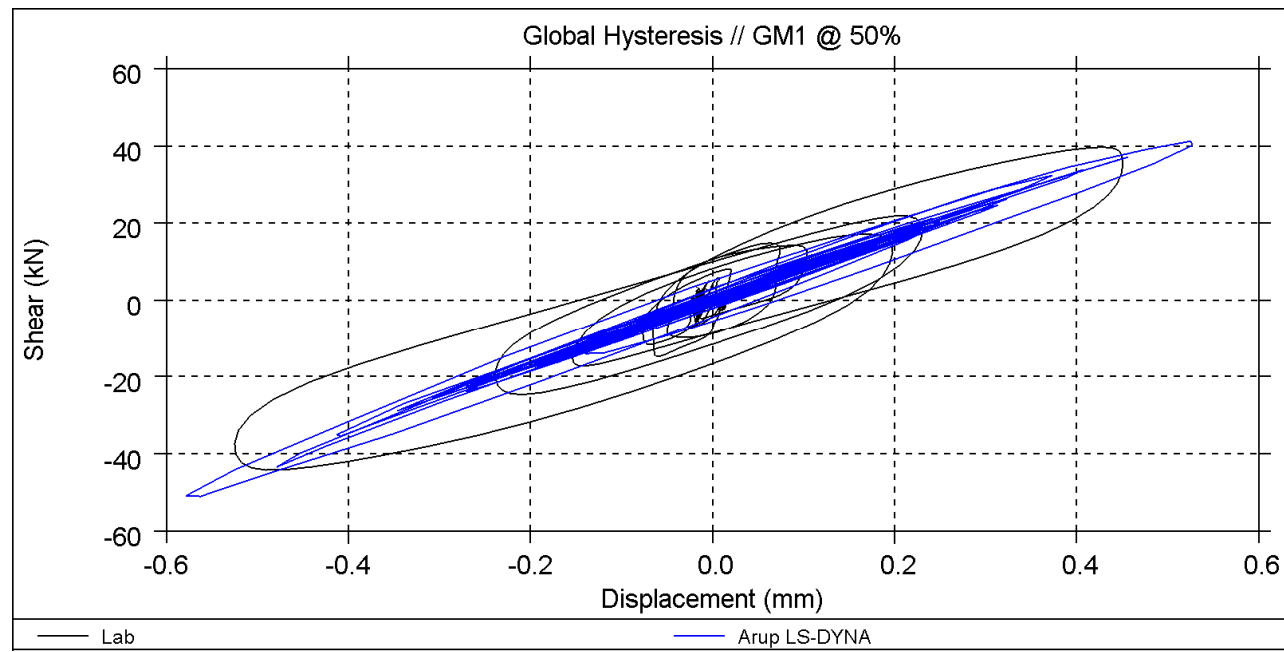


EQ1 at 50%



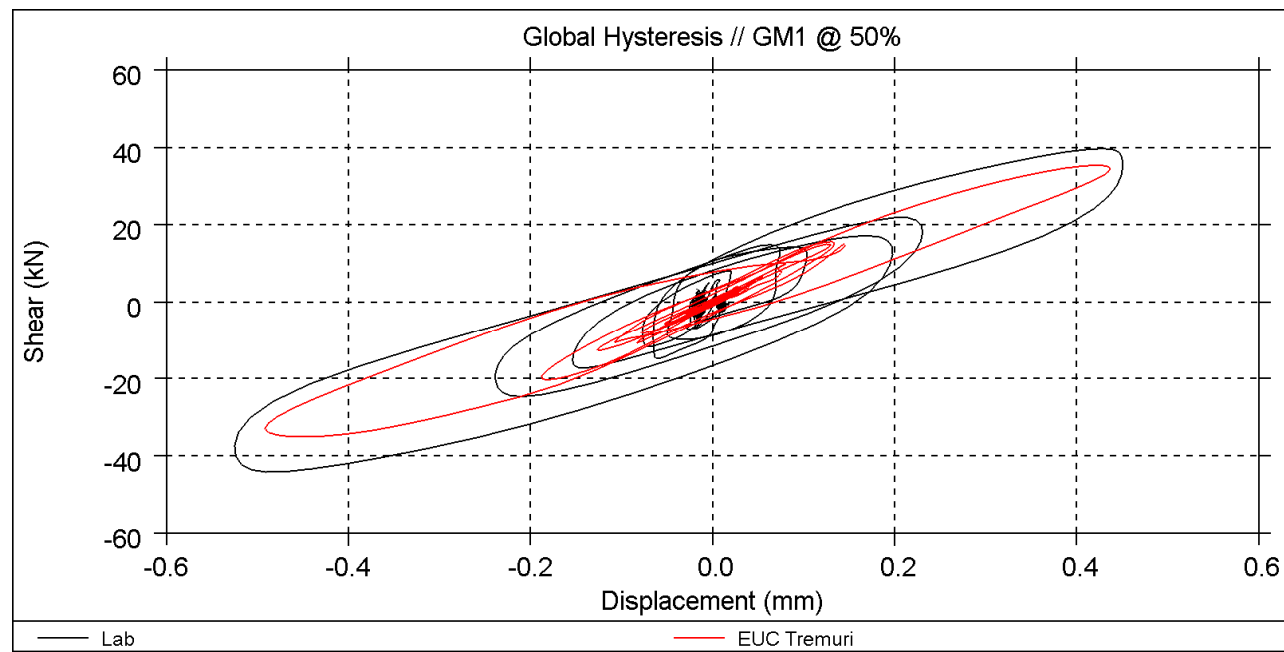
EQ1 at 50%

Global Hysteresis <sup>1</sup>



Arup

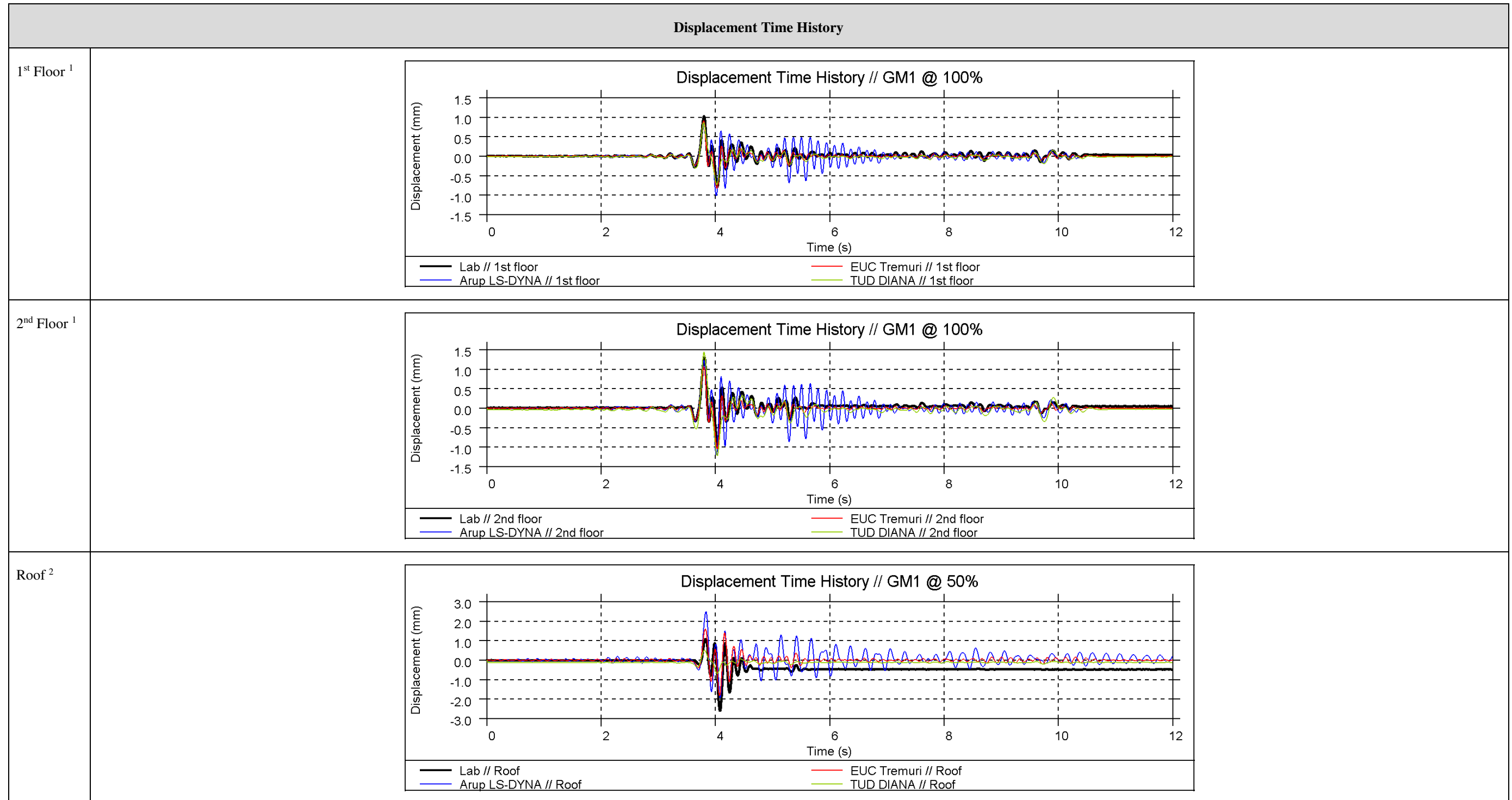
TU-Delft



EUCENTRE

<sup>1</sup> Base shear vs. 2<sup>nd</sup> floor displacement

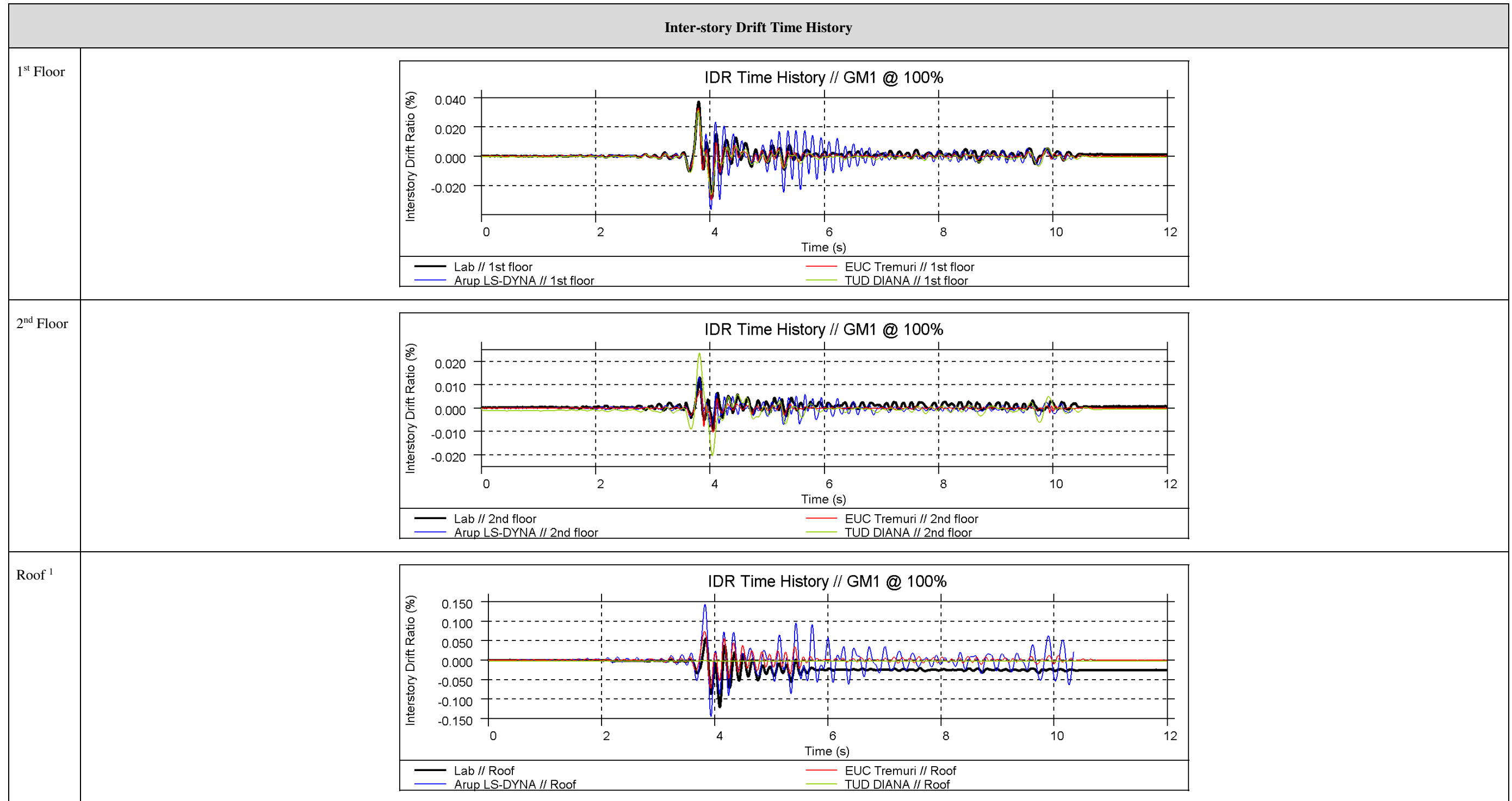
EQ1 at 100%



<sup>1</sup> Displacement of the 1<sup>st</sup> floor and 2<sup>nd</sup> floor is calculated as the average displacement measured at the four corners of the slab

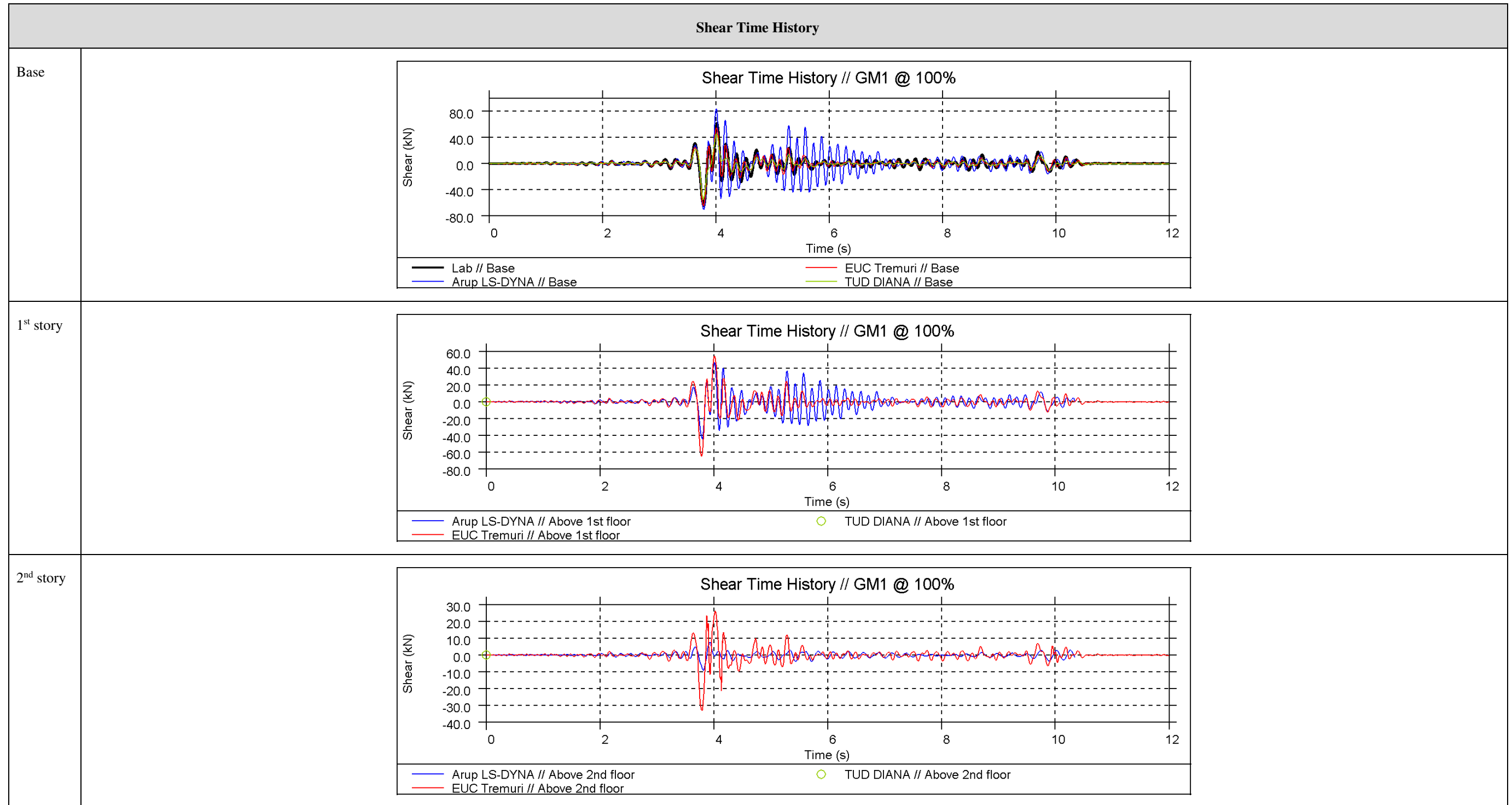
<sup>2</sup> Displacement of the roof is measured as the average displacement at the two ends of the ridge beam

EQ1 at 100%



<sup>1</sup> Roof drift is calculated using a diagonal length from the gable peak to the 2<sup>nd</sup> floor along the roof slope (3.5m)

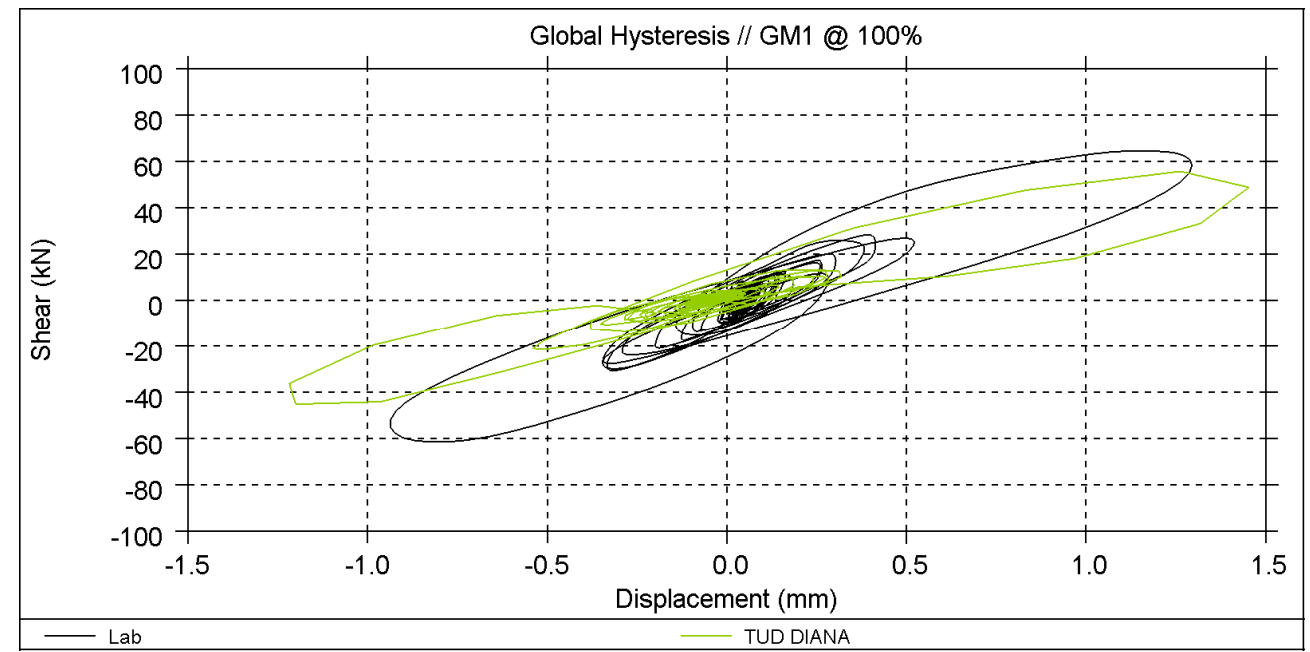
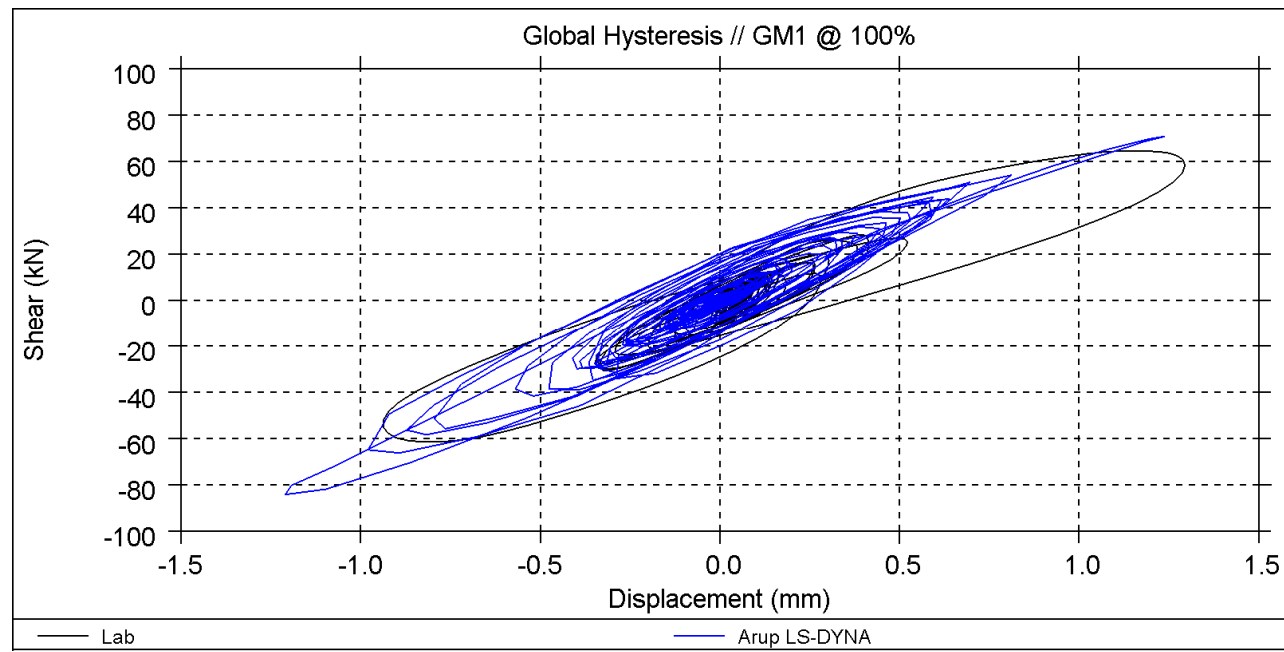
EQ1 at 100%





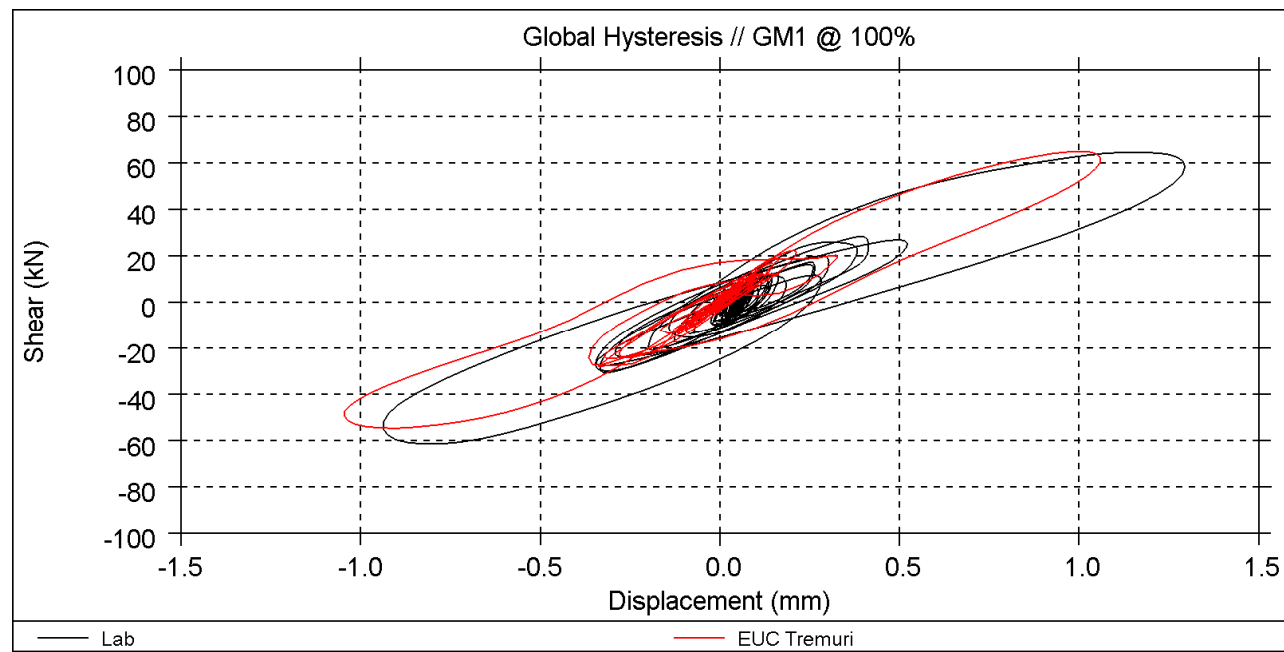
EQ1 at 100%

Global Hysteresis <sup>1</sup>



Arup

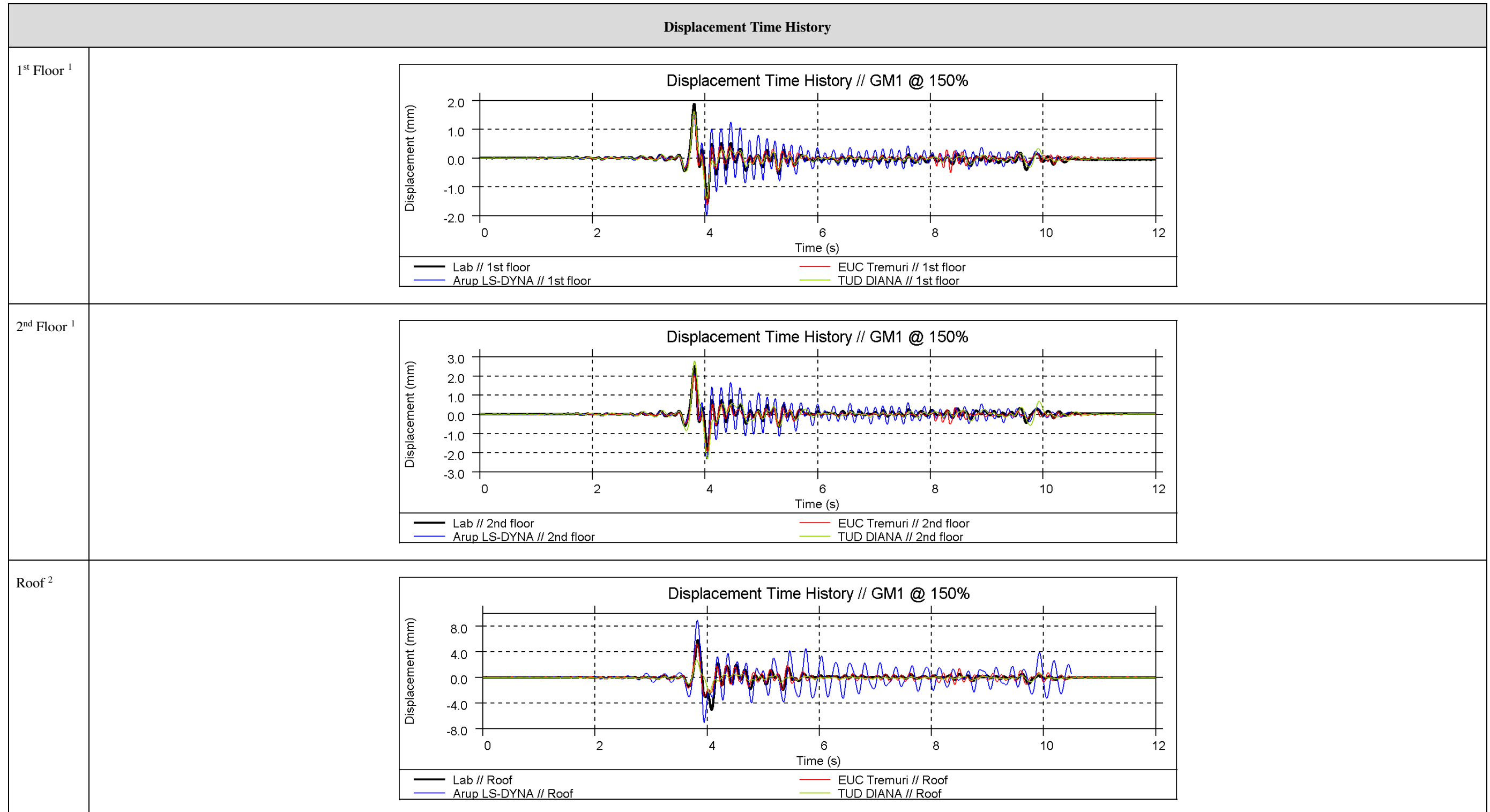
TU-Delft



EUCENTRE

<sup>1</sup> Base shear vs. 2<sup>nd</sup> floor displacement

EQ1 at 150%



<sup>1</sup> Displacement of the 1<sup>st</sup> floor and 2<sup>nd</sup> floor is calculated as the average displacement measured at the four corners of the slab

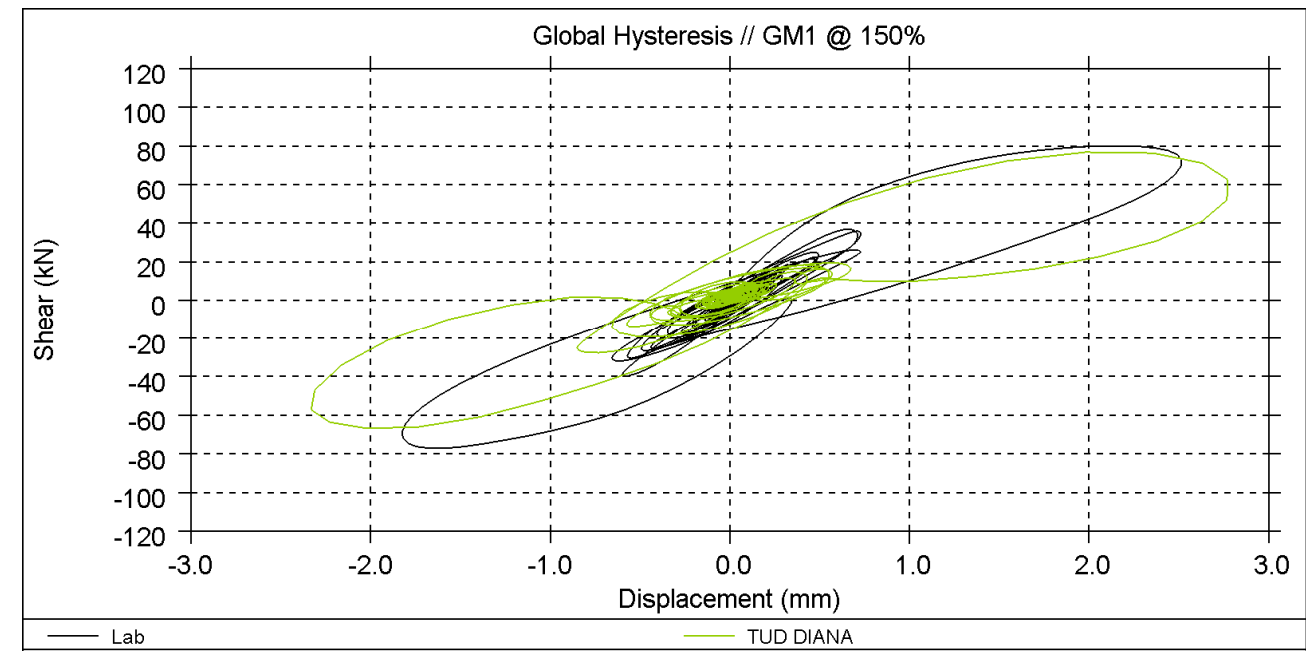
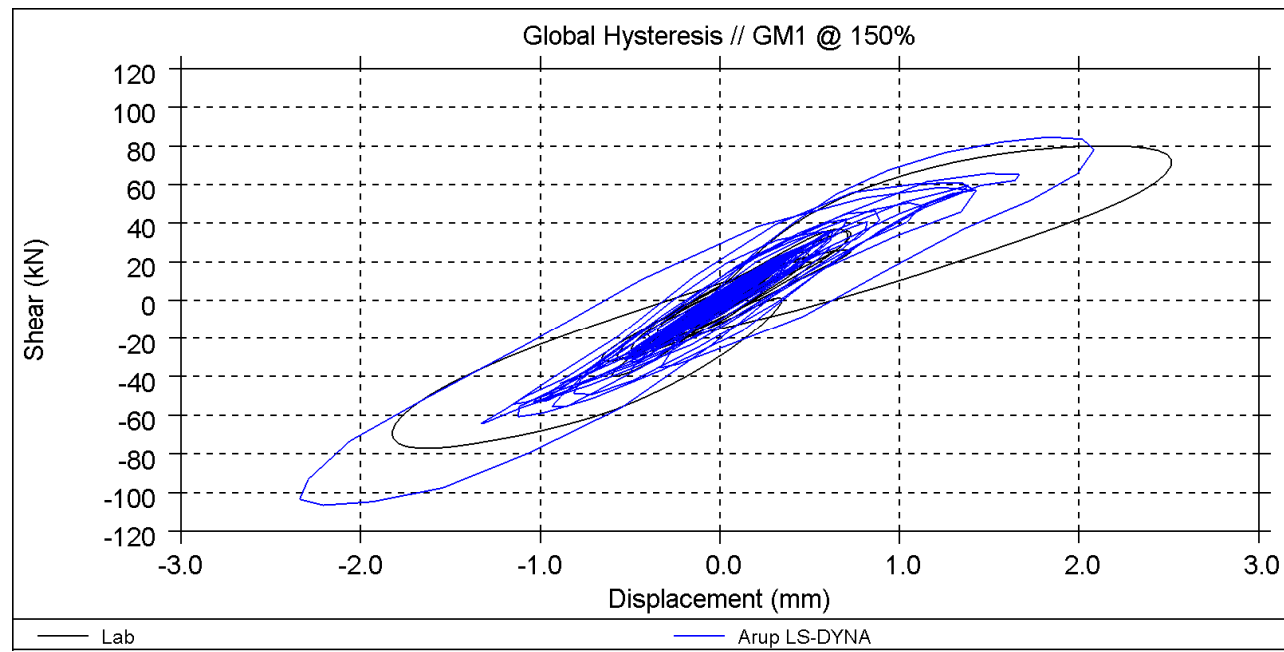
<sup>2</sup> Displacement of the roof is measured as the average displacement at the two ends of the ridge beam





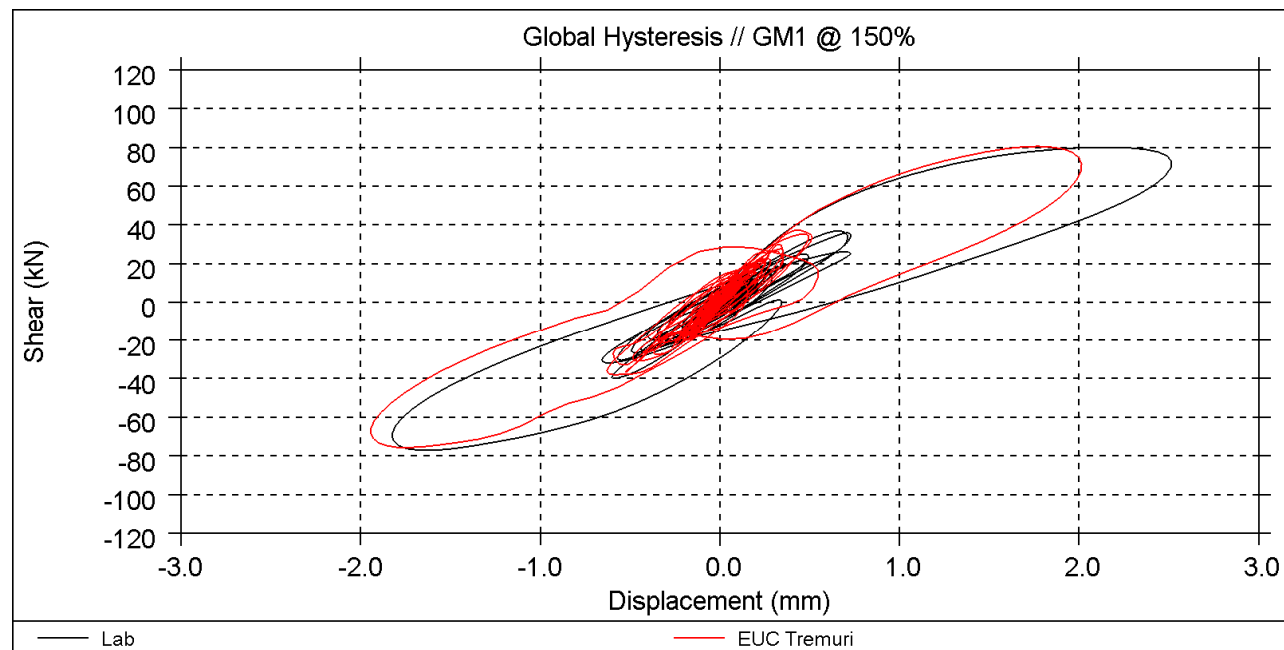
EQ1 at 150%

Global Hysteresis <sup>1</sup>



Arup

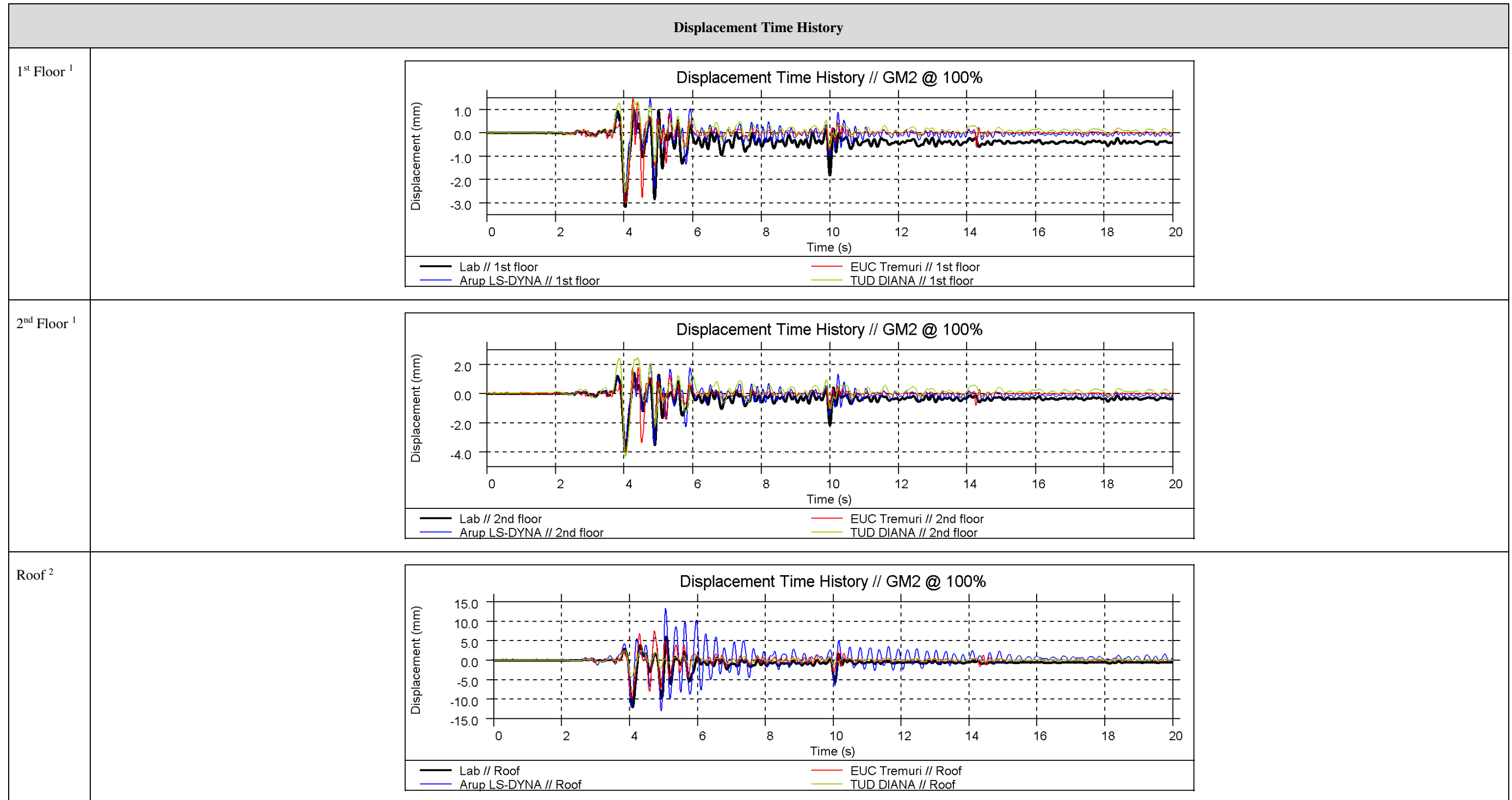
TU-Delft



EUCENTRE

<sup>1</sup> Base shear vs. 2<sup>nd</sup> floor displacement

EQ2 at 100%



<sup>1</sup> Displacement of the 1<sup>st</sup> floor and 2<sup>nd</sup> floor is calculated as the average displacement measured at the four corners of the slab

<sup>2</sup> Displacement of the roof is measured as the average displacement at the two ends of the ridge beam

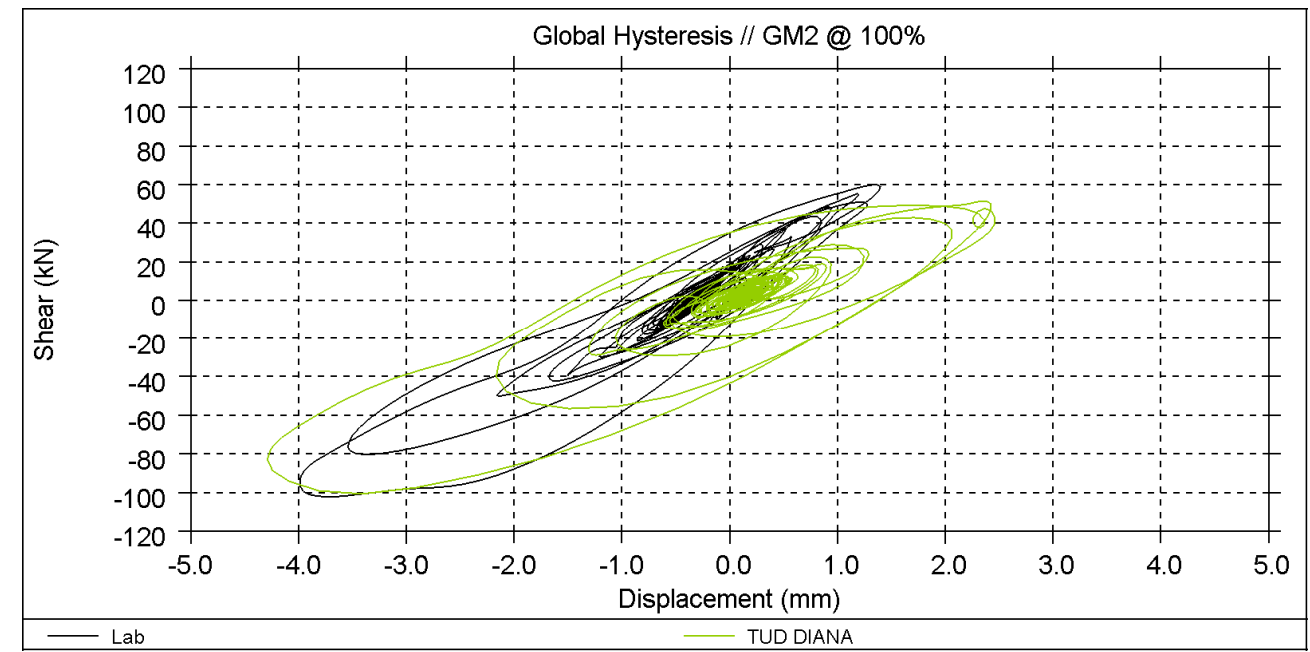
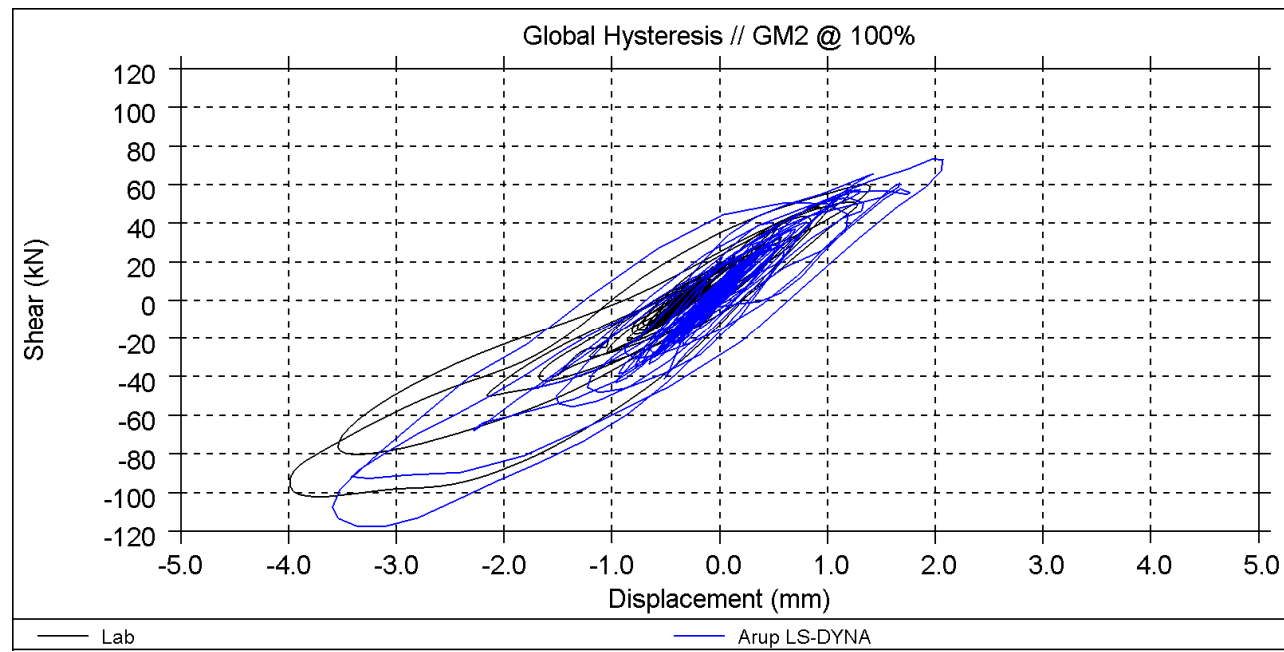






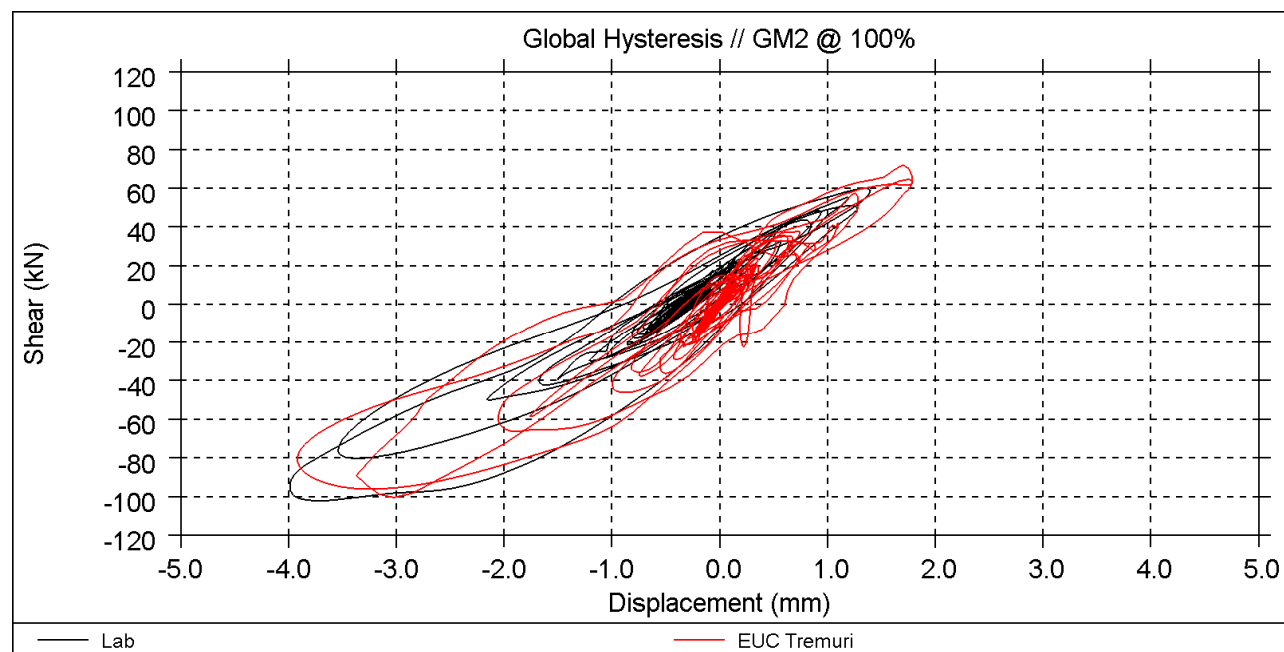
EQ2 at 100%

Global Hysteresis <sup>1</sup>



Arup

TU-Delft



EUCENTRE

<sup>1</sup> Base shear vs. 2<sup>nd</sup> floor displacement

EQ2 at 100%

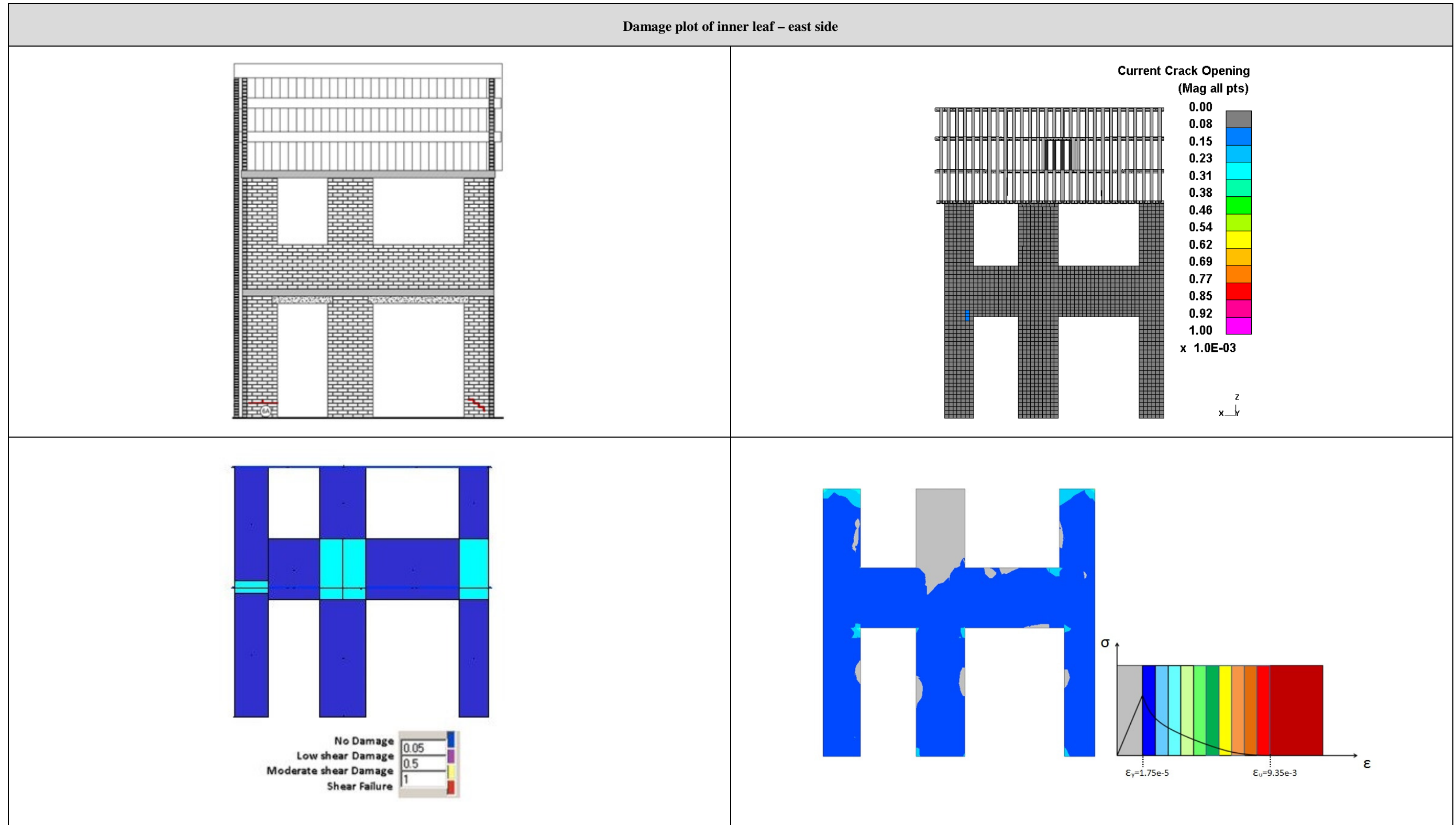


Figure 33: Damage plot of inner leaf - east side of test result (top left), Arup LS-DYNA (top right), EUCENTRE (bottom left), and TU-Delft (bottom right)

EQ2 at 100%

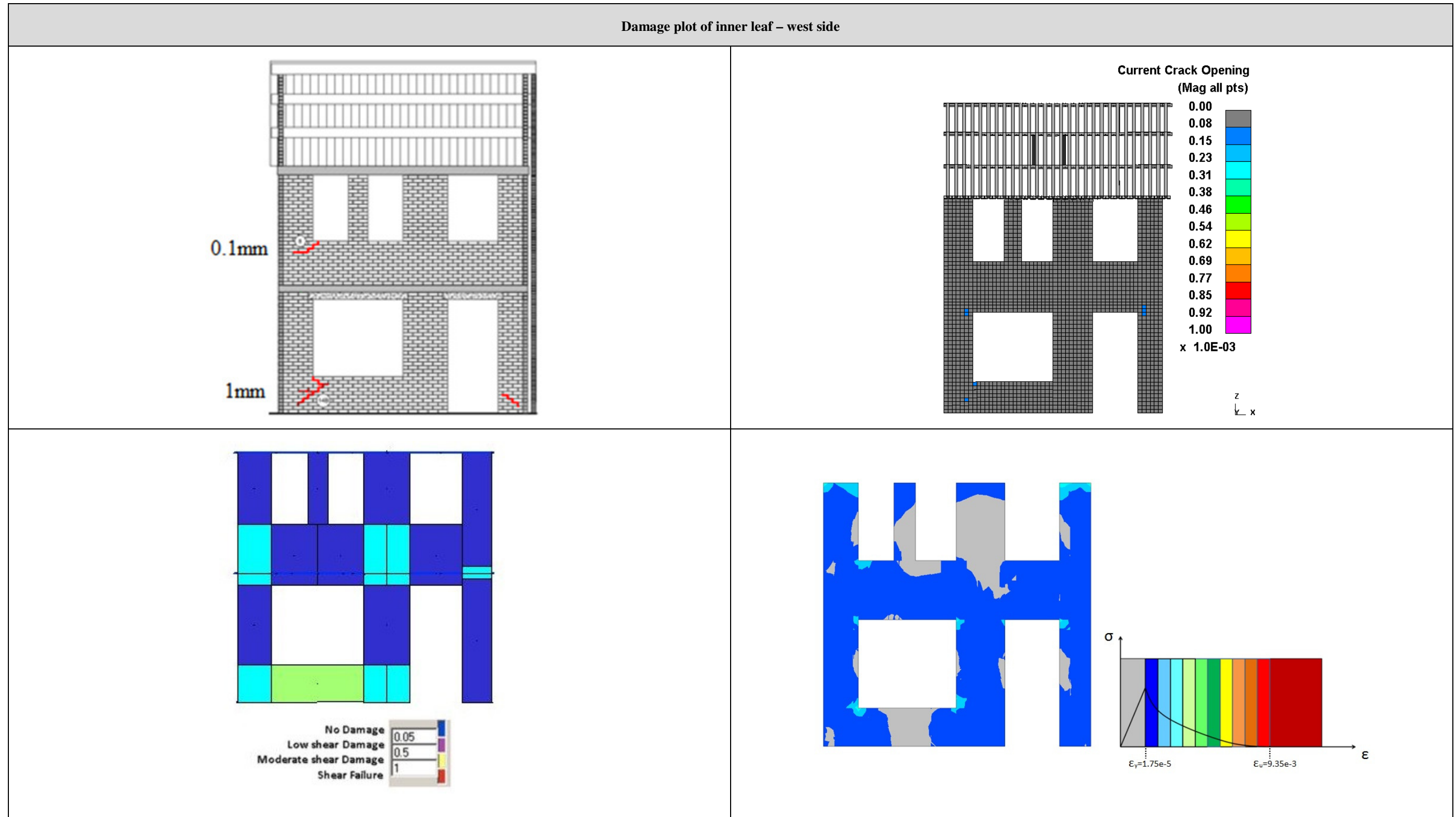
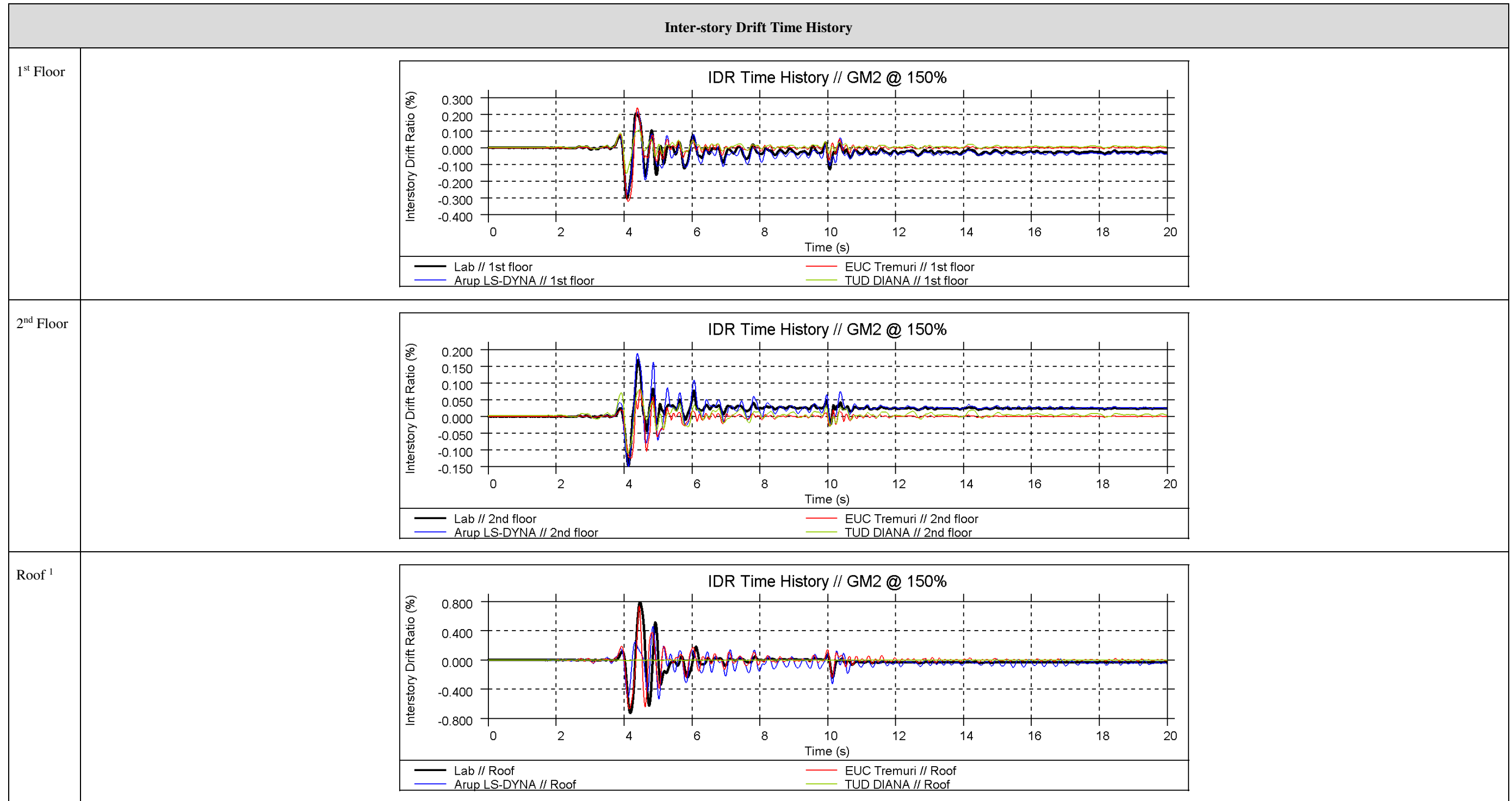


Figure 34: Damage plot of inner leaf - west side of test result (top left), Arup LS-DYNA (top right), EUCENTRE (bottom left), and TU-Delft (bottom right)



EQ2 at 150%

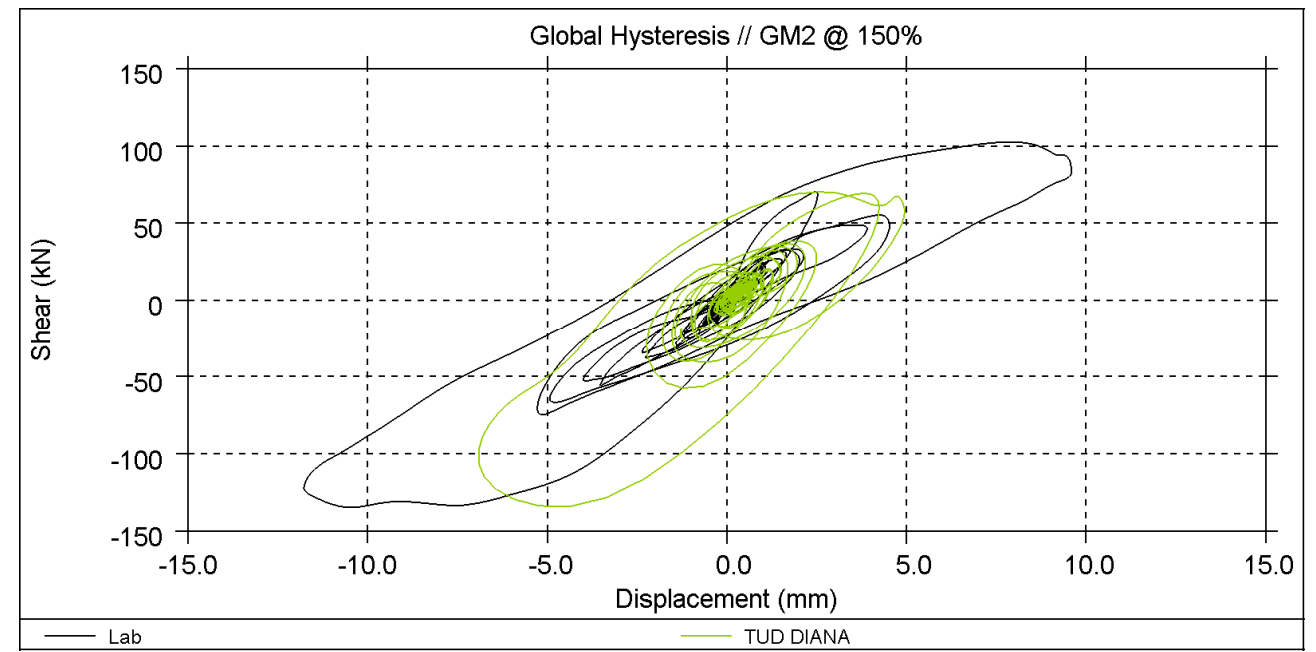
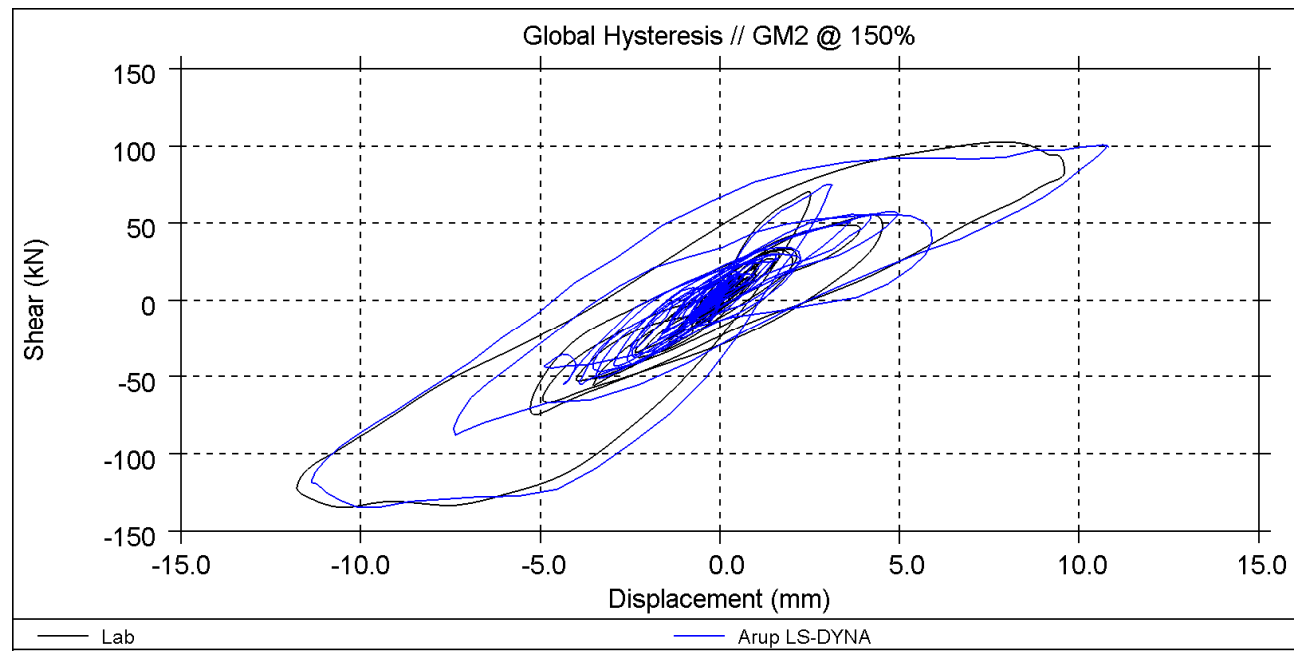


<sup>1</sup> Roof drift is calculated using a diagonal length from the gable peak to the 2<sup>nd</sup> floor along the roof slope (3.5m)



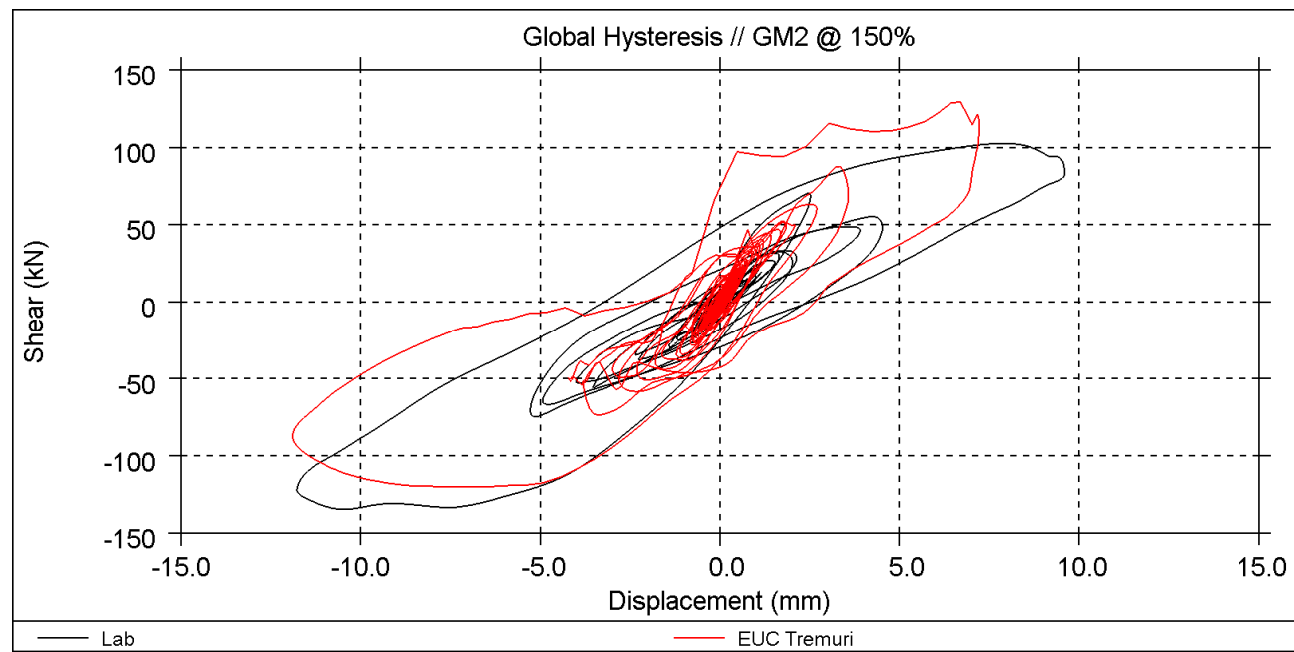
EQ2 at 150%

Global Hysteresis <sup>1</sup>



Arup

TU-Delft



EUCENTRE

<sup>1</sup> Base shear vs. 2<sup>nd</sup> floor displacement

EQ2 at 150%

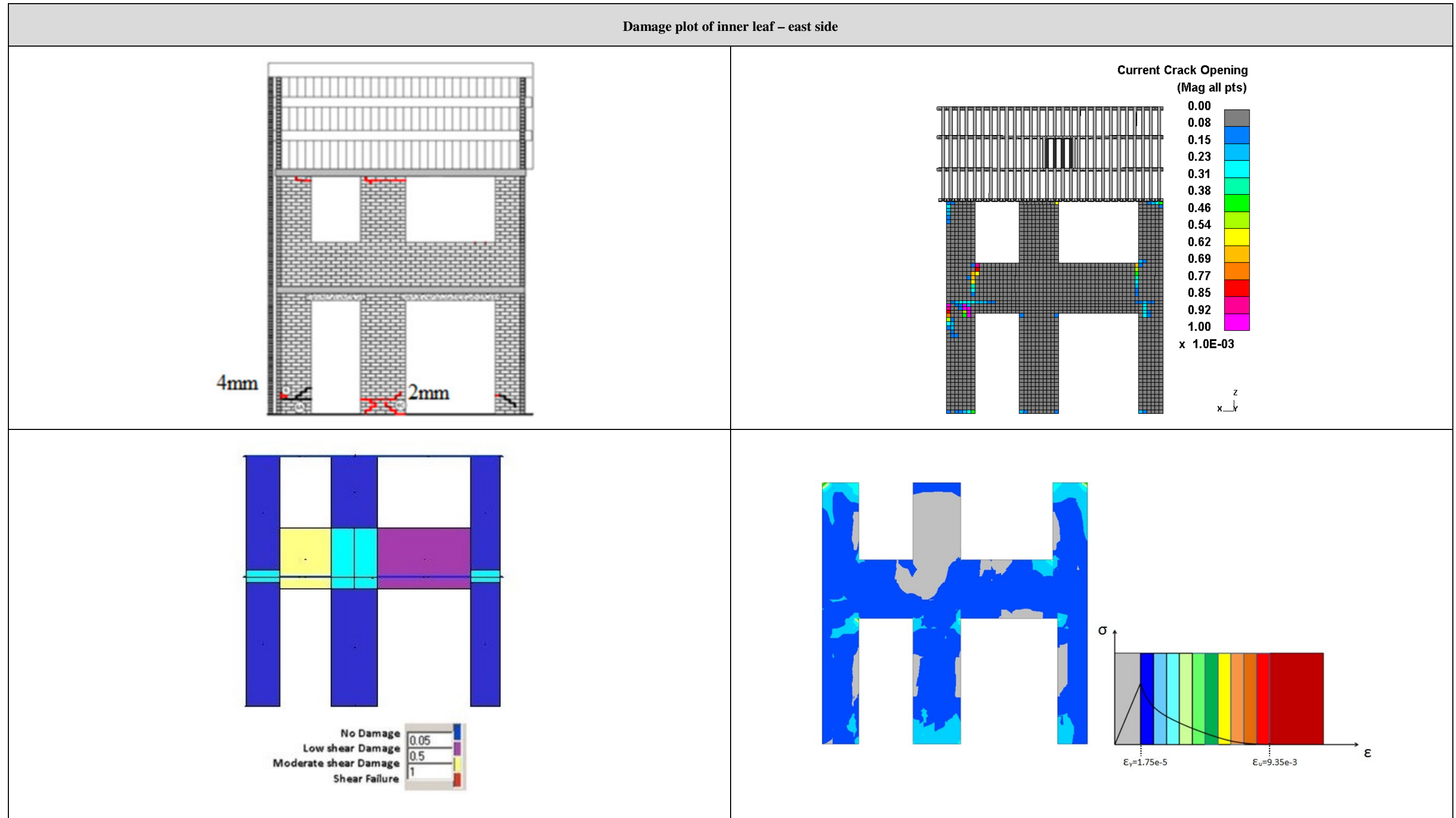


Figure 35: Damage plot of inner leaf - east side of test result (top left), Arup LS-DYNA (top right), EUCENTRE (bottom left), and TU-Delft (bottom right)



EQ2 at 150%

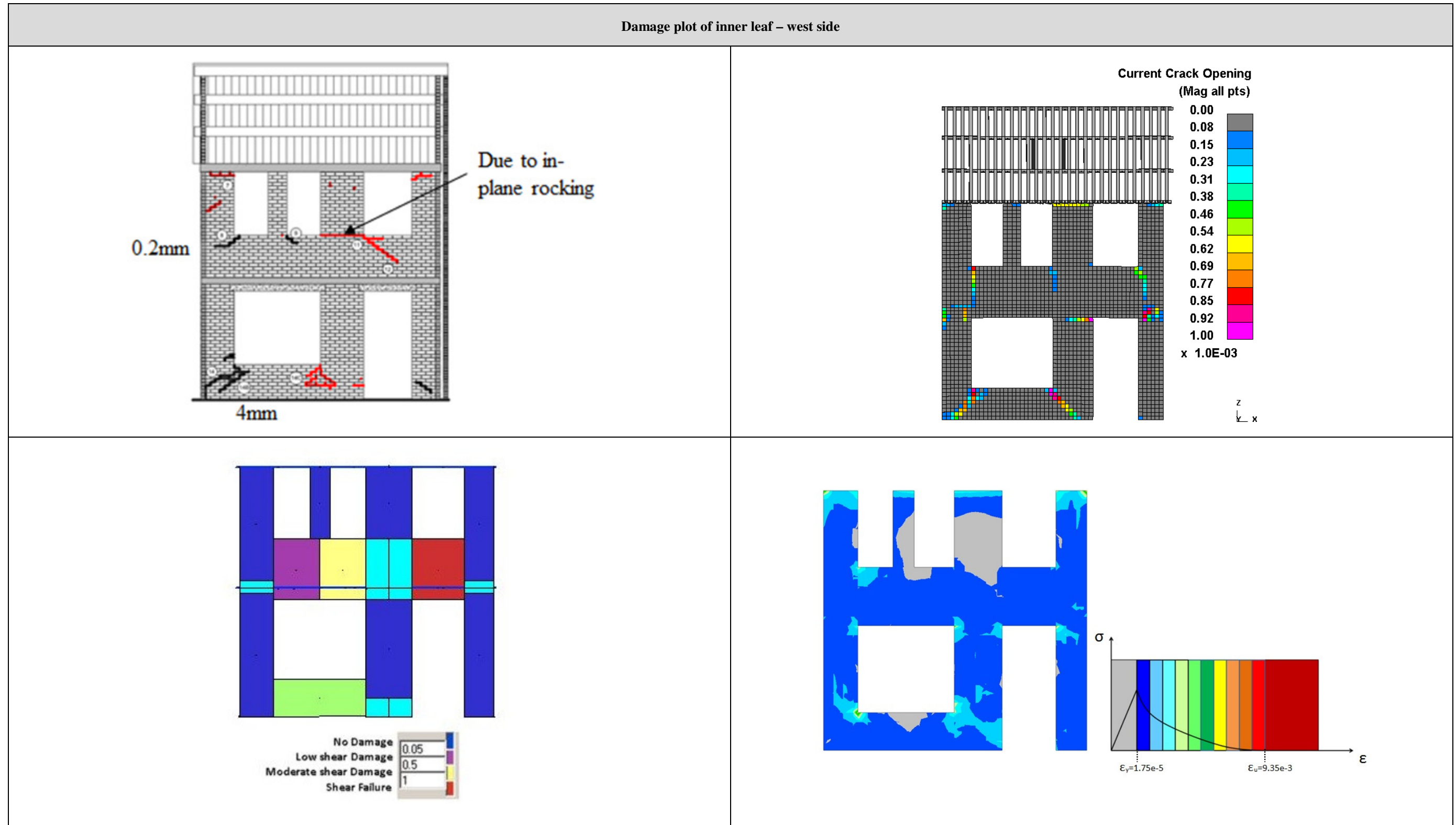
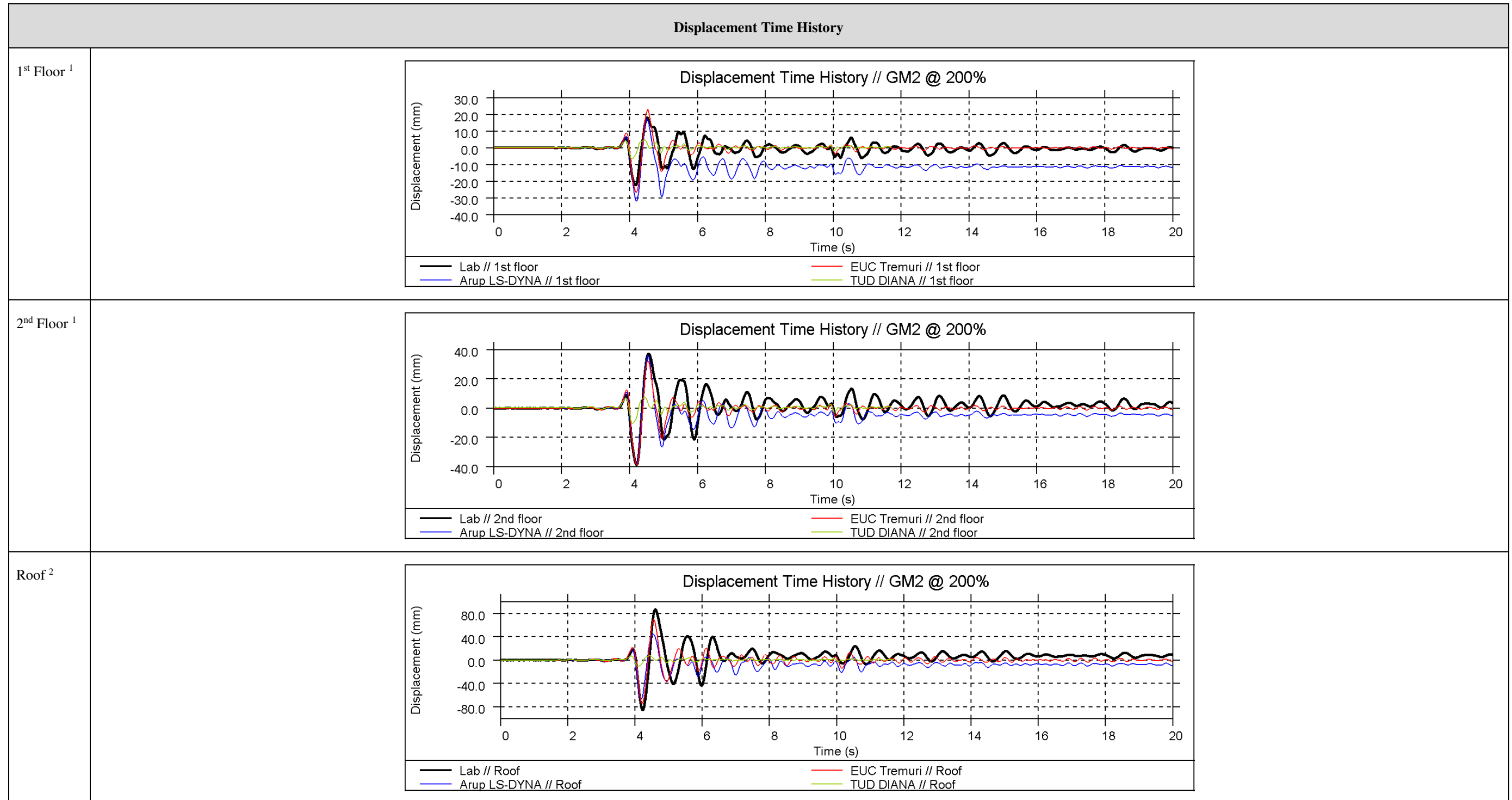


Figure 36: Damage plot of inner leaf - west side of test result (top left), Arup LS-DYNA (top right), EUCENTRE (bottom left), and TU-Delft (bottom right)

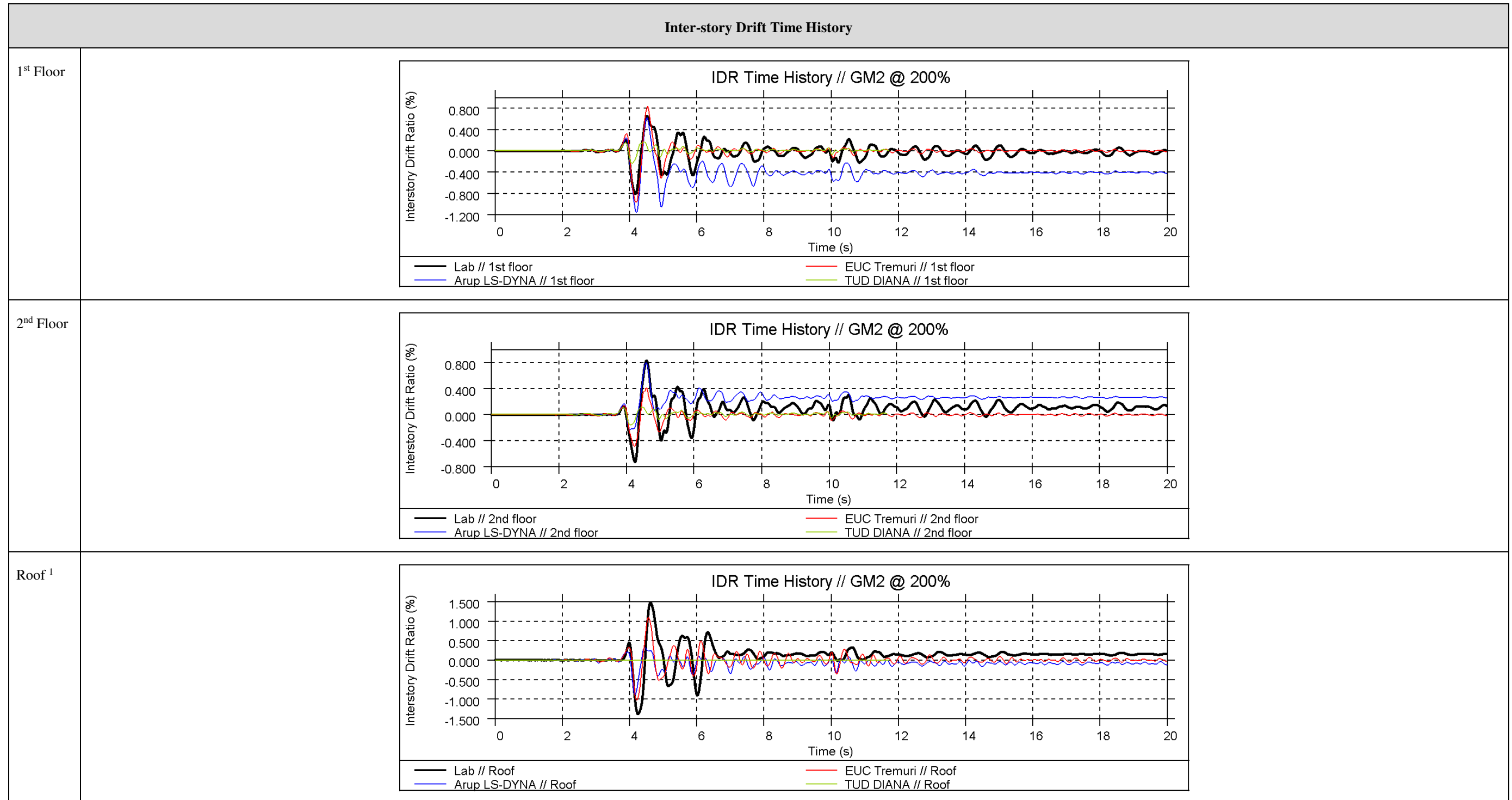
EQ2 at 200%



<sup>1</sup> Displacement of the 1<sup>st</sup> floor and 2<sup>nd</sup> floor is calculated as the average displacement measured at the four corners of the slab

<sup>2</sup> Displacement of the roof is measured as the average displacement at the two ends of the ridge beam

EQ2 at 200%

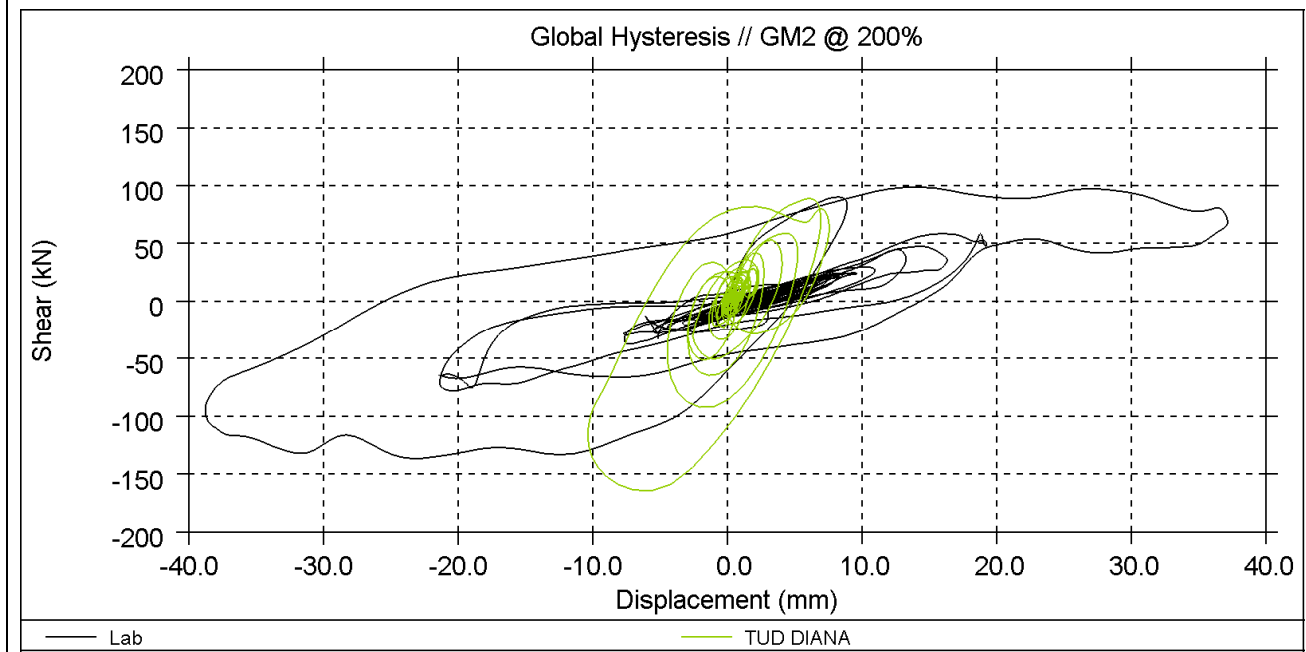
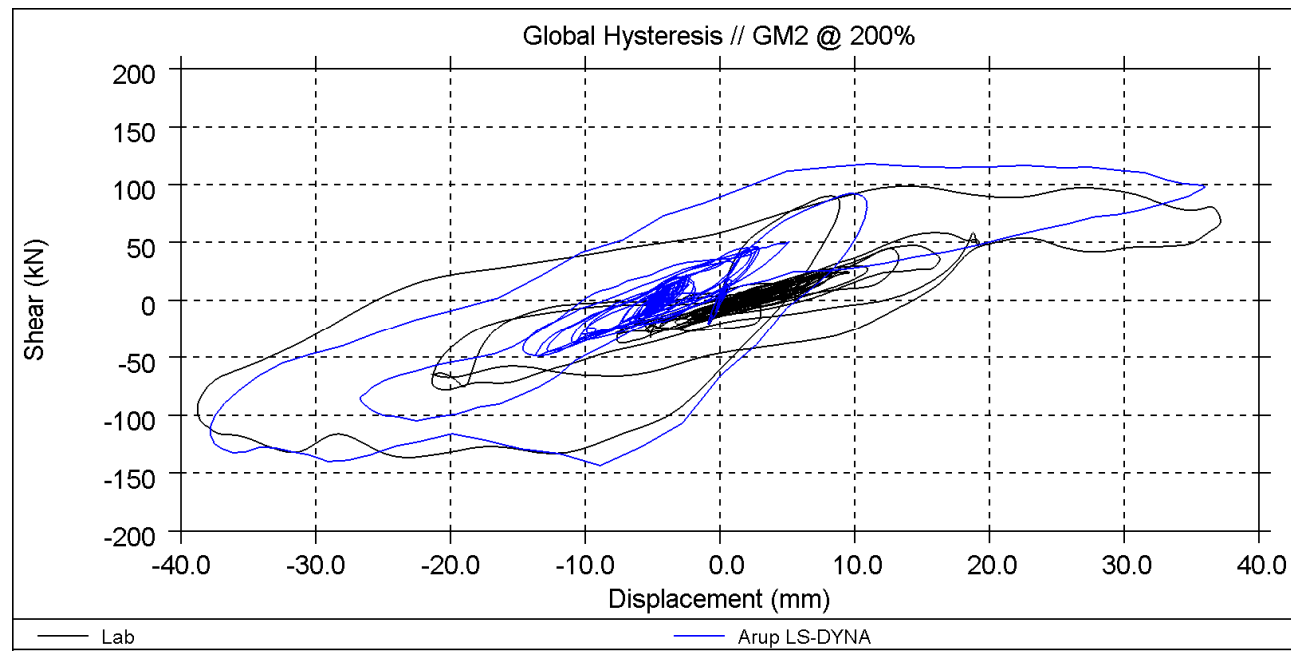


<sup>1</sup> Roof drift is calculated using a diagonal length from the gable peak to the 2<sup>nd</sup> floor along the roof slope (3.5m)



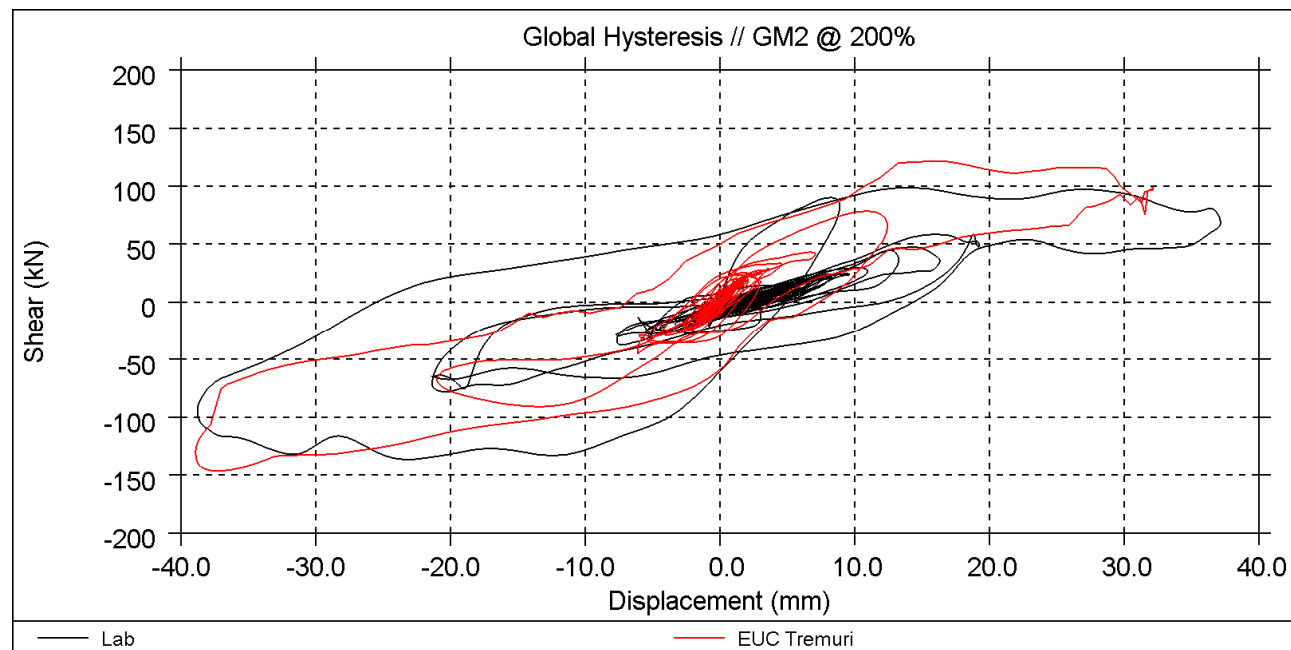
EQ2 at 200%

Global Hysteresis <sup>1</sup>



Arup

TU-Delft



EUCENTRE

<sup>1</sup> Base shear vs. 2<sup>nd</sup> floor displacement

EQ2 at 200%

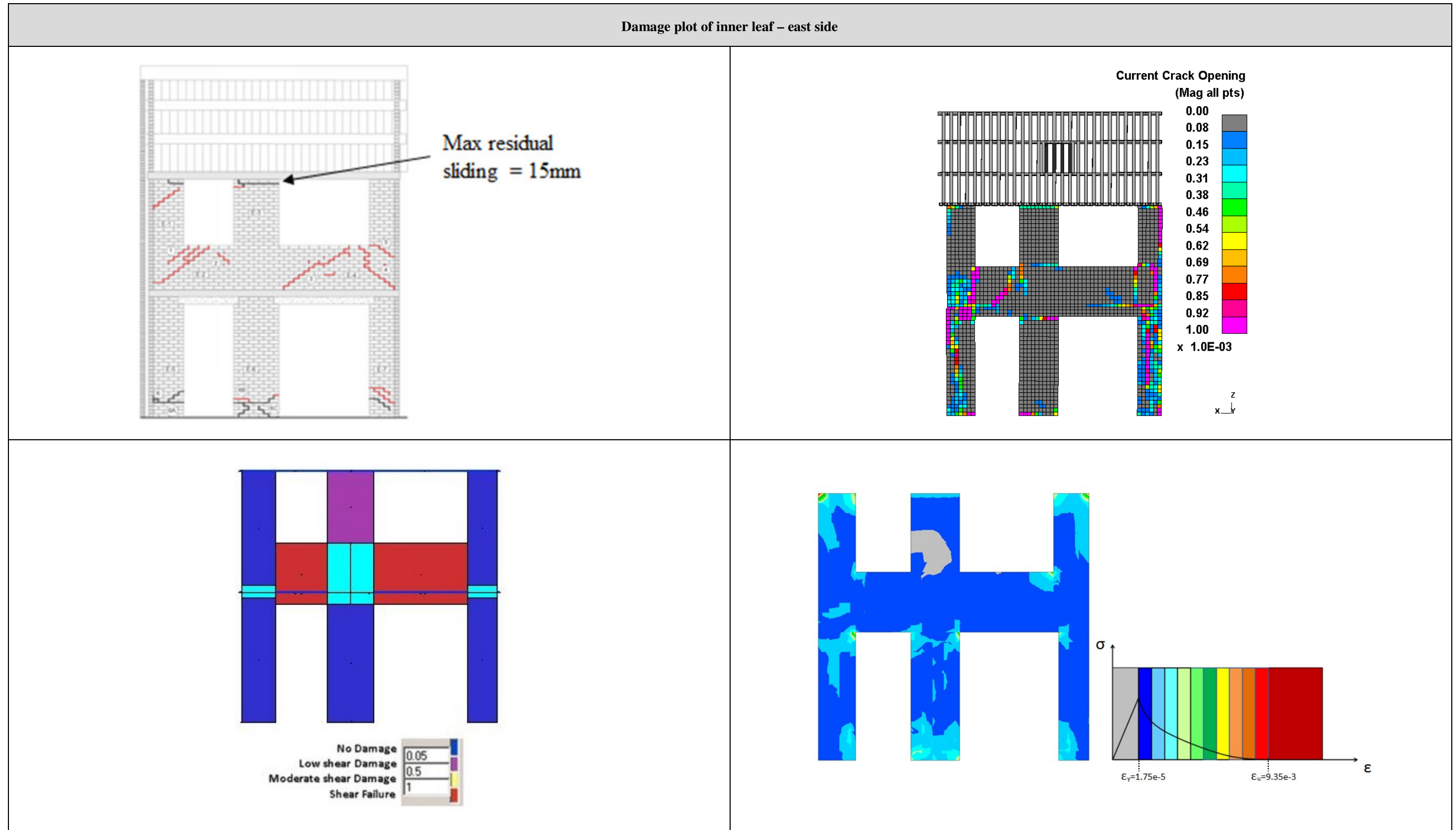


Figure 37: Damage plot of inner leaf - east side of test result (top left), Arup LS-DYNA (top right), EUCENTRE (bottom left), and TU-Delft (bottom right)

EQ2 at 200%

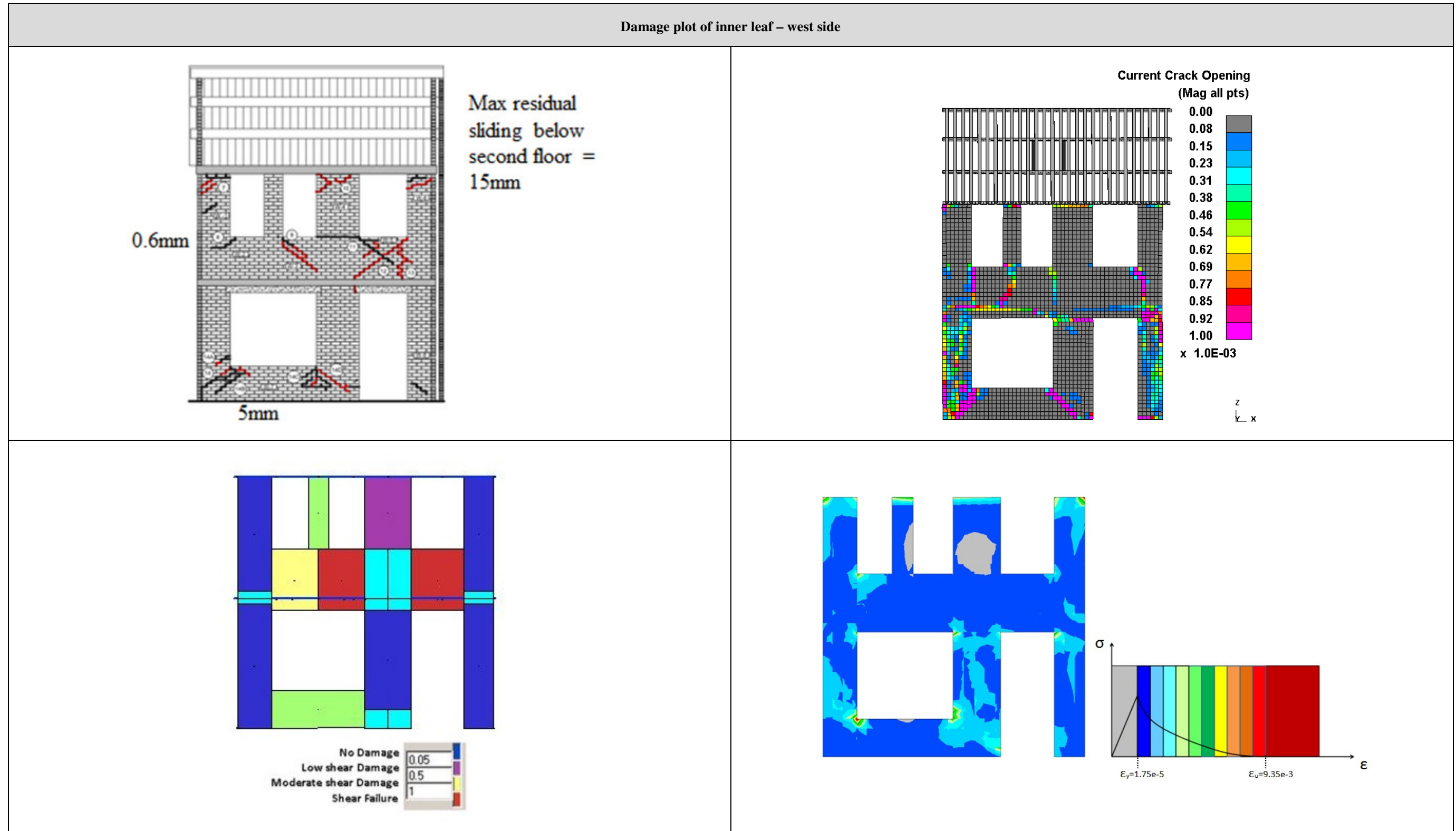


Figure 38: Damage plot of inner leaf - west side of test result (top left), Arup LS-DYNA (top right), EUCENTRE (bottom left), and TU-Delft (bottom right)

EQ2 at 200%

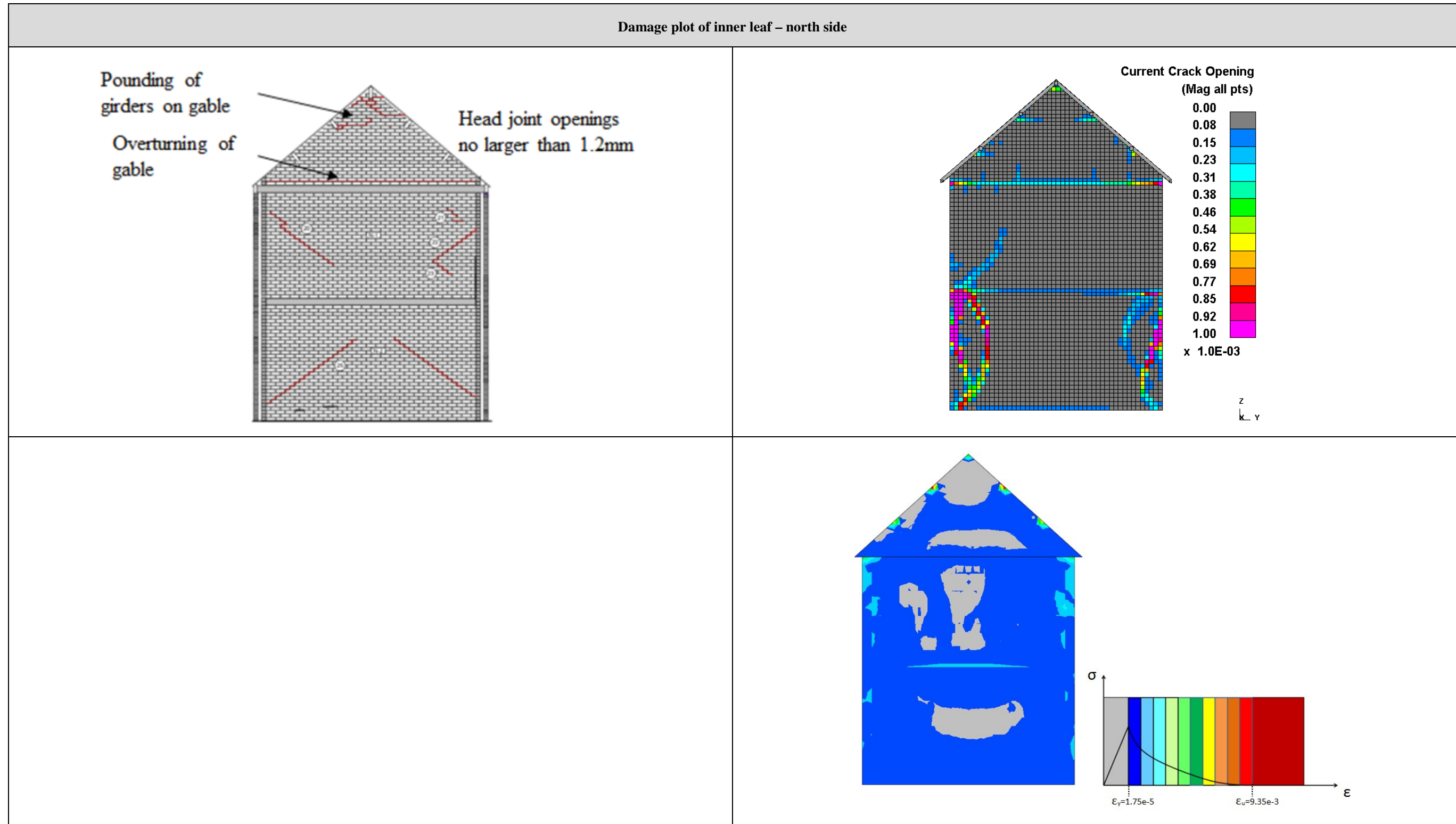


Figure 39: Damage plot of inner leaf - north side of test result (top left), Arup LS-DYNA (top right), and TU-Delft (bottom right)



EQ2 at 200%

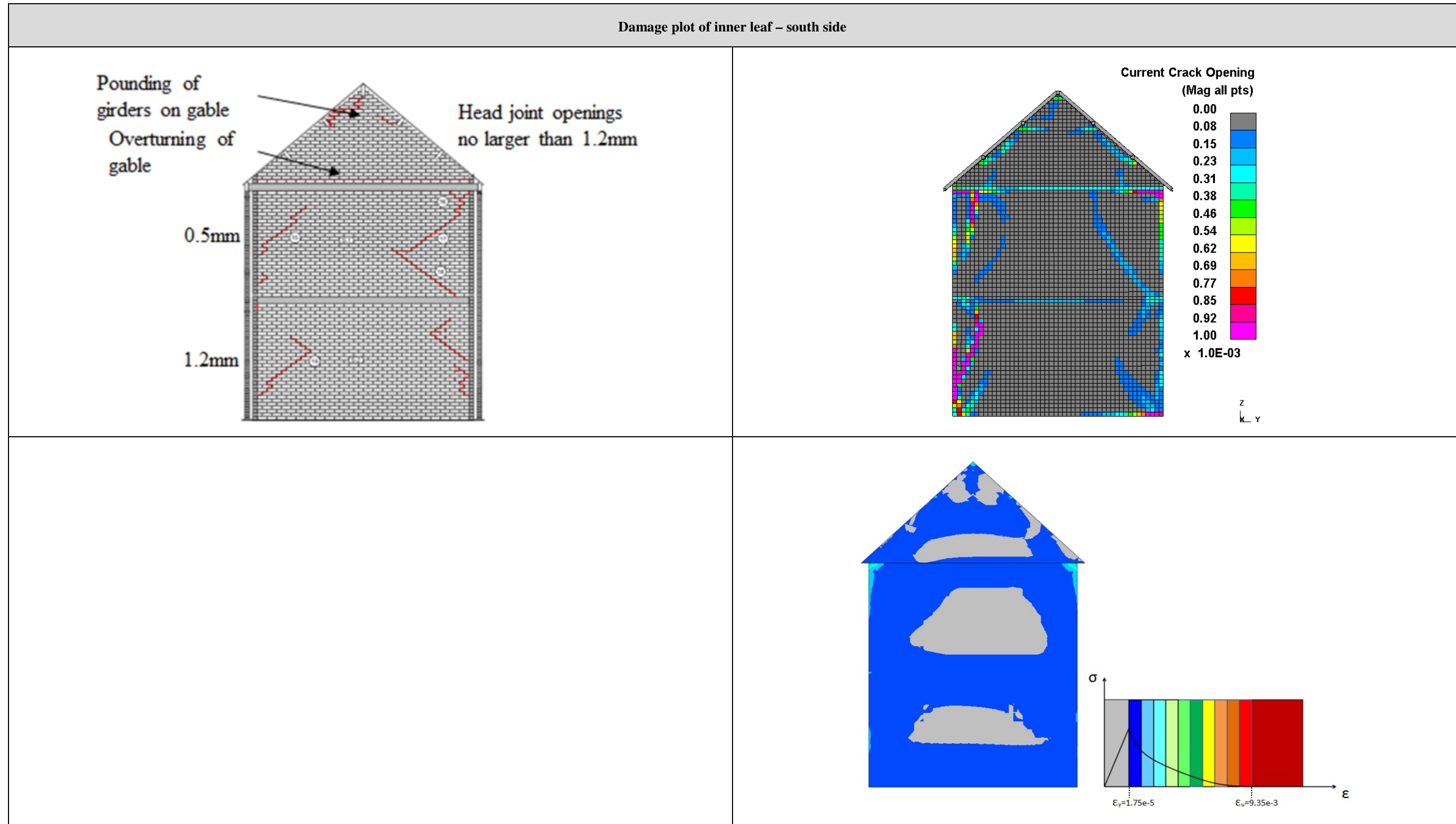


Figure 40: Damage plot of inner leaf - south side of test result (top left), Arup LS-DYNA (top right), and TU-Delft (bottom right)

EQ2 at 200%

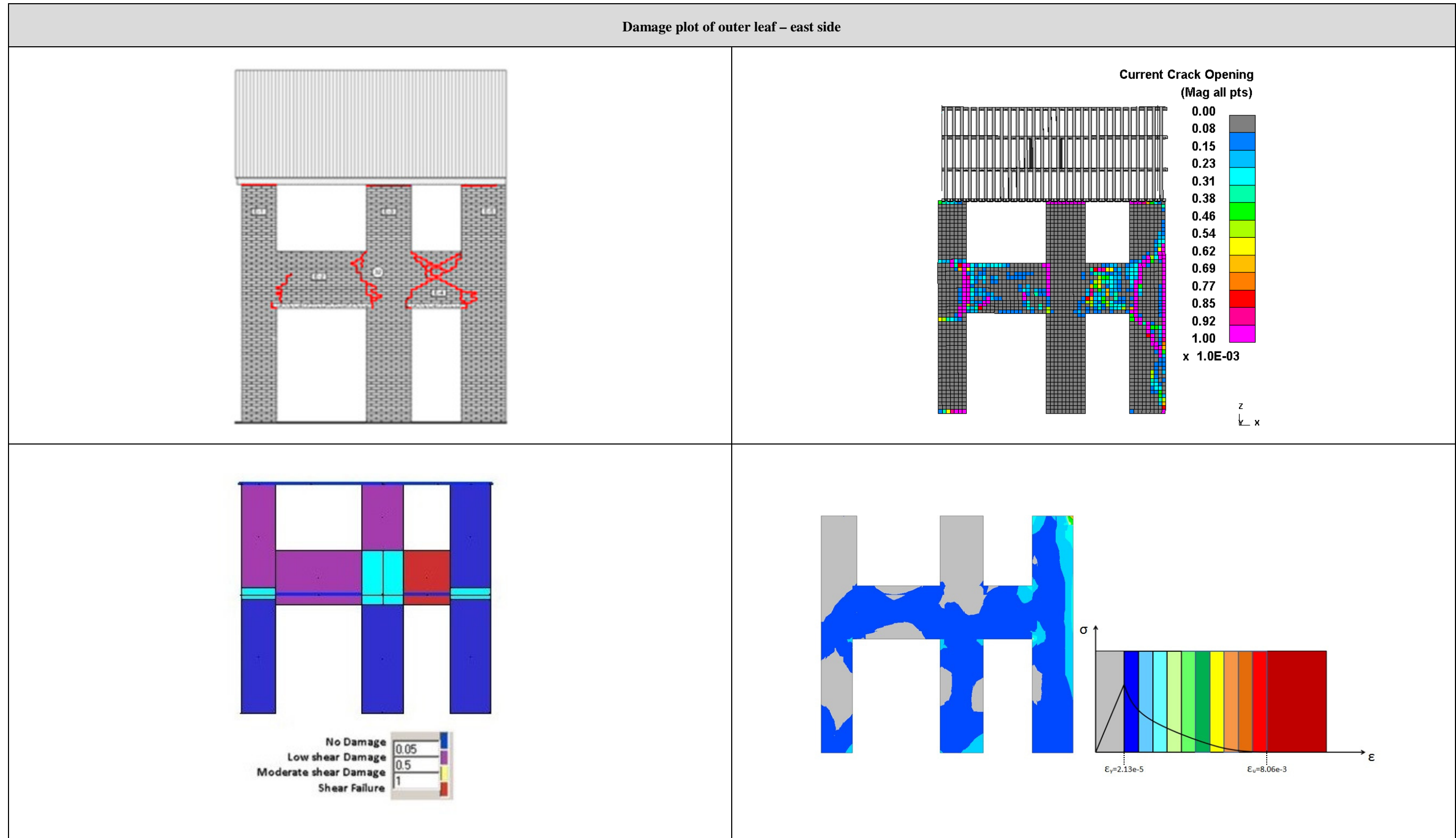


Figure 41: Damage plot of outer leaf - east side of test result (top left), Arup LS-DYNA (top right), EUCENTRE (bottom left), and TU-Delft (bottom right)

EQ2 at 200%

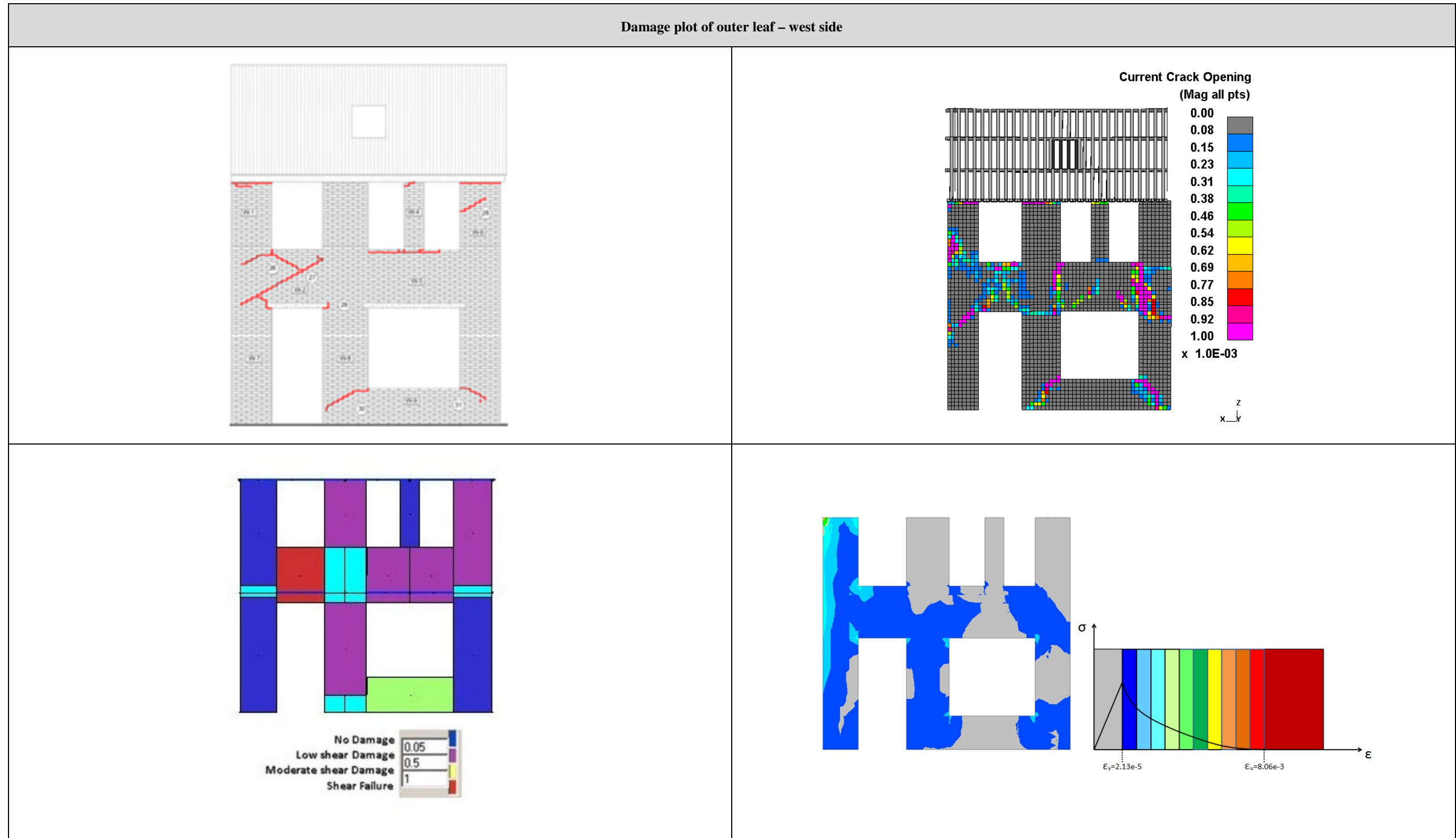


Figure 42: Damage plot of outer leaf - west side of test result (top left), Arup LS-DYNA (top right), EUCENTRE (bottom left), and TU-Delft (bottom right)

EQ2 at 200%

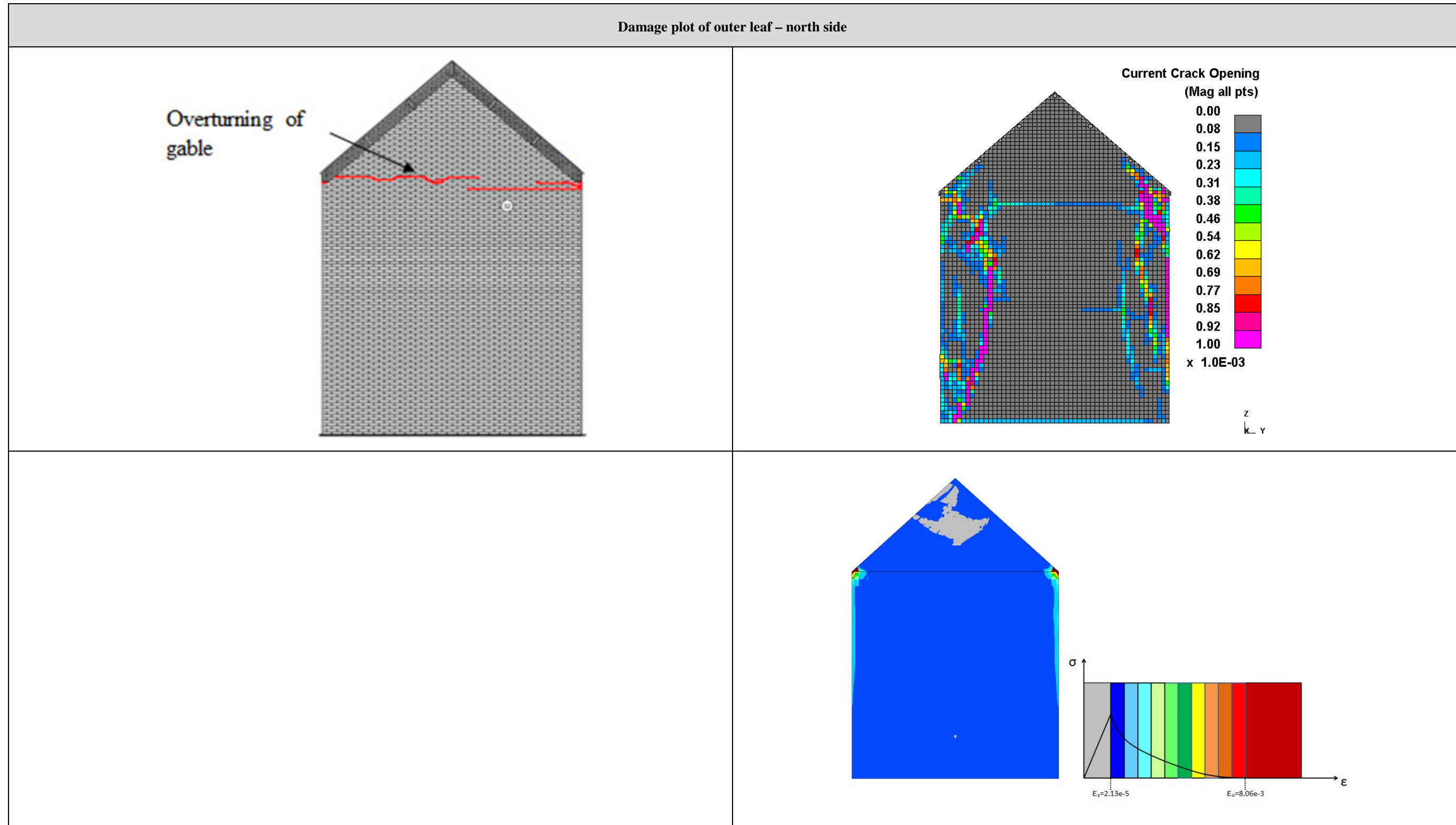


Figure 43: Damage plot of outer leaf - north side of test result (top left), Arup LS-DYNA (top right), and TU-Delft (bottom right)

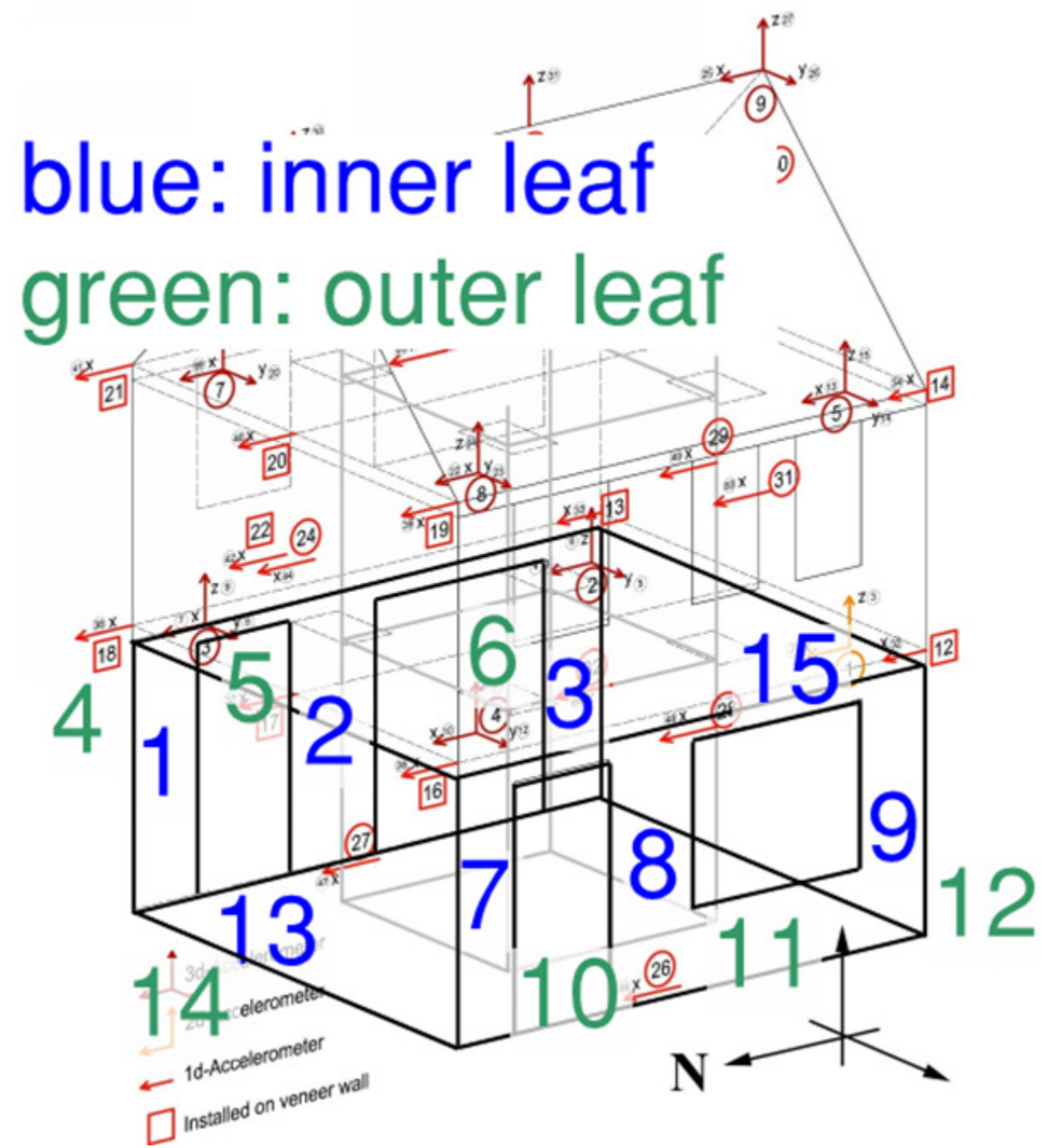


Figure 44: Legend for pier labelling. Refer to tables below

Table 31: Axial force summary (kN) <sup>1</sup>

		Total	East wall, inner			East wall, outer			West wall, inner			West wall, outer			North wall, inner	North wall, outer	South wall
			Pier 1	Pier 2	Pier 3	Pier 4	Pier 5	Pier 6	Pier 7	Pier 8	Pier 9	Pier 10	Pier 11	Pier 12	Pier 13	Pier 14	Pier 15
t = 0	Arup	558	20.0	20.5	18.7	12.1	14.4	9.45	17.4	17.9	15.9	10.8	13.3	8.83	141	68.2	151
	EUCENTRE	561	20.9	16.0	18.6	12.6	14.5	12.4	18.1	17.9	30.7	11.0	17.3	15.9	146	66.6	142
	TU-Delft	527	17.4	14.9	16.0	15.4	20.2	21.3	15.5	13.1	14.9	13.8	18.4	20.6	117	81.8	126
EQ1 @ 50%	Arup	560	26.1	21.9	12.6	19.3	17.8	12.4	22.1	13.7	16.6	16.3	9.22	17.1	125	38.0	171
	EUCENTRE	559	20.4	14.7	18.3	12.3	12.1	9.15	18.1	19.0	30.5	9.96	16.9	12.1	152	78.0	136
	TU-Delft	529	13.2	13.9	19.8	11.6	17.5	19.9	12.0	15.5	15.5	11.0	19.1	17.6	131	98.0	113
EQ1 @ 100%	Arup	560	32.1	22.8	6.80	25.5	18.4	14.7	26.8	10.0	14.3	20.7	4.04	22.0	110	17.2	188
	EUCENTRE	561	22.3	19.2	18.2	25.2	21.7	17.1	17.8	22.3	30.3	13.7	23.4	23.3	132	25.2	149
	TU-Delft	529	7.75	14.3	24.7	6.93	14.9	18.3	7.43	17.3	17.0	7.51	19.5	14.3	114	146	98.8
EQ1 @ 150%	Arup	554	40.6	25.9	1.78	32.4	19.2	18.1	33.2	9.06	7.53	27.8	1.71	22.6	79.2	1.18	198
	EUCENTRE	558	25.0	18.7	19.2	30.4	18.7	19.2	19.3	22.8	35.4	14.7	19.0	27.5	123	19.3	146
	TU-Delft	530	3.15	15.6	29.6	2.55	13.2	16.8	3.26	19.8	19.4	4.09	19.5	11.1	159	128	85.8

<sup>1</sup> Unless noted otherwise, reported axial forces occur at time "A." Time "A" is the time at which the total base shear force is the absolute maximum during that run

Table 32: Axial force summary (kN) (continued)<sup>1 2</sup>

		Total	East wall, inner			East wall, outer			West wall, inner			West wall, outer			North wall, inner	North wall, outer	South wall
			Pier 1	Pier 2	Pier 3	Pier 4	Pier 5	Pier 6	Pier 7	Pier 8	Pier 9	Pier 10	Pier 11	Pier 12	Pier 13	Pier 14	Pier 15
EQ2 @ 100%	Arup	564	45.5	28.7	1.79	36.9	21.6	21.0	38.4	9.48	4.85	27.9	3.62	21.3	63.4	-5.02	206
	EUCENTRE	563	24.6	18.0	26.1	25.5	9.24	4.66	18.8	29.7	62.5	19.9	20.6	11.6	155	64.9	72.4
	TU-Delft	523	33.7	20.1	1.01	30.5	29.0	25.8	30.9	7.37	5.79	26.3	14.5	33.4	74.6	11.7	178
EQ2 @ 150%	Arup	572	34.5	40.5	-0.235	49.7	27.6	24.1	53.0	7.44	3.49	47.2	5.29	28.4	29.1	-23.6	208
	EUCENTRE	571	40.8	20.0	46.7	35.9	7.29	5.46	32.5	32.7	63.6	30.9	17.2	9.53	149	37.4	41.4
	TU-Delft	520	38.5	22.6	-2.75	34.2	32.2	27.2	35.5	6.45	3.46	29.4	12.4	36.7	63.7	-9.77	190
EQ2 @ 200%	Arup	598	29.9	35.4	-1.51	60.0	21.0	28.2	55.3	3.42	1.43	58.8	7.59	34.1	40.6	-20.8	204
	EUCENTRE	647	68.8	30.5	42.4	26.6	14.3	7.21	54.3	55.6	64.0	17.5	21.8	8.45	89.6	74.0	72.4
	TU-Delft	533	42.0	24.3	-4.41	37.4	36.4	29.2	39.2	5.94	3.12	32.2	9.03	40.4	52.9	-10.2	195

<sup>1</sup> Unless noted otherwise, reported axial forces occur at time "A." Time "A" is the time at which the total base shear force is the absolute maximum during that run<sup>2</sup> Positive values are compression loads. Negative values are tension loads due to uplift.

Table 33: Base shear force summary (kN): EQ1 @ 50%

			Total	East wall, inner			East wall, outer			West wall, inner			West wall, outer			North wall, inner	North wall, outer	South wall
				Pier 1	Pier 2	Pier 3	Pier 4	Pier 5	Pier 6	Pier 7	Pier 8	Pier 9	Pier 10	Pier 11	Pier 12	Pier 13	Pier 14	Pier 15
EQ1 @ 50%	t = A <sup>1</sup>	Arup	51.0	3.16	4.17	2.23	4.68	4.86	2.51	2.19	1.19	0.745	3.58	0.823	0.967	0.565	0.920	2.14
		EUCENTRE	-35.4	-1.54	-2.64	-0.870	-2.80	-3.30	-1.86	-1.15	-4.97	-2.99	-1.29	-4.90	-3.89	-0.910	-1.31	-0.980
		TU-Delft	-19.3	-1.03	-2.76	-1.78	-2.13	-2.53	-0.760	-0.610	-1.26	-0.830	-1.40	-1.30	0.420	-1.22	-1.90	-0.200
	Max Envelope	Arup		3.16	4.19	2.24	-4.79	4.91	2.53	2.19	-1.39	0.749	-3.78	-2.01	0.967	-1.52	-2.07	2.20
		EUCENTRE		1.55	2.70	1.12	2.81	3.31	1.86	1.17	5.22	4.21	1.57	5.00	3.93	0.910	1.77	1.22
		TU-Delft		2.64	2.76	1.78	2.13	2.53	1.14	1.97	1.26	0.850	1.48	1.30	0.810	1.23	1.91	1.37

<sup>1</sup> Time "A" is the time at which the total base shear force is the absolute maximum during that run



Table 34: Base shear force summary (kN): EQ1 @ 100%

			Total	East wall, inner			East wall, outer			West wall, inner			West wall, outer			North wall, inner	North wall, outer	South wall
				Pier 1	Pier 2	Pier 3	Pier 4	Pier 5	Pier 6	Pier 7	Pier 8	Pier 9	Pier 10	Pier 11	Pier 12	Pier 13	Pier 14	Pier 15
EQ1 @ 100%	t = A	Arup	84.1	5.18	7.10	3.90	6.76	7.48	4.72	3.54	1.64	2.42	4.69	1.39	3.24	1.34	2.00	3.62
		EUCENTRE	64.9	-3.09	-4.53	-1.97	-5.63	-5.63	-3.09	-2.22	-8.11	-6.18	-2.61	-8.64	-6.85	-2.88	-1.22	-2.27
		TU-Delft	-40.8	-2.94	-5.19	-3.37	-4.24	-4.88	-1.78	-2.04	-3.27	-1.26	-2.91	-2.00	0.240	-2.35	-3.64	-1.21
	Max Envelope	Arup		5.18	7.10	3.90	6.76	7.48	4.72	3.54	-3.59	2.43	-5.29	-4.92	3.35	-2.58	-5.64	3.62
		EUCENTRE		3.15	4.55	2.07	5.66	5.63	3.11	2.26	8.11	7.18	2.61	8.64	6.94	2.88	2.69	2.27
		TU-Delft		4.03	5.19	3.37	4.24	4.88	1.81	2.99	3.46	1.26	2.91	2.00	0.990	2.35	3.64	2.08

Table 35: Base shear force summary: EQ1 @ 150%

			Total	East wall, inner			East wall, outer			West wall, inner			West wall, outer			North wall, inner	North wall, outer	South wall
				Pier 1	Pier 2	Pier 3	Pier 4	Pier 5	Pier 6	Pier 7	Pier 8	Pier 9	Pier 10	Pier 11	Pier 12	Pier 13	Pier 14	Pier 15
EQ1 @ 150%	t = A	Arup	107	7.34	8.96	4.44	8.82	8.45	5.90	4.93	1.25	5.58	6.48	1.86	5.48	1.99	2.00	5.86
		EUCENTRE	-80.5	-3.82	-5.45	-2.59	-7.38	-6.10	-4.02	-2.67	-10.2	-8.48	-3.32	-8.84	-9.50	-3.68	-1.38	-3.07
		TU-Delft	-56.5	-4.04	-6.94	-4.90	-5.55	-6.52	-2.76	-2.86	-4.66	-1.32	-3.86	-2.74	0.150	-3.42	-5.20	-1.91
	Max Envelope	Arup		7.62	9.03	-4.93	8.82	8.45	5.90	5.04	-5.75	5.82	6.54	-6.39	5.77	-3.99	-11.1	5.96
		EUCENTRE		4.00	5.45	3.14	7.49	6.14	4.03	2.77	11.4	11.7	3.52	11.0	9.52	3.81	2.98	3.12
		TU-Delft		5.66	7.13	5.09	5.80	6.52	2.85	4.31	5.20	1.86	4.08	2.79	1.31	3.42	5.20	2.88

Table 36: Base shear force summary: EQ2 @ 100%

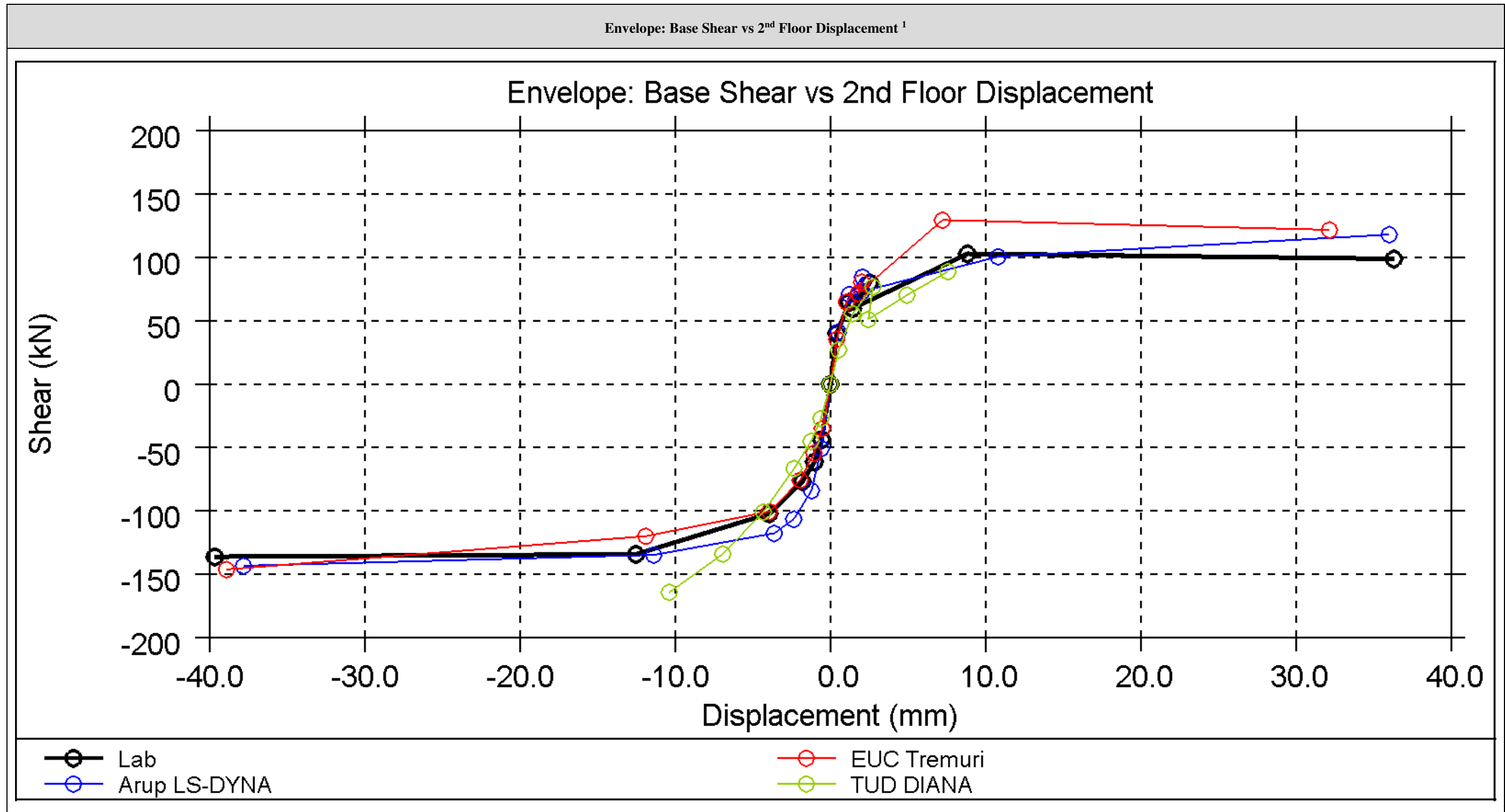
			Total	East wall, inner			East wall, outer			West wall, inner			West wall, outer			North wall, inner	North wall, outer	South wall
				Pier 1	Pier 2	Pier 3	Pier 4	Pier 5	Pier 6	Pier 7	Pier 8	Pier 9	Pier 10	Pier 11	Pier 12	Pier 13	Pier 14	Pier 15
EQ2 @ 100%	t = A	Arup	118	8.87	10.0	4.58	9.29	9.07	6.30	5.92	1.19	6.61	5.99	1.14	4.61	3.13	2.34	8.64
		EUCENTRE	101	3.33	5.84	2.94	11.0	10.0	4.67	2.35	14.2	11.0	5.35	16.8	8.38	1.58	1.47	1.69
		TU-Delft	68.4	7.83	8.69	3.09	9.04	9.97	4.61	5.91	-3.51	3.37	6.24	0.850	1.93	2.17	3.71	4.51
	Max Envelope	Arup		9.03	10.3	-5.08	9.42	9.07	6.35	6.03	-5.25	6.74	5.99	-5.89	5.16	-3.68	-12.7	8.93
		EUCENTRE		4.21	7.09	4.12	11.0	10.5	5.02	2.76	16.2	16.8	5.35	17.2	10.8	5.19	3.68	3.92
		TU-Delft		7.83	8.69	3.90	9.04	9.97	4.61	5.91	4.50	3.44	6.24	2.22	1.97	2.61	4.09	4.51

Table 37: Base shear force summary: EQ2 @ 150%

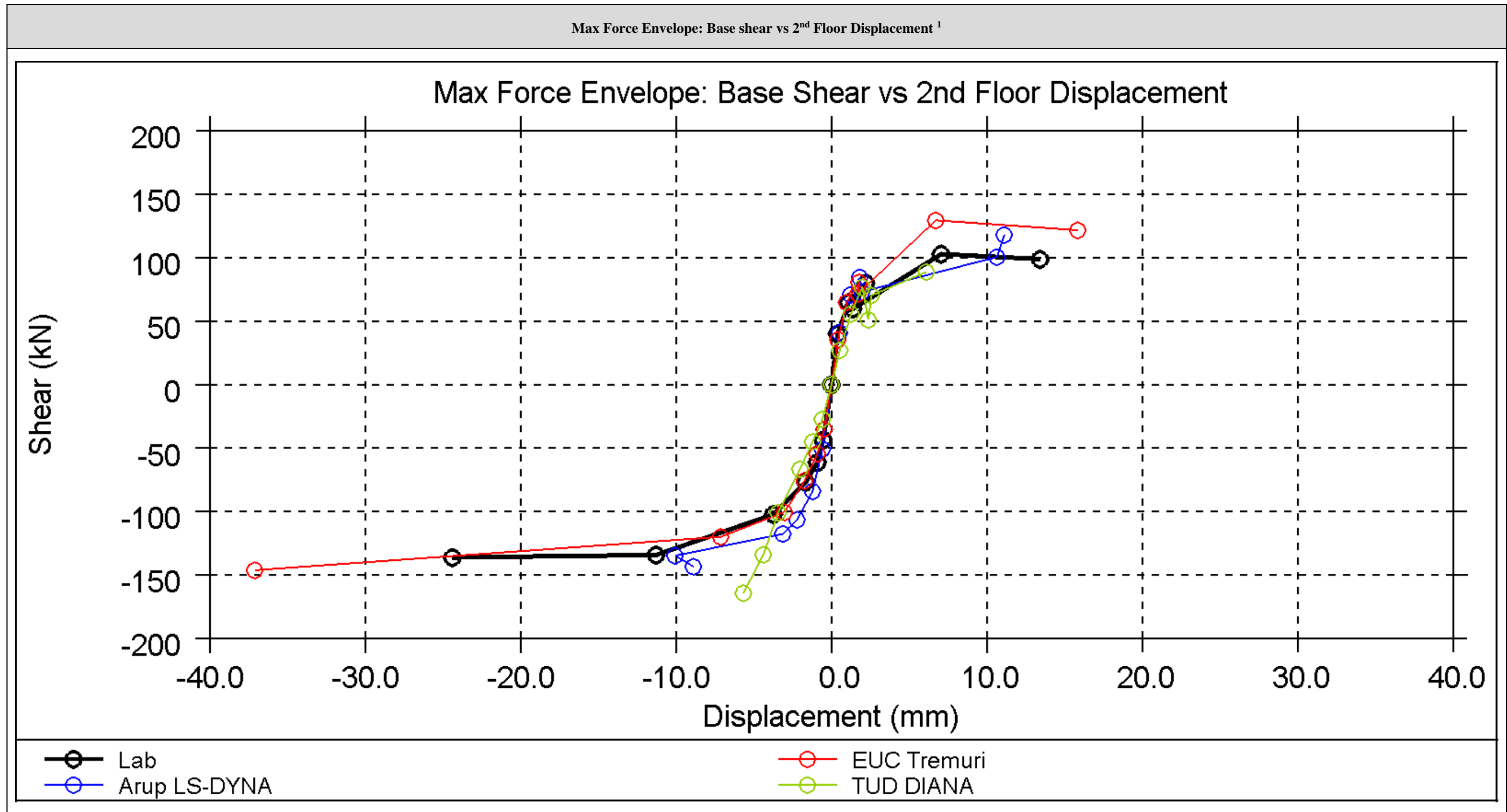
			Total	East wall, inner			East wall, outer			West wall, inner			West wall, outer			North wall, inner	North wall, outer	South wall
				Pier 1	Pier 2	Pier 3	Pier 4	Pier 5	Pier 6	Pier 7	Pier 8	Pier 9	Pier 10	Pier 11	Pier 12	Pier 13	Pier 14	Pier 15
EQ2 @ 150%	t = A	Arup	135	8.32	13.7	0.780	10.7	10.6	6.29	9.94	0.234	2.53	8.89	1.28	7.86	3.23	1.53	24.4
		EUCENTRE	-129	-8.93	-11.3	-4.98	-7.74	-3.78	-3.15	-6.05	-15.7	-6.95	-4.74	-19.3	-9.86	-4.03	-18.2	-4.59
		TU-Delft	91.3	10.2	11.3	3.84	11.9	13.6	6.36	7.63	-4.33	4.41	8.47	0.940	2.99	3.50	4.06	6.51
	Max Envelope	Arup		10.0	13.7	-10.2	11.4	10.9	6.50	9.95	-13.6	6.19	8.89	-8.60	8.00	-20.6	-15.7	25.2
		EUCENTRE		9.88	11.5	7.89	16.7	23.0	9.01	6.59	16.6	11.9	9.22	19.4	23.5	6.19	18.2	5.48
		TU-Delft		10.3	11.5	5.14	11.9	13.8	6.44	7.72	6.09	4.55	8.47	2.83	3.62	3.50	5.47	6.56

Table 38: Base shear force summary: EQ2 @ 200%

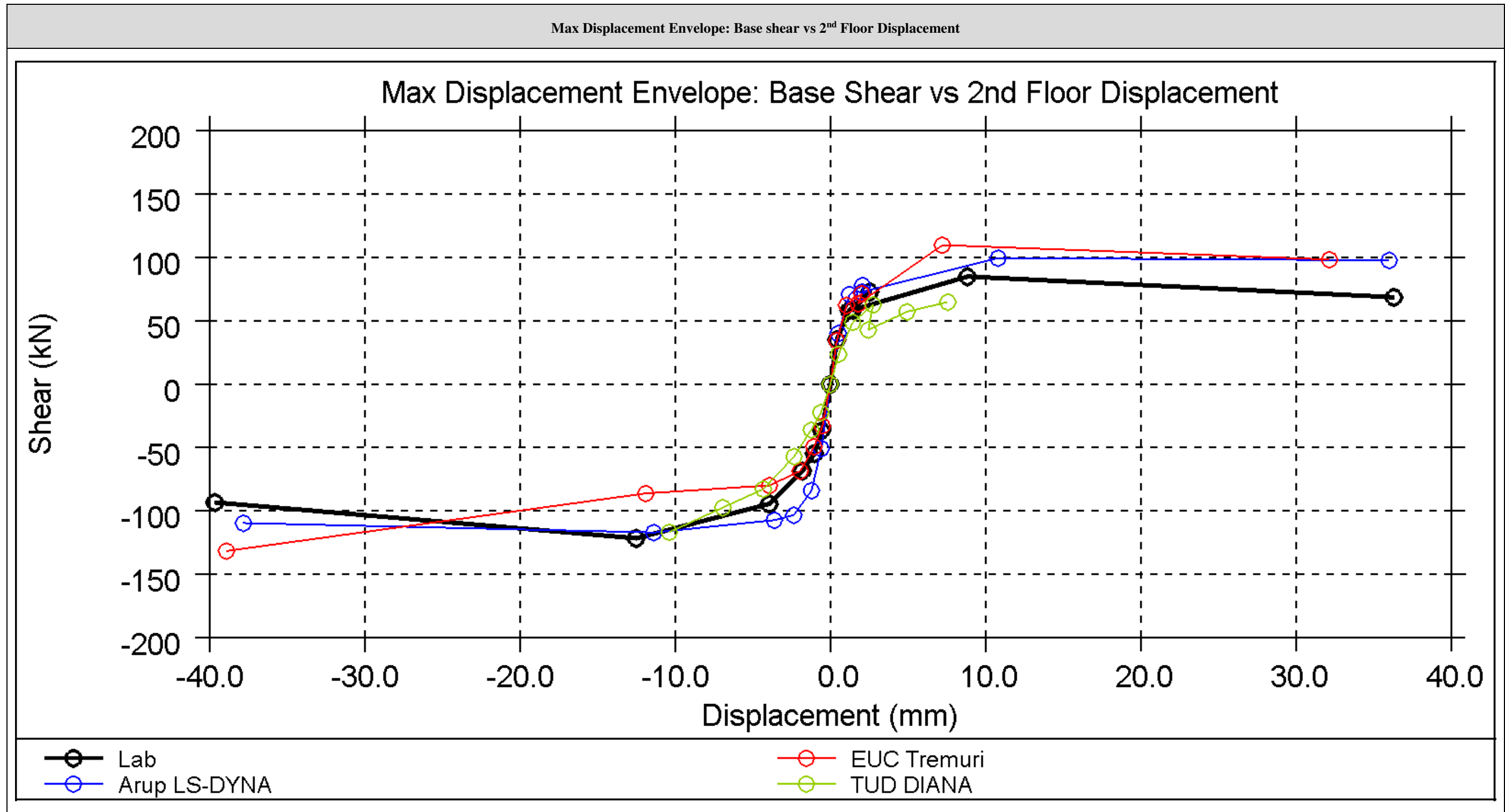
			Total	East wall, inner			East wall, outer			West wall, inner			West wall, outer			North wall, inner	North wall, outer	South wall
				Pier 1	Pier 2	Pier 3	Pier 4	Pier 5	Pier 6	Pier 7	Pier 8	Pier 9	Pier 10	Pier 11	Pier 12	Pier 13	Pier 14	Pier 15
EQ2 @ 200%	t = A	Arup	143	8.39	12.6	0.704	11.8	7.42	7.59	11.5	1.46	1.10	12.1	2.21	11.0	5.09	0.432	23.1
		EUCENTRE	146	13.7	12.1	9.17	7.64	6.17	2.60	9.40	24.0	14.8	4.23	10.2	2.74	2.41	4.78	22.2
		TU-Delft	110	12.3	13.6	4.25	14.6	17.4	7.98	9.38	-5.06	4.89	10.5	-1.95	5.00	4.22	4.53	8.30
	Max Envelope	Arup		9.59	20.8	-13.1	11.8	18.7	12.3	11.5	-23.3	-2.81	12.1	-9.16	12.5	-28.9	-15.1	24.4
		EUCENTRE		15.0	19.3	10.6	7.65	6.87	5.85	9.64	26.6	16.3	4.23	11.0	6.40	18.9	7.34	30.6
		TU-Delft		12.3	13.8	6.43	14.6	17.5	8.14	9.43	7.79	5.99	10.5	3.96	6.14	5.00	6.78	8.35



<sup>1</sup> Plot is defined as maximum base shear in +x direction vs. maximum displacement in +x direction, and maximum base shear in -x direction vs. maximum displacement in -x direction for each ground motion.



<sup>1</sup> Plot is defined as maximum base shear in +x direction vs. corresponding displacement at that instant, and maximum base shear in -x direction vs. corresponding displacement at that instant for each ground motion.



<sup>1</sup> Plot is defined as instantaneous base shear vs. maximum displacement in +x direction, and instantaneous base shear vs. maximum displacement in -x direction for each ground motion.

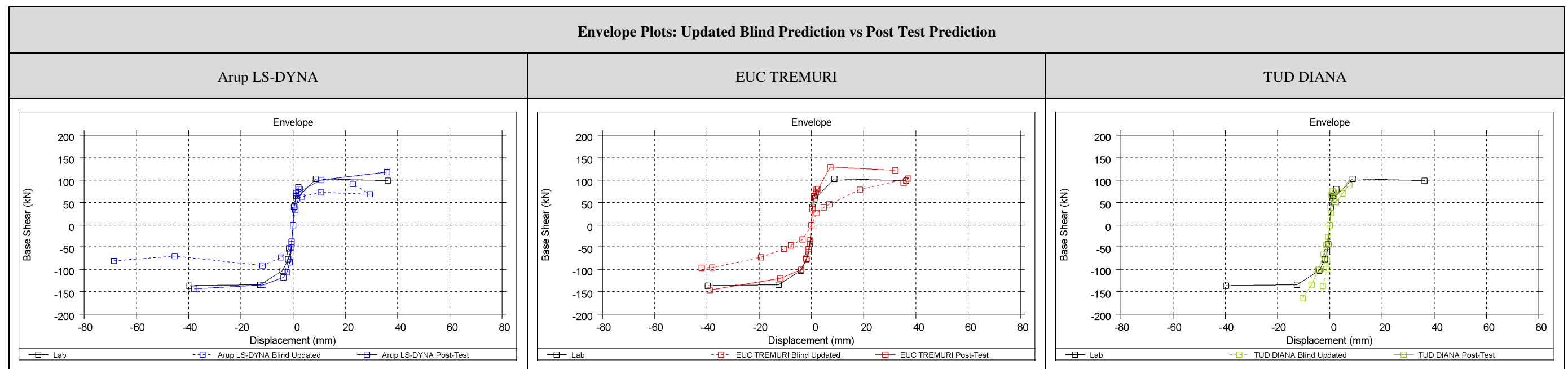


### 2.3.6 Conclusion

First, to give a brief summary of the behaviour of the lab specimen, the building tolerated 0.17g PGA with little damage and was in a near-collapse state after 0.31g PGA. At the end of EQ2 scaled at 200%, the structure may have been approaching a near-collapse state due to extensive damage in the spandrel beams (both shear and in-plane bending cracks) at the first floor level and the out-of-plane overturning mechanism activated in the gable walls. This is evident in the crack patterns presented in section 2.3.5 above. No significant shear damage occurred in masonry piers, whereas sliding occurred at the top of masonry walls parallel to the table motion (East and West walls).

The absence of significant shear failures in the experimental response of masonry piers did not allow to exploit any possible improvement in the finite element models which had not performed well in the simulation of the in-plane cyclic tests of piers failing in shear (component tests).

All numerical models achieved improved results with each post-test refined prediction model. The LS-DYNA post-test refined model of the full scale shake table building results in more accurate predictions and simulation of observed behaviour in the laboratory in comparison to the blind prediction model, and the model now well predicts the building deformation experienced during the application of EQ2. Nevertheless, the intrinsic damping of the CaSi masonry is higher than assumed, which affects the predictions at low levels of response but has less influence at higher response levels. For the TREMURI model, the implemented improvements in the new refined model have a significant impact in simulating with a more precise way the response of the test-house. Compared to the blind prediction model, the post-test improved TREMURI model exhibits a general response noticeably closer to the real dynamic response of the test building, during the whole test protocol. In order to better match the last stage of the test (EQ2-200%) the interface elements on top of the veneers were removed, allowing for free sliding (this could also be done by activating the element expiration feature of the macroelement model at the attainment of a given shear drift). For the DIANA model, the refinement of the finite element model for the post-test prediction leads to an improvement in terms of stability of the solution, since the whole loading protocol has been applied without experiencing any numerical divergence. Compared to the blind prediction, the global behaviour is significantly closer to the experiment. Nevertheless, the model still presents a behaviour that is too stiff for higher PGAs (EQ2-150% and 200%) leading to underprediction of the displacements for the last 2 applied ground motions and absence of a clear plateau in the base shear - top displacement curve.



As a result of performing the blind prediction and post-test refined prediction of the EUCENTRE full scale shake table building, the following LS-DYNA, TREMURI, and DIANA software pros and cons have been gathered and compared in Table 39 below.

Table 39: Comparison of software pros and cons

	Arup LS-DYNA	EUCENTRE TREMURI	TU-Delft DIANA
Pros	<ul style="list-style-type: none"> <li>• Collapse and near-collapse scenarios can be predicted</li> <li>• Effect of details of construction and geometry are well captured</li> <li>• Any improvement of input data is reflected in more accurate building response</li> <li>• Realistic representation of building modelling limits the amount of assumptions needed</li> <li>• Material model improvements can be added quickly [developed in-house]</li> </ul>	<ul style="list-style-type: none"> <li>• Provides the capability to reliably simulate the actual nonlinear response of masonry buildings.</li> <li>• Easy-to-use tool for both capacity assessment and direct time-history response evaluation. Immediate interpretation of failure modes in structural members.</li> <li>• Permits the performance of non-linear seismic analyses with a limited number of d.o.f. and is suitable for efficient parametric analysis on many structural models with limited computational burden. Being a dedicated masonry nonlinear analysis tool, TREMURI provides an excellent compromise between accuracy of results and analysis time (orders of magnitude shorter than detailed FEM models).</li> </ul>	<ul style="list-style-type: none"> <li>• Multi-purpose program with wide library of element types all supporting nonlinearity in tension/compression and smeared cracking</li> <li>• Relatively simple model generation, no need to replicate exact brick arrangements</li> <li>• Possibility to use interfaces to model connections</li> <li>• Good embedment in the Dutch engineering community</li> <li>• Short line to the developers (TNO-DIANA)</li> </ul>
Cons	<ul style="list-style-type: none"> <li>• Detailed modelling requires longer run time</li> <li>• LS-DYNA model-building requires experience with the program</li> </ul>	<ul style="list-style-type: none"> <li>• Simultaneous modelling of out-of-plane and in-plane response of the same walls is not possible.</li> <li>• Does not provide detailed cracking pattern.</li> </ul>	<ul style="list-style-type: none"> <li>• Difficulties in obtaining numerical convergence can arise in implicit integration scheme due to negative stiffness contributions related to softening</li> <li>• Need for improvement of constitutive model for masonry to include orthotropy, different failure modes, improve loading/unloading paths and hysteresis – <i>ongoing</i></li> <li>• Overstiff behaviour and stress locking especially related to out-of-plane behaviour (to be included in the improvement of the material model)</li> </ul>

Table 40 presents the lessons learnt from this exercise from each consultant, as well as combined lessons learnt agreed by all consultants

Table 40: Summary of lessons learnt

Arup LS-DYNA	EUCENTRE TREMURI	TU-Delft DIANA
<ul style="list-style-type: none"> <li>Numerical model is sensitive to the assumptions made on the structural connections. Increased knowledge on the connections can be directly incorporated into the model and can be used to improve upon previously made assumptions.</li> <li>Extreme variability of strength of CaSi masonry due to sensitivity to weather conditions and level of craftsmanship has a significant effect on results. If reliable predictions for low strength masonry were required in future, further validation against component tests on such masonry would be desirable.</li> <li>Intrinsic damping of CaSi material is higher than assumed</li> </ul>	<ul style="list-style-type: none"> <li>Attention should be given on proper modelling of the connections.</li> <li>Material properties assumed significantly affect the performance of the model, in particular E and G of masonry, as no tension is assumed and no shear failures occur until the last stages of the tests.</li> <li>The reliable prediction of their overall behavior mainly depends on the proper representation of characteristics of each single structural member and mass distribution.</li> </ul>	<ul style="list-style-type: none"> <li>Improvement of constitutive masonry model is ongoing, so as to include orthotropy, more specific distinction between tensile and shear modes, and loading/unloading hysteresis. This will most likely also solve the problem of having highly stiff behaviour in the final stage.</li> <li>Importance of a proper modelling of connections between floors and walls</li> <li>Sensitivity of results to material properties that should be carefully assessed</li> </ul>
<ul style="list-style-type: none"> <li>Understanding the behavior of structural connections and properly implementing them in the numerical models is key in order to achieve a more accurate prediction.</li> <li>More validation regarding the variability of masonry material properties, such as calcium-silicate material, is recommended</li> </ul>		

More detail is provided in the individual sections below.

### Arup LS-DYNA

The LS-DYNA post-test refined model of the full scale shake table building results in more accurate predictions and simulation of observed behaviour in the laboratory in comparison to the blind prediction model. The model now well predicts the building deformation experienced during the application of EQ2. This is mainly due to the changes made in the modelling of the connections as described in section 2.3.2. The deformation of the second floor slab is no longer overestimated as was found with the blind prediction model. This results in improvement of the global hysteresis loops with better prediction of stiffness, strength, and deformation. Nevertheless, the intrinsic damping of the CaSi masonry is higher than assumed. This is evident in the free vibration that the model experiences during earlier runs (i.e., EQ1) that is evident in the time history graphs. This affects the predictions at low levels of response but probably has less influence when non-linear energy dissipation due to cracking, sliding etc. occurs at higher response levels.

The deformation predicted by the LS-DYNA post-test refined model compares reasonably well to the damage observed in the laboratory. While the damage is slightly underestimated during the application EQ2 scaled at 100% and 150%, damage is better predicted during the application of the final run of EQ2 scaled at 200%. There is some over-prediction of damage to the narrow piers of the CaSi East and West inner leaves and in the clay North outer leaf but better concentration of damage predicted in the CaSi North and South inner leaves and the clay East and West outer leaves. Diagonal crack pattern exhibited extending from the corner of openings as well as observed damage to the spandrels are well captured in the LS- DYNA model.

### EUCENTRE TREMURI

Through the comparison of the global hysteresis curves as resulted from the post-test refined prediction model and the lab tests, it can be immediately inferred that the improvements implemented in the new refined TREMURI model have a significant impact in simulating with a more precise way the response of the test-house. Compared to the blind prediction model, the post-test improved TREMURI model exhibits a general response noticeably closer to the real dynamic response of the test building, during the whole test protocol.

The model provides an accurate simulation of the structure's response when subjected to GM1, capturing in a satisfying degree the global stiffness of the specimen, and predicting maximum displacements and base shears close to those achieved during the shaking table tests. This claim is further strengthened by the excellent coincidence of the base shear, displacement as well as IDR time histories observed when compared with the corresponding experimental waveforms.

The improvements achieved in the post-diction have been guided by the knowledge of the crack pattern and of the local failure of specific connections (sliding of the timber beam above the outer leaf). In general, such information is not available a priori. Still, with little adjustments the model was able to obtain good results maintaining the low computational effort of a macro-modelling approach, confirming how such simplified approach can be usefully adopted in complement to more refined and detailed modelling (which can provide a preliminary insight regarding connections and crack patterns) for the execution of numerous parametric nonlinear dynamic analyses with reduced computational effort.

The TREMURI model presents the same great efficiency in predicting the structure's response during the application of GM2. The good match made when comparing the displacement and shear time histories is also reflected in the agreement between the numerical and experimental hysteresis curves of the structure when subjected to 100% of GM2. When subjected to 150%, despite capturing fairly well the main features of the building's response, the model slightly underestimates the maximum 2<sup>nd</sup> floor displacement attained in the lab for the positive direction of motion, a deficit that is also identified when looking at the 2<sup>nd</sup> storey's IDR time histories. Nevertheless, it succeeds in accurately attributing the response of the 1<sup>st</sup> storey and the gable in terms of IDRs, as well as in reproducing a well-aimed base shear time history. During the test at 200% of GM2 the test-building is more flexible, and as in the case of the blind prediction model, the post-test refined TREMURI model is able to capture well enough the general response with slight under-prediction of the displacements for the positive direction of motion, which could be partially attributed to the relatively high value of damping ratio assumed during this run ( $\xi=4\%$ ). The above mentioned remarks can also be easily derived from the examination of the base shear vs 2<sup>nd</sup> floor displacement envelope, which approximate satisfactorily the experimental results.

The damage pattern given by TREMURI at the end of the different runs shows a good consistency with the damage reported in the lab. Being able to indicate locations where shear damage is expected, TREMURI model well-predicts the evolution of damage of the spandrels during the testing procedure, as well as their final failure.

Given the significant improvement that is achieved in the results with small adjustments and limited additional modelling effort as described in section 2.3.3, it is confirmed how the simplified macroelement modelling approach can be used in conjunction with more refined and detailed modelling (which can provide a preliminary insight regarding connections and crack patterns) for the development of parametric nonlinear dynamic analyses with reduced computational effort.

## TU-Delft DIANA

The refinement of the finite element model for the post-test prediction leads to an improvement in terms of stability of the solution, since the whole loading protocol has been applied without experiencing any numerical divergence. The application of multiple ground motions in sequence starting from low level PGAs helped the improvement of the convergence since the damage slowly increased into the structure. Also, the removal of overconstrained nodes had a beneficial effect on this respect.

The results of the post-test refined prediction show a good estimation of shear levels and an improvement of the global envelopes of shear-displacement trends with respect to the blind predictions. The comparison between experimental and DIANA numerical results in terms of hysteresis plots shows a good agreement until EQ2-100%. Nevertheless, the model still presents behaviour that is too stiff for higher PGAs (EQ2-150% and 200%) leading to underprediction of the displacements for the last 2 applied ground motions. This is most likely due to the current constitutive model for masonry in DIANA which reacts too stiff in the fully cracked stage. An improved constitutive model is currently in development and calibrated against the component tests.

Displacements of 1st and 2nd story and IDRs are correctly predicted for low to medium PGAs (till EQ2-100%). IDR of the roof level is instead underpredicted for all PGAs, possibly due to the modelling of the connection between the facades, the 2nd story and the roof, free to move in plane, causing the roof to "slide" on top of the piers because of lack of in-plane connection.

The damage pattern for in-plane behaviour of piers in the facades is predicted quite well. Rocking of piers and cracks developing from the corners of the windows are quite consistent with the experiment. Damage of spandrels and out-of-plane walls is not always consistent with the experiment, possibly due to lack of connection at the floor levels.

## References

---

- [1] Arup, 229746\_032.0\_REP127, “Modelling and Analysis Cross-Validation – Arup, EUC, TU Delft”, July 2015, Rev A.01.
- [2] Tomassetti U., Graziotti F., Penna A., Magenes G. (2015). A single degree of freedom model for the simulation of the out-of-plane response of unreinforced masonry walls. Proc. Italiana National Conference on earthquake engineering, L’Aquila.
- [3] NAM, Basis for Design: Seismic Structural Upgrading of Existing Buildings in the Groningen Area, Rev 3, March 2015, Doc Ref: EP201403208456
- [4] Lagomarsino S., Penna A., Galasco A., Cattari S., (2013) “TREMURI Program: an equivalent frame model for the nonlinear seismic analysis of masonry buildings”, ENGINEERING STRUCTURES, 56(11): 1787-1799.
- [5] Penna A., Lagomarsino S., Galasco A., (2014) “A nonlinear macro-element model for the seismic analysis of masonry buildings”, EARTHQUAKE ENGINEERING & STRUCTURAL DYNAMICS, 43(2): 159-179.

## Appendix A

### Modelling Approach and Assumptions

## A1 Arup

Table 41: Arup general modelling notes

Component	Description
Analysis team	Arup
Analysis software and formulation	LS-DYNA – Explicit time integration scheme
Overview of modelling approach	<ul style="list-style-type: none"> <li>• Explicit time integration scheme is used for nonlinear pushover and response history analysis</li> <li>• Homogenized masonry material model with fully integrated shell elements that evaluate the behaviour of masonry where the damage is assumed to be lumped at the joints. Crack plane directions are pre-defined to model mortar bonds</li> <li>• Shell elements, beam elements, and discrete (spring) elements are used to model other components of the tests.</li> <li>• Material properties are either defined based on the median material properties defined in the Basis for Design issued by NAM or on available test data for masonry characterisation tests, using a consistent methodology across all tests.</li> </ul>
Model units	SI units (kg, m, sec)
Mesh size	0.1m x 0.1m

Table 42: Arup model properties

Input	Description
Element formulation	2D, fully integrated shell elements. Two through-thickness integration points for models subjected strictly to in-plane action. Five through-thickness integration points for all other models.
Shell material type	MAT_SHELL_MASONRY*
Damping	<p>DAMPING_PART_STIFFNESS, with damping coefficient 0.05, for numerical stability without affecting primary behaviours</p> <p>DAMPING_FREQUENCY_RANGE_DEFORM, with damping coefficient 0.015 for frequency range 1-30 Hz</p>

\*This material model is under development. For the analyses reported in this document, the 2015 version was used. This version offers bed joint sliding and opening capabilities. This version of the material model has the potential for stepped diagonal pattern failures. It has the potential for toe-crushing and vertical cracks through the bricks and head joints, but the input properties were such that these failure modes did not occur in the analyses reported in this document. Developments in progress will address these limitations.



## A2 EUCENTRE

Table 43: EUCENTRE general modelling notes

Component	Description
Analysis team	EUC-Pavia
Analysis software and formulation	TREMURI – Equivalent-frame formulation based on a macro-element model
Overview of modelling approach	<p>The adopted equivalent-frame modelling strategy implemented in the TREMURI program [Lagomarsino et al., 2013] [4] is based on the effective non-linear macro-element modelling approach.</p> <p>The macro-element model represents the cyclic non-linear behaviour associated with the two main in-plane masonry failure modes, bending-rocking and shear mechanisms, with a limited number of degrees of freedom (8 d.o.f) and internal variables which describe the damage evolution [Penna et al., 2014] [5]. The two-node macro-element, suitable for modelling piers and spandrel beams, can be ideally subdivided into three parts: a central body where only shear deformation can occur and two interfaces, where the external degrees of freedom are placed, which can have relative axial displacements and rotations with respect to those of the extremities of the central body. In the two interfaces, infinitely rigid in shear, the axial deformations are due to distributed system of zero-length springs with no-tension and limited compression behaviour.</p> <p>Due to the concentration of the axial and flexural deformations in the interfaces, the spring stiffness equal to <math>k = 2E'/h</math>, where <math>E'</math> is an effective elastic modulus and <math>h</math> is the element length (height in case of pier elements), is set differently as far as axial or lateral stiffness need to be more accurately reproduced. The following settings apply for <math>E'</math>:</p> <p><math>E' = E</math> (masonry Young's modulus in compression) when axial stiffness is concerned;</p> <p><math>E' = 1.5E</math> when lateral stiffness is concerned in a cantilever wall;</p> <p><math>E' = 3E</math> when lateral stiffness is concerned in a double-fixed wall;</p> <p><math>E'</math> is usually set to <math>2E</math> when lateral stiffness is concerned in a building model with intermediate boundary conditions for the different structural elements.</p> <p>The macroscopic shear model is based on a combination of equivalent cohesion, <math>\bar{c}</math>, and friction, <math>\bar{\mu}</math>, parameters. The determination of the model parameters from the "local" mechanical parameters derived from characterisation tests depends on the governing shear failure mode:</p> <ul style="list-style-type: none"> <li>For diagonal shear cracking (with cracks passing through bricks), the following relations apply,</li> </ul> $\begin{cases} \bar{\mu} = \frac{1}{4.6(1+\alpha_v)\sqrt{1+N_o/f_{bt}lt}} \\ \bar{c} = \frac{f_{bt}}{2.3(1+\alpha_v)}\sqrt{1+N_o/f_{bt}lt} - \bar{\mu}\frac{N_o}{lt} \end{cases}$ <p>where <math>f_{bt}</math> is the longitudinal unit tensile strength, <math>N_o</math> is the axial force and <math>\alpha_v=h_o/l</math> is the shear span ratio (ratio between the zero moment height and the wall length);</p>

	<ul style="list-style-type: none"> <li>For shear failure with sliding along bed-joints the following relations apply,           <math display="block">\begin{cases} \bar{\mu} = \frac{\mu}{(1+\alpha_v)\left(1+\frac{2\mu\Delta_y}{\Delta_x}\right)} \\ \bar{c} = \frac{c}{(1+\alpha_v)\left(1+\frac{2\mu\Delta_y}{\Delta_x}\right)} \end{cases},</math> <p>where <math>c</math> and <math>\mu</math> are the joint cohesion and friction coefficient, and <math>\Delta_y</math> and <math>\Delta_x</math> are the unit height and length, respectively. Reduced values of <math>\mu</math> (50%) can be used to account for loading reversal effects.</p> <p>The TREMURI computer program performs several types of linear and nonlinear analyses: modal analysis, incremental static analyses (Newton-Raphson) with force or displacement control, 3D pushover analyses with fixed and adaptive load pattern and 3D time-history dynamic analysis (Newmark integration method; Rayleigh viscous damping).</p> <p>Floor and roof diaphragms are modelled by means of linear 3-node and 4-node orthotropic membrane elements.</p> </li> </ul>
Model units	SI units (kg, m, sec)

## A3 TU-Delft

Table 44: TU-Delft general modelling notes

Component	Description
Analysis team	TU-Delft
Analysis software and formulation	DIANA implicit solver
Overview of modelling approach	<ul style="list-style-type: none"> <li>Total strain based smeared crack model for masonry, with non-linearity in tension and compression.</li> <li>Plasticity model for wall ties in tension and compression.</li> <li>Geometrical nonlinearity</li> </ul>
Model units	SI units (kg, m, sec)
Mesh size	0.20 m x 0.20 m on average
Assumptions	<ul style="list-style-type: none"> <li>Gravity loads of floors applied as line loads on top of the S-N walls to avoid excessive cracking during dead load application.</li> <li>Tyings have been used to reproduce some connections between structural elements. <ul style="list-style-type: none"> <li>The inner leaf of E/W walls has been connected to the first floor for the out-of-plane displacements only.</li> <li>The plywood has been clamped to the girders but disconnected from the masonry walls.</li> <li>The upper boundary of the E/W walls (both leaves) have been set as free to move in plane, since during the construction phase, the concrete floor has been kept separated from these walls and subsequently the gap has been filled with mortar. Due to the negligible vertical load transferred to these walls, the friction effect of the filling mortar has been neglected in this stage of the analysis.</li> </ul> </li> <li>Boundary condition at the bottom of the building is fixed</li> </ul>

Table 45: TU-Delft model properties

Input	Description
Element formulation	<ul style="list-style-type: none"> <li>Quadratic shell elements were used to reproduce in-plane/out-of-plane behaviour of the single walls in the 3D configuration.</li> <li>Beam elements have been used for the timber girders and for the concrete lintels with linear elastic behaviour.</li> <li>Truss elements have been used for the ties, with elastic perfect plastic behaviour.</li> <li>Shell elements with linear behaviour have been used for the concrete floors and the timber plywood.</li> </ul>
Damping	5% damping assumed with Rayleigh coefficients, determined on the base of the first 2 main frequencies in the X direction.

# Instruments full-scale test-house Eucentre Laboratory

*EUCENTRE, Pavia*

# Specimen Instrumentation

Monitoring building displacement and deformations:

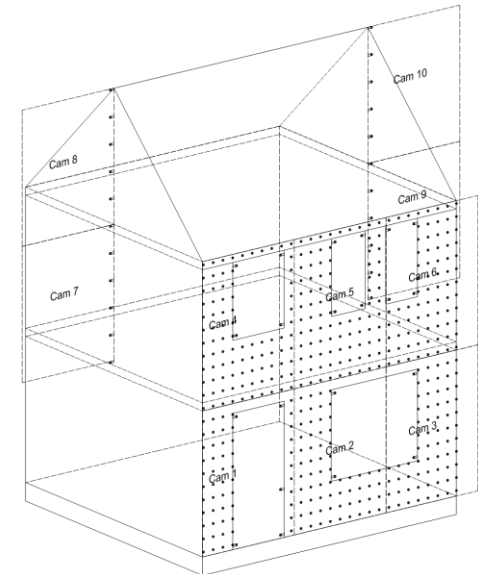
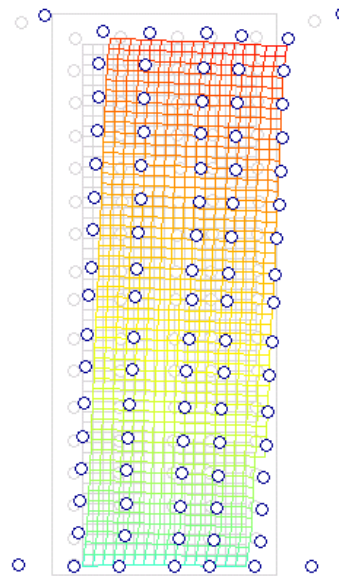
- Traditional Acquisition Systems

Accelerometers: recording acceleration time histories

Linear and Wire Potentiometers

- 2d Optical Acquisition System

- 3d Optical Acquisition System

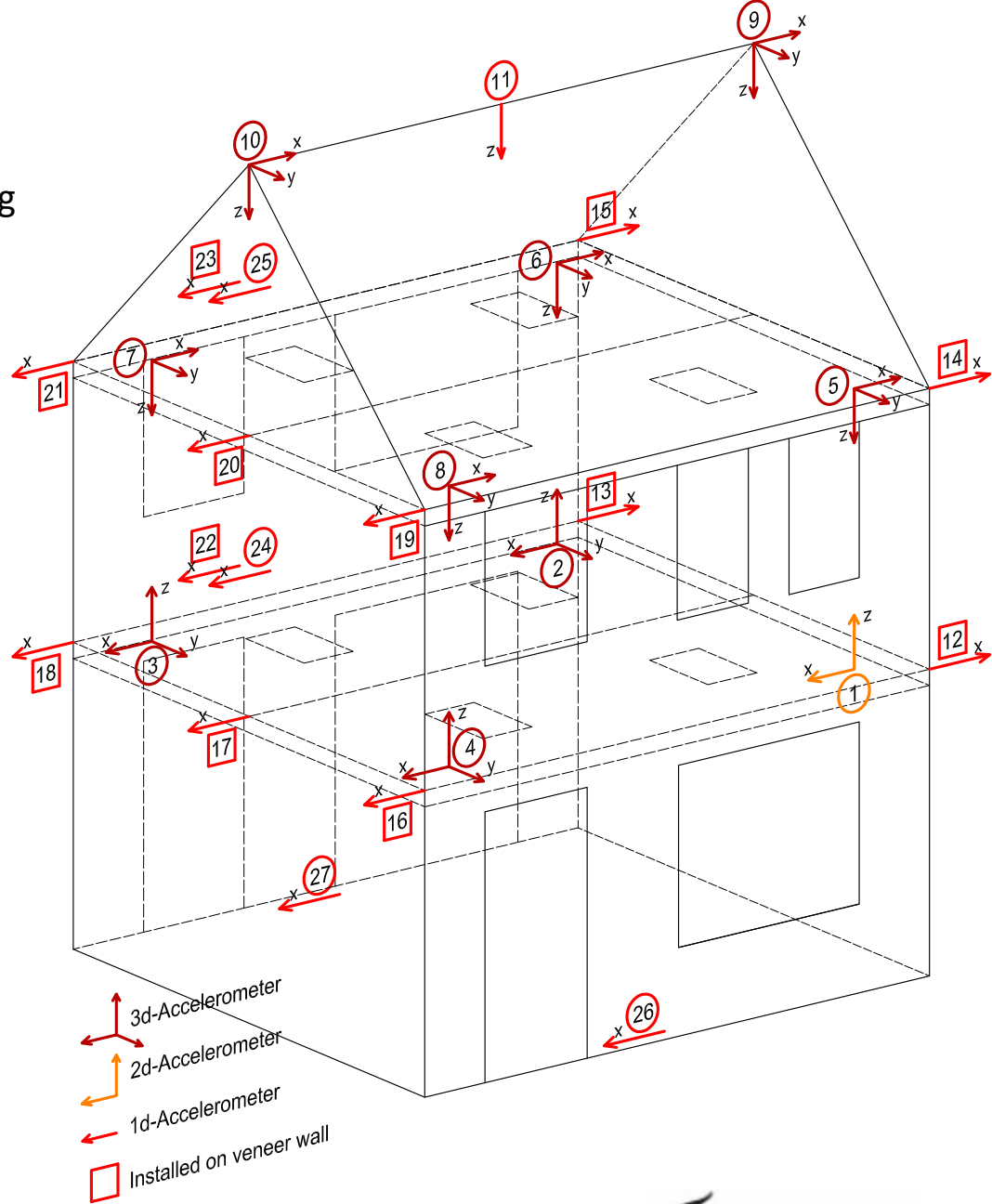


# Specimen Instrumentation:

## 1) Accelerometers

Traditional acquisition data system recording acceleration time histories.

- 3d Accelerometers
- 2d Accelerometers
- 1d Accelerometers

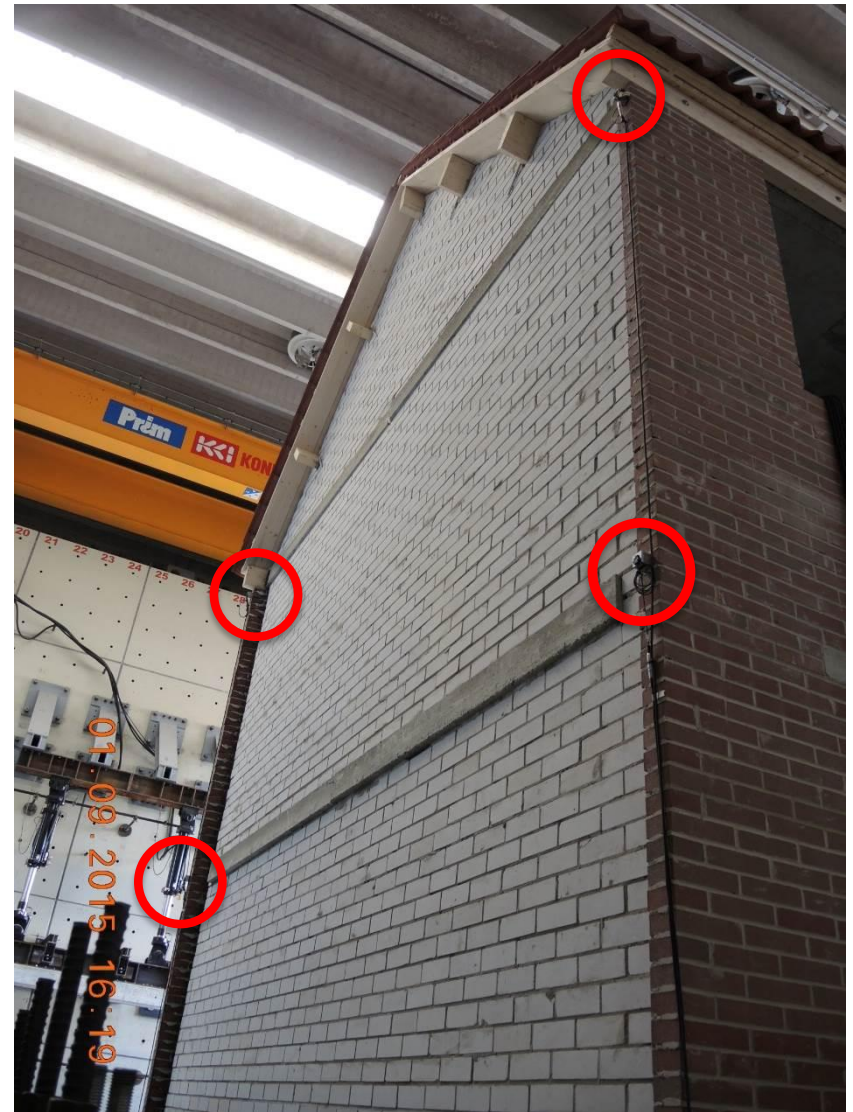


# Specimen Instrumentation:

## 1) Accelerometers

Traditional acquisition data system recording acceleration time histories.

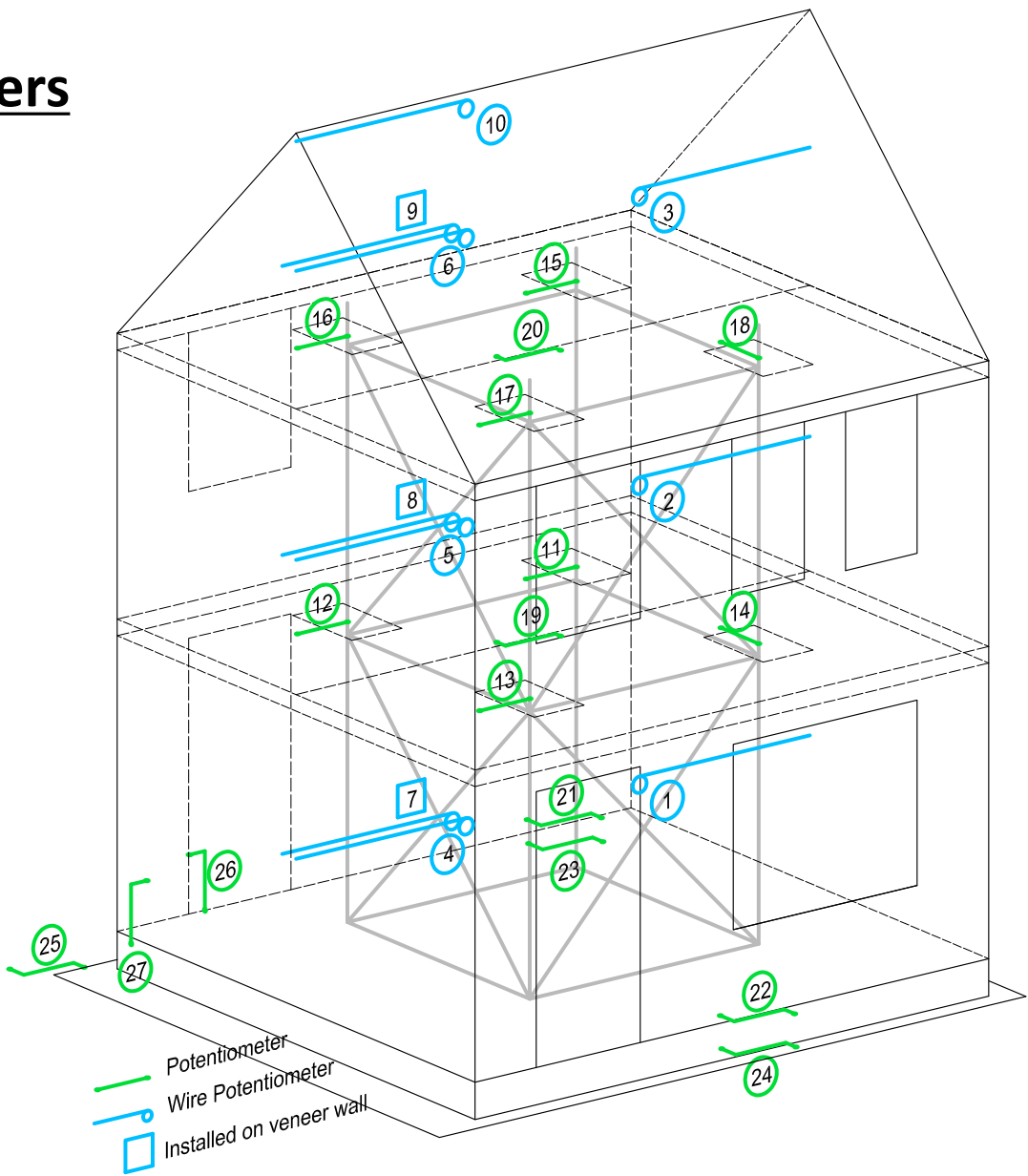
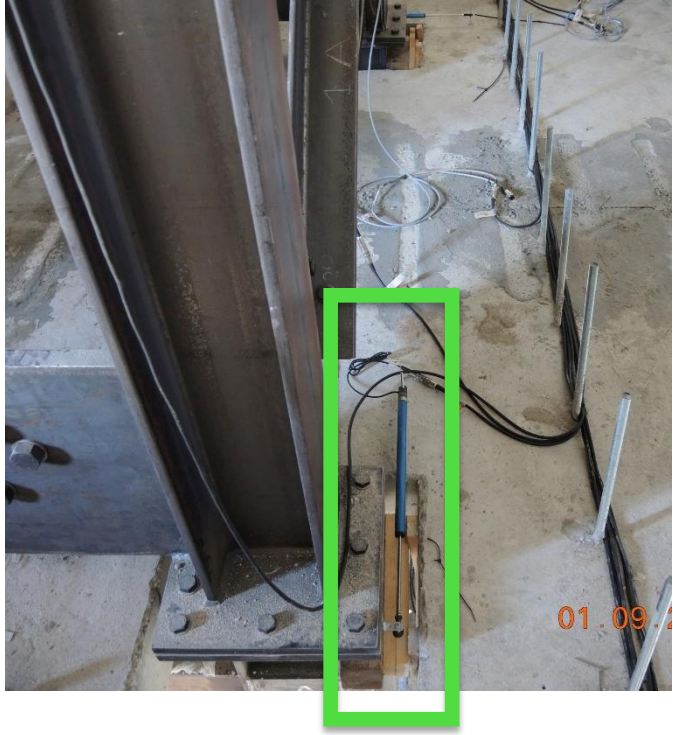
- 3d Accelerometers
- 2d Accelerometers
- 1d Accelerometers



# Specimen Instrumentation:

## 2) Linear & Wire Potentiometers

Traditional acquisition data system monitoring:  
-floor displacements and rotations  
-mid-height out-of-plane wall displacements ( North and South Facades)





# Specimen Instrumentation:

## 2) Linear & Wire Potentiometers

Traditional acquisition data system monitoring:

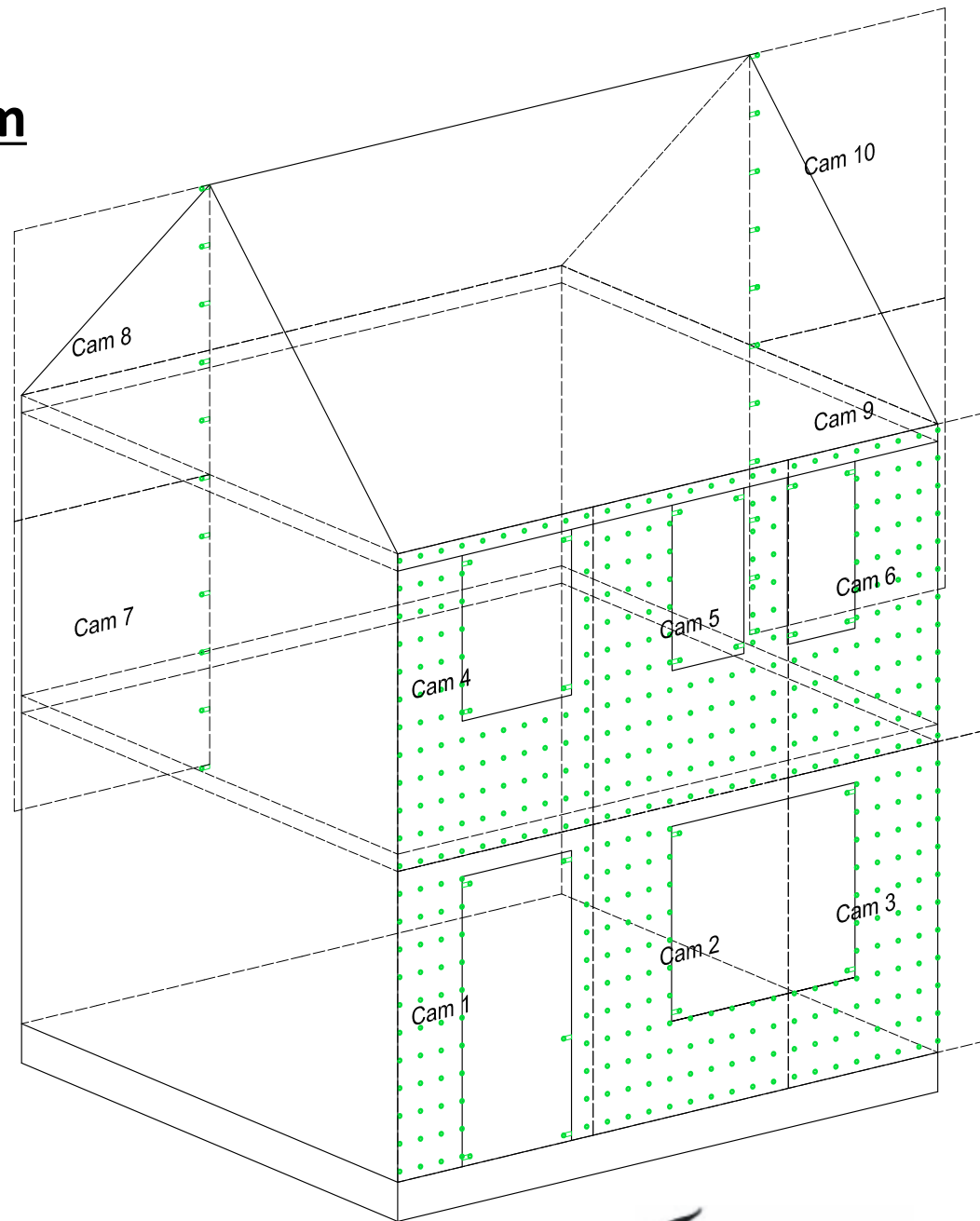
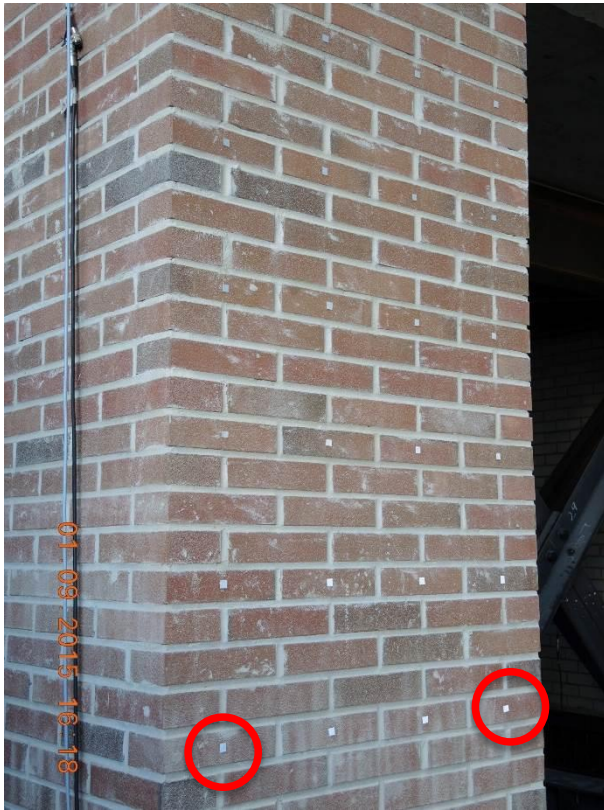
- floor displacements and rotations
- mid-height out-of-plane wall displacements ( North and South Facades)



# Specimen Instrumentation:

## 3) 2D Optical acquisition system

X & Y displacement time histories of each marker positioned in the West facade and in the Out-of-plane walls



# Specimen Instrumentation:

## 3) 2D Optical acquisition system

X & Y displacement time histories of each marker positioned in the West facade and in the Out-of-plane walls

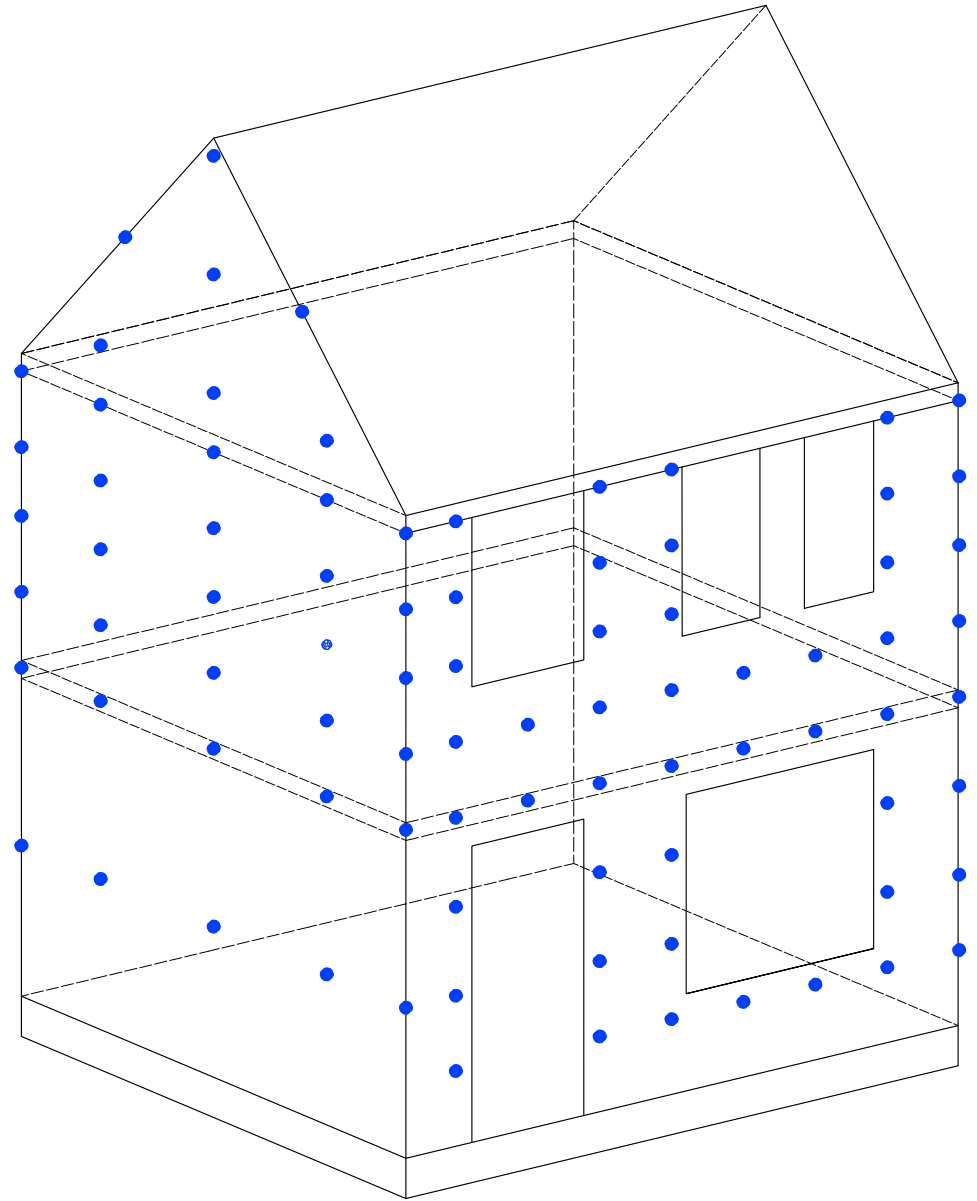
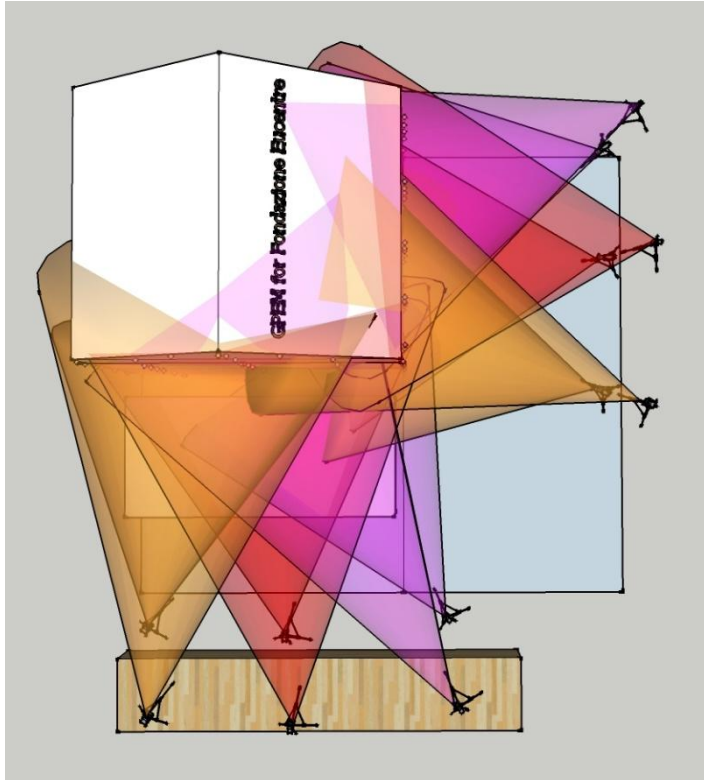


Detail of installation of markers on the CS inner wall.

# Specimen Instrumentation:

## 4) 3D Optical acquisition system

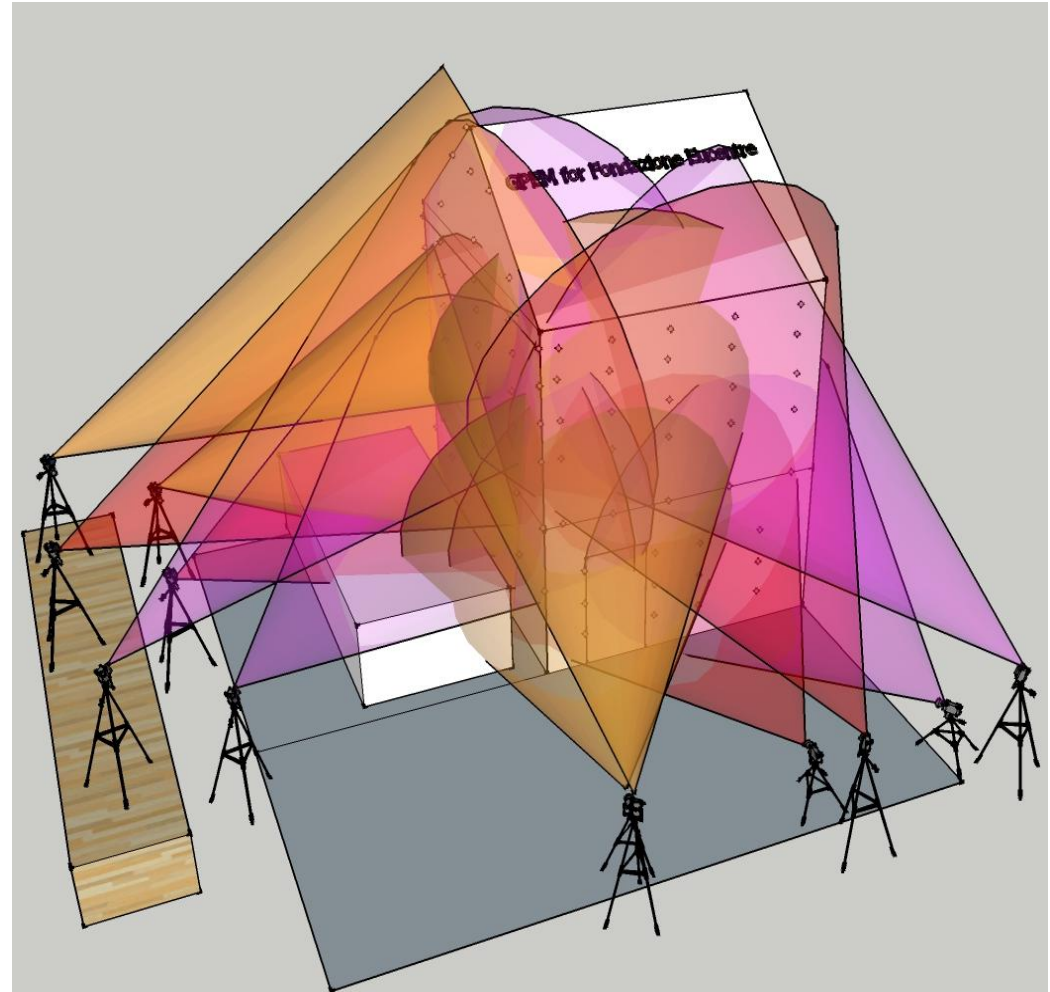
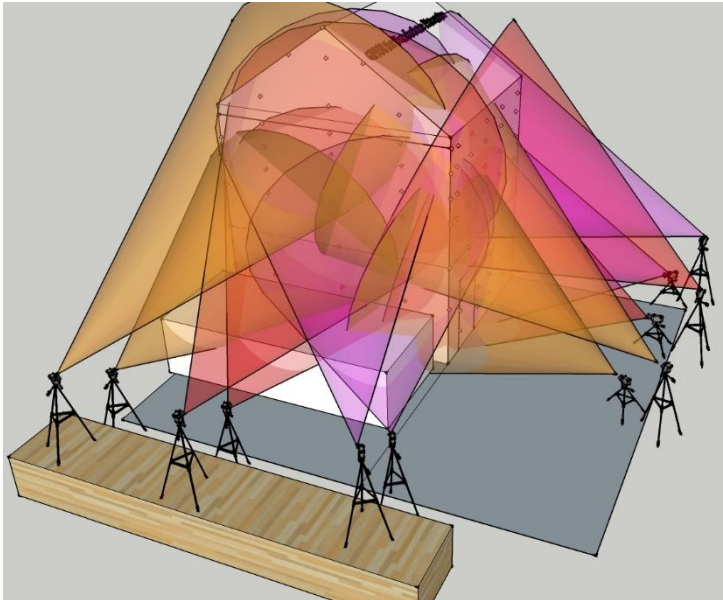
X, Y and Z displacement time histories of each marker positioned in the West and North facades



# Specimen Instrumentation:

## 4) 3D Optical acquisition system

X, Y and Z displacement time histories of each marker positioned in the West and North facades





# Protocol for Shaking Table Test on Full Scale Building (Eucentre) V\_1

## 1. Scope and application field

The aim of this document is to define the procedure for the dynamic shaking table test on a masonry building specimen representing a terraced house typical of the Groningen area.

## 2. Specimen description

A detail specimen description is contained in Appendix A.

## 3. Input time histories

The specimen will be subjected to incremental dynamic test runs, namely a series of table motions of increasing intensity. The table input motions will consist of accelerograms aiming to reproduce a realistic simulation of possible ground motions in the study area, corresponding to scenarios with different return periods. Prior to a test with a specific accelerogram it will be necessary to calibrate the shake table by means of low intensity table motion; such calibration will be needed every time a different type of accelerogram is to be applied to the table. In order not to accumulate excessive damage in the structure there is the need to limit the number of different inputs. A detailed study on the seismic hazard characteristics (Appendix B) identified 2 main scenarios. Two records were chosen from those scenarios in order to maximize the outcome of the test, taking into account the final goal: i.e. to develop a solid experimental reference for the development of fragility models for urm buildings in the Groningen area.

During the test the specimen will be subjected to 3 different type of motions: a white noise (WN) (for table calibration and structural identification purposes) and two types of earthquake signals (EQ1, EQ2), each associated to a different scenario.

Table 1. Summary of the selected records.

	Waveform #	Database	EQ. Name	EQ Date	5-75% significant duration [s]
WN	White noise	-	-	-	20
EQ1	00201L	NGA	Imperial Valley-07	15/10/1979	0.375
EQ2	01703L	NGA	Northridge-06	20/03/1994	1.72

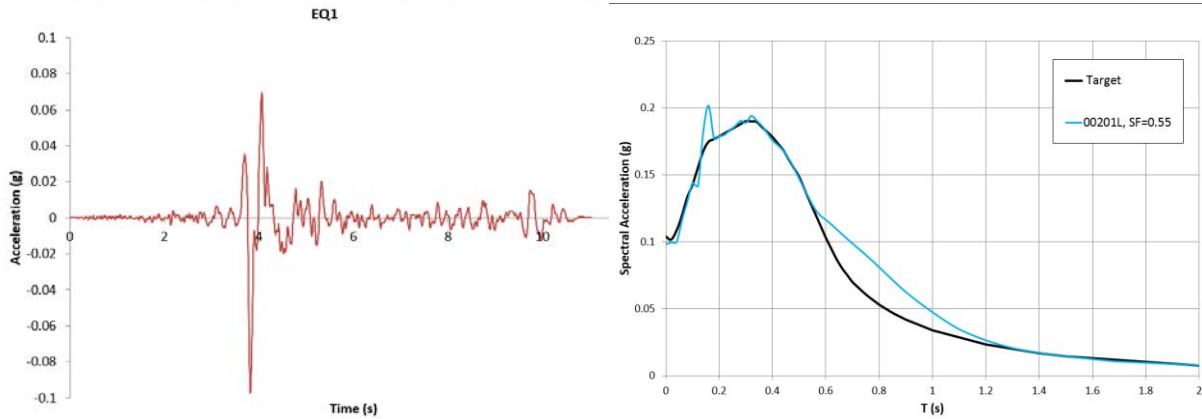


Figure 1. EQ1: time history and 5% damping acceleration elastic response spectrum.

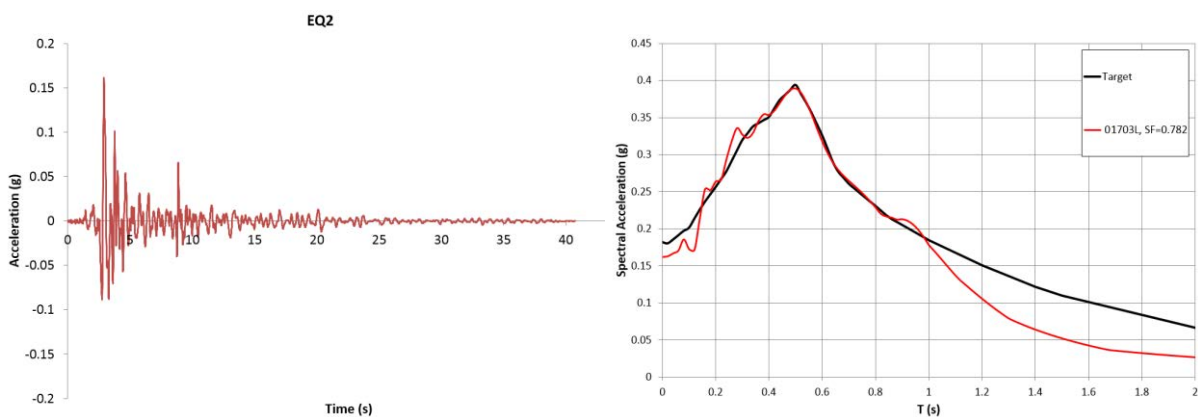


Figure 2. EQ2: time history and 5% damping acceleration elastic response spectrum.

The next table reports the currently planned sequence of dynamic inputs. The sequence may be changed (in intensity) during the test, depending on the actual response of the structure. The signals that will be used for calibration purpose are reported in grey.

#	Type	Intensity [m/s <sup>2</sup> ]	Scaling Factor	Sa <sub>0.2s5%</sub> [m/s <sup>2</sup> ]
1	WN	0.5	-	-
2	EQ1	0.25	25%	0.44
3	EQ1	0.5	50%	0.88
4	EQ1	1	100%	1.75
5*	EQ1	1.5	150%	2.63
6	WN	0.5	-	-
7	EQ2	0.8	50%	1.74
8	EQ2	1.6	100%	3.48
9	EQ2	2.4	150%	5.22
10	EQ2	3.2	200%	6.96
11	EQ2	...	...	...

\*to be defined during the test



## 4. Annexes

Appendix A: Report on the “as built” test specimen

Appendix B: Selection of Acceleration Time-Series for Shake Table Testing of Groningen  
Masonry Building

Accelerograms: .txt file in m/s<sup>2</sup>, sampling 256 Hz



## Full-scale test-house (V.4\_8\_15)

This document has the purpose to show the real geometry of the test-house and its phases of construction. The house was built directly on the shake-table in the Eucentre Lab. the contact surface between the steel foundation and the first layer of mortar is concrete.

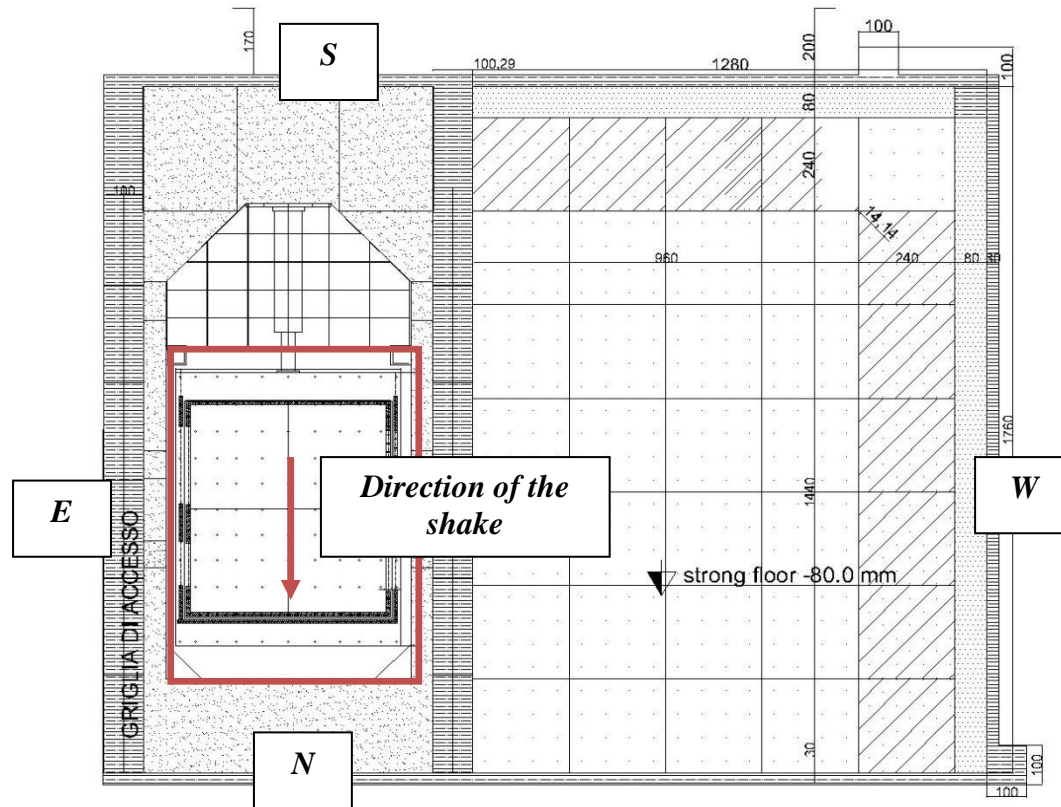


Figure 1. Plan view of the Eucentre Lab. and position of the shake-table and the walls of the test-house

The test-house is a two-storey building, with a wood roof and RC slabs. The bearing system is provided by cavity walls. They are composed by two leaves of unreinforced masonry, separated by a gap of about 8 cm. The inner calcium silicate wall is the bearing one. The outer leaf, made by clay bricks, gives no contribution to sustain the vertical loads. A series of steel ties connects the two leaves, 2 each square meter.

The house is 5.82 m long, 5.46 m wide and about 7.76 m height.

The bricks dimension are:

calcium silicate bricks: 212x102x71 mm

clay bricks: 210x100x50 mm

The mortar used for the calcium silicate bricks is different from the one used for the clay bricks. The thickness of the layers were about 1 cm for both masonries. The following Figure shows the identification code of these two materials.



Mortar for C.S. bricks	Mortar for clay bricks
0920150102 t.h.t.: 19-08-2016 705 ITALY	1401151030 t.h.t.: 28-09-2016 705 BM2 PAVIA/DELFT

Figure 2 Mortar types

Because the materials are different, the water content is not the same for the two types of mortar used. Table 1 shows the percentage of water, respect to the weight of the mortar, that has to be used.

Table 1. Water content

	WATER (lt=kg)	MORTAR (kg) - one bag	W/M (% weight)
Mortar for CS bricks	2.9	25	12%
Mortar for Clay bricks	3.75	25	15%



The following Figures show the geometry of the test-house and its dimension.

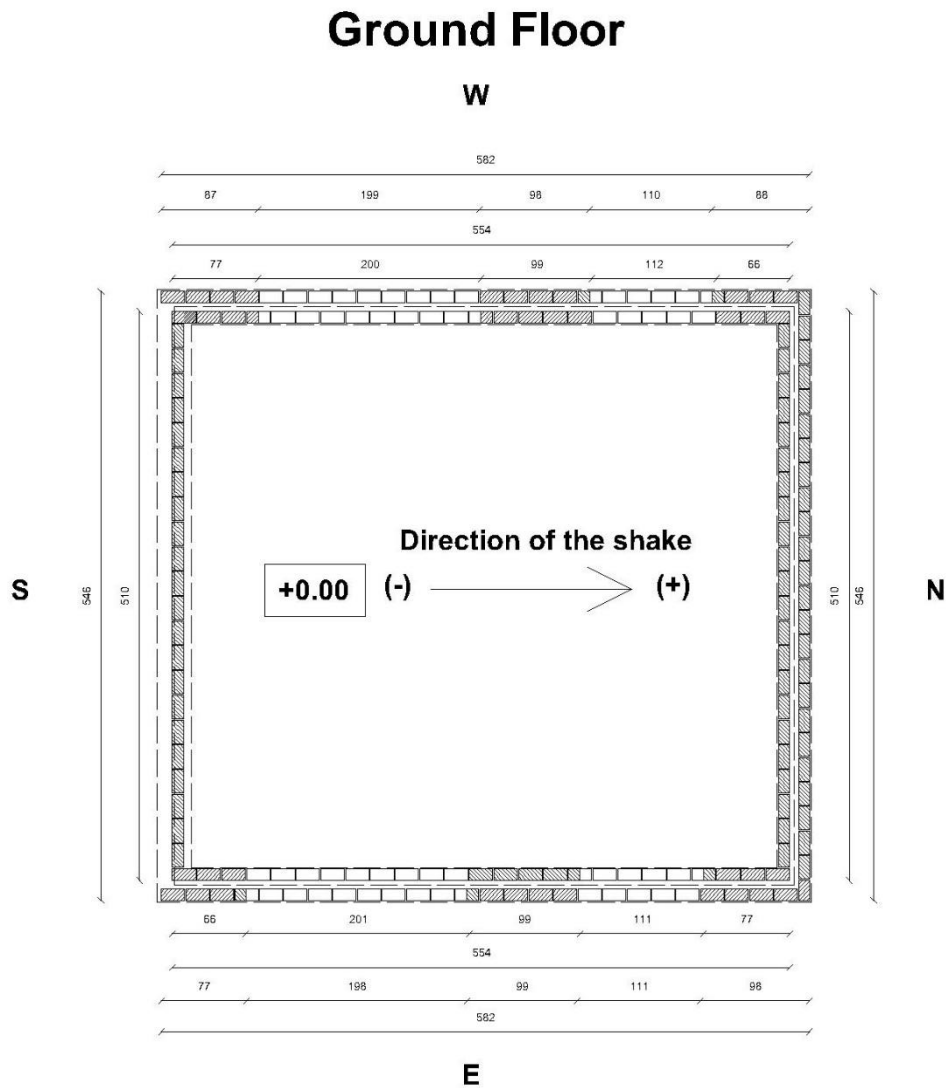


Figure 3. Plan view of the test-house - ground floor



## First Floor

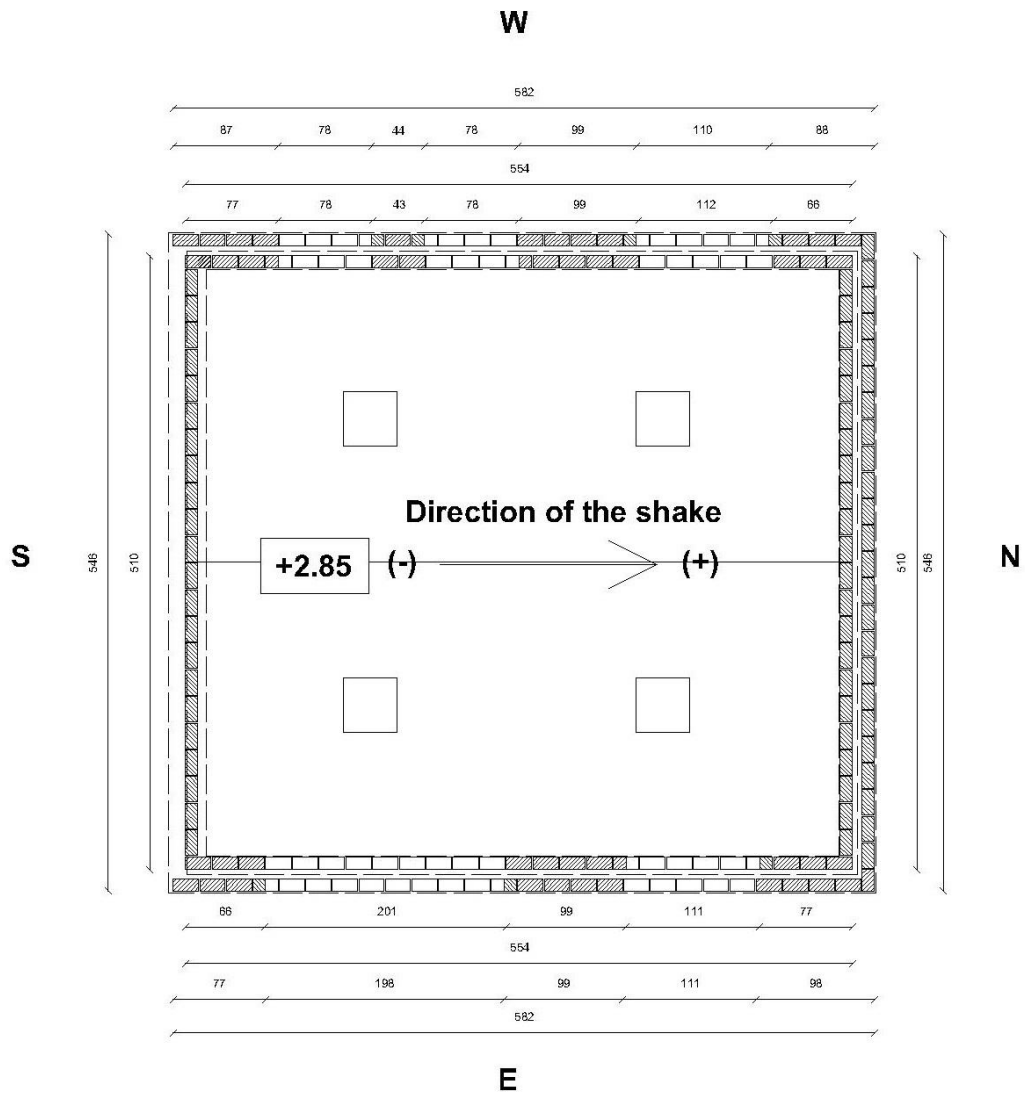


Figure 4. Plan view of the test-house - first floor

The inner leaf (calcium silicate bricks) is continuous all along the perimeter of the test-house, while the outer leaf (clay bricks) is not present in the south-side.

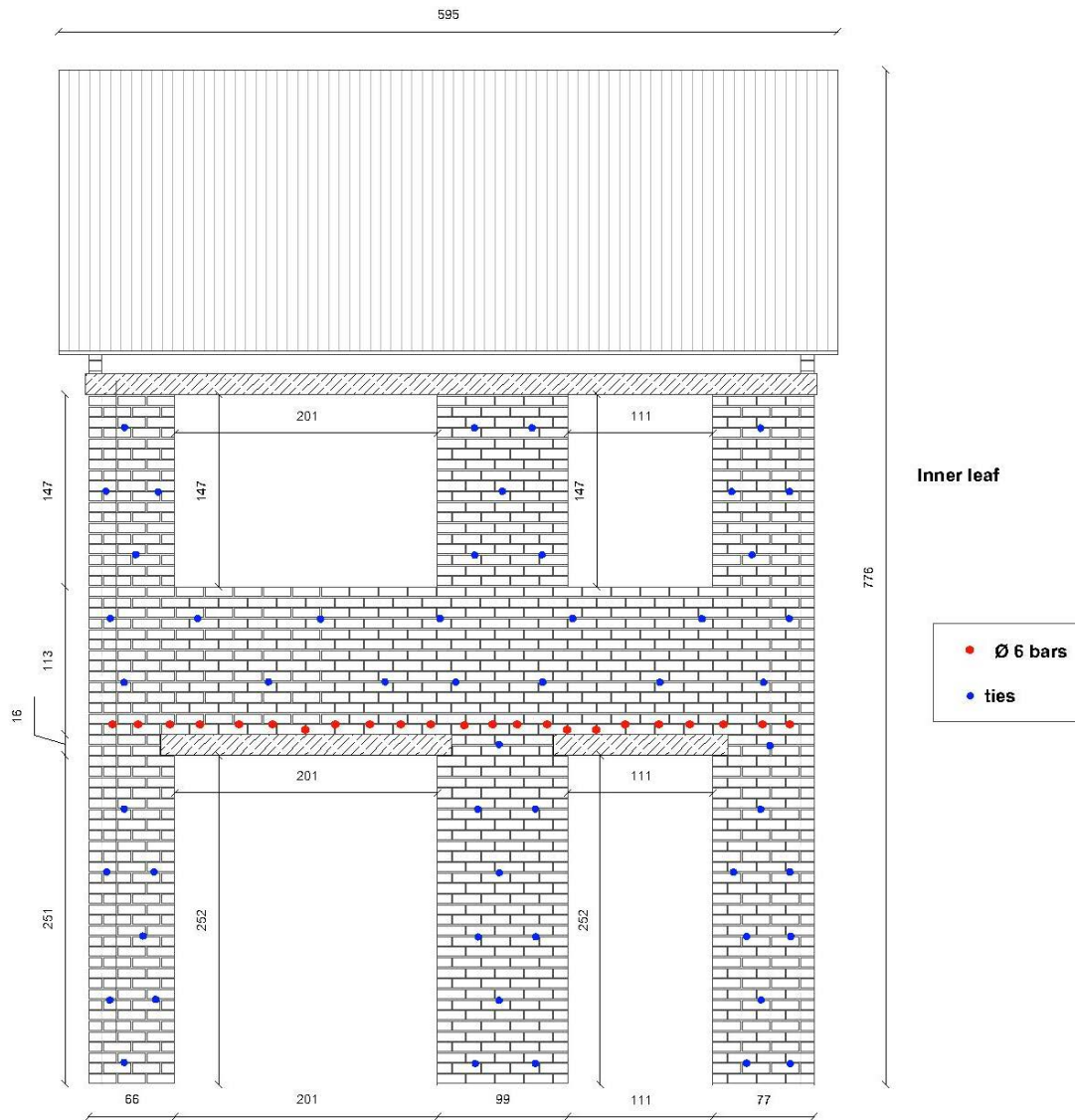


Figure 5. Elevation view of the test-house - inner leaf - west-side

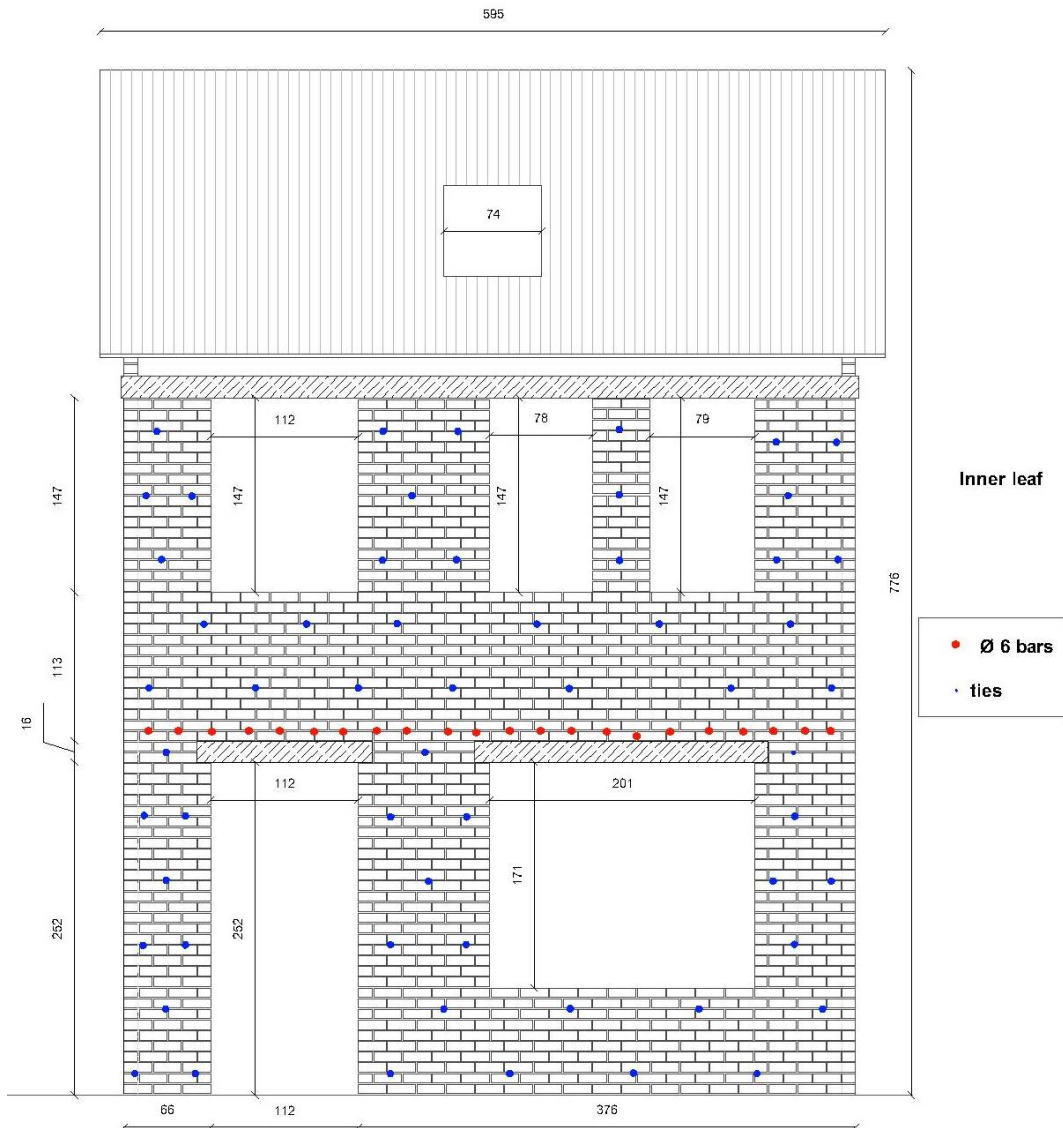


Figure 6. Elevation view of the test-house - inner leaf - east-side

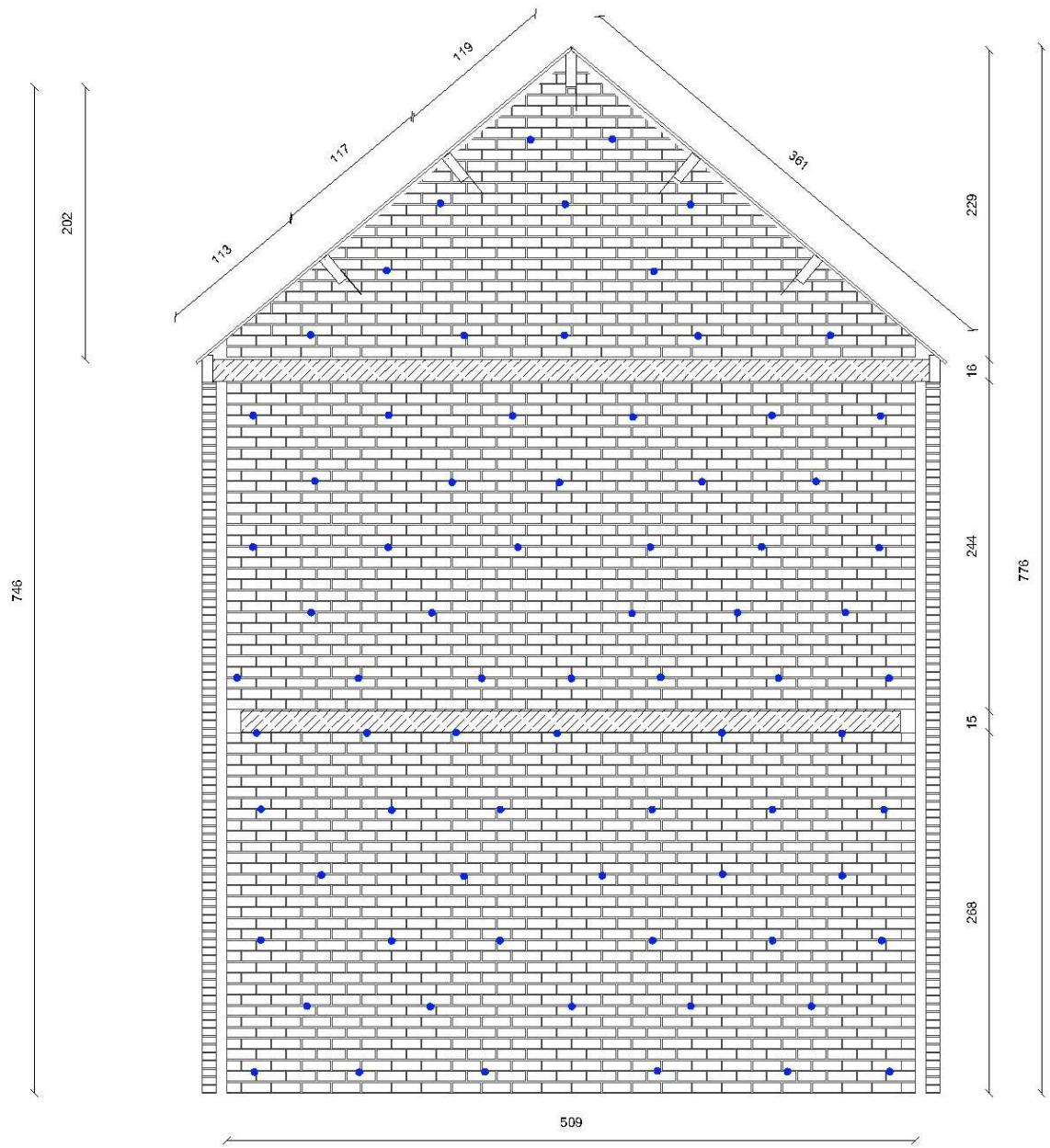


Figure 7. Elevation view of the test-house - inner leaf - north side

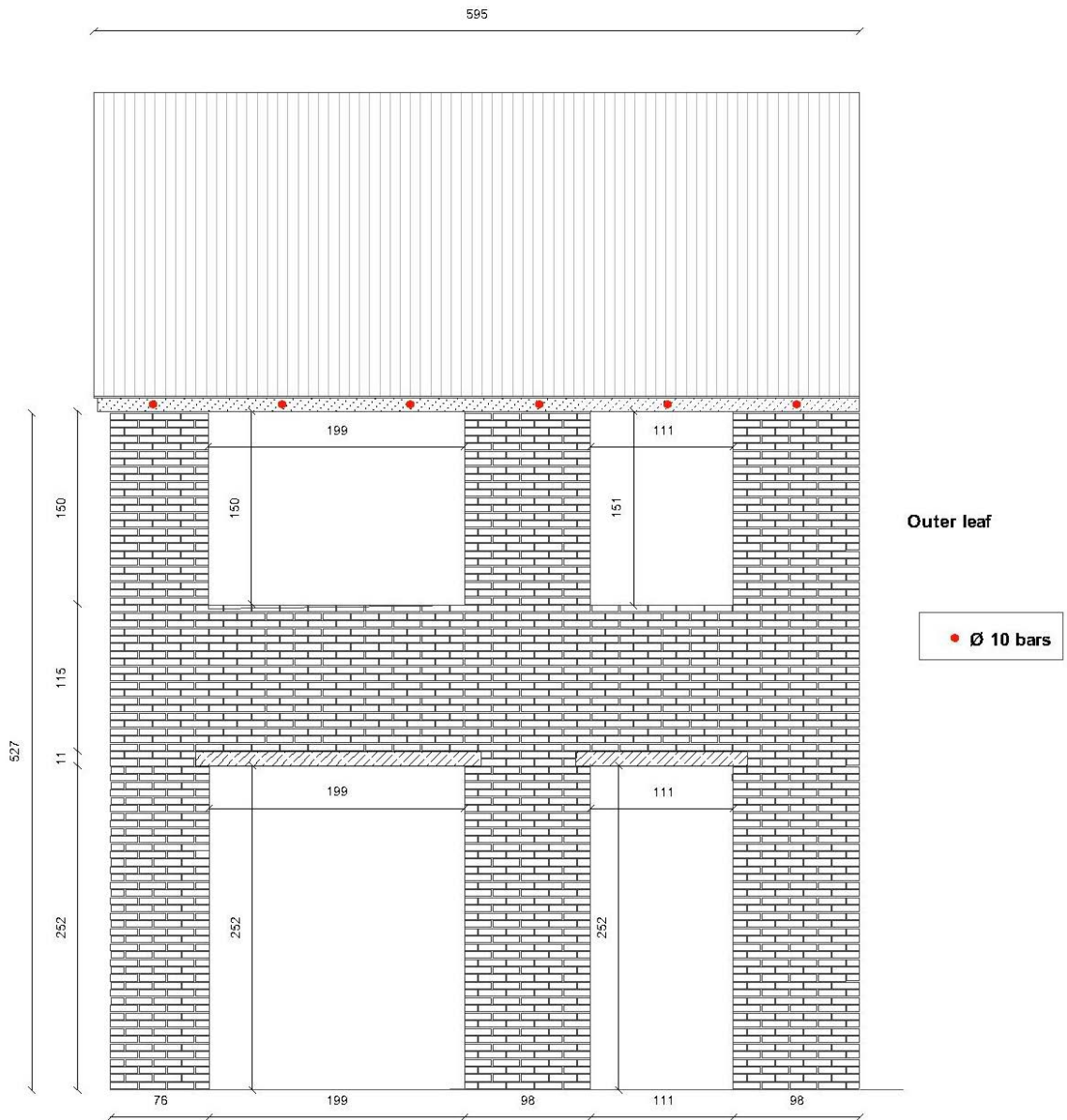


Figure 8. Elevation view of the test-house - outer leaf - west-side





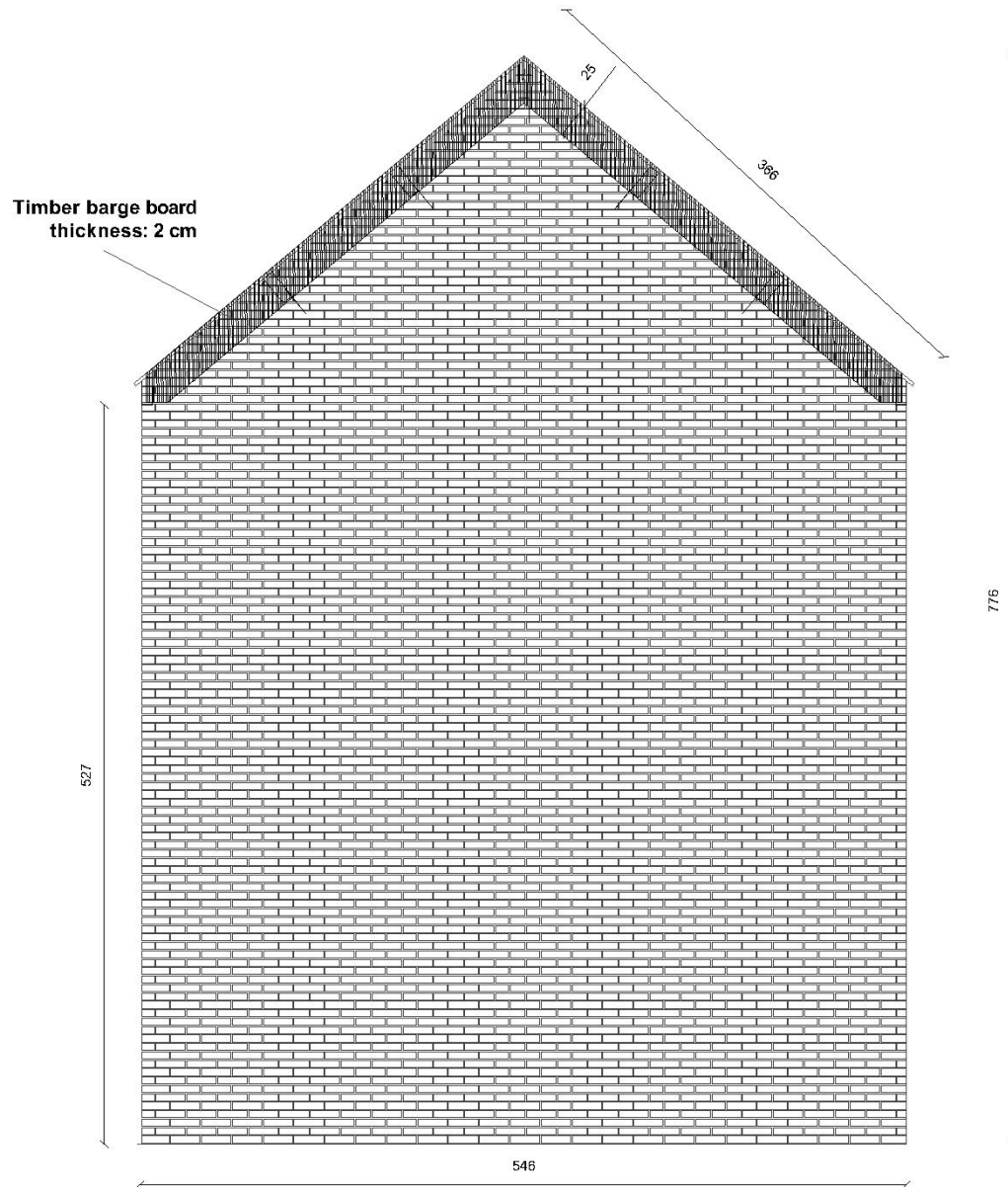


Figure 10. Elevation view of the test-house - outer leaf - north and south side



## Details

### Lintels

Above the openings (doors and windows) of the first floor there are lintels, for both inner and outer walls. The lintels are made in reinforced pre-casted concrete. The following Figure shows their geometry.

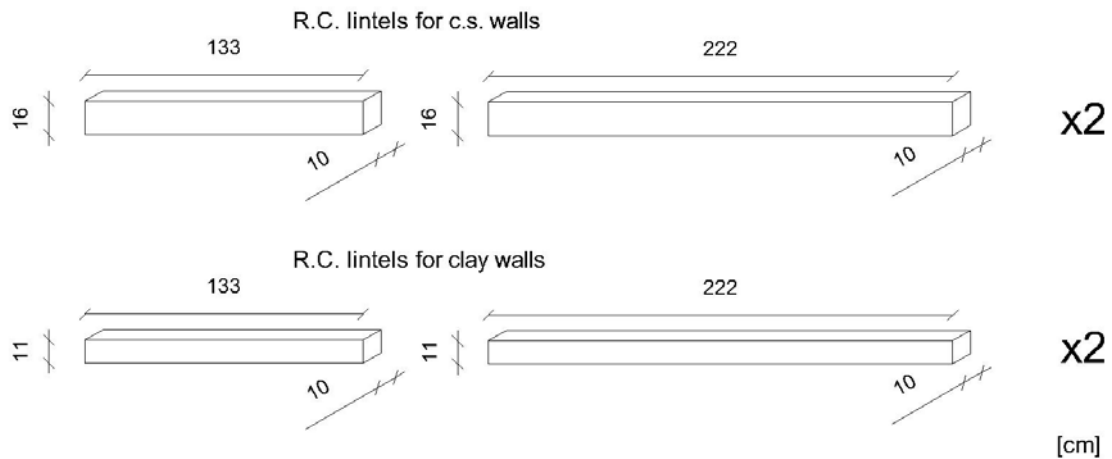


Figure 11. Lintels dimensions and geometry

### Ties

The two walls are connected by steel ties 20 cm long. They are inserted in the mortar joint during the laying of the bricks. The edge with the hook is in the inner leaf (calcium silicate bricks), for a length of about 7 cm.



Figure 12. Ties dimensions and geometry



Figure 13. Laying of the ties

**Detail of the connection between the RC slab of the first and second floor and the inner leaf (c.s. walls) - South side**

The slabs in reinforced concrete lays only on the north and south inner walls. The N/S walls were built up to an height of 268 cm, then the slab were laid on an approx. 1 cm mortar layer. A series of temporary supports supported the slab during the mortar maturation. The same procedure is repeated for the slab of the second floor. The vertical distance between the two slabs is 244 cm.

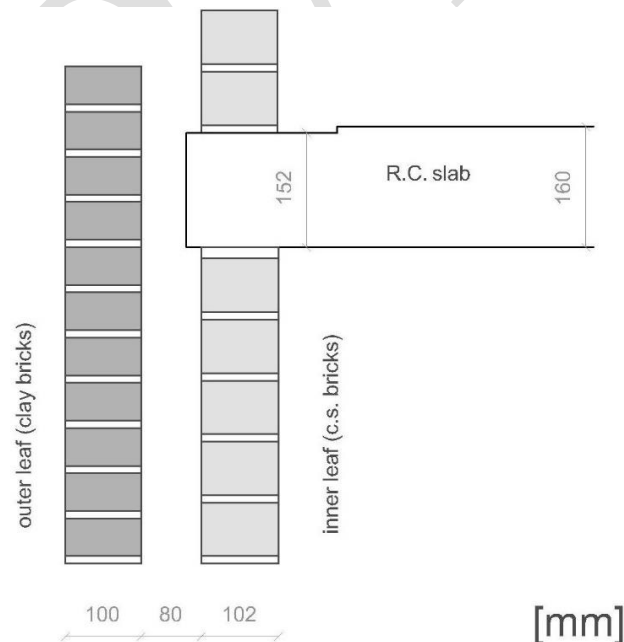


Figure 14. Detail of the connection between the r.c. slab of the first and second floor and the inner leaf (c.s. walls) - South side

### Detail of the connection between the r.c. slab of the first floor and the inner leaf (c.s. walls) - East and West side

The slab of the first floor is not laying directly on the lateral (east and west) walls, but they are connected with them by means of threaded bars. The system is shown in the following Figure.

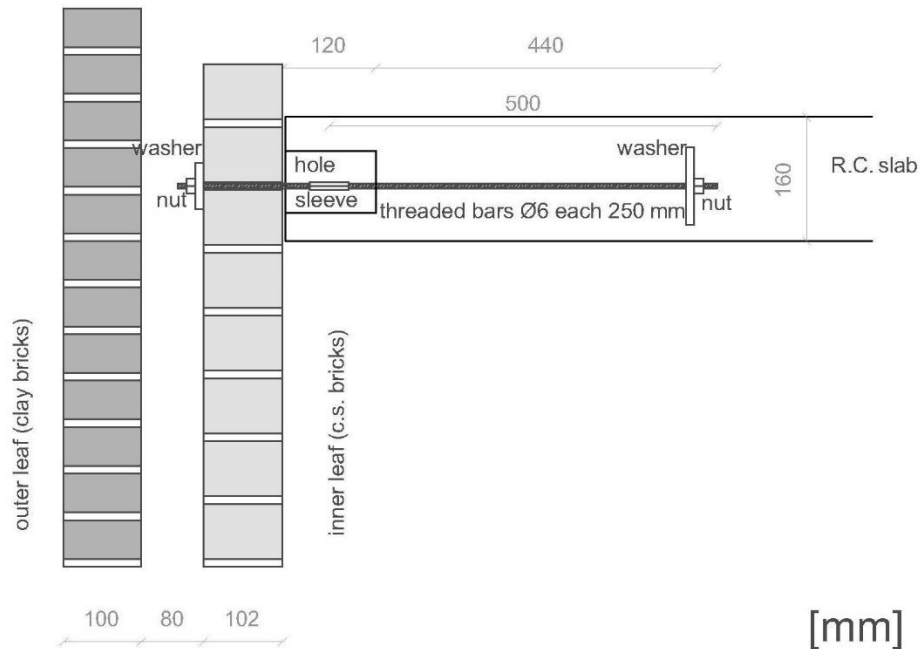


Figure 15. Detail of the connection between the r.c. slab of the first floor and the inner leaf (c.s. walls) - East and West side



Figure 16. Positioning of the r.c. slab of the first floor - East side



Figure 17. View of the r.c. slab of the first floor - East side

**Detail of the connection between the r.c. slab of the second floor and the inner leaf (c.s. walls) - East and West side**

The slab of the second floor is connected with the lateral timber beams by a series of threaded bars  $\phi 10$  each meter. When the slab is laid does not touch directly the lateral (east and west side) walls but laid only on the south and north inner walls and the temporary supports. The gap between the lateral walls and the slab was filled after the removal of the supports.

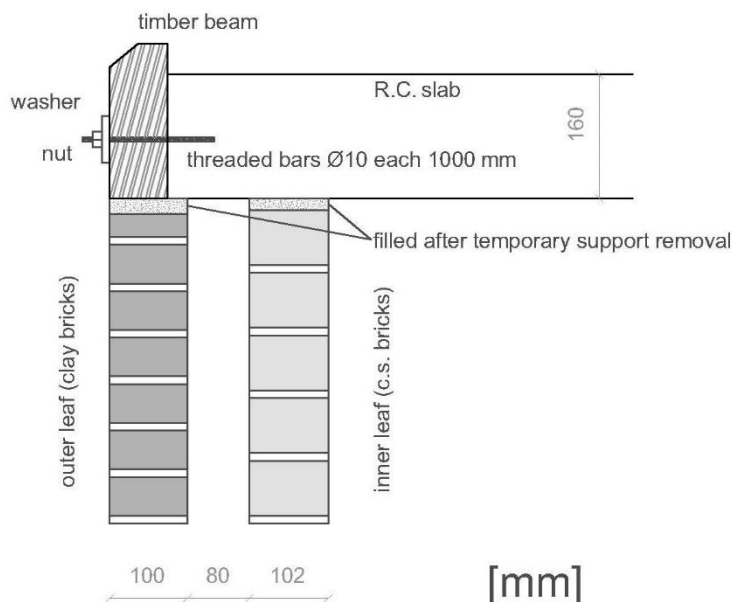


Figure 18. Detail of the connection between the r.c. slab of the second floor and the inner leaf (c.s. walls) - East and West side

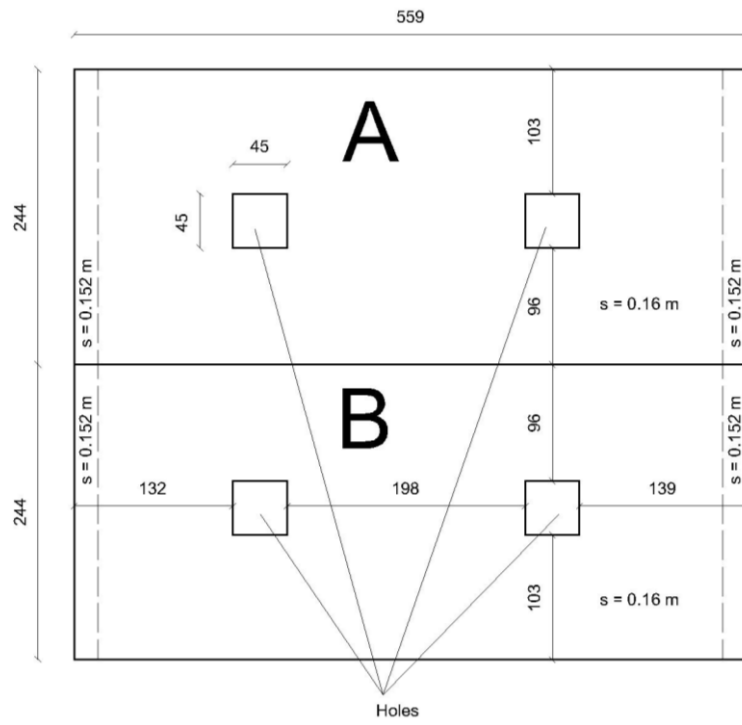


Figure 19. Slab of the first floor

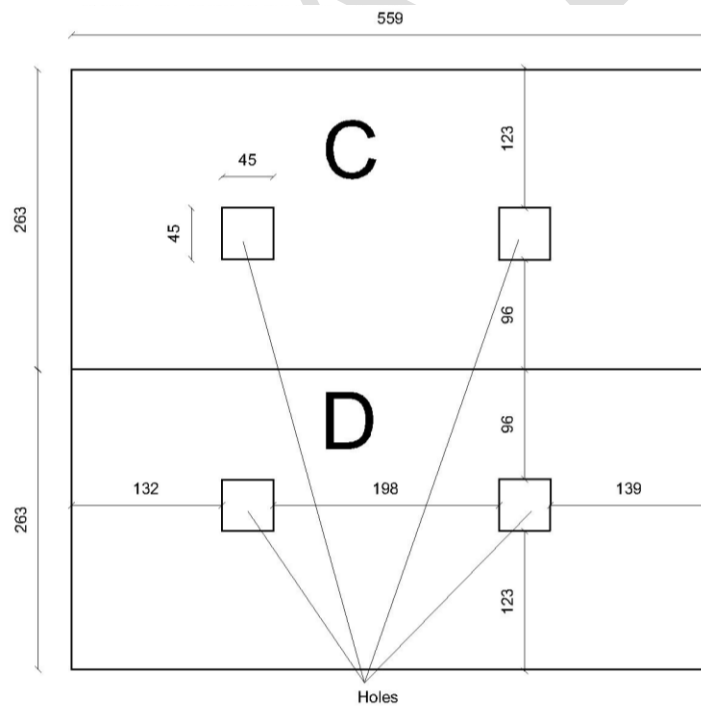


Figure 20. Slab of the second floor



Figure 21. Detail of the connection between the r.c. slab of the second floor and the inner leaf (c.s. walls)- view of the gap - West side

### Detail of the roof

The roof was built according specifications. In particular two 60x2 mm nails each intersection were used to connect each tongue and groove plank with the below timber beam. The counter and tile battens are shown in next figure.

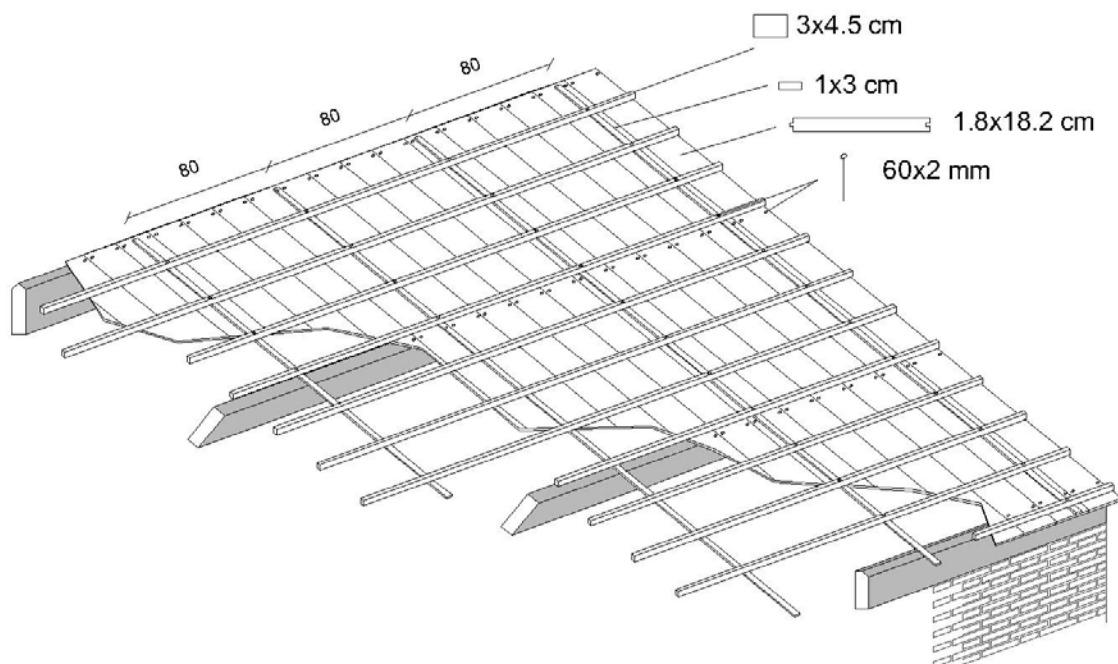


Figure 22. Detail of the roof



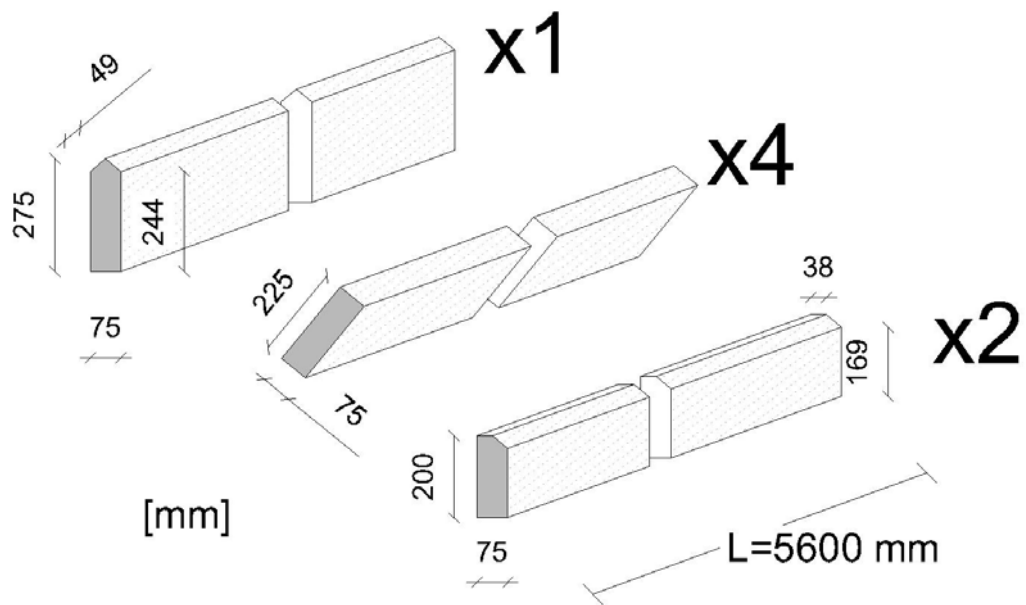


Figure 23. Sections of the girders



Figure 24. Roof and c.s. gable - South side

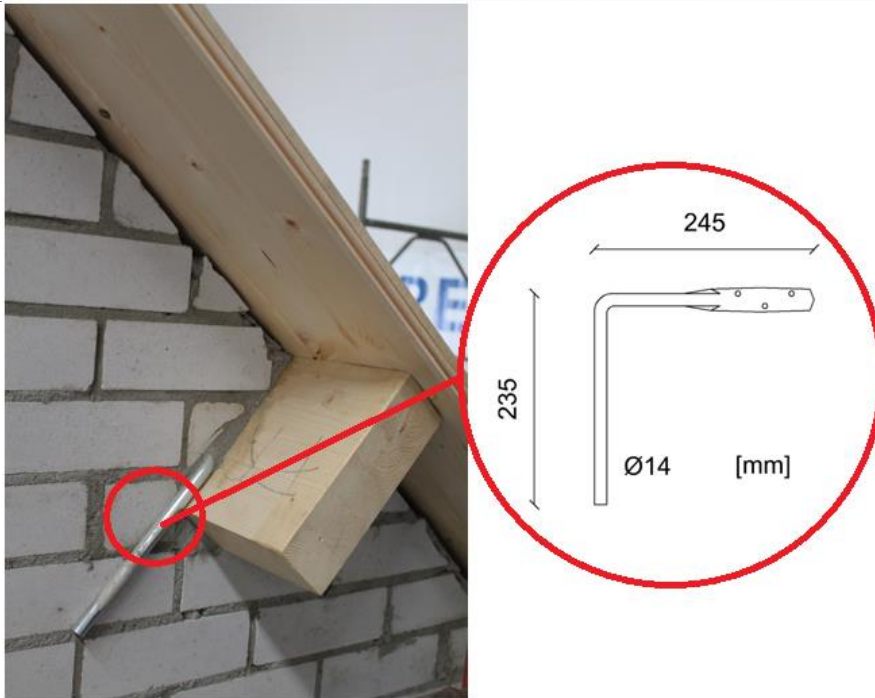


Figure 25. Roof and c.s. gable - South side - detail of the connection with the steel tie



Figure 26. Roof - West side

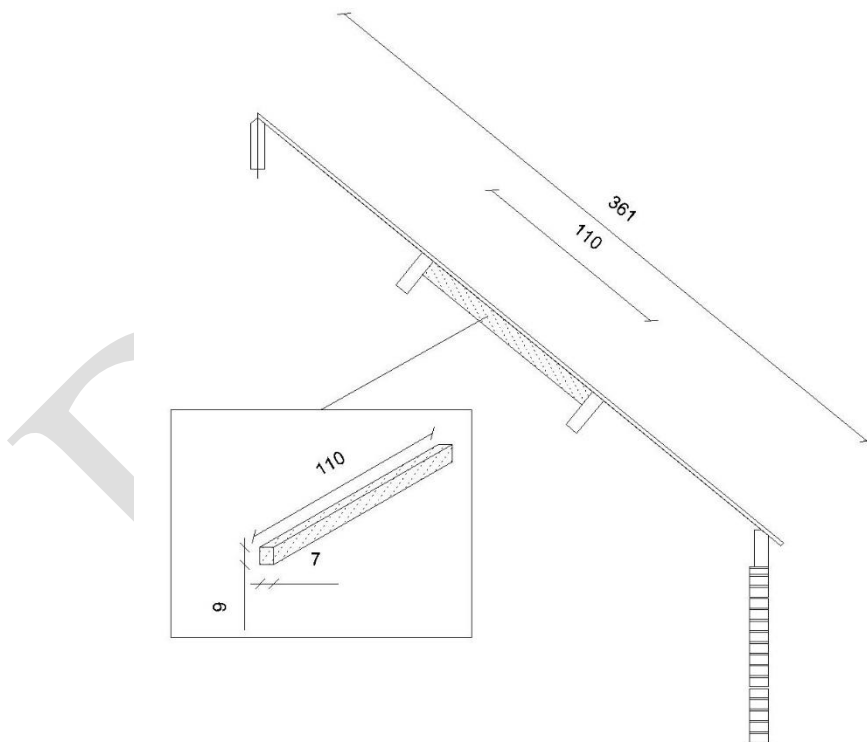
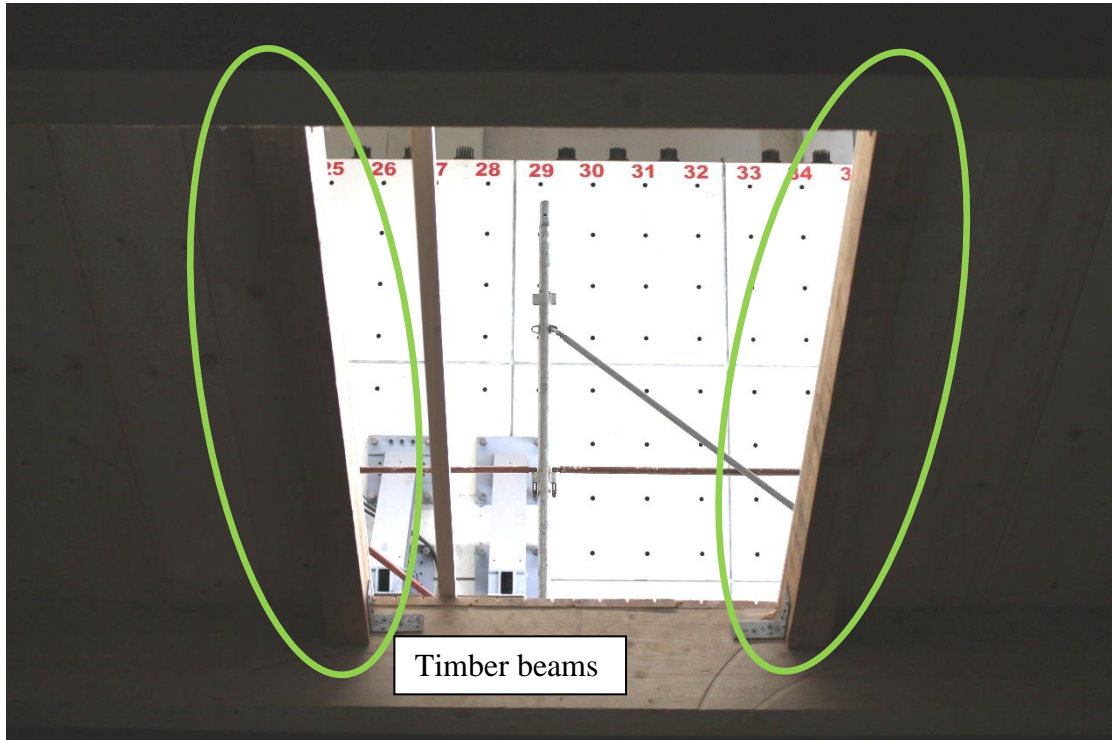


Figure 27. Section of the roof - detail of the opening and the timber beams



*Figure 28. Detail of the connection between the timber beam of the opening and the girder*



*Figure 29. Detail of the connection between the girder and the clay gable - 1*



*Figure 30. Detail of the connection between the girder and the clay gable - 2*



*Figure 31. Detail of the connection between the girder and the clay gable - 3*



## MODEL SNELDEK

Collectie geprofileerde dakpannen



### 'Ik wil zekerheid, de ultieme garantie'

U houdt van degelijk: u wilt blind op uw dak kunnen vertrouwen, jaar in jaar uit. Weer of geen weer. De Sneldek is een betrouwbare, tijdloze pan. En hij heeft zijn sporen verdiend. Hij wordt al tientallen jaren toegepast op woningen en levert een herkenbaar, vriendelijk dak op. Behalve een prima prijs-kwaliteitverhouding biedt de Sneldek u het comfort van jarenlange zekerheid.

Het NIBE (Nederlands Instituut voor Bouwbiologie en Ecologie) heeft betondakpannen als meest milieuvriendelijk dakbedekkingsmateriaal gekwalificeerd. MONIER heeft duurzaamheid hoog in het vaandel staan en levert met al haar betondakpannen dus een dakbedekking met een zeer lage milieubelasting.

### TROTS OP HET DUBOKEUR



MONIER vindt duurzaamheid belangrijk en beschikt als enige over het DUBOkeur voor dit model. Kiest u voor deze betondakpan, dan weet u dus zeker dat u bijdraagt aan de bescherming van het milieu! De productie van betondakpannen levert een CO<sub>2</sub>-uitstoot die tot 60% lager ligt dan die van andere dakbedekkingsmaterialen.

### TECHNISCHE GEGEVENS

<b>Betondakpan</b>		
Afmeting (l x b)	420 x 332 mm	
Gemiddelde werkende breedte	300 mm	
Gewicht	42 N	
Gemiddeld aantal per m <sup>2</sup> overlap 75 mm	9,7	
Gemiddeld gewicht per m <sup>2</sup> overlap 75 mm	ca. 410 N	
Dakhelling minimaal	17,5°	
van 15° tot 17,5° advies vragen bij de afdeling Dakservice		
<b>Latafstand</b>		
dakhelling (°)	maximale latafstand (mm)	minimale overlapping (mm)
≥ 30	345	75
25 - 30	335	85
17,5 - 25	325	95
bij toepassing van gevelpannen is de minimale latafstand 295 mm		
<b>Modelgebonden dakstelselcomponenten</b>		
Euro-panhaak rvs, rekenwaarde	265 N	



De kleuren van de getoonde dakpannen benaderen zoveel mogelijk de werkelijke kleuren. Vraag voor de juiste kleuruncering altijd monsters aan.

\* De coating van deze dakpannen bevat een geringe hoeveelheid conserveringsmiddel met bestanddeel biocide THOR MKB3

Figure 32. Tiles spec.

# **Selection of Acceleration Time-Series for Shake Table Testing of Groningen Masonry Building at the EUCENTRE, Pavia**

Version: 1<sup>st</sup> August 2015

## **Scope**

As part of NAM's data acquisition and analysis programme to develop a seismic hazard and risk model for induced earthquakes in the Groningen gas field, dynamic tests are being performed on structural elements and a full-scale model of a masonry building typical of those encountered in the region. The purpose of this document is to document the selection and preparation of acceleration time-series for the shake table testing on the full-scale model that is scheduled for 10<sup>th</sup> September 2015.

This document is developed jointly by members of the Hazard & Risk Team (Bommer, Crowley, Pinho, Polidoro) and members of the Masonry Structures Group at the EUCENTRE (Magenes, Penna, Graziotti, Mandirola, Bracchi) to ensure that the motions provided for the testing are compatible with the requirements of the testing and also consistent with the seismic hazard in the field.

## **Testing Requirements**

The shake table tests will be performed as uniaxial dynamic loading of the structural model with the objective of ascertaining the ultimate capacity and failure mode of the building but without causing collapse (because of potential collateral damage to the laboratory). The structure is estimated to have a fundamental vibration period of 0.15 seconds in the direction of loading as determined from eigenvalue analyses. However, it is probably more appropriate to use the cracked vibration period of the structure, which has been estimated from bilinear approximations of the capacity curves from pushover analyses to be in the range of 0.25-0.33 s (Figure 1), depending on the assumed lateral force distribution. The yield capacity, in terms of spectral accelerations, has been estimated to be in range of 0.15-0.20g, which is a very important constraint in view of the requirement not to cause collapse. The yield displacement is estimated as 0.0025 m and the ultimate displacement capacity as 0.04 m (Figure 2).

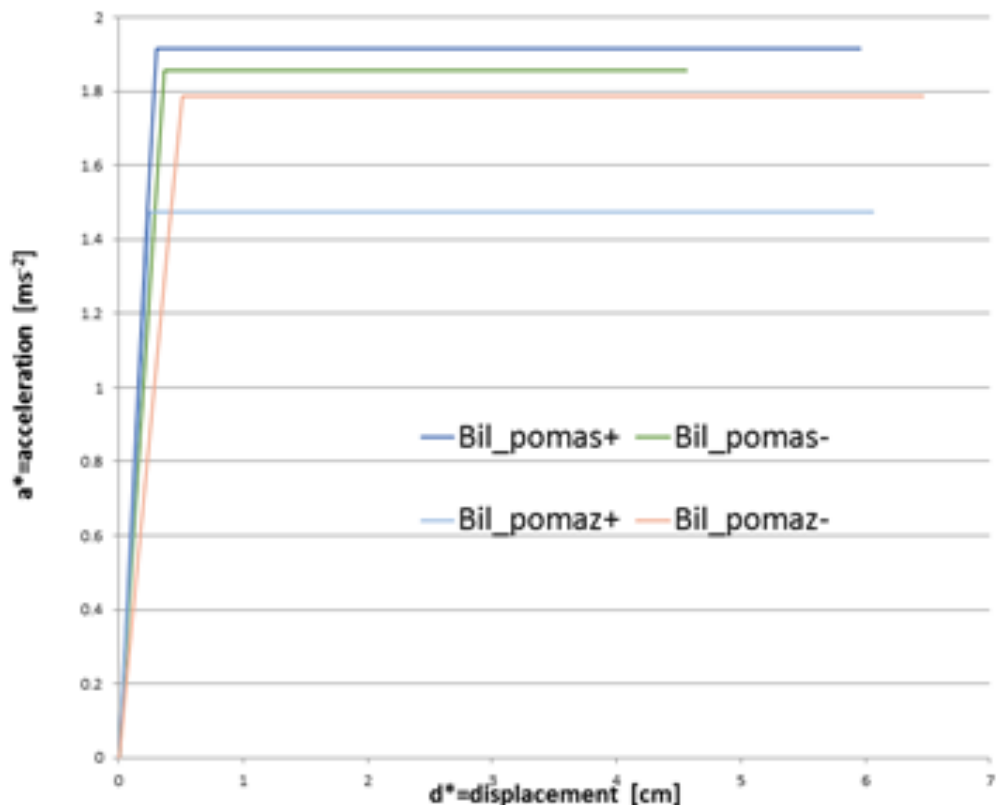


Figure 1. Bilinearised capacity curves for the masonry structure to be tested

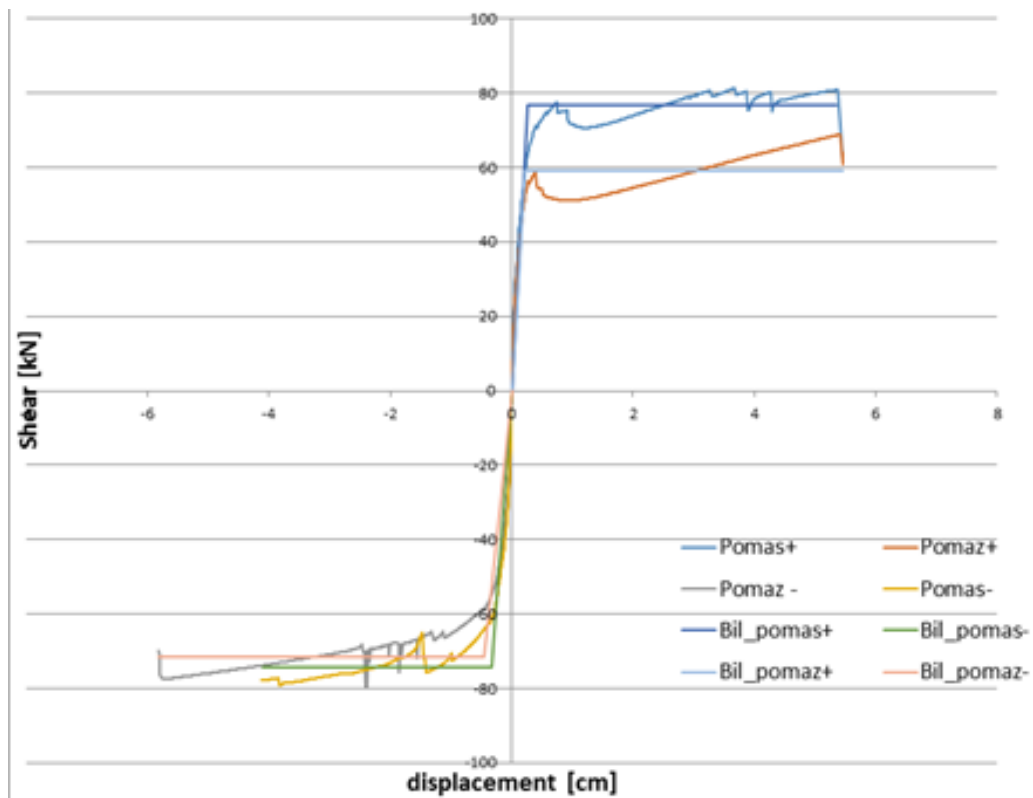


Figure 2. Pushover curves for the masonry structure



There are different requirements in terms of dynamic inputs for the testing:

1. Low-level motions with a broad frequency content for calibration runs
2. A series of realistic motions of increasing amplitude that will eventually lead to failure of the structure

For #1 it is understood that the EUCENTRE will use a generic white-noise signal. For #2, a fundamental choice is whether to use a single acceleration time-history that is scaled through various amplitude levels or to use a series of records that capture not only the increase of amplitude but also other features that may be expected with more severe loading cases. The EUCENTRE requests that no more than two or three records be provided because of the need to re-calibrate for each time-history and the dangers of accumulated damage due to repeated low-level excitation.

Since it is important to avoid total collapse of the structure during the test—or at least at a premature stage of the testing—it is important to estimate *a priori*, from element tests and/or numerical modelling, the intensity levels that would be expected to lead to catastrophic failure of the structure.

## Seismic Hazard Characteristics

In order to identify the controlling earthquake scenarios that dominate the hazard at different annual exceedance probabilities, the hazard was calculated by Dr Stephen Bourne of Shell for Loppersum (the village closest to the current location of highest hazard in the field, with RD coordinates of 245598 X ,594788 Y) using the V1 hazard model and a production period of 5-years (July 2016 to July 2021, consistent with the 2016 Winningsplan). The hazard was calculated in terms of the spectral accelerations at 0.01, 0.2, 0.5, 1 and 2 seconds (Figure 3). The hazard results at selected return periods are listed in Table 1. From the values in the table it can be immediately appreciated that for range of periods defined for the building, yielding can be expected even under the 50-year return period ground motions.

Table 1. Hazard results.

Return Period	Spectral Accelerations (g)				
	0.01 s	0.2 s	0.5 s	1.0 s	2.0 s
50	0.10	0.21	0.16	0.04	0.01
100	0.16	0.32	0.26	0.07	0.02
500	0.36	0.61	0.67	0.22	0.08
1,000	0.48	0.95	0.95	0.33	0.12
2,500	0.69	1.32	1.43	0.53	0.21
5,000	0.89	1.69	1.90	0.70	0.28

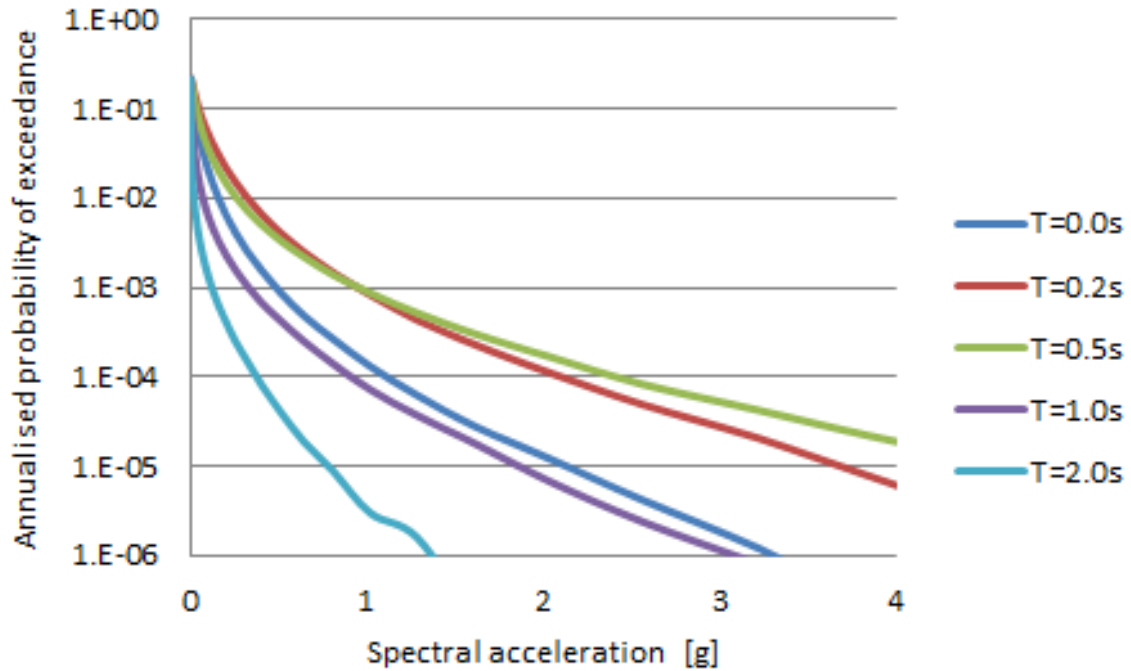


Figure 3. Mean seismic hazards for Loppersum

The hazard estimates were then disaggregated for return periods of 50, 100, 500, 1000, 2500 and 5000 years in terms of contributions by magnitude, distance and epsilon (number of standard deviations above the median prediction). The results show that for the location of highest hazard in the field, the dominant distance is not strongly sensitive to either oscillator period or return period (Figure 4). Although the disaggregation is artificially truncated at a minimum epicentral distance of 3 km, it is clear that for all response periods and return periods the dominant contribution comes from very short distances. This observation simplifies the investigation of the problem because the only parameters of interest become magnitude and epsilon. The disaggregation in terms of contributions by magnitude and epsilon bins are presented graphically in Figures 5 and 6, respectively, and summarised in Table 2. The recurrence of certain values, particularly for epsilon, reflect the resolution at which the disaggregations are performed and the values may therefore be interpreted as indicative approximations rather than exact to three decimal places.

The patterns observed in the results are consistent with expectations, with the values of both the modal magnitude and epsilon increasing with the return period. Additionally, there is an increase in the modal magnitude with the oscillator period. This latter observation highlights the importance of taking into account the natural period of vibration of the structure being tested, although the modal magnitude is more sensitive to return period than to oscillator period.

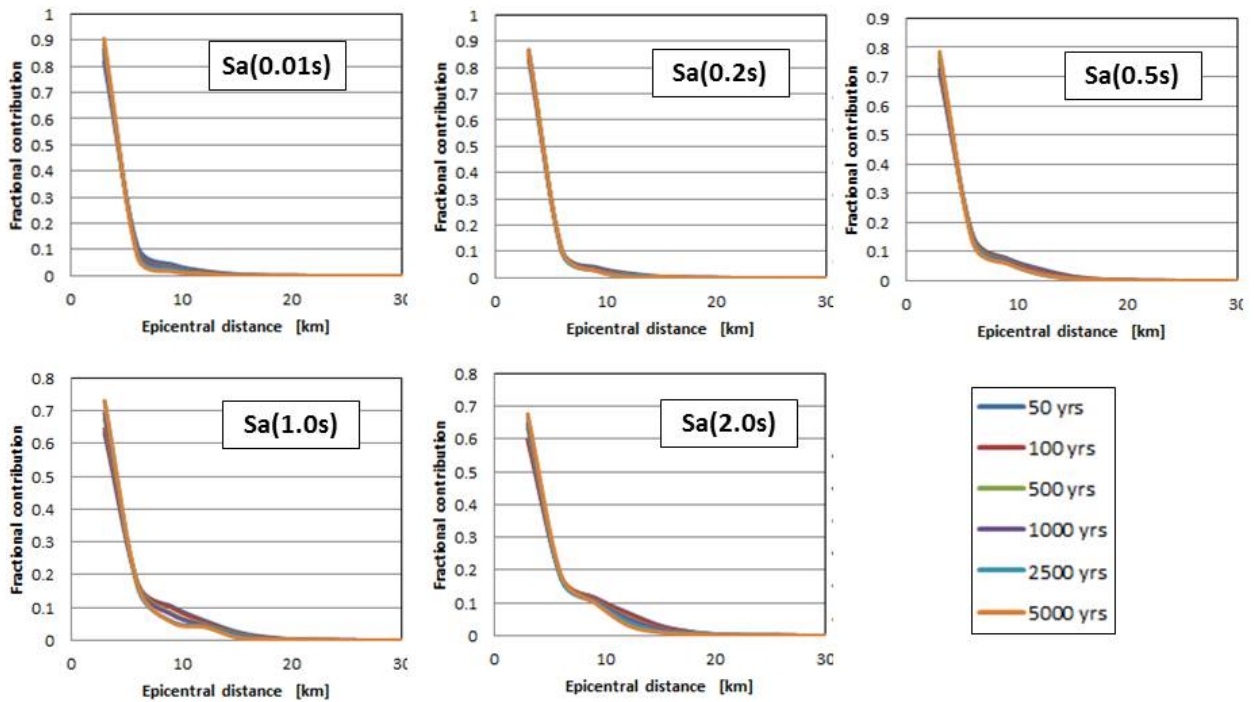


Figure 3. Disaggregation plots for hazard contributions by distance (the truncation at 3 km is unintentional and a result of the software originally being coded for hypocentral distance)

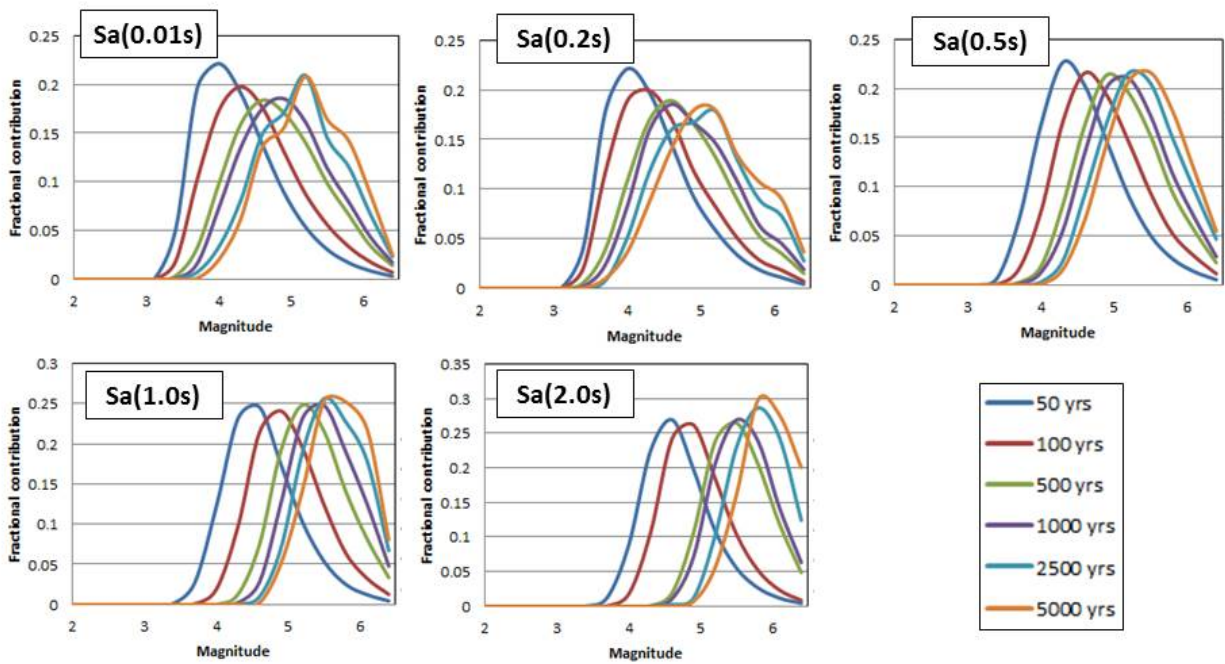


Figure 5. Disaggregation plots for hazard contributions by magnitude

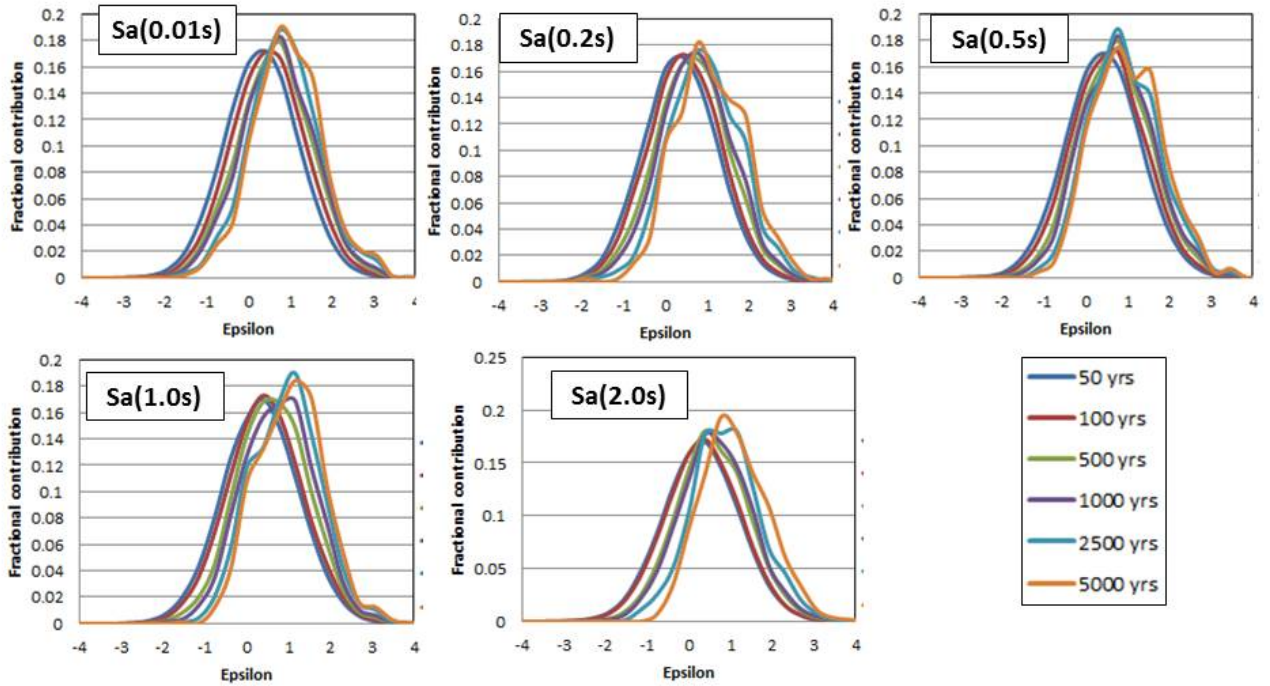


Figure 6. Disaggregation plots for hazard contributions by epsilon

Table 2. Modal contributions of magnitude and epsilon

Return Period	0.01 s		0.2 s		0.5 s		1.0 s		2.0 s	
	M	$\epsilon$	M	$\epsilon$	M	E	M	$\epsilon$	M	$\epsilon$
50	4	0.384	4	0.384	4.3	0.384	4.6	0.384	4.6	0.384
100	4.3	0.384	4.3	0.384	4.6	0.768	4.9	0.384	4.9	0.384
500	4.6	0.768	4.6	0.768	4.9	0.768	5.2	0.384	5.5	0.384
1,000	4.9	0.768	4.6	0.768	5.2	0.768	5.5	1.151	5.5	0.384
2,500	5.2	0.768	5.2	0.768	5.2	0.768	5.5	1.151	5.8	1.151
5,000	5.2	0.768	5.1	0.768	5.5	0.768	5.5	1.151	5.8	0.768

An important observation concerns the epsilon values, which in some cases seem to exhibit somewhat erratic patterns. This appears to be related to convergence issues, as in the case of Sa(2s) and the unusually high value for the 2,500-year return period. As can be appreciated from Figure 4, the disaggregation curve shows a bi-modal behaviour from which it might be inferred that a more appropriate value might lie between the two peaks (which would yield a value similar to that for the 5,000-year return period).

A point worthy of note here is that it has been shown that there is a marked negative correlation between the residuals of spectral accelerations and residuals of durations for the Groningen motions. This fact might allow the selection of a reduced number of accelerograms—which could then be scaled in amplitude as needed—since while the modest increases in modal magnitudes as the return periods increase from 50 to 5,000 years would result in motions of longer durations, this would be at least

partially offset by the smaller durations resulting from the negative correlation coupled with the positive epsilons on accelerations.

A final point that needs to be noted is that the accelerations in Table 1 and the magnitudes in Table 2, especially for the longer return periods, are likely to be over-estimates of the ‘true’ values as a result of the absence of soil non-linearity in the current GMPEs. This means that in reality the increase in dominant magnitude values with increasing return period may actually be smaller than indicated by the values in Table 2.

### Selection and Scaling/Matching Criteria

As already noted, the data in Table 1 show that the yield capacity of the structure is likely to be reached under the action of ground motions with a return period of 50 years, from which it is concluded that only the shorter return periods are relevant. Using the same non-linear static procedures (NSP) that were deployed for the derivation of the V1 fragility functions (Crowley *et al.*, 2015b), it is estimated that under the action of the 50-year UHS, the displacement demand is 0.0047 m—which means that the structure will be responding inelastically—with a corresponding effective period of 0.3 seconds. We make the assumption that the disaggregation information for the acceleration response at 0.2 seconds can be used as a surrogate in this case, which yields a dominant (modal) magnitude of 4.0 and an epsilon of about 0.4 (Table 2). Under the action of the 500-year UHS, the structure has an effective period of 0.5 seconds and displacement demand of 0.034 m, which is a little below the estimated ultimate capacity for the structure. The disaggregation of this scenario yields a modal magnitude of 4.9 and an epsilon of about 0.8 (Table 2). These calculations thus yield two suites of parameters that can be used to define the selection and scaling criteria for the records, as summarised in Table 3.

Table 3. Characteristics of scenarios for record selection

Scenario	Return Period (years)	$T_{\text{eff}}$ (s)	M	$R_{\text{epi}}$ (km)	Epsilon
1	50	0.3	4.0	0.0	0.38
2	500	0.5	4.9	0.0	0.77

The next step is to generate target response spectra for these scenarios. Since the records will be scaled to different amplitudes for input to the shake table tests, it is the spectral shape rather than the absolute amplitudes that are of particular interest. For this reason, it is considered sufficient to generate the scenario spectra using only the central V1 GMPE rather than the weighted average of the three models (lower, central and upper; Bommer *et al.*, 2015a) as used in the hazard calculations presented earlier. Using the full suite of coefficients at multiple response periods

together with the interpolated sigma values, scenario spectra are generated for both scenarios in Table 3. Additionally, using the period-to-period correlations of Akkar *et al.* (2014b), the conditional mean spectra, or CMS (Baker & Cornell, 2006; Baker, 2011), are also generated for both scenarios, conditioned in each case on the spectral acceleration at the effective period. It should be noted that for the scenario of zero epicentral distance, there is no adjustment to be made to the sigma value for geometrical effects of the fault rupture. These four spectra are illustrated in Figure 7. The CMS are presented for interest but in view of the inherent uncertainties in the estimated vibrations periods for the structure, it is considered more appropriate to use the scenario spectra as the targets.

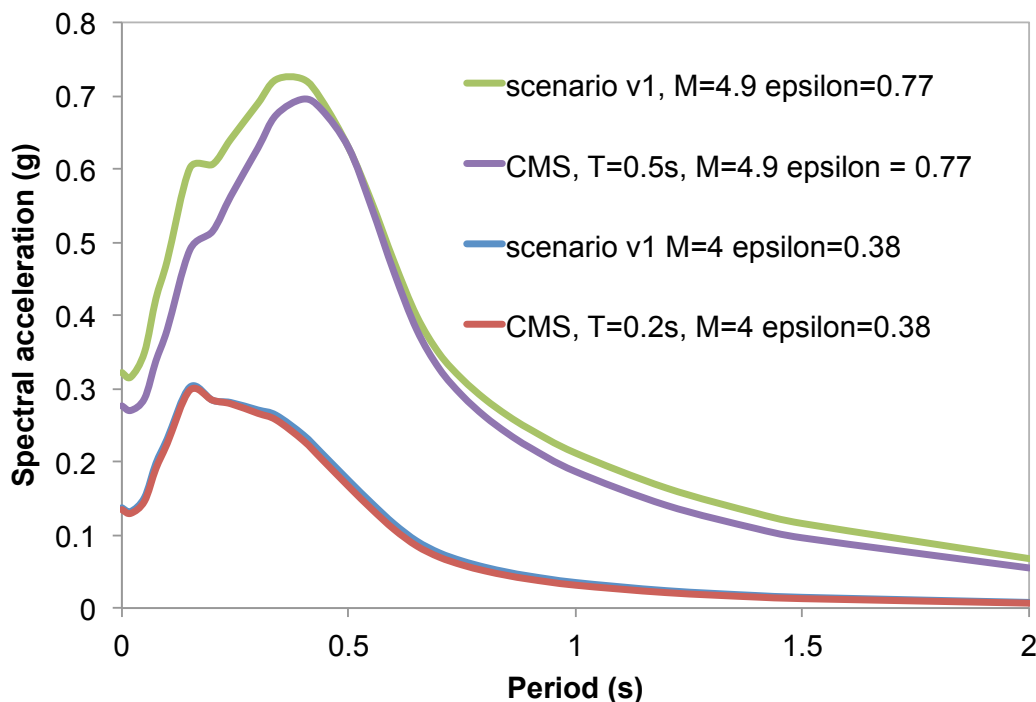


Figure 7. Scenario and conditional mean spectra for the scenarios in Table 3.

An acknowledged shortcoming of the V1 GMPEs is that they only model linear site response; even though the magnitudes of the controlling scenarios in Table 3 are modest, the short source-to-distances mean that the motions may be strong enough to induce non-linear response in the soft soils that cover most of the Groningen field, particularly in the northern parts. Two different approximate adjustments for non-linearity are made by using available non-linear site amplification functions. For both procedures the linear response is firstly removed to transform the motion to some reference baserock horizon, and then the non-linear site amplification functions are applied to bring the baserock motions back to the surface.

In particular, the first approach is the same followed by Crowley *et al.* (2015a) to generate suites of records for structural analyses of Groningen buildings. The

reference rock spectrum is obtained by removing the linear amplification from the v1 linear amplified response spectra according to Sandıkkaya *et al.* (2013). Once the reference spectral acceleration values have been estimated, the nonlinear site amplification term calculated with the same model (Sandıkkaya *et al.*, 2013) is used to define the nonlinear amplified response spectra.

The second approach instead, starting from the v1 linear amplified response spectra, adopts the suite of non-linear site response amplification functions derived for the ground surface at the Groninger Forum site as part of a site-specific assessment of earthquake loads (Bommer *et al.*, 2015b). The amplification function (AF) is defined as in the Equation 1 where  $f_1$ ,  $f_2$  and  $f_3$  are parameters (Bommer *et al.*, 2015b),  $S_{a,rock}$  is the baserock acceleration (g) and  $\varepsilon$  is the zero-mean random variable with standard deviation  $\sigma_{\ln AF}$ .

$$\ln AF = f_1 + f_2 \cdot \ln \left( \frac{S_{a,Rock} + f_3}{f_3} \right) + \varepsilon \quad (1)$$

As in the previous formulation the linear amplification function is represented by the parameter  $f_1$ , the reference rock spectra is obtained by simply dividing the v1 linear spectral accelerations by the exponent of  $f_1$ . Hence, Equation 1 is used to calculate the nonlinear amplified response spectra.

Figure 8 and 9 show the v1 linear amplified response spectra and the nonlinear amplified response spectra (obtained by following the two different approaches) calculated for each scenario respectively. When the second approach is used, nonlinear amplified response spectra are calculated for the two different soil profiles (5a and 6S) described in Bommer *et al.* (2015b).

Given that the Groninger Forum nonlinear response spectra are smoother and are more conservative at longer periods of vibration, and the two soil profiles produce similar results, it has been decided to use their mean, also shown in the same figures, as the target spectra for the record selection and matching. These target spectra are provided in the Excel file appended to this document.

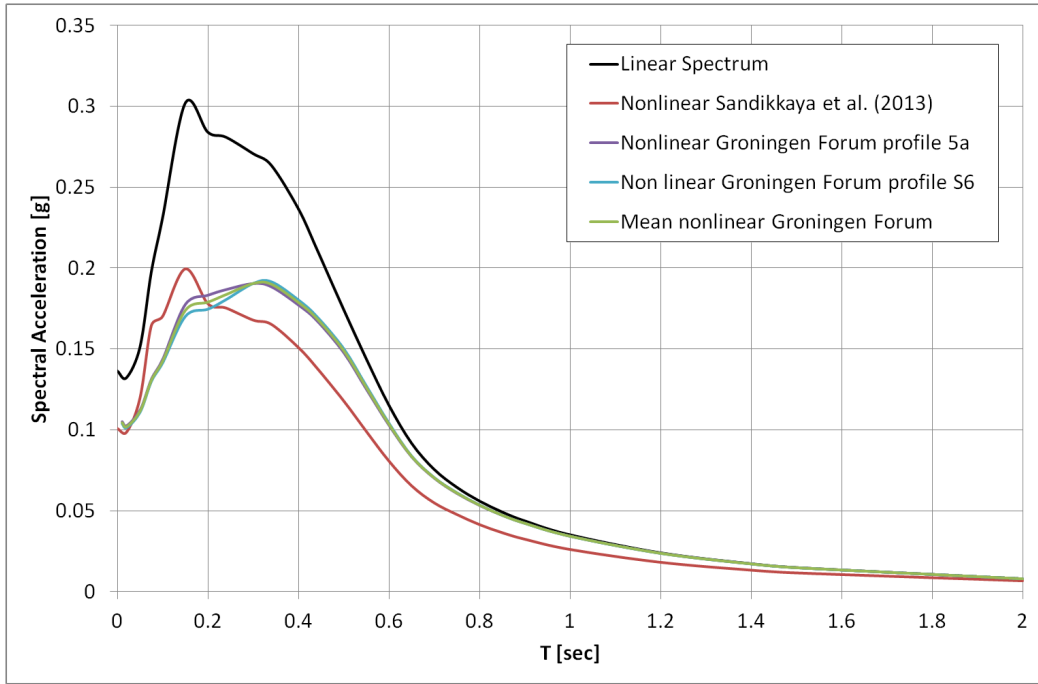


Figure 8. Nonlinear amplified spectra for the scenario 1 based on the Sandikkaya *et al.* (2013) and the non-linear site response amplification functions derived for the ground surface at the Groninger Forum site.

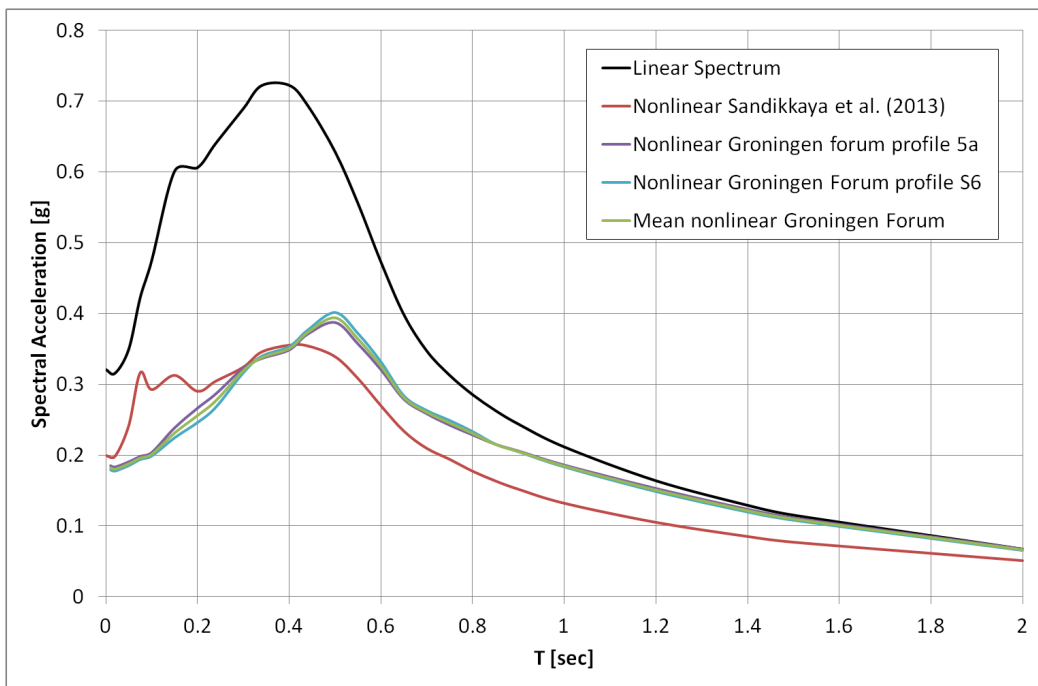


Figure 9. Nonlinear amplified spectra for the scenario 2 based on the Sandikkaya *et al.* (2013) and the non-linear site response amplification functions derived for the ground surface at the Groninger Forum site.



A final consideration in defining the selection criteria is the duration of the ground motion. For the V1 hazard and risk modelling, it was concluded that the predictive equation of Kempton & Stewart (2006) for the significant duration based on the 5-75% accumulation of Arias intensity yielded acceptable approximations to the Groningen data when applied, in the CBL format, with an assumed basin depth ( $Z_{1.5}$ ) of 600 m and an assumed  $V_{S30}$  of 200 m/s;  $R_{rup}$  is approximated by  $R_{hyp}$ , which for the scenarios in Table 3 is 3 km. Equation 2 illustrates the formulation adopted to calculate the duration for the two different scenarios.

$$\ln(D_s) = \ln \left[ \frac{\left( \frac{\exp(6.02)}{10^{1.5M+16.05}} \right)^{\frac{1}{3}}}{1.568 \times 10^7} + 0.07 \cdot R_{rup} + 2.73 - 0.0013(V_{S30}) - 0.00075(Z_{1.5}) \right] \quad (2)$$

However, it was noted by Bommer *et al.* (2015a) that this model does overestimate the durations of the Groningen motions at very short distances, which is a pertinent observation for this application. Moreover, a negative correlation was found between the residuals of spectral acceleration from the V1 GMPEs and the residuals of duration with respect to this adopted model (Bommer *et al.*, 2015a); following the results of Bradley (2011), the correlation coefficient for spectral acceleration at 0.2 s can be used as a substitute for that at 0.3 seconds. Table 4 summarises the calculated  $D_{S5-75}$  values.

Table 4. Calculated durations for the two design scenarios

Scenario	Median $D_{S5-75}$	$\rho[D_{S5-75}, Sa(T_{eff})]$	$\epsilon_{D_{S5-75}}$	$\sigma_{D_{S5-75}}$	Conditional mean $D_{S5-75}$
1	2.25	-0.316	-0.12	0.53	2.11
2	2.28	-0.392	-0.30	0.53	1.96

Noting the observation that at short distances, the Kempton & Stewart (2006) model tends to overestimate durations for small-magnitude Groningen earthquakes, the values in the final column of Table 4 may be treated as upper bounds.

### Selection, Scaling and Matching of Acceleration Records

A pre-selection of records from the NGA database (<http://ngawest2.berkeley.edu>) has been undertaken by identifying horizontal components that have a 5-75% significant duration lower than the conditional mean value defined in Table 4, that is 2.11s for scenario 1 and 1.96s for scenario 2, ensuring that the maximum usable period is greater than or equal to 0.5 seconds.

Using this reduced set of waveforms, the final selection is made by linearly scaling the records to minimize the difference with respect to the target horizontal spectra, across the 0.2 to 0.4 second period range for scenario 1 and 0.3 to 1 second period range for scenario 2. The absolute sum of squared errors (SSE) is used to quantify the match between the response spectral ordinates of the records and the target spectrum over the period range of interest. Hence, the waveforms have been ordered in terms of SSE and the top five records with the lowest SSE values have been selected for the spectral matching.

In order to include a recording from the Groningen field for scenario 1, the database used to develop the v1 GMPEs (Bommer *et al.*, 2015a) has been used. Also in this case a pre-selection of records has been made by identifying horizontal components that have a 5-75% significant duration of less than 2.11s. Hence, the same procedure of linear scaling is applied and the waveforms have been ordered in terms of SSE. The first five records with the lowest SSE plus the record with the lowest SF have been selected for the spectral matching.

Once the horizontal components from the two different databases have been selected for each scenario, accelerograms have been linearly scaled and then spectrally matched to the target horizontal spectra using the spectral matching algorithm described in Hancock *et al.* (2006) and embedded within the SeismoMatch software (Seismosoft, 2015). To avoid dramatic modifications to the frequency content of the original records, a maximum of 30 iterations have been applied in the matching algorithm.

After matching, for scenario 1 two recordings from the NGA database and one from the Groningen database having the best match over a wide period range have been selected, whilst for scenario 2 the top three recordings from the NGA database with the lowest SSE values have been chosen.

Figures 10 and 11 show the target and matched response spectra for the selected recordings, for scenario 1 and 2 respectively, whilst Figures 12 and 13 show the comparison of the original and the scaled/matched time-histories.

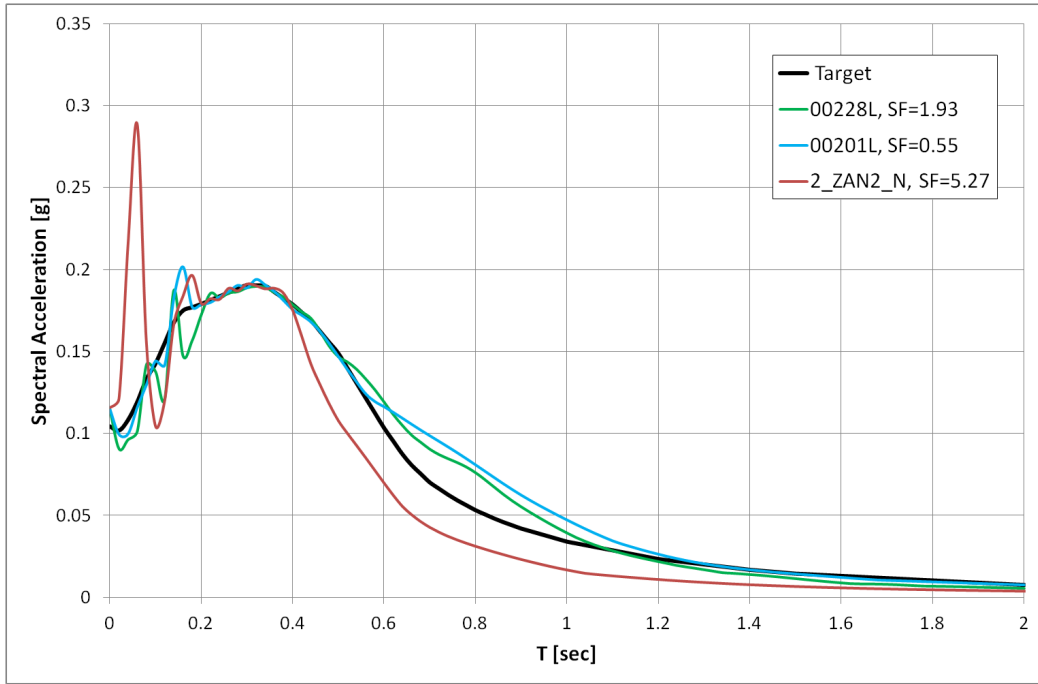


Figure 10. Comparison of target spectrum and matched spectra for scenario 1.

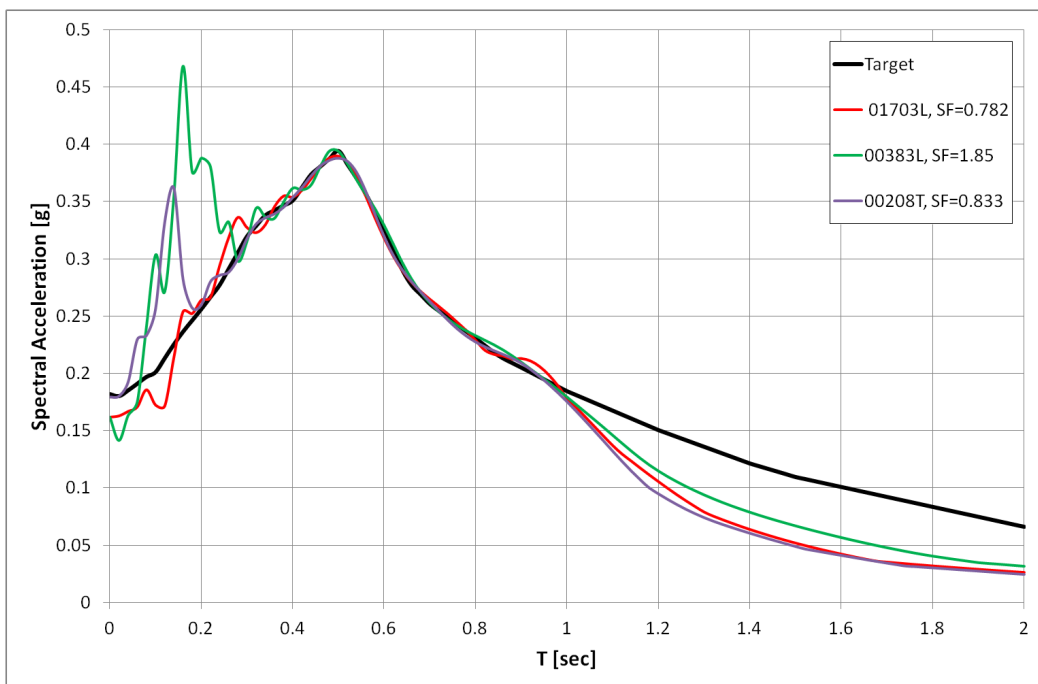


Figure 11. Comparison of target spectrum and matched spectra for scenario 2.

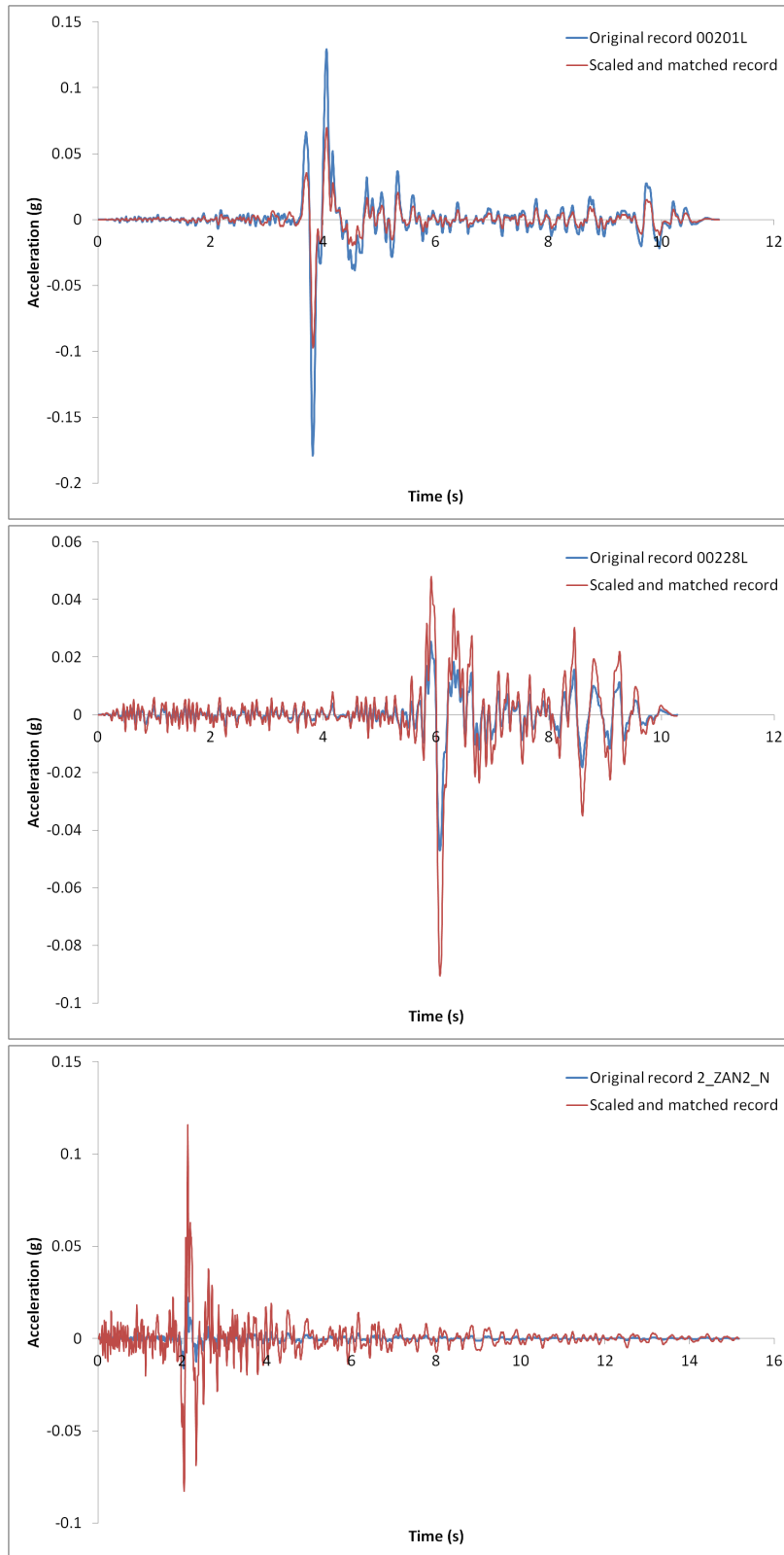


Figure 12. Comparison between the original and scaled and matched records for scenario 1.

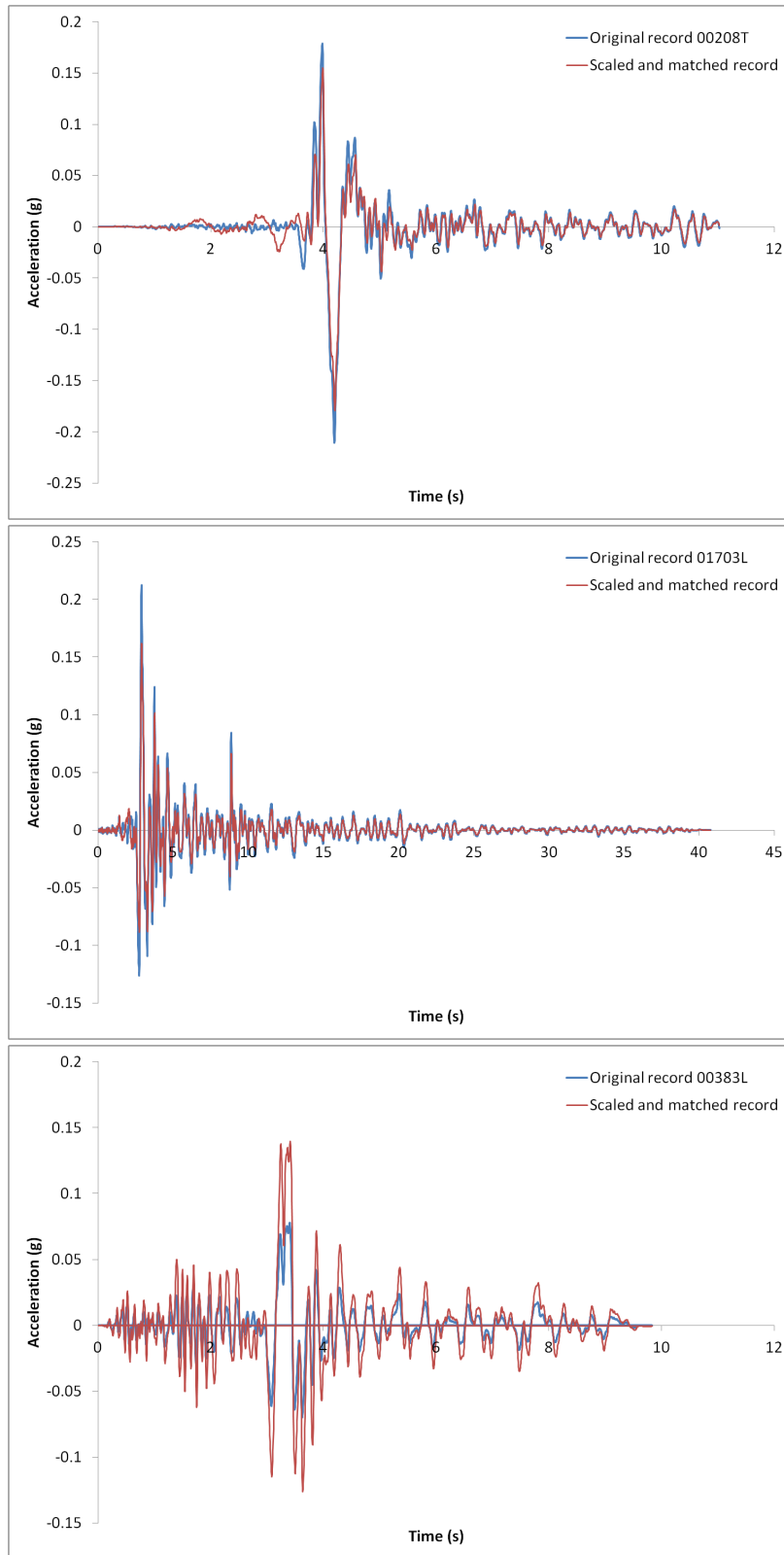


Figure 13. Comparison between the original and scaled and matched records for scenario 2.

As the spectral matching can change the 5-75% significant duration, this has been recalculated for each matched horizontal component to ensure that the value was still lower than the upper bound defined in Table 4.

Information and significant durations of the selected and matched ground motions are reported in Table 5 for scenario 1 and in Table 6 for scenario 2.

Table 5. Summary of records selected for scenario 1.

No.	Waveform No.	Database	EQ Name	EQ Date	Mw	Repi (km)	5-75% significant duration (s)
1	00228L	NGA	Anza (HorseCanyon)	25-02-1980	5.19	41.25	1.05
2	00201L	NGA	Imperial Valley-07	15/10/1979	5.01	15.28	0.375
3	ZAN2_N	Groningen	2	30/10/2008	3.1	3.36	0.395

Table 6. Summary of records selected for scenario 2.

No.	Waveform No.	Database	EQ Name	EQ Date	Mw	Repi (km)	5-75% significant duration (s)
1	01703L	NGA	Northridge-06	20/03/1994	5.28	9.19	1.72
2	00383L	NGA	Coalinga-02	09/05/1983	5.09	8.23	1.97
3	00208T	NGA	Imperial Valley-07	15/10/1979	5.01	7.85	0.40

### Final Selection of Records for Shake Table Test

Accelerograms with a smoother response spectra are preferred for the shake table test, for higher control of both the shake table and the response of the structure, and thus waveforms 00228L, 00201L (scenario 1) and 01703L (scenario 2) are preferred. For scenario 1, it is felt that the shorter duration waveform (00201L) would be more representative of the local hazard, given that it has a significant duration similar to the Groningen recording. Even though this duration is much lower than the target significant duration, it is known that the formula that has been used overestimates the duration of recordings from the field at short distances.

Hence, the waveforms 00201L for scenario 1 and 01703L for scenario 2 have been selected for the shake table test. The shake table test will be an incremental dynamic analysis, with a number of levels of shaking being applied to the structure, as described in the testing protocol. Scenario 1 will be scaled down to 50% to obtain the response of the structure under lower levels of shaking, and scenario 2 will be scaled by up to 2 times for the highest levels of shaking. It has been deemed appropriate to scale scenario 2 by this much given that the disaggregated scenario for spectral

acceleration at 0.5 seconds does not change significantly from 500 to 2500 years. For levels of shaking between scenario 1 and scenario 2, it would be justified to scale either scenario and a practical choice to remain with scenario 1 has been made.

## References

Akkar, S., M.A. Sandıkkaya & J.J. Bommer (2014a). Empirical ground-motion models for point- and extended-source crustal earthquake scenarios in Europe and the Middle East. *Bulletin of Earthquake Engineering* **12**(1), 359-387. *Erratum*: **12**(1), 389-390.

Akkar, S., M.A. Sandıkkaya & B.Ö. Ay (2014b). Compatible ground-motion prediction equations for damping scaling factors and vertical-to-horizontal spectral amplitude ratios for the broader European region. *Bulletin of Earthquake Engineering* **12**(1), 517-547.

Baker, J.W. (2011). Conditional mean spectrum: tool for ground motion selection. *ASCE Journal of Structural Engineering* **137**, 322-331.

Baker, J.W. & C.A. Cornell (2006). Spectral shape, epsilon and record selection. *Earthquake Engineering & Structural Dynamics* **35**, 1077–1095.

Bommer, J.J., S.J. Bourne, H. Crowley, B. Edwards, P. Kruiver, S. Oates & A. Rodriguez-Marek (2015b). *Seismic design loads for the Groningen Forum*. Version 3, 26 June, 88 pp.

Bommer, J.J., P.J. Stafford, B. Edwards, M. Ntinalexis, B. Dost & D. Kraaijpoel (2015a). *Development of Version 1 GMPEs for response spectral accelerations and strong-motion durations*, Version 1, 16 March, 278 pp.

Bradley, B.A. (2011). Correlation of significant duration with amplitude and cumulative intensity measures and its use in ground motion selection. *Journal of Earthquake Engineering* **15**(6), 809-832.

Crowley, H., J.J. Bommer & R. Pinho (2015a). *Selection of records for nonlinear dynamic analysis of Groningen buildings*. Version 1.0, 13 May, 17 pp.

Crowley, H., D. Grant & R. de Vries (2015b). *Development of V1 fragility functions for structural failure*. 1 July, 63 pp.

Hancock, J., J. Watson-Lamprey, N.A. Abrahamson, J.J. Bommer, A. Markatis, E. McCoy & R. Mendis (2006). An improved method of matching response spectra of recorded earthquake ground motion using wavelets. *Journal of Earthquake Engineering* **10**(special issue 1), 67-89.

Kempton, J.J. & J.P. Stewart (2006). Prediction equations for significant duration of earthquake ground motions considering site and near-source effects. *Earthquake Spectra* **22**(4), 985-1013.

Sandıkkaya, M.A., S. Akkar & P.-Y. Bard (2013). A nonlinear site-amplification model for the next pan-European ground-motion prediction equations. *Bulletin of the Seismological Society of America* **103**(1), 19-32.

Seismosoft (2015) SeismoMatch Version 2.1, Available from URL: <http://www.seismosoft.com/downloads>